INFORMATION TO USERS

This manuscript has been reproduced from the microfilm master. UMI films the text directly from the original or copy submitted. Thus, some thesis and dissertation copies are in typewriter face, while others may be from any type of computer printer.

The quality of this reproduction is dependent upon the quality of the copy submitted. Broken or indistinct print, colored or poor quality illustrations and photographs, print bleedthrough, substandard margins, and improper alignment can adversely affect reproduction.

In the unlikely event that the author did not send UMI a complete manuscript and there are missing pages, these will be noted. Also, if unauthorized copyright material had to be removed, a note will indicate the deletion.

Oversize materials (e.g., maps, drawings, charts) are reproduced by sectioning the original, beginning at the upper left-hand corner and continuing from left to right in equal sections with small overlaps.

Photographs included in the original manuscript have been reproduced xerographically in this copy. Higher quality 6" x 9" black and white photographic prints are available for any photographs or illustrations appearing in this copy for an additional charge. Contact UMI directly to order.

Bell & Howell Information and Learning
300 North Zeeb Road, Ann Arbor, MI 48106-1346 USA
800-521-0600

A Numerical Modelling Study of Transport Phenomena in Wood Drying

by

Ahmad Hashemi Esfahanian
B.A., Isfahan University of Technology, 1987
M.Sc., Isfahan University of Technology, 1990

A Submitted in Partial Fulfillment of the
Requirements for the Degree of
DOCTOR OF PHILOSOPHY
in the
Department of Mechanical Engineering.

We accept this thesis as conforming
to the required standard

[Dr. B. Tabarrok], Co-supervisor (Dept. of Mechanical Engineering)

Dr. S. Dost, Co-supervisor (Dept. of Mechanical Engineering)

Dr. Z. Dong, Member (Dept. of Mechanical Engineering)

Dr. M. D. Whale, Member (Dept. of Mechanical Engineering)

Dr. R. Lueck, Member (School of Earth and Ocean Sciences)

Dr. Luiz Oliveira, External Examiner (Forintek Canada)

Supervisors: [Dr. B. Tabarrok] and Dr. S. Dost

Abstract

This thesis presents a numerical simulation study for the heat and mass transfer in- and out-side individual boards of a stack during kiln drying of wood and on the effect of side gaps between the boards. The objective is to optimize the drying process for efficiency and high quality products.

A literature survey in the area is presented. The importance of the correct link between the transport processes in wood, and heat/mass transfer and fluid flow in the surrounding drying air is emphasized. Objectives, motivations and needs for the present study are also presented. This is followed by a detailed account of the governing equations, description of models, physical properties, and discretization and solution procedures used in the present study.

A sample stack of planks has been used to evaluate the performance of various turbulence models and upwinding schemes of the CFX software developed for predicting the transport parameters in air. Given a typical stack set up for drying 105×105 mm western hemlock lumber, the effects of side gaps on surface coefficients are studied for different air velocities. An optimum gap size for maximum heat/mass transfer is suggested.

The model developed for heat and mass transfer inside the wood is validated for a one dimensional case by comparing the numerical results with published results. The improved performance using a newly proposed relationship for the diffusivity of bound water has been demonstrated. Also a new relationship for the mass transfer boundary condition at the surfaces was proposed to incorporate the effect of the surface resistance. Relative effects of model unknowns in predicting the average moisture content and board center temperatures are discussed.

A Fortran program was developed to solve the two-dimensional coupled heat and mass transfer equations inside the wood during the drying process. The model considers the changes in air temperature and humidity due to heat and mass transfer to and from the boards. The iterative SOR (Successive Over Relaxation) method was modified to increase accuracy and stability. Predictions for average and local moisure content are in good agreement with experiments. The effect of side gap on the drying process inside the wood was also examined. A plot of standard deviation of each board versus the board average moisture content is suggested for the judgement about the uniformity of the products. Results indicate that without using the extra gap size there exists a considerable difference between the maximum and minimum final average moisture content of the boards in each row. The first and last boards are usually over-dried. By using the previously suggested gap size the maximum difference of the final average moisture content is almost half the case without the extra gap.

Average diffusion and surface coefficients are extracted from the experimental data of drying a stack without side gap. A software tool has been developed to solve the simple unsteady one-dimensional diffusion problem. Results are compared with experiments. The introduced method can be used to obtain the average diffusion and surface coefficients.

Examiners:

[Dr. B. Tabarrok], Co-supervisor (Dept. of Mechanical Engineering)

Dr. S. Dost, Co-supervisor (Dept. of Mechanical Engineering)

Dr. Z. Dong, Member (Dept. of Mechanical Engineering)

Dr. M. D. Whale, Member (Dept. of Mechanical Engineering)

Dr. R. Lueck, Member (School of Earth and Ocean Sciences)

Dr. Luiz Oliveira, External Examiner (Forintek Canada)

Table of Contents

List of Tables

List of Figures

Acknowledgements

First I have to thank God for providing me guidance, ability, knowledge and patience. Thank you very much my father and mother for your full love and support during my whole life, without which I could not reach this position. Many thanks to my wife, Sima, for her patience, love and support. I appreciate your understanding when you had to quit temporarily your study for staying with me and when I had to stay late at the University.

Posthumous appreciation is given to Dr. Behrouz Tabarrok's role as co-supervisor for his guidance, encouragement and support. I also would like to thank my co-supervisor, Dr. Sadik Dost, for all his efforts, guidance and support throughout this research.

I am very gateful for the financial support provided by: the Ministry of Culture and Higher Education of I. R. of Iran, National Science and Engineering Research Council of Canada, and the University of Victoria fellowship. I would like to acknowledge Ms. Min Li and Dr. I. Hartley for providing the experimental data which were necessary for completion of this work. I would like also to thank the external examiner and other members of the supervisory committee Drs. L. Oliveira, Z. Dong, M. Whale and R. Lueck for their generous cooperation and assistance. Also instrumental in the completion of this work were the discussions I had with fellow graduate students Ian Spearing, Shafei Zeidan, Anotai Suksangpanomrung, Jon Pharoah and Martin Bowers and Drs. Shafei Zeidan and Ibrahim Dincer.

To my parents, brothers and sisters

To my wife, my children (Niloofar and Amin) and my wife's family

Nomenclature

A	coefficient in calculating capillary pressure
A_1	coefficient in Eqn. 8.1
B	coefficient in calculating capillary pressure
B_1	coefficient in Eqn. 8.1
B_2	coefficient in Eqn. 8.1
B_X, B_T	coefficients in calculating the flux of bound water
c_u, c_k	coefficients for describing u^+ in turbulent flows
c_p	specific heat capacity
$c_{\epsilon 1}, c_{\epsilon 2}$	coefficients used for $\epsilon-$ equation in turbulent flows
D	apparent moisture diffusion coefficient of wood
D_{AB}	un-delayed water vapour diffusion coefficient
D_a	diffusion coefficient of drying moist air
D_{av}	average diffusion coefficient of moisture in wood
D_b	bound water diffusion coefficient
D_{eff}	effective water vapour diffusion coefficient
D_h	hydraulic diameter of the duct
D_μ	coefficient of the drying model related to bound water
E_l	effective permeability to liquid flow in wood

F_X	coefficient in calculating the flux of free water
G	turbulent kinetik energy generation
g	side gap size
h	convective heat transfer coefficient from surface
h_a	enthalpy of air
h_b	enthalpy of bound water
h_f	enthalpy of free water
h_v	enthalpy of water vapour
h_m	convective mass transfer coefficient from surface
J	vector of total moisture flux
J_a	vector of air mass flux in wood
J_b	vector of bound water mass flux
J_f	vector of free water mass flux
J_v	vector of water vapour mass flux
K_l	permeability of unsaturated wood to liquid water flow
K_{ls}	permeability of saturated wood to liquid water flow
k	kinetik energy of the fluctuation motion in turbulent flows
$\dot{m}$	mass transfer rate
m_v	molar mass of water
Nu	Nusselt number
n_{st}	number of stacks per kiln
P_c	capillary pressure
Pe	Peclet number
P_l	liquid water pressure
Pr	Prandtl number
P_{sv}	saturation water vapour pressure in wood

P_v	partial water vapour pressure in wood
Q	heat transfer
q	heat transfer per unit volume of lumber
R	ideal gas constant
R_h	relative humidity of the drying air
s	molar entropy
S	saturation
S_{av}	average surface mass transfer coefficient
Sc	Schmidt number
S_{err}	summation of errors in SOR method
S_{min}	minimum saturation for free water flow
Sh	Sherwood number
S_T	coefficient of the drying model related to bound water
t	time
T	temperature
$\overline{T}$	local time average temperature of air
u^+	dimensionless velocity in turbulent flows
u_a	internal energy of dry air inside the wood
u_b	internal energy of bound water
u_d	internal energy of the dry wood
u_f	internal energy of free water
u_v	internal energy of water vapour
v	molar volume
V	volume
V_i, V_j	velocity components
V_X, V_T	coefficients in calculating the flux of water vapour

x_i, x_j	Cartesian coordinate
X	local moisture content in wood
X_{eq}	equilibrium moisture content of the drying air
X_{FSP}	moisture content at the fibre saturation point
X_{max}	moisture content if the entire void structure is filled with water
X_{min}	minimum moisture content for liquid flow
x_v	vapour mole fraction in humid air
y^+	dimensionless distance from wall in turbulent flows
Y	air humidity, dry basis

Greek symbols

α	attenuation factor of wood structure in eqns. 5 and 7
δx	distance between two adjacent ponits in x direction
δy	distance between two adjacent ponits in y direction
Δt	time step
Δx	x direction step size
Δy	y direction step size
ε	viscous dissipation in turbulent flows
ϵ	void fraction
η_l	viscosity of liquid water
λ_a	thermal conductivity of air
λ	thermal conductivity of moist wood
μ	viscosity of air
μ_b	chemical potential for bound water
μ_t	turbulent eddy viscosity
ξ	residue at each point in the SOR method
ρ, ρ_a	density of air
ρ_b	density of bound water
ρ_l, ρ_f	density of liquid (free) water
ρ_d	density of dry wood
ρ_v	density of water vapour
ρ_{wt}	total moisture density in wood
τ_w	wall shear stress
Φ	dissipation term in turbulent flows
$\psi(X,T)$	coefficient for partial vapor pressure in wood

ω	absolute humidity of the drying air
Ω	over relaxation factor in the SOR method

Superscripts

.	time rate
$-$	turbulent time average values
$'$	turbulent fluctuation terms
n	time step number

Subscripts

a	air
b	bound water
$cell$	wood cell
d	dry wood
db	dry-bulb (temperature)
eff	effective
FSP	fiber saturation point
f	free water
l, w	liquid water
n	normal to the surface
s	values at the surface
∞	free stream values
(i, j)	location numbers of control volume cell
v	water vapour
wb	wet-bulb (temperature)
x	component in the x-direction
y	component in the y-direction

Acronynms

ADI	alternating direction implicit
FSP	fiber saturation point
SOR	successive over relaxation
TDMA	three diagonal matrix

Chapter 1

Introduction

Drying is an energy intensive process. This process is used in a variety of applications ranging from food processing to wood drying. For wood drying, there is great interest in studying this process because the wood industry is one of the largest industries in British Columbia and Canada as well as in other countries.

Canada is a major producer of wood. It is certain that the lumber industry and wood products will continue to play a key role in Canada's economy over the next century. The total energy consumption of this industry excluding pulp, paper and printing industries, is approximately 1% (27 Pega Joules in 1998) of the total industrial energy consumption in Canada[1]. Due to its importance, the Canadian wood industry spends about twenty five million dollars annually on research and development related to wood[1].

Material properties of wood are influenced by the amount of its moisture content. Most mechanical properties, such as strength, are better for dry wood than for green wood, with the exception of toughness and shock resistance. For most applications, wood serves best at specific levels of *moisture content*. The moisture content is the

amount of moisture in wood expressed as a percentage of the weight of the dry wood substance. Wood is a hygroscopic material, that is it gives off or takes in moisture until it is in balance with the air surrounding it. When wood has attained such a balance, it is said to have reached its equilibrium moisture content(EMC). Therefore, wood should be dried ideally to a moisture content close to the EMC that it will attain in service. The values of moisture content in EMC condition vary between 12 to 18 percent for the manufacture of articles for outdoor use, and between 5 and 10 percent for indoor articles[2].

One of the reasons for drying lumber before shipping to the processing workshops, is that the transport charges for lumber, moved by rail or truck, are based on the shipping weight. Principally for this reason, more than 70 percent of non-coastal lumber in Canada is dried[3].

A certain amount of moisture content is necessary in wood to prevent decaying caused by destroying organisms. Based on this fact, the lumber shipped by sea before long trips, e.g. to Japan, is dried even though in this case the transport charges are based on volume. In addition, wood must be relatively dry before it can be satisfactorily painted with oil-based paints, glued or treated with preservatives.

There are two main methods for drying wood, *kiln drying* and *air drying*. Kiln drying is used almost exclusively in preference to air drying, because kiln drying permits a producer to gear production to demand and avoids rental of drying yards and, furthermore, provides a more uniform product.

The process of removing moisture from wood in a kiln can be very costly due to: (a) the cost of supplying equipment, labor and energy to accelerate the process, and (b) losses from damage caused to the wood during drying.

Researchers in the field of lumber drying are making efforts in improving the drying process, the main motivation being to reduce the manufacturing costs and degrade

losses so that wood products will continue to be competitive with other products such as plastics and metals.

In order to highlight the importance of improving the energy efficiency of wood drying, it should be noted that, in Canada, the total energy which is used for wood and wood products industry comes almost exclusively from petroleum products. In 1998, it was about 2.2 percent of the total petroleum products consumed in the industrial sector and about 70 percent of this usage is for wood drying[3]. It can be understood that even small improvements in the energy efficiency of wood drying would bring about significant energy savings and environmental benefits. This improvement would decrease the energy consumption per unit of output which decreases both pollution and the release of greenhouse gases such as CO_2.

Research in lumber drying is currently concerned with such issues as:

- developing a better understanding of the drying process inside the wood,

- analysing the numerically predicted moisture content and temperature fields in order to obtain the internal stresses during drying,

- determining energy requirements for lumber drying,

- establishing drying procedures for species of wood not previously processed, to obtain their full potential.

In the drying process of lumber of particular species and thickness, the temperature and humidity conditions of the drying air are set by the *kiln schedule*. Changes of the kiln conditions are usually made at predetermined time intervals, or when preselected levels of moisture content have been reached. The schedule used should dry the lumber in as short a time as possible, while minimizing drying degrade to acceptable levels. Over the years, kiln-drying schedules have been developed based on experience. Research continues to improve these schedules by taking advantage of

new technologies and meeting the demands of the kiln drying industry. It should be noted that there are many schedule combinations due to changes in the velocity, temperature and relative humidity of the drying air. Also there are different lumber sizes which can be loaded in different configurations. With this wide range of parameters researchers have attempted to improve the schedules to reach optimum choices. In this direction, a complete analysis of the complex process of heat and mass transfer which drives the moisture movement during drying is necessary.

The forces involved in moving the moisture are complex. Such complexities increase with increasing temperature and moisture gradient inside the wood. The objective of kiln drying is to make these forces as high as possible without causing lumber damage and decreasing the quality of lumber. This is usually done by increasing the kiln temperature and by increasing the wet bulb depression (the difference between the dry- and wet-bulb temperatures). For some species, there is a practical limit to the intensity of temperature which may cause discolouration, kiln burn or reduced mechanical strength. Besides the dry- and wet-bulb temperatures, there are other parameters which have significant effects on moisture removing forces, such as: wood structural characteristics, air velocity, and stack configuration. For example, using higher air velocities could result in faster drying. Less obvious factors include the arrangement of the boards in the kiln. In this study the effect of the gaps between the boards is investigated and its importance is brought to light. Of course the introduction of gaps reduces the number of boards that can be placed in a kiln. Thus, these are trade-off effects that open the way for optimization.

When the relative humidity of the drying air is kept very low, in order to provide a high moisture content gradient inside the wood, and the lumber is still wet, some difficulties such as *checking* arise. High moisture content gradients during drying induce surface shrinkage while the core is unable to shrink. If the resulting stresses

are greater than the strength of the wood, *checking* will occur as cracks on the wood surface. Checks can be avoided by maintaining a higher relative humidity for air. particularly in the early stages of drying. But this will increase the drying time, total energy consumption, and subsequently the total cost of drying. One of the questions might be: "Can the usage of side gap between the boards, without changing the other parameters of the drying schedule, reduce the total time and cost required for drying a certain amount of lumber?"

Some undesirable conditions such as *case hardening* can set up high internal stresses that cause defects in the dried lumber during later processes such as sawing. These stresses arise when rapid drying causes shrinkage of the surface while the core remains wet and swollen. Further drying, when the surface is very dry and unyielding. does not facilitate the shrinkage of the core.

Detailed analysis of the state of strain and stress at different locations of different boards of the stack needs a thorough knowledge of the temperature and moisture distributions in the boards. It will be shown in the following chapters that comprehensive analysis of the latter type has yet to be undertaken. Although there are some experimental data for temperature and moisture content at some locations of the boards, an extensive experimental set of data for these quantities. at different locations, is not available for different combinations of stack geometry and kiln schedules. Experimental data collection for such a variety of variables is of course very costly and time consuming.

The processes of heat and mass transfer in wood drying can be described by the associated governing differential equations. These equations, however, are nonlinear and coupled, and can only be solved numerically. The main difficulty, however, is not in finding general numerical soloutions for the governing equations but the lack of data on certain physical properties needed to obtain specific solutions.

Outline of Thesis

In this thesis, Chapter 2 presents a literature review on the relevant theoretical, numerical and experimental studies of wood drying. In Chapter 3, the objectives and motivations of the present work are discussed. The equations governing the heat and mass transfer and fluid flow are presented for the drying air and the wood in Chapter 4. Also discussed are the models for migration and physical properties of different phases of water inside the wood. Turbulence models and schemes used for drying air flow are also included in this chapter. Chapter 5 begins with studying the performance of different turbulence models and schemes in predicting the air flow characteristics and convective heat/mass transfer surface coefficients for a benchmark case. Then the effect of side gap on the heat transfer between the drying air and board surfaces of a stack is investigated. A procedure is developed to determine the optimum gap size. Based on the results, the optimum gap size is suggested for different air velocities. In Chapter 6, the numerical model proposed for the wood in Chapter 4 is validated against other numerical and experimental results by a one-dimensional simulation. Also the relative effects of some model parameters are brought to light in this Chapter. Chapter 7 presents the two dimensional numerical simulation for the drying of a stack under a selected drying schedule. The effect of air velocity and side gap on the drying process is investigated as well. In Chapter 8, a simple one-dimensional diffusion case is used to study the middle part of the drying process. Finally in Chapter 9, a summary of conclusions is presented and recommendations for future work are given.

Chapter 2

Literature review

It is evident that for an accurate optimum design and control of the wood drying process, a better understanding of moisture movement and accurate prediction of important parameters inside the wood, such as temperature and moisture content, are essential. Studies in this field require mathematical models that describe the process and experimental findings for the needed physical properties. Also heat/mass transfer coefficients between wood surfaces and the drying air are required in boundary conditions for numerical and theoretical studies.

2.1 General models

Research in wood drying started with modelling the mass transfer as a simple diffusion process based on Fick's law[4]. Later this type of model was expressed for moisture concentration, moisture content and water vapour pressure[5]. Then a number of steady state and unsteady state models for finding the diffusion coefficient were described. It was indicated by Choong[6] that moisture movement through wood, due

to the diffusion process, involves two mechanisms:
(1) vapour movement through cells and
(2) bound water movement through the cell walls of the wood.
Experimental results also showed that the bound water and vapour diffusion coefficients in wood vary with moisture content, temperature and direction[2].

Stamm[7] modelled the wood as a bundle of capillaries of equal length. He indicated that the movement of free water in the drying wood, above the fiber saturation point, is a pressure controlled phenomena. Comstock[8] modeled the flow of free water through wood by using Darcy's law.

Since the moisture content of wood during the drying process can be below or above the fiber saturation point (FSP), it is necessary to develop a general model to include both diffusion and capillary transport. Spolek and Plumb[9] developed an analytical model for the heat and mass transfer in wood drying. A set of coupled partial differential equations for moisture content and temperature, as a function of space and time, were developed. The experimental results of Plumb *et al*[10] showed that capillary transport was dominant at moisture contents above the saturation point.

Some proposed diffusion models for non-isothermal diffusion and capillary movement of water in wood, based on irreversible thermodynamics, are compared by Siau[11].

2.2 Numerical studies

2.2.1 Approaches

The literature survey shows that in wood drying there have been two main approaches toward numerical simulation of heat and moisture transfer. One approach is based on using the simple diffusion equation for the whole process. Some of the studies that have used the diffusion coefficient are: [12-15]. Others have considered the diffusion tensor [16,17]. In this approach, diffusion coefficients are based on an average value from previous experiments for one dimensional cases with constant boundary conditions. All of the investigations in this field have been undertaken for a single board with constant boundary conditions over all the boundaries. Due to changes of moisture content and phases in space and time, this approach is not sufficient for prediction of local moisture content, especially where the geometry is complicated and boundary conditions change in space and time. Also the proposed diffusion coefficients are based on experiments for boards with low moisture content (below the fiber saturation point).

The second approach is based on a system of differential equations which takes into consideration the effect of the gradient of the thermodynamic properties of different water phases on the various moisture fluxes, by using different forms of driving forces for water transport.

2.2.2 Investigations

A two-dimensional, time-dependent wood drying model, based on local three phase equilibrium, was developed by Kayihan[18]. The model assumes separate governing equations for mass conservation of each phase, and uses the partial pressure of each

phase as one of the main parameters. The model predictions show that various portions of the drying curve are sensitive to convective transfer and to individual diffusion coefficients.

Stanish *et al.*[19] improved the above model by introducing some new sub-models for each phase and applied it to a one-dimensional case. Results were in very satisfactory agreement with experimental findings. But the model was complex and required the solution of three coupled differential equations.

Mitchel and Bigbee[20] used the model of Kayihan[18] for an industrially motivated study of western hemlock kiln drying. The purpose was to evaluate the relative effect of various wood and kiln parameters on the final outcome of the kiln schedule in an effort to understand the variability that results in kiln drying. The changes in the parameters such as dry and wet bulb temperatures of drying air, air velocity, initial moisture content and wood density were studied. The authors neither mentioned the model unknowns nor compared their results with experimental data. The model was one-dimensional, and as in the case of Kayihan[18], the constant bound water diffusion and fully developed formulation for surface coefficient were used. The effect of heat and mass transfer to and from the upstream boards on the conditions of drying air was not considered. The results of this study brought some insight in understanding the significant impact of variations in the mentioned parameters. However, due to above mentioned shortfalls, the results were neither sufficient nor accurate enough to draw definitive conclusions.

Josserand *et al.*[13] used a simple one-dimensional diffusion equation for an isothermal unsteady case. This model, which assumes that the diffusion coefficient is a function of moisture content, was applied to a two-dimensional case with constant boundary conditions. Some researchers, e.g. Simpson and Liu[14], have tried to determine the dependence of the diffusion coefficient, in an isothermal problem, on

moisture content. Such coefficients have been used in three dimensional problems for an orthotropic material[17].

The non-isothermal model for diffusion process was improved by Siau[11]. The same problem was numerically solved by Avramidis *et al.*[21] by taking water chemical potential as the driving force for diffusion. They derived the temperature gradient coefficient in the mass balance equation based on the principles of non-equilibrium thermodynamics. The numerical predictions of average moisture content and temperature, using finite difference method, were in good agreement with the experimental data of desorption from an initial 20 percent moisture content (MC). But the results of the model were not compared with cases with higher MC. In this study, the constant temperature and moisture content were assumed as surface boundary conditions since the air side resistance to heat/mass transfer is assumed to be relatively small.

A two dimensional time dependent finite-element model of isothermal wood drying, based on water potential concept, was presented by Cloutier *et al.* [22]. This study also used a constant surface mass transfer coefficient.

In 1993, Colignan *et al.*[23] provided a method of estimating the macroscopic drying kinetics curve and described the internal moisture content profiles of a maritime-pine wood. Moisture gradients and the time evolution of the parameters were analysed as a function of the air drying parameters (dry-bulb, wet-bulb and the velocity) and the product parameters (thickness and density).

They assumed that moisture diffusion occurs only through the main faces of the board and not through the edges. It was also assumed that the heat transfer has a quasi steady nature and, therefore, the energy equation was not solved. The diffusion process was divided into two stages based on whether moisture content of the wood surface is below the fiber saturation point (FSP) or above it. The authors attempted to find the best fit for diffusion coefficients and surface convective coefficients giving

the best fit for the experimental data at each stage. This method is inappropriate for expressing time dependency of local moisture content near the edges, especially for initial stages of drying.

The results of the above study were used as inputs for a model developed for predicting the stresses in the wood which gives rise to flaws called shakes[24]. The model was based on a simplified description of the normal internal stresses. The aim was to evaluate the differences in degradation by the type of drying procedure. The model was based on the assumption that the change in strain between two subsequent times is the sum of a shrinkage due to local variation of moisture content, and an elastic strain. The normal stress at each location was then found and compared with the allowable stress.

The approach in the above two studies has some limitations:
a) it is one-dimensional,
b) it neglects the effects of edges on the moisture content distribution, and
c) it is an isothermal model, does not consider the temperature effects on the moisture content.

Liu *et al.*[25] developed a mathematical model for coupled heat and mass transfer. The model separated the moisture flux into that of the liquid and that of the vapour phase. The authors applied the model to a one dimensional time dependent case and used the constant surface coefficients based on the boundary layer theory.

Hernandez and Puiggali[26] simulated the drying of a wood sample using the model proposed by Stanish *et al.*[19]. They also studied the drying process using microwaves. The main purpose of this study was to investigate the drying kinetics (changes of moisture and its gradients with respect to temperature over a period of time).

Avramidis and Hatzikiriakos[27] solved a dynamic non-isothermal set of coupled

partial differential equations for one dimensional heat and mass transfer inside a wood specimen using the Galerkin finite element method. The analysis showed that the moisture-time and temperature-time curves were strongly affected by the values of convective mass and heat transfer coefficients. These coefficients were based on fully developed flow, and the edge and entrance effects were not considered.

There has been an effort, by Dincer and Dost[12], in proposing an analytical model to determine the moisture diffusivities in geometrical solid objects (namely, infinite slab, infinite cylinder, sphere) during the drying process. Comparison with the available data showed the validity of the model for different ranges of Biot numbers (Bi), namely the ratio of internal resistance to external resistance during heat/mass transfer. The authors applied their model to a slab of wood[15].

The profiles of the surface and centre temperature and also average moisture content in the drying of a single *pinus radiata* board were predicted as a function of time by Pang *et al.*[28]. In this work, the heat and mass transfer inside the wood along the air stream direction was not taken into account. The governing equations were solved in the direction perpendicular to the air stream. Since the numerical results of previous studies were not satisfactory[29-31], the direct experimental data of surface coefficients were applied to the equations. The same process was repeated for different locations of stream wise direction considering separate boundary conditions for each location. They reported that variations have been noted in the external mass transfer coefficients in the stream wise direction which leads to differential drying of the board. The effect of reversing the air flow periodically was studied to determine the reduction of these differences in the extent of drying across each board, and some practical suggestions were given.

For the following reasons, the model and suggestions of [28] cannot be extended to study an array of boards. Firstly, the heat/mass transfer of upstream boards will

affect the temperature and relative humidity of air downstream. This problem was not addressed since the [29] study considered only one board. In other words, the surface mass/heat transfer coefficients defined were based on entrance values of concentration/temperature instead of the mean values. Secondly, due to the complexity of flow and having a limited number of boards in a row, the distribution of local surface coefficients for each board is different from that for the other boards in the same row. Thirdly, in the experiments, mass/heat transfer occurred from one board and the other boards did not take part in the process. Fourthly, the mass transfer of naphtaline, which was used in tests would provide the boundary condition of surface concentration/temperature across the test section. But in the real process this changes with time and space. Finally, the mass/heat transfer for side edges of the boards were not considered neither in the experiments nor in computations. This may suggest a lower drying rate and in consequence a higher predicted moisture content than the actual values during drying.

Recently, Turner[32] formulated a two-dimensional mathematical model for an orthotropic single wood board and developed a numerical code based on the finite volume approach. He expressed the governing equations in the longitudinal and stream wise directions. The effect of air stream temperature was studied while the surface coefficients were assumed to be independent of time and space. Although the heat and mass transfer across the wood thickness is much more significant than those in the stream wise direction, they were neglected. In solving the model equations, it was assumed that the board is a perfectly symmetrical body and the external transfer coefficients over the end are the same as those over the flat surfaces.

A simplified one dimensional description of drying kinetics was obtained for the drying behaviour of an array of *pinus radiata* by Pang *et al.*[33]. Mass and heat balances over a control volume in the stream wise direction were coupled with simplified

characteristic drying curves. It was assumed that the drying rate curves for a specific material will remain similar, irrespective of the external condition, and it contains three main periods: initial constant drying rate, and two falling periods with different slopes[34]. This assumption would not hold for locations near the edges of the boards especially when there is a large gap between boards. The study determined the changes in air condition (humidity and temperature) and local average moisture content through the stack using the above simplified one dimensional approach. The influence of air flow reversals under different strategies were investigated in order to make some suggestions for decreasing moisture content differences along the stack.

Gong and Plumb[35,36] proposed a theoretical model for the effect of heterogenous and anisotropic nature of wood on heat and mass transfer process. They implemented their model using a finite difference program capable of predicting the two-dimensional distribution of moisture content and temperature in wood. They conducted experiments using a γ-ray attenuation system and a near-infrared reflectance analyzer. The internal and surface moisture content were measured by the mentioned instruments. Their main concern was the difference between the transfer process in radial and tangential directions, and that the process in any other direction could be determined based on these two ones. In the model, they ignored the contribution of the gradient of temperature in the mass transfer equation and the gradient of moisture content in the energy equation. Also in the energy equation, the changes in the enthalpy and internal energy of each phase were not considered separately. Instead, a temperature and moisture content dependent relationship for moist wood specific heat was employed (similar to the works of Pang *et al.*[28] and Avramidis *et al.*[27]). Also heat of vaporization and rate of changing the liquid to vapor at any point were used for the mentioned parameters.

Kamke and Vanek[37] compared the performance of a number of wood drying

models using a common set of drying data for spruce lumber. Experimental data of the initial values of relevant parameters were supplied to the authors from 16 countries, for comparison of predicted average moisture contents, and moisture content near the surfaces and in the core. The majority of the simulation results were not in good agreement with the test runs. Some explanations were given for poor agreements such as: uncertain coefficients for the models considered as the most important reason; nature of simplifications; and the solution methods used for heat and mass transfer equations. The review emphasized that "there is no universal model available for wood drying, but rather models which are best suited for specific problems due to performance or ease of use". From the comparison of different simulations with experimental data presented in [37], it can be observed that the following programs perform better than others: WOODRY-S originated from Sutherland *et. al.*[38]; SALINA related to Salin's thesis[39]; SAHA developed by Ranta-Maunus[40]; and PROFIL based on Vogel's work[41].

The model by Salin was developed following the earlier work by Stanish *et al.*[19]. It considers different phases of moisture but neglects the bulk flow of water vapor and air. The model considers the drying of each wood board as an isothermal one dimensional process. The treatment of bound water diffusion as a function of moisture content and temperature is the most important modification of this model compared to its original version. Solution is by the finite difference method, and the convective surface coefficients are velocity dependent.

The original SAHA program is a one-dimensional isotropic model which only considers the diffusion mechanism for mass transfer driven by a gradient in moisture content. The value of the diffusion coefficient was determined by experiments over a range of moisture contents, temperature and density for heartwood and sapwood. Heat transfer is governed by conduction. For the boundary condition at the surface.

the partial water pressure difference with drying air is used instead of the moisture content. The surface coefficients are determined by experiments.

The methodology used in PROFIL is based on a one-dimensional solution to a system of isotropic unsteady state mass diffusion and heat conduction. Here, moisture gradients drive the mass transport. The mass diffusion coefficient is obtained using the procedure proposed by Siau[2] which applies an electrical analogy for parallel and series resistance to bound water and water vapor diffusion. In the heat transfer equation, the contributions of bulk flow and advection term were not taken into account.

A more recent study based on this program, by Akulich and Militzer[42], obtained the solution for a two dimensional nonisothermal moisture transfer in the anisotropic structure of an specimen. Like the original version, the effect of different phases was not considered separately. Instead, the density and specific heat of vaporization of moist wood were used in the energy equation. The contribution of moisture content in the energy equation was absent while the effect of temperature gradient on the mass transfer was considered. The set of equations was a simplified Luikov equation. The two-dimensional system of equations of heat and mass transfer were solved iteratively by a locally one-dimensional method. The effect of surface resistance was considered by introducing an unknown correction factor, named phase transition. Its value was obtained by a trial and error method, but not as a function of wood properties. Another shortfall is the assumption of constant surface coefficients of fully developed flow. After obtaining the moisture content and temperature fields, the internal stresses in the wood were calculated based on the elasticity theory. The model considers the shrinkage due to drying below the fiber saturation point as the only cause. A Galerkin method was applied and solution was limited to three terms of the infinite series.

Tarasiewicz *et al.*[43-45] proposed a nonlinear one dimensional system of partial differential equations for predicting the air conditions and average moisture contents of boards in a stack array. The model did not include the heat and mass transfer inside the wood, and considered each board of having a uniform temperature and moisture content. It divides the behaviour of the drying rate curve versus moisture content into four stages. Instead of solving the Navier-Stokes and heat and mass transfer equations for the drying air at every single point of the air duct, the model considers small control volumes extended between the centerlines of two adjacent boards. Then the momentum equation in the main-stream direction as well as the balance of mass and energy are expressed for such control volumes. The effect of heat and mass transfer on the drying air temperature and humidity are taken into account. While the study provides a fast look into the average moisture content and temperature of the boards across a stack, it does not give insight toward local variables even for the drying air. In addition, the same surface coefficients are used for all boards, and the effect of two-dimensionalities in air flow, such as separation and entrance or exit, are not considered.

2.3 Experimental studies, surface coefficients

Apart from the studies in references [12-17], all the cited numerical studies contain experimental results. Temporal changes of moisture content and temperature inside the board were usually reported. The aim of such studies was to determine the diffusion coefficient to model the diffusion component of the drying process. Surface to air convective mass transfer can also be obtained from these experimental data using mathematical approximations. The diffusion coefficient is related to the resistance of moisture leaving the wood surface and being transferred to the ambient drying air.

2.3.1 Investigations

Time dependent moisture content and temperature distribution inside red pine and white birch lumber were reported by Bai and Garrahan[46]. Results of the drying tests indicated:

a) interior temperature increases in direct relation to elapsed time,

b) moisture content drops exponentially with elapsed time, and

c) an exponential relationship exists between the average moisture content and the core temperature of the lumber. The authors mentioned that monitoring of the lumber drying process through measurements of the interior wood temperature may be feasible.

Plumb *et al.*[47] studied the transport of heat and mass during drying of southern pine and investigated the accuracy of the measurements of moisture content with gamma attenuation. The measured drying rate above the fiber saturation point (FSP), was not a well defined function of moisture content. The drying rate did not appear to be highly temperature dependent at high moisture contents. Below the FSP, the effect of temperature on the dominant diffusion process were evident.

Rice and Young[48] determined the shape of the moisture profile in flat sawn red oak under different conditions during the early periods of drying. Their aim was to investigate differential moisture losses during the early stages of drying which are critical to the development of stresses that result in checking and associated degradation.

Simpson[49] determined the diffusion coefficient of northern red oak as a function of moisture content based on his experiments. He compared the experimentally determined desorption times and local moisture content gradients with those calculated by the diffusion model. The effect of thickness was also investigated.

Soderstrom and Salin[50], after presenting some of the previously published data for surface emission factors, mentioned the large differences between the values obtained from experiments carried out with various wood species under different conditions. They showed that the discrepancies can be explained by the fact that a mathematically incorrect method was used. Also the wrong type of heat and mass transfer sealing of some lateral surfaces, in order to ensure unidirectional moisture flow, was criticized. The authors presented a method to measure the surface emission factors correctly and to analyse the diffusion problem theoretically for wood drying.

A review of the heat and mass transfer coefficients for individual boards and board surfaces was presented by Salin[51]. He aimed to extract results from the vast literature on heat and mass transfer, on situations that are similar enough to kiln stack geometry, and present them in a usable form. Among these cases were: fully developed turbulent flow between parallel plates; entry region in flow between parallel plates; plate(s) in parallel flow; single and multiple rectangular cylinders in cross flow. From the review, it transpired that experimental results are only available for specific geometries and Re numbers. Also the distribution of coefficients on vertical edges were not investigated at all. The only available numerical study for horizontal edges did not reach an accuracy of ± 10 percent.

Li *et al.*[52,59] studied the effects of air gaps and air velocities on the drying characteristics of *Western Hemlock* 105 $\times$ 105 mm boards using a conventional kiln dryer. It was observed that side gaps reduced kiln drying times of planks of similar dry density. They concluded that when pieces of lumber are stacked with vertical air gaps, higher air velocities can reduce drying times, especially when the average moisture content is above the FSP. Higher air velocities did not seem to affect drying times, when vertical gaps were absent. The effect of two different air gaps on degradation did not show the same trend. The total number of case hardened specimen was

increased 15 percent by using 10 mm gaps and decreased 50 percent by using 20 mm gaps, with respect to the case without gaps. The effects of airflow reversal, changing the air temperature, and its relative humidity were not investigated. It seems that a combination of the certain increases in the air velocity with a specific air gap would result in a substantial drying time reduction with acceptable degree of degradation. This issue is still open for investigation.

Chapter 3

Objectives and motivations

As noted in the previous chapters, there has been a constant effort to find ways to improve kiln schedules for wood drying. This, however, requires a detailed knowledge of the complex processes of heat and mass transfer occuring during the drying process. Accurate predictions of the two key parameters, namely, moisture content and temperature, inside the wood in space and time are essential for the understanding of the drying process. Once these parameters are determined accurately, other related wood parameters, such as the shrinkage, strain, stress, defects, and degradation, can be evaluated. There have been numerous experimental efforts to obtain information about these parameters. But it is not feasible to perform a large number of tests for a wide variety of stack configurations and air conditions. Numerical techniques provide a valuable tool for optimization and control of the kiln drying process from view point of energy consumption, time, degradation, and cost. Such an analysis should relate the air parameters (air conditions and stack configurations) to the parameters associated with the wood.

One-dimensional models, by their nature, cannot predict the moisture and heat losses from the vertical surfaces of the boards. These types of models can provide

better predictions for lumber with higher aspect ratios (ratio of width to thickness), when the heat/mass transfer in the main air flow direction becomes negligibly small. Such a simplification will predict a lower drying rate and, as a result, a higher predicted moisture content than the actual values. Otherwise, a higher external transfer coefficient has to be used to compensate for the unaccounted moisture losses. For boards with aspect ratios close to one and especially the square cross sections, a two dimensional model will be necessary.

There are no reported experimental or numerical results for the convective surface coefficients of heat/mass transfer from the vertical faces of the boards. In the measured experimental data for horizontal faces, the local Nu/Sh numbers have been defined based on the inlet temperature/concentration instead of the mean values which should be used in the internal flows. In such tests, the heat/mass transfer occurs only from one surface and the effect of the transfer process from the upstream surfaces is not considered. Also the reported data cannot be used for other blockage ratios ($\frac{board\ thickness}{board\ thickness+sticker\ thickness}$) due to differences in flow characteristics.

A majority of the modelling studies in the literature have not addressed a number of important aspects. For instance, constant Nu/Sh values of the fully developed flow were used and the effect of the entrance and separation bubbles were neglected. The other common incorrect assumption was the application of the surface coefficients to the inlet temperature/concentration instead of the mean parameters. Heat and mass transfer between the drying air and the board surfaces upstream at any location in the stack affects the air wet- and dry-bulb temperatures at that point and thus the drying ability of air downstream. This point was also not included in some models. Even when this was considered, the application of the surface coefficients to the inlet air conditions instead of the mean values resulted in inaccurate predictions of the drying air conditions at all locations of the stack. Another point to be mentioned

is that some relationships for the external boundary flow surface coefficients have been used, and some studies have adopted isothermal assumptions. Such models do not provide accurate information in the critical initial stages of drying and when air temperature changes continuously or is kept constant for only short periods.

In addition, some of the assumptions made in the derivation of the governing equations may also be the source of poor agreement between numerical and experimental results. Some models used for determining the fluxes of water phases need improvements for better accuracy. Almost all numerical models discussed in the present literature, are based on finite difference or finite element methods. These methods need special treatment in order to satisfy the basic laws (conservation of mass and energy) in each control volume, especially when the convective terms are retained. Such an approach is followed in the *finite volume* method presented by Patankar[53].

Based on the above discussions, the main objectives of the present work can be summarized as follows.

1-Development of a procedure for numerical analysis of fluid flow and heat/mass transfer in the drying air, using the best available turbulence method and scheme. leading to local Nu/Sh numbers distributions on horizontal and vertical surfaces of the boards, and some relations for these dimensionless numbers.

2-Numerically analyse the heat and mass transfer for detailed time-dependent local moisture content and temperature distributions in the boards. The study uses the finite volume approach and the ADI and Fully Implicit methods for discretization and TDMA and SOR methods to solve the governing equations and sub-models implemented within them.

3-Development of a new model for the diffusion process in the wood and also the verification of the model with experiments.

4-Verification of the numerical procedure by experiments.

5-Study the effects of different combinations of air velocities on the drying process.

6-Investigation of the effects of side gap between the boards and proposing a procedure for optimizing its value based on dimensionless geometrical and flow characteristics, total drying time, surface coefficients distributions, and total heat/mass transfer rate across the stack.

3.1 Practical applications

As a practical application, kiln drying of $105 \times 105mm$ *Western hemlock* (*Tsuga hetrophylla*) boards, the so-called baby squares, will be studied. Western hemlock is the most abundant species in British Columbia. In 1997, about 40 percent of the growing volume of various species in the coastal B.C. were of this type[54]. From the perspective of mature standing and log production, it ranked among the first.

Baby squares are very popular in Japan for construction of wooden houses. Japan is the second largest consumer of B.C. wood products and the largest potential market for B.C. dimensional lumber[54]. In 1991, baby squares accounted for about 70 % of all the BC hemlock exported to Japan. Since thick hemlock lumber are quite hard to dry and also because of considerable degradation during kiln drying, about 95 percent of the B.C. exported baby squares are in green condition[54]. Current prices for baby squares are about US$ 432-445/m^3, and the value of kiln-dried baby squares is estimated to increase by 15 percent[55]. Evidently, by selling kiln-dried baby squares, larger revenues can be generated by the B.C. forest products industry. Also moulding developed on green lumber during 40 days journey of lumbers is not acceptable to the Japanese customers, since most of the construction lumber is exposed to view.

While traditional *air drying* of baby squares results in a good quality lumber, a one-year time requirement makes it inefficient[56]. Kiln drying is called *conventional* when kiln temperature is less than 100^0C, usually between 60 to 90^0C. The drying schedules for conventional kiln drying of baby squares are about sixteen to twenty four days[56]. The long drying schedule, non-uniformity of final moisture content, and subsequent degradation are major problems in conventional kiln drying of hemlock[56]. According to the National Lumber Grades Authority, lumber with moisture content above 19 percent is considered wet or under-dried. The under-dried lumber must be re-dried, requiring additional drying time and cost. The percentage of under-dried hemlock lumber, using the conventional kiln schedule, is about 5 to 10 percent, depending on the wood quality[52]. The improvement in drying of different sizes of hemlock boards is still under study[59]. Experiments conducted thus far, due to the limitations of the number of tests and their costs, are not sufficient to reach an optimum choice for the drying process. Numerical modelling can provide a better perspective for optimization and quality control of this process. It can suggest a few alternatives for optimum choices to be verified by experiments. Neither has there been reported defined coefficients for western hemlock which can be used in modelling the simple diffusion case nor separate diffusion coefficients of bound water and capillarity of free water and water vapour for the sub-models.

There are other reasons which motivated the present study; the two dimensionality of moisture movement process in baby squares, especially when extra side gaps are applied, and large values of lumber thickness (105 mm), to mention just two. The prediction of improving the quality of final products and reducing the total time of drying by introducing side gaps between boards were parts of the motivations behind the experimental work of Li[52]. Naturally, such an experimental program could not separately study the effects of the side gap between the boards and air velocity, due to

differences of moisture content and density of the stack boards. Such a study requires the distribution of surface coefficients on both vertical and horizontal faces of the planks. Also the number of tests performed in[52] was not sufficient for obtaining a final conclusion for optimization of stack arrangement.

Chapter 4

Governing equations

Moisture in wood exists in two forms: *bound* or hygroscopic water and *free* water. *Bound water* is found in the cell wall and is hydrogen bounded to the hydroxyl groups of cellulose, hemicellulose and lignin. Physical properties of wood change gradually and continuously with increasing moisture content till saturation of cells with bound water (Fiber Saturation Point, FSP). After that, an abrupt change in physical properties of wood occurs and additional water is held as *free water* in the voids of wood. Due to evaporation during drying, there is also water vapour (mixed with air) in void spaces. Moisture transfer inside the wood takes place due to different mechanisms. Several mechanisms are cited in the literature, including: diffusion of bound water due to chemical potential driving force, free water movement as a result of capillary pressure, diffusion of water vapour in pores due to water vapour concentration pressure (water vapour concentration) gradient and total pressure gradient, moisture transfer driven by temperature gradient.

In this section, the governing equations of the present model are presented for the wood (solid phase) and for the drying air (fluid phase). We consider heat and mass transfer in the solid phase, and heat and mass transfer and fluid flow in the fluid

phase.

4.1 Heat and mass transfer equations in the solid

The basic equations governing the mass and heat transfer in the solid are presented below.

a) The conservation of mass requires that the rate of change of water mass inside a control volume, is equal to the net flux of water from the surfaces of the control volume. Thus by defining:

$$X = \frac{mass\ of\ water\ inside\ wood}{mass\ of\ dry\ wood} \quad , \tag{4.1}$$

and:

$$\rho_d = \frac{mass\ of\ dry\ wood}{volume\ of\ dry\ wood} \quad , \tag{4.2}$$

we write:

$$-\rho_d \frac{\partial X}{\partial t} = \nabla . \mathbf{J} = \frac{\partial J_x}{\partial x} + \frac{\partial J_y}{\partial y} + \frac{\partial J_z}{\partial z} \quad , \tag{4.3}$$

where J is the total mass flux vector entering the control volume and ρ_d is the dry wood density. Since J is a vector, we have:

$$\mathbf{J} = J_x i + J_y j + J_z k \quad , \tag{4.4}$$

where, i, j, and k are unit vectors and J_x, J_y and J_z are components of the vector J in x, y, and z directions, respectively.

The total mass flux can be written as:

$$\mathbf{J} = \mathbf{J}_v + \mathbf{J}_b + \mathbf{J}_f \quad , \tag{4.5}$$

where $\mathbf{J}_v$, $\mathbf{J}_b$, and $\mathbf{J}_f$ are the fluxes of moisture due to water vapour, bound water, and free water, respectively.

b) The balance of energy yields the heat transfer equation:

$$\frac{\partial}{\partial t}(\rho_a u_a + \rho_b u_b + \rho_f u_f + \rho_v u_v + \rho_d u_d) + \nabla.(\mathbf{J}_a h_a + \mathbf{J}_b h_b + \mathbf{J}_f h_f + J_v h_v) = \nabla.(\lambda \nabla T) \quad , \tag{4.6}$$

where T is the temperature, and ρ_a, ρ_b, ρ_f, ρ_v, ρ_d; u_a, u_b, u_f, u_v, u_d; and h_a, h_b, h_f, h_v are respectively the densities; specific internal energies and enthalpies of the air, bound water, free water and water vapour phases and the dry wood. All these parameters are functions of temperature. It should be noted that density of all phases are not the same as the usual thermodynamic property with the same name. These densities, representing the amount of moisture in any phase, are related to the moisture content and the total moisture density, ρ_{wt}, as:

$$\rho_{wt} = \rho_f + \rho_v + \rho_b = \rho_d X \quad , \tag{4.7}$$

The energy balance expresses the equality of the change in internal energy in the element to the differences in the incoming and outgoing enthalpy flows as well as conductive heat flows. Implementation of fluxes of heat and mass transfer at the boundaries of the element will be followed in the present work during the discretization of the governing equations.

Since the total internal pressure gradient is negligible and pressure is assumed to be equal to the ambient pressure, no separate mass balance for air in the wood is required. This implies that air in the wood is immobile with negligible heat capacity. Therefore, two terms representing the contributions of air, namely $\frac{\partial}{\partial t}\rho_a u_a$ and $\nabla.\mathbf{J}_a h_a$, are neglected.

Before writing the conservation of mass and energy in final forms, expressions for the fluxes appearing in Eqn. (4.5) will be developed.

4.1.1 Movement of water vapour

Flow of water vapour in the porous body of wood occurs according to two different mechanisms. First, the mixture of vapour and air (humid air) may flow as a consequence of the total pressure gradient. Due to the small size of the pores,the flow is laminar in nature and the vapour flux can be expressed by Darcy's law[2]. Secondly, vapour migrates due to its concentration (partial pressure) gradient by gas diffusion. In the present work, there is no bulk flow of the humid air since the total pressure gradient is assumed to be negligibly small. Therefore, vapour diffusion may be expressed according to Fick's law as follows:

$$\mathbf{J}_v = -cm_v D_{eff} \nabla x_v \quad , \tag{4.8}$$

where:

c = mole density of humid air $(mole/m^3)$,

m_v = water molecular weight (kg/mol), and

x_v = vapour mole fraction in humid air.

Here, D_{eff} is the effective diffusivity of water vapour. In wood, however, the diffusion of water vapour is slowed down by the solid matrix structure of the wood, and therefore, D_{eff} must be defined to include this effect[19]:

$$D_{eff} = \epsilon^2 \alpha D_{AB} \quad , \tag{4.9}$$

where D_{AB} is the unhampered diffusivity of water vapour in air, ϵ^2 accounts for the volume occupied by the solid and the tortuosity of the void space and α is an attenuation factor specified for the structure of the wood. While ϵ, the porosity of wood, is a function of T and X, α is one of the unknowns of the model. D_{AB} is given by the empirical correlation[19]:

$$D_{AB} = \frac{1.2146 \times 10^{-4} (T)^{1.75}}{p_a + p_v} \quad , \tag{4.10}$$

where T is the temperature in K and p_a is the partial air pressure in wood. When these expressions are combined with the assumption of vapour as ideal gas, the final result, after some modifications, is found to be

$$\mathbf{J}_v = -\frac{1.2146 \times 10^{-4} m_v \epsilon^2 \alpha(T)^{0.75}}{R} \nabla P_v \quad , \tag{4.11}$$

where R is the ideal gas constant. P_v, the partial vapour pressure is given by the correlation proposed by Simpson and Rosen[57] as

$$P_v = P_{sv}(T)\psi(X,T) \quad , \tag{4.12}$$

and P_{sv} is the saturation water pressure, calculated from the empirical relationship which is curve fitted to the steam table values by Simpson and Rosen[57]. In order to obtain a better accuracy for the present work, we modified his relationship as:

$$P_{sv}(T) = 132.9020 \times 10^{f(T)} \quad , \tag{4.13}$$

where:

$$f(T) = 16.3737 - \frac{2818.6}{T} - 1.6908 log_{10} T - 5.7546 \times 10^{-3} T + 4.0070 \times 10^{-6} T^2 \tag{4.14}$$

$\psi(X,T)$ is given by the following empirical correlation as proposed by Turner *et al.*[32]:

$$\psi(X,T) = exp[a_1 \times a_2^{92X}] \quad , \tag{4.15}$$

where:

$$a_1 = 17.8840 - 0.1423T + 23.6300 \times 10^{-5} T^2 \quad , \tag{4.16}$$

$$a_2 = 1.0327 - 67.4000 \times 10^{-5} T \quad . \tag{4.17}$$

Considering the above equations, the gradient of P_v can be expressed as:

$$\nabla P_v = (\frac{\partial P_{sv}}{\partial T}\psi + P_{sv}\frac{\partial \psi}{\partial T})\nabla T + P_{sv}\frac{\partial \psi}{\partial X}\nabla X \quad . \tag{4.18}$$

The final expression for the flux of water vapor is:

$$\mathbf{J}_v = -\frac{1.2146 \times 10^{-4} m_v \epsilon^2 \alpha(T)^{0.75}}{R}[(\frac{\partial P_{sv}}{\partial T}\psi + P_{sv}\frac{\partial \psi}{\partial T})\nabla T + P_{sv}\frac{\partial \psi}{\partial X}\nabla X] \ . \quad (4.19)$$

This can be rewritten as:

$$\mathbf{J}_v = -V_X \nabla X - V_T \nabla T \quad . \quad (4.20)$$

where V_X and V_T are positive and defined as

$$V_X = \frac{1.2146 \times 10^{-4} m_v \epsilon^2 \alpha(T)^{0.75}}{R} P_{sv}\frac{\partial \psi}{\partial X} \quad , \quad (4.21)$$

$$V_T = \frac{1.2146 \times 10^{-4} m_v \epsilon^2 \alpha(T)^{0.75}}{R}(\frac{\partial P_{sv}}{\partial T}\psi + P_{sv}\frac{\partial \psi}{\partial T}) \quad . \quad (4.22)$$

ϵ_d, ϵ and phase densities

Porousity ϵ is one of the most important characteristics of wood in relation to moisture transport. Its value when wood is completely dry, sometimes called the dry wood void fraction, ϵ_d, can be obtained from:

$$\epsilon_d = \frac{V_{ad}}{V_T} = 1 - \frac{\rho_d}{\rho_{cell}} \quad , \quad (4.23)$$

where V_T and V_{ad} are the total volume of wood and air volume inside the dry wood structure, respecively. ρ_{cell} is the density of the cell which is almost constant and its value is $1500\frac{Kg}{m^3}$ (see Siau[2]). It is assumed that the void space between the cells is filled with free water, air and water vapour. The density of water vapor is neglected compared to the free water. Therefore, the porousity of wet wood is calculated as

$$\epsilon = \frac{V_a}{V_T} = 1 - \frac{\rho_d}{\rho_{cell}} - \frac{\rho_v + \rho_f}{\rho_w} \simeq 1 - \frac{\rho_d}{1500} - \frac{\rho_f}{\rho_w} \quad , \quad (4.24)$$

where ρ_w is the density of water at the corresponding temperature.

The moisture in wood is first stored as the bound water till the Fiber Saturation point (FSP). Siau[2] proposed a correlation to calculate X_{FSP}, the moisture content at fiber saturation point. We modified his correlation by changing the constant value of 0.3 to 0.28. The modified relationship is:

$$X_{FSP} = 0.28 - 0.001(T - 293.15) \ . \tag{4.25}$$

Further, water after the FSP is not stored as the bound water. Therefore, if $X > X_{FSP}$:

$$\rho_b = \rho_d X_{FSP} \ . \tag{4.26}$$

On the other hand, based on the definition of ψ:

$$\rho_v = \epsilon \rho_{sv} \psi(X, T) \quad , \tag{4.27}$$

where ρ_{sv} is the saturated water vapor density at wood temperature. The rest is the free water density:

$$\rho_f = \rho_d X - \rho_v - \rho_b \simeq \rho_d X - \rho_b \ . \tag{4.28}$$

For $X < X_{FSP}$, $\rho_f = 0$ and:

$$\rho_b = \rho_d X - \rho_v \simeq \rho_d X \ . \tag{4.29}$$

In both cases, the semi-equilibriums may be used for initial guesses of the densities and by trial and error, the final densities may be calculated.

4.1.2 Movement of bound water

Bound water diffusion occurs mostly when the moisture content is below the fiber saturation point (FSP). The flux of bound water can be expressed by (see Salin[39])

$$J_{b-i} = -D_b \frac{\partial \mu_b}{\partial x_i} \quad , \tag{4.30}$$

where μ_b is the chemical potential of bound water, D_b is the bound water transfer coefficient, and J_{b-i} is the flux of bound water in the i direction. Stanish *et al.*[19] included a factor of $(1-\epsilon_d)$ where ϵ_d is the fractional void space of the dry solid. This factor was considered for the amount of conductive cell wall material in the volume. Salin[39] did not find any clear dependence on wood density and excluded this factor. He did not find D_b to be a constant, as Stanish *et al.*[19] had supposed. The following correlation was suggested by Salin[39] for the dependence of D_b on moisture content and temperature:

$$D_b = D_\mu exp(\frac{40\rho_b}{\rho_d} - \frac{4100}{T}) \quad . \tag{4.31}$$

where D_μ is a constant. During the present work, it was concluded that the term $exp(\frac{40\rho_b}{\rho_d} - \frac{4100}{T})$ should be modified to obtain physically meaningful and stable as well as more accurate distributions for moisture content and temperature. It should be noted that:

$\frac{\rho_b}{\rho_d} = X_{FSP}$ for $(X > X_{FSP})$ and

$\frac{\rho_b}{\rho_d} = X - \frac{\rho_v}{\rho_d} \simeq X$ for $(X < X_{FSP})$.

Thus, the term $\frac{40\rho_b}{\rho_d}$ is always positive which causes the previously mentioned shortfalls. Also the dependence of D_b on temperature for different species should be considered. Based on the above discussions and after trying different combinations, we propose the following relationship for D_b:

$$D_b = D_\mu exp[40(\frac{\rho_b}{\rho_d} - X_{FSP}) - \frac{S_T}{T})] \quad . \tag{4.32}$$

where D_μ and S_T are unknown constants for the specific species. Changing the constant value of 40 did not show any significance in the model. By this combination, the multiplication factor has the following characteristics:

- is always less than 1,

- above FSP, is not a function of X and acts almost like $exp(-\frac{1}{T})$ function with respect to T, and
- below FSP, acts like $exp(X)$ which has the fastest change with respect to X.

The significance of this modification can be better understood if we recall that in most of the drying process, $X_{av} < X_{FSP}$ and bound water diffusion is the dominant process. Also the shrinkage of wood, causing the internal stresses and subsequent degredations, starts when moisture content is below the fiber saturation point.

For local thermodynamic equilibrium, the chemical potential of bound water, μ_b, is the same as that for the vapour, μ_v, and it follows that:

$$m_w \frac{\partial \mu_b}{\partial x_i} = m_w \frac{\partial \mu_v}{\partial x_i} = -s\frac{\partial T}{\partial x_i} + v\frac{\partial p_v}{\partial x_i} \; . \tag{4.33}$$

The molar entropy, $s(J/mol/K)$, and molar specific volume, $v(m^3/mol)$, are state functions of temperature and pressure. Stanish *et al.*[19] assumed that the vapour obeys the ideal gas law and the above relationship can be transformed into a computable form in which the chemical potential is related to the local temperature and pressure gradients as follows:

$$\mathbf{J}_b = -\frac{D_b}{m_v}\{-[187 + 35.1ln(\frac{T}{298.15}) - 8.314ln(\frac{P_v}{101325})]\nabla T + 8.314\frac{T}{P_v}\nabla P_v\} \; . \tag{4.34}$$

The partial vapour pressure, P_v, can be estimated from the thermodynamic relationship of moisture content-temperature, as given by previous equations. The final equation can be expressed in terms of gradients of X and T as:

$$\mathbf{J}_b = -B_X \nabla X + B_T \nabla T \quad , \tag{4.35}$$

where B_T and B_X are positive and defined as:

$$B_T = \frac{D_b}{m_v}\{[187 + 35.1ln(\frac{T}{298.15}) - 8.314ln(\frac{P_v}{101325})] - 8.314\frac{T}{P_v}(\frac{\partial P_{sv}}{\partial T}\psi + P_{sv}\frac{\partial \psi}{\partial T})\} \quad , \tag{4.36}$$

$$B_X = 8.314 \frac{D_b}{m_v} \frac{T}{\psi} \frac{\partial \psi}{\partial X} \ . \tag{4.37}$$

4.1.3 Movement of free water

The movement of free water, which only occurs for moisture contents higher than FSP, is due to capillarity between liquid and vapour phase within the cell lumens of the wood. The flux of this phase, therefore, is obtained from Darcy's law[2] as:

$$\mathbf{J}_f = -E_l \nabla P_l = E_l \nabla P_c \quad , \tag{4.38}$$

where P_c is the capillary pressure and E_l is the effective permeability to free water flow. The latter is related to the measured permeability, K_l, by:

$$E_l = \frac{K_l \rho_l}{\eta_l} \quad , \tag{4.39}$$

where ρ_l and η_l are, respectively, the density and viscosity of the liquid water. Spolek and Plumb[9] assumed that the capillary pressure is a simple function of saturation as follows:

$$P_c = A.S^{-B} \quad , \tag{4.40}$$

where A=10,000 and B=0.61 . The saturation of wood is calculated by:

$$S = saturation = \frac{liquid\ volume}{void\ volume} = \frac{X - X_{FSP}}{X_{max} - X_{FSP}} \ . \tag{4.41}$$

The moisture content at the fiber saturation point is X_{FSP} while X_{max} is the moisture content of wood when the entire void structure is filled with liquid. It can be obtained as:

$$X_{max} = \epsilon_d \frac{\rho_w}{\rho_d} \ . \tag{4.42}$$

The minimum saturation for liquid flow is S_{min}. When the saturation is below this point, liquid flow is impossible. Combining the above equations, the flux of free water may be expressed as:

$$\mathbf{J}_f = \frac{-A.B.E_l(X_{max} - X_{FSP})^B}{(X - X_{FSP})^{(1+B)}} \nabla X \ . \tag{4.43}$$

The liquid permeability of wood, K_l, decreases with reduction of the wood saturation. It may be related to the permeability at saturation, K_{ls}, by using the correlation of Stanish *et al.*[19]:

$$K_l = K_{ls}\{1 - cos[\frac{\pi}{2}.\frac{S - S_{min}}{1 - S_{min}}]\} \ . \tag{4.44}$$

Therefore, the final expression for the flux of free water is:

$$\mathbf{J}_f = -F_X \nabla X \quad , \tag{4.45}$$

where F_X is positive and defined by:

$$F_X = \frac{A.B.K_{ls}\rho_l(X_{max} - X_{FSP})^B}{\eta_l(X - X_{FSP})^{(1+B)}}\{1 - cos[\frac{\pi}{2}.\frac{X - X_{min}}{X_{max} - X_{min}}]\} \ . \tag{4.46}$$

It should be mentioned that based on experiments:

$\mathbf{J}_b \ll \mathbf{J}_f$ for $(X \gg X_{FSP})$ and

$\mathbf{J}_f = 0$ for $(X < X_{FSP})$ or $(S < S_{min})$.

In this study the flux of bound water was not neglected due to smaller differences between the initial moisture content and X_{FSP}.

4.1.4 General form of the equations for internal nodes

Combining the expressions for the fluxes of different moisture phases we obtain:

$$\mathbf{J} = -(V_X + B_X + F_X)\nabla X - (V_T - B_T)\nabla T \ . \tag{4.47}$$

Using the above expression in Eqn. 4.3, the conservation of mass yields:

$$\rho_d \frac{\partial X}{\partial t} = \nabla[(V_X + B_X + F_X)\nabla X + (V_T - B_T)\nabla T] = \nabla(D_X \nabla X + D_T \nabla T) \quad (4.48)$$

where D_X and D_T are positive coefficients.

For the balance of energy, in Eqn. 4.7, since the changes in moisture contents are extremely slow with time, we can neglect the term $\frac{\partial \rho_{b,v,f}}{\partial t}$ for all the water phases ($\rho_d = constant$). Therefore, the balance of energy becomes:

$$[\Sigma \rho_k \frac{\partial u_k}{\partial T}]\frac{\partial T}{\partial t} = \nabla[(\lambda + h_v V_T - h_B B_T)\nabla T] + \nabla[(h_v V_X + h_b B_X + h_f F_X)\nabla X] \quad (4.49)$$

or:

$$(\rho C_p)_{eff} \frac{\partial T}{\partial t} = \nabla(\lambda_{eff} \nabla T + \lambda_X \nabla X) \quad , \quad (4.50)$$

where $(\rho C_p)_{eff}$, λ_{eff} and λ_X are positive coefficients. The above set of equations are non-linear and coupled.

4.1.5 Boundary conditions

Boundary conditions at the surfaces are obtained from heat and mass transfer between board surface and the surrounding air. For the mass transfer at the surfaces, we have:

$$J_{s_n} = h_m \epsilon_s \rho_v [X_s - X_{eq}(M)] \quad , \quad (4.51)$$

where ρ_v is the density of water vapour at the surface, index s refers to surface values, and m refers to the mean (bulk) values defined for internal flows. $X_{eq}(M)$, the equilibrium moisture content of the drying air can be obtained as[57]:

$$X_{eq}(M) = \frac{18}{W}[\frac{k_1 k_2 \phi}{1 + k_1 k_2 \phi} + \frac{k_2 \phi}{1 - k_2 \phi}] \quad , \quad (4.52)$$

where ϕ is the relative humidity of the dying air. k_1, k_2, and W are modified for temperatures in degrees Kelvin as:

$$k_1 = -45.6988 + 0.3216T - 5.0123 \times 10^{-4}T^2 \quad , \tag{4.53}$$

$$k_2 = -0.1722 + 4.7317 * 10^{-3}T - 5.5534 \times 10^{-6}T^2 \quad , \tag{4.54}$$

$$W = 1416.502 - 9.4302T + 0.01853T^2 \ . \tag{4.55}$$

The author believes that ϵ_s should be used when J_{s_n} is calculated in order to consider the surface resistance to mass transfer in addition to air resistance represented by h_m. Salin[58] after reviewing the experimental data concluded that the mass transfer coefficient is often one order of magnitude smaller than what could be expected from the analogy between heat and mass transfer. Such phenomenon was first observed by Plumb *et. al*[10]. Also Gong[36] reported the correction factor values between 0.7 and 0.3, depending on surface moisture content and temperature. The term ϵ_s, where ϵ_s is the porousity of the surface, provides such order of magnitude.
Heat balance at surface requires that:

$$Q_s/A = h(T_s - T_M) + J_{s_n} h_{v-s} \quad , \tag{4.56}$$

where the h_{v-s} is the enthalpy of water vapour at the surface. The values of convective heat and mass transfer coefficients at each point of the surfaces, h and h_m, are obtained by solving the heat/mass transfer and fluid flow equations in the air.

The integration of heat and mass transfer between the stack inlet and each location in the stack, provides the mean temperature and mean equilibrium moisture content of the drying air.

At the center of the board, the symmetry condition about the x axis requires that:

$$\frac{\partial \phi}{\partial y} = 0 \quad , \tag{4.57}$$

where ϕ will be either temperature T, or moisture content X, or their derivatives.

4.1.6 Physical properties

Various physical and thermodynamical properties of wood and moisture phases appear in the equations of the present model. Previously, relationships for some of them were presented like: the saturation water pressure, $P_{sv}(T)$; $\psi(X,T)$; moisture content at Fiber Saturation Point, X_{FSP}, etc. For the rest of the parameters the following relationships have been used in the modelling.

Free water and water vapor characteristics

Free water and water vapor thermodynamic characteristics (except the density) are the same as the liquid water and water vapor, respectively, at saturation temperature. Relationships has been proposed in the present work for the steam table data in the range of temperature observed in conventional kiln drying. The relationships are in polynomial format and predict the related parameters with better than 0.5 percent accuracy.

Bound water characteristics

The bound water specific heat, enthalpy, and internal energy can be obtained by formulations suggested by Stanish *et.al* [19] as:

$$C_{Pb} = C_{Pf} - 0.4(C_{Pv} - C_{Pf})[1 - \phi_b + \frac{1}{3}\phi_b^2] \quad . \tag{4.58}$$

$$h_b = h_f - 0.4(h_v - h_f)[1 - \phi_b + \frac{1}{3}\phi_b^2] \quad , \tag{4.59}$$

$$u_b = u_f - 0.4(u_v - u_f)[1 - \phi_b + \frac{1}{3}\phi_b^2] \quad , \tag{4.60}$$

where f and v subscripts are referred to free water (or saturated water) and water vapor (saturated water vapor),

$$\phi_b = \frac{\rho_b}{\rho_{bFSP}} \quad , \tag{4.61}$$

and ρ_{bFSP} is the density of bound water at fiber saturation point obtained as:

$$\rho_{bFSP} = \rho_d X_{FSP} \ . \tag{4.62}$$

Wood characteristics

The dry wood specific heat and internal energy, and heat conductivity for moist wood can be calculated by relationships proposed by Stanish *et.al* [19] as

$$C_{Pd} = 1112.0 + 4.85(T - 273.15) \quad . \tag{4.63}$$

$$u_d = 123010 - 212.05T + 2.425T^2 \quad , \tag{4.64}$$

$$\lambda = \frac{\rho_d}{\rho_w}[0.2 + 0.5\frac{\rho_t}{\rho_d}] + 0.024 \ . \tag{4.65}$$

4.2 Governing equations in the fluid phase

In this section the drying air flow is modelled. The Re number in the duct flows is one of the parameters which specifies the flow regime and is defined as $Re = \frac{2s\rho u_{av}}{\mu}$. It involves: fluid properties, ρ and μ density and viscosity; average main flow velocity. u_{av}; and duct characteristic, $2s$= *hydraulic diameter*, where s is the sticker thickness. For $Re > 2000$ flow regime is turbulent. Based on the average velocities observed in the stack, flow regime is expected to be turbulent. For turbulent flows, Reynolds[60]

separated the instantaneous values of the flow parameters into mean and fluctuating parts, e.g.:

$$V_i = \overline{V_i} + V' \quad , \tag{4.66}$$

$$P = \overline{P} + P' \quad , \tag{4.67}$$

$$T = \overline{T} + T' \quad , \tag{4.68}$$

$$Y = \overline{Y} + Y' \quad , \tag{4.69}$$

where, P, T, V_i, and Y are instantaneous values of pressure, temperature, components of velocity vector and water vapor concentration, respectively. The superscripts $(-)$ and $(')$ refer to the time-mean and corresponding fluctuations about the mean, respectively. The time average of a dependent variable, e.g. T, for a statistically steady flow is defined as:

$$\overline{T} = \frac{1}{\Delta t} \int_{t_0}^{t_0+\Delta t} T dt \quad , \tag{4.70}$$

where Δt should be selected in a way that it will be long enough compared with the time scale of the turbulent motion and small compared with the time scale of the mean flow.

The air is assumed to be a heat conductive, incompressible, viscous, Newtonian fluid. Under these conditions, the governing equations of the fluid phase are[61]:

Incompressibility:

$$\frac{\partial \overline{V_i}}{\partial x_i} = 0 \quad , \tag{4.71}$$

Momentum balance:

$$\rho[\frac{\partial \overline{V_i}}{\partial t} + \overline{V_j}\frac{\partial \overline{V_i}}{\partial x_j}] = -\frac{\partial \overline{P}}{\partial x_i} + \frac{\partial}{\partial x_i}(\mu \frac{\partial \overline{V_i}}{\partial x_i}) - \rho \frac{\partial}{\partial x_j}(\overline{V_i' V_j'}) \quad . \tag{4.72}$$

Energy balance:

$$\frac{\partial(\rho C_{pa}\overline{T})}{\partial t} + \frac{\partial(\rho C_{pa}\overline{V_j T})}{\partial x_j} = \frac{\partial}{\partial x_i}(\lambda_a \frac{\partial \overline{T}}{\partial x_i}) - \frac{\partial}{\partial x_i}(\rho C_{pa}\overline{V_i' T'}) + \Phi \quad , \tag{4.73}$$

where Φ is the dissipation term which will be neglected due to low velocities. The first two equations are called Reynolds averaged Navier-Stokes equations.

Mass conservation for water vapour yields:

$$\frac{\partial \overline{Y}}{\partial t} + \overline{V_j}\frac{\partial \overline{Y}}{\partial x_j} = \frac{\partial}{\partial x_i}(D_a \frac{\partial \overline{Y}}{\partial x_i}) - \frac{\partial}{\partial x_i}(\overline{V_i' Y'}) \ . \tag{4.74}$$

It can be seen that the mass transport and energy equations in the absence of viscous dissipation term, have similar forms. Indeed, if the Lewis number ($Le = \frac{Prandtl\ Number(Pr)}{Schmidt\ Number(Sc)} = \frac{\rho C_{pa} D}{\lambda_a}$) is about one, their dimensionless solutions will be the same. The Lewis number for diffusion of water vapour into air, in the temperatures of the kiln ($50 - 80^0 C$), is about 1.06-1.09. Therefore, there is no need to solve both Eqs.4.73 and 4.74 for temperature and water concentration. The results of energy equation 4.73 for surface coefficients and heat flux at walls will also be used to provide the parameters of mass transport.

4.2.1 Turbulence modelling

In order to solve the above sets of equations, the terms $-\rho\frac{\partial}{\partial x_j}(\overline{V_i' V_j'})$ and $-\frac{\partial}{\partial x_i}(\rho C_{pa}\overline{V_i' T'})$ must be related to the unknowns of the model. Such a knowledge is obtained by a process of introducing additional algebraic or differential equations, which is called "*turbulence modelling*". A brief review of the turbulence models used in the present work is presented next. Description of other approaches in turbulence modelling can be found in [62].

One of the two terms which should be modelled is $-\rho\frac{\partial}{\partial x_j}(\overline{V_i' V_j'})$, the so called "*Reynolds stresses*". Bousinesq[63] suggested that, in analogy to the viscous stresses in laminar flows, the turbulent stresses are proportional to the mean velocity gradients or:

$$-\rho\frac{\partial}{\partial x_j}(\overline{V_i' V_j'}) \equiv \mu_t(\frac{\partial \overline{V_i}}{\partial x_j} + \frac{\partial \overline{V_j}}{\partial x_i}) \quad , \tag{4.75}$$

where μ_t is the turbulence eddy viscosity. One approach for determining μ_t is the "*Two Equation Approach*" in which μ_t is defined based on two new parameters. One of these two parameters is the kinetic energy of the fluctuating motion, k, defined by:

$$k = \frac{1}{2}\sum \overline{V_i' V_i'} \ . \tag{4.76}$$

For each of these two new parameters a separate partial differential equation is derived from Navier-Stokes equations. These new partial differential equations contain new terms which are modelled using empirical relations. The system of the new equations and Navier-Stokes equations are then solved for all parameters.

The "*Prandtl-Kolmogorov*" relation determines the turbulent eddy viscosity as[64]:

$$\mu_t = c_\mu \rho \frac{k^2}{\varepsilon} \quad , \tag{4.77}$$

where c_μ is an empirical constant and ε is the "*Viscous dissipation*" defined by:

$$\varepsilon = -\frac{\mu}{\rho}\left(\overline{\frac{\partial V_i'}{\partial x_j}\frac{\partial V_j'}{\partial x_i}}\right) . \tag{4.78}$$

In heat/mass transfer equation, a direct analogy between turbulent momentum transport and the turbulent heat/mass transport is often assumed. Therefore, the latter is related to the gradient of transported quantity, ϕ as:

$$\overline{-V_i' \phi'} = \Gamma \frac{\partial \overline{\phi}}{\partial x_i} \quad , \tag{4.79}$$

where Γ is the turbulent diffusivity of heat/mass transfer. Γ depends on the state of turbulence and is not a fluid property. The Reynolds analogy between heat/mass and momentum transport suggests that:

$$\Gamma = \frac{\mu_t}{\rho \sigma_t} \quad , \tag{4.80}$$

where σ_t is called the turbulent *Prandtl/Schmidt* number. Therefore,

$\phi = T \ , \ \sigma_t = Pr_t \ , \ \Gamma = \lambda \quad ,$

$\phi = Y \ , \ \sigma_t = Sc_t \ , \ \Gamma = D \ .$

Standard $k-\varepsilon$ turbulence model

This model was proposed by Launder and Spalding[65] and uses the following equations, in addition to Eqs. 4.75-4.78:

k-equation:

$$\overline{V_j}\frac{\partial k}{\partial x_j} = \frac{1}{\rho}\frac{\partial}{\partial x_j}[(\mu + \frac{\mu_t}{\sigma_k})\frac{\partial k}{\partial x_j}] + \rho G - \rho\varepsilon \quad , \tag{4.81}$$

ϵ *-equation*:

$$\overline{V_j}\frac{\partial \varepsilon}{\partial x_j} = \frac{1}{\rho}\frac{\partial}{\partial x_j}[(\mu + \frac{\mu_t}{\sigma_\epsilon})\frac{\partial \varepsilon}{\partial x_j}] + c_{\epsilon 1}\frac{\rho G\varepsilon}{k} - c_{\epsilon 2}\frac{\rho\epsilon^2}{k} + E \quad , \tag{4.82}$$

where G, the turbulent kinetic energy generation, is:

$$G = \frac{\mu_t}{\rho}(\frac{\partial \overline{V_i}}{\partial x_j} + \frac{\partial \overline{V_j}}{\partial x_i})\frac{\partial \overline{V_i}}{\partial x_j} \quad , \tag{4.83}$$

and $E = 0$, $c_\mu = 0.09$, $c_{\epsilon 1} = 1.44$, $c_{\epsilon 2} = 1.92$, $\sigma_k = 1.0$, and $\sigma_\epsilon = 1.3$.

Here, it is assumed that except the near wall region, $\mu_t >> \mu$.

Wall function

The form of standard $k-\epsilon$ model is valid for high Re number flows. Near the walls, the kinetic energy, k, tends to zero while the dissipation, ϵ, have a finite value at the wall. This causes a singularity in the last two terms of ϵ-equation. Also near the walls, the stresses due to viscosity, μ, cannot be neglected compared to the turbulent stresses. An alternative is to estimate the near wall region with wall functions. These functions, based on experiments, assume that flow close to the wall is like a one dimensional boundary flow where the stream wise gradient is negligible and there is a layer in which flow behaves like a laminar flow. This layer is called the "*Laminar sublayer*".

Assuming τ_w representing the wall shear stress, the dimensionless velocity, u^+, is defined as:

$$u^+ = \frac{u}{u_\tau} = \frac{u}{\sqrt{\frac{\tau_w}{\rho}}} . \tag{4.84}$$

In the same way, the dimensionless distance from wall, y^+, is defined as:

$$y^+ = \frac{u_\tau \rho y}{\mu} = \frac{\sqrt{\frac{\tau_w}{\rho}}\rho y}{\mu} = \frac{y\sqrt{\tau_w \rho}}{\mu} . \tag{4.85}$$

Here it can be seen that y^+ looks like a Re number. The laminar sub-layer has the limit of $y^+ < 5$ to 12, depending on the surface roughness. The velocity profile in this region is linear and, based on the above definitions, is described as[66]:

$$u^+ = y^+ . \tag{4.86}$$

There is another region called "*Outer layer* ", for $y^+ > 30$, in which flow is fully turbulent. The velocity profile in this region is defined based on logarithmic profile such as:

$$u^+ = \frac{1}{c_u} ln(y^+) + c_k \quad , \tag{4.87}$$

where $c_u = 0.41$ is the "*von Karman constant*" and c_k is a function of surface roughness. The distance between these two regions is called "*Buffer layer*". In this region an interpolation between the two velocity profiles of laminar and outer layers is used.

The integration of $k-$ and $\varepsilon-$equations from fully turbulent region to the wall results in this equation for the wall shear stress:

$$\tau_w = \frac{\rho c_u {c_\mu}^{1/4} k^{1/2}}{ln(y^+)} \overline{U} \quad , \tag{4.88}$$

where $\overline{U}$ is the average velocity component parallel to the wall. Similarly, the following expression is obtained for ϵ near the wall region:

$$\varepsilon = \frac{c_\mu^{3/4} k^{3/2}}{c_u y} ln(c_k y^+) . \tag{4.89}$$

Low Re $k-\varepsilon$ model of Launder and Sharma

Launder and Sharma[67] used the original idea of Standard $k-\varepsilon$ turbulence model.This model, like the other low Re number models, does not implement the law of the wall for velocity profile near the wall. Instead it uses other types of velocity profile, e.g. linear or quadratic, with more nodes close to the wall for a better accuracy of velocity profile. A couple of nodes inside the laminar sublayer are needed for such accuracy.

In the standard $k-\varepsilon$ model, the value of ε at wall as a boundary condition for ε−equation comes from the integration of $\varepsilon-$ equation between the wall and the outer layer using the wall function. In the Launder and Sharma model, this value is considered from the distribution of k near wall such as:

$$\varepsilon_w = 2\frac{\mu}{\rho}(\frac{\partial\sqrt{k}}{\partial y})^2 \ . \tag{4.90}$$

Launder and Sharma proposed new non-constant expressions for c_μ and $c_{\epsilon 2}$ based on a newly defined turbulent Re number. This Re number is defined as:

$$R_T = \frac{\rho k^2}{\mu\varepsilon} \ . \tag{4.91}$$

The expression for c_μ and $c_{\epsilon 2}$ are exponential decaying functions of R_T so that at high Re numbers they become the same as the constants used in standard version. The following expressions can be used along with the Eqs. 4.81 and 4.82:

$$c_\mu = 0.09exp[\frac{-3.4}{(1+\frac{R_T}{50})^2}] \quad , \tag{4.92}$$

$$c_{\epsilon 2} = 1.92[1-0.3exp(-R_T^2)] \ . \tag{4.93}$$

The other difference with the standard model is using a non-zero E term in the ε-equation as:

$$E = \frac{2\mu}{\rho}\frac{\mu_t}{\rho}(\frac{\partial^2 U}{\partial y^2}) \ . \tag{4.94}$$

One can interprete that in the standard version it is assumed where either μ or μ_t is considerable the other one is negligible and the E term in the ε-equation is neglected due to multiplication of them.

General form of the governing equations

The system of Eqs. 4.71-4.73, 4.81 and 4.82, can be written in the general form:

$$\frac{\partial(\rho\phi)}{\partial t} + \frac{\partial(\rho\phi\overline{V_j})}{\partial x_j} = \frac{\partial}{\partial x_j}(\Gamma\frac{\partial\phi}{\partial x_j}) + S_\phi \quad , \tag{4.95}$$

where ϕ represents either of ($\overline{V_j}$, $\overline{P}$, $\overline{T}$, k, ϵ) and S_ϕ is the source term. The source term may be dependent on ϕ and other variables. Therefore, it is linearized as:

$$S_\phi = S_P\phi_P + S_U \quad , \tag{4.96}$$

where subscript P refers to the point in which the equation is written. S_U and S_P are calculated from the last values during iteration. Patankar[53] has presented the guidelines for linearization of the source term.

4.2.2 Discretization process

The CFX software uses the integration technique of governing equations over the control volume surronding a node. This method known as "*Finite volume*" guarantees the conservation of mass and momentum over any arbitrary group of control volumes as well as the entire computational domain. In the non-staggered grid system used by the software, the scalar variables as well as the velocity components are stored at the centres of control volumes.

When the general form of the equation is integrated over the control volume, the diffusion and advection flux terms at the surfaces of computational cells appear.

For diffusion terms, the diffusion coefficients at the surfaces can be obtained from harmonic average between two adjacent points as suggested by Patankar[53].

The integration of the advection term $\frac{\partial(\rho\phi\overline{V_j})}{\partial x_j}$ at the control surfaces between points (i,j) and $(i+1,j)$ results in terms like $\rho\overline{V_l}_{(i+\frac{1}{2},j)}\cdot\phi_{(i+\frac{1}{2},j)} = C_{(i+\frac{1}{2},j)}\phi_{(i+\frac{1}{2},j)} = L_{(i+\frac{1}{2},j)}$. The way such terms are dealt with is related to "*Upwinding schemes*". Here some of the upwinding schemes related to the present work are discussed.

Central Differencing Scheme (CDS)

In this scheme, $L_{(i+\frac{1}{2},j)}$ is an arithmatic average of L values at two neighboring points of (i,j) and $(i+1,j)$ after considering the changes of cell length. While this scheme is second order accurate, it is subject to instabilities especially at high Re numbers.

Upwind Differencing Scheme (UDS)

This scheme was first put forward by Courant, Isaacson and Rees[68]. The scheme assumes that the advection term is much larger than the diffusion one or $Pe >> 1$. Here, $Pe = \frac{\overline{\rho V_l}\delta x}{\Gamma}$, the "*cell Peclet number*" is the ratio of advection to diffusion flux at each control volume. Therefore, the advection term value at the intermediate face is the value at the grid point on the upward side of the face or:

$$L_{(i+\frac{1}{2},j)} = L_{(i,j)} \; if \; V_{l(i+\frac{1}{2},j)} > 0 \quad ,$$

$$L_{(i+\frac{1}{2},j)} = L_{(i+1,j)} \; if \; V_{l(i+\frac{1}{2},j)} < 0.$$

This scheme is first order accurate and unconditionally stable, but produces false diffusion and is not recommended for $Pe < 2$.

Hybrid Differencing Scheme (HDS)

This is a modification to upwind scheme. In this method Central differencing is used if absolute Pe number is less than 2. Otherwise, Upwind Differencing is used. This scheme is stable and provides a relative good accuracy but suffers from the false diffusion when $1 < Pe < 30$ [53].

Quadratic Upwind Differencing Scheme (QUICK)

This is a third-order accurate upwinded scheme. It uses two upstream points and one downstream point. The formulation for $V_{l(i+\frac{1}{2},j)} > 0$ is:

$$L_{(i+\frac{1}{2},j)} = \frac{3}{8}L_{(i+1,j)} + \frac{3}{4}L_{(i-1,j)} - \frac{1}{8}L_{(i+2,j)} \ . \tag{4.97}$$

Bounded Quadratic Upwind Differencing Scheme (CCCT)

While $QUICK$ scheme has a high order accuracy, it can suffer from non-physical overshoots in its solutions. For example, turbulent kinetic energy can become negative. $CCCT$ is a modification of the $QUICK$ scheme which is bounded and can eliminate these overshoots. For the similar case of QUICK it has the form of:

$$L_{(i+\frac{1}{2},j)} = (\frac{3}{8} - \alpha)L_{(i+1,j)} + (\frac{3}{4} + 2\alpha)L_{(i-1,j)} - (\frac{1}{8} + \alpha)L_{(i+2,j)} \quad . \tag{4.98}$$

where α depends on the curvature of the variable ϕ. The scheme is then treated like the QUICK scheme. Full details of the calculations of α are given by Alderton and Wilkes[69].

Chapter 5

Numerical simulation of air flow in stack

5.1 Bench mark case (Kho's geometry)

In this section we consider the air flow over a stack of planks arranged in a pattern which will be referred to as the Kho's geometry[29]. In each row, five boards, each 100x25 mm, are placed next to each other without side gaps in a way to provide a 500 mm long passage between two rows of boards. The distance between two rows of boards is the same as each row thickness (D), D=25 mm. Therefore, the blockage ratio is 50 percent and the length of each passage is 20 D. Due to large ratios of l/D in commercial kilns, where l is the length of each board in the third direction, the flow can be considered as two-dimensional. The configuration of flow and computational domain is shown in Figure 5.1. This case was also investigated numerically by Langrish *et al*[30-31], but comparisons of their results with experimental data were not satisfactory. Figures 5.2 and 5.3 present typical flow patterns after the leading and

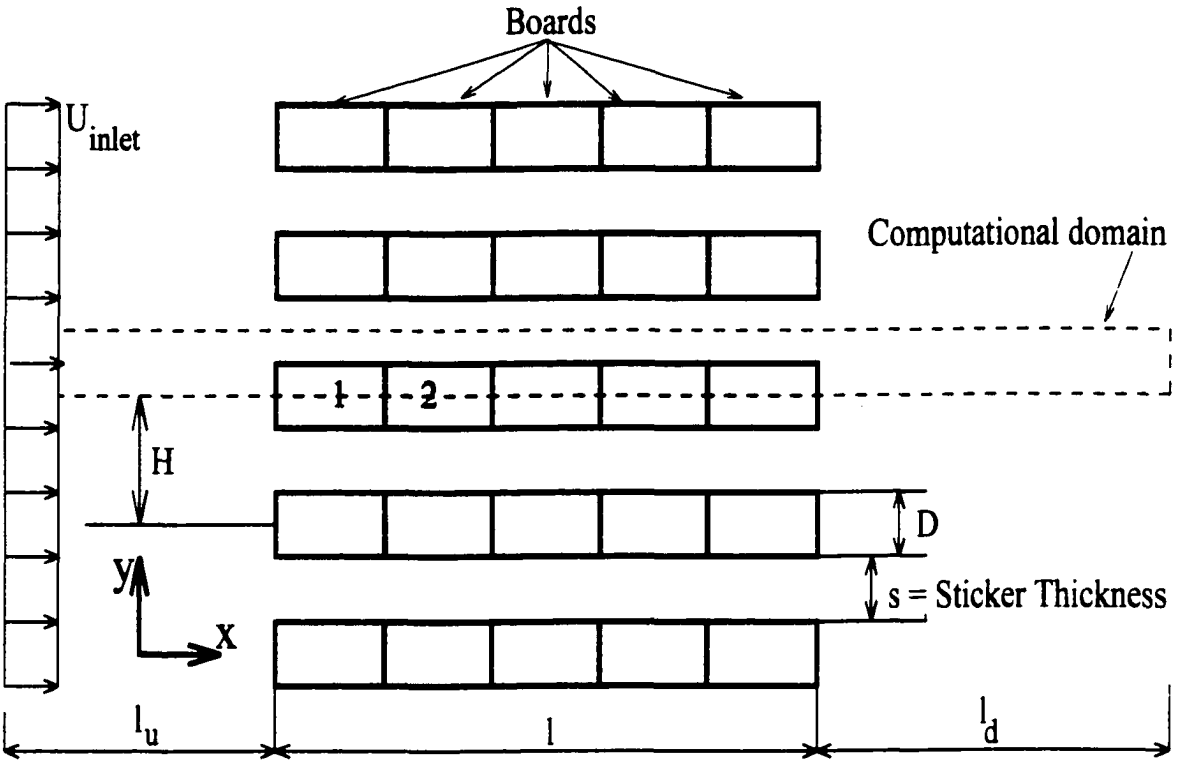

Figure 5.1: Configuration of stack plank investigated by Kho *et al* [29]

trailing edges of the stack, respectively. The separation bubbles and air recirculation due to backward flow inside them can be seen in these figures.

5.1.1 Solution method

This study was conducted with the standard $k-\varepsilon$ and low Reynolds number turbulence models. The following differencing schemes were used: hybrid, QUICK, and CCCT (bounded QUICK). In the first step, a finite volume formulation of $k-\varepsilon$ turbulence model and hybrid discretization scheme along with the logarithmic wall treatment were chosen from the menus of the CFX-F4.1 software to solve the isothermal flow of air at $54.3°C$. For the uniform flow boundary condition at inlet, the kinetic energy and the dissipation rate were chosen based on the values measured by Kho

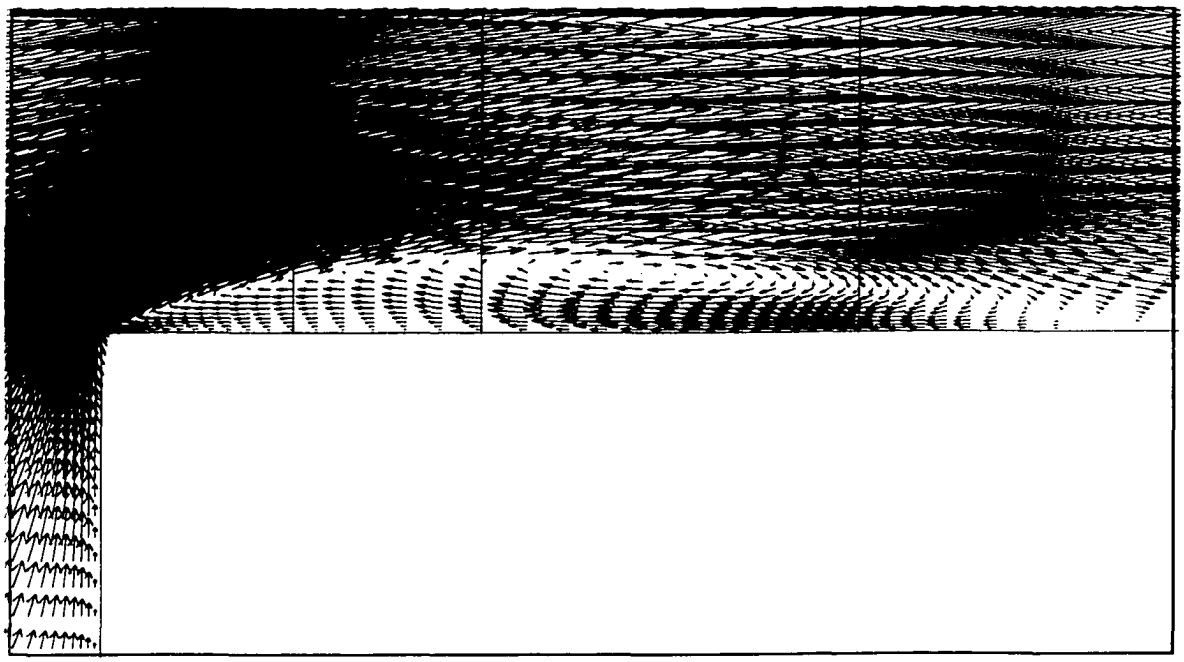

Figure 5.2: Typical velocity vectors near the leading edge at $Re_{D_h} = 8200$

et al [29]. Because of symmetry, the computational domain was considered between the centre line of the boards and the centre line of the space between the boards. The following boundary conditions were imposed: zero stream wise gradient across the outlet, zero gradients with respect to y-direction and zero y- velocity component along the axis of symmetry.

5.1.2 Effect of the inlet and outlet locations

To determine the effect of the locations of inlet and outlet boundaries, l_u and l_d, some computations were carried out for an intermediate Reynolds number of $Re = \frac{\rho u_{av} \cdot 2s}{\mu} = 13660$ ($u_{inlet} = 2.5m/s$) for a relatively fine grid. Here, μ and ρ are the viscosity and the density of the drying air, u_{av} is the average air velocity between the boards, and $s = D$ is the sticker thickness which is half the hydraulic diameter of the duct. For $l_u > 10D$, the location of inlet boundary was found to have no noticeable effect on the

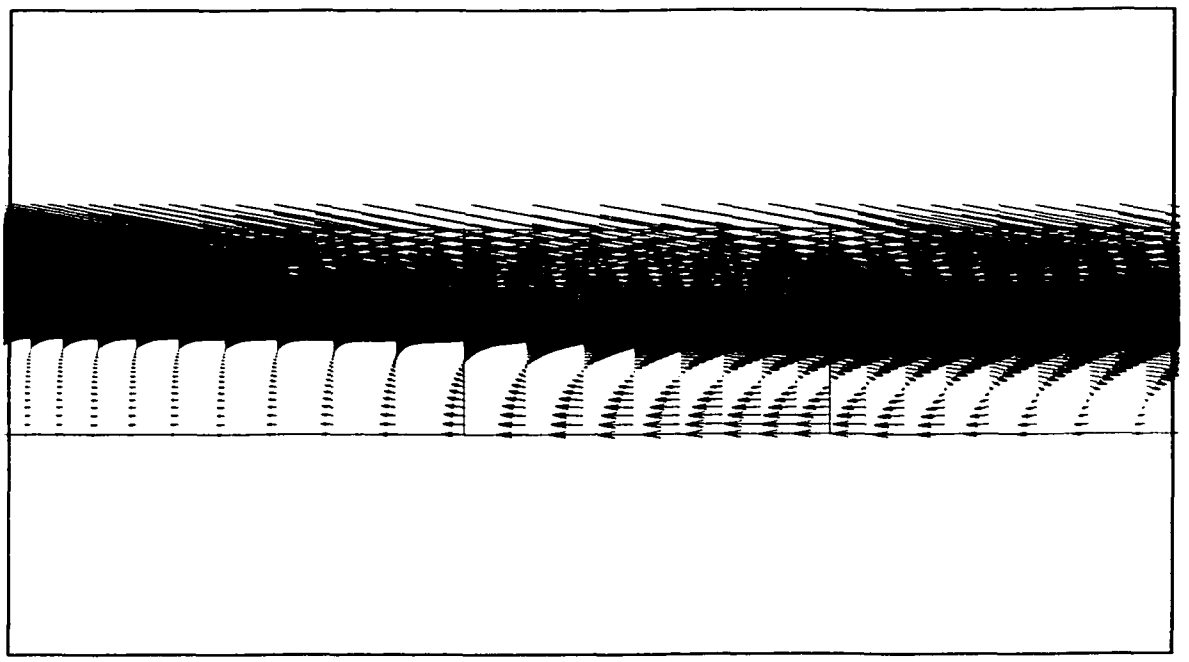

Figure 5.3: Typical velocity vectors after the trailing edge at $Re_{D_h} = 8200$

flow in the recirculation region after the leading edge (typically less than 0.4 percent change in the length of the separation bubble). The same phenomena was observed for the effect of $l_d > 14D$ on the recirculation zone downstream the trailing edge of the board (less than 0.1 percent change in the length of the down-stream separation bubble). Therefore, in all subsequent computations $l_u = 11D$ and $l_d = 16D$ were used.

5.1.3 Mesh arrangement

A proper refinement of grids immediately upstream and around the leading and trailing edge corners was performed to obtain a more accurate solution. A typical grid distribution is shown in Figures 5.4 and 5.5. The expansion factors in grid generation, E_x and E_y, were chosen based on some of the values suggested by Djilali *et al*[70]. For the y-direction, since all grids are within the important area, $E_y < 1.1$ was up-

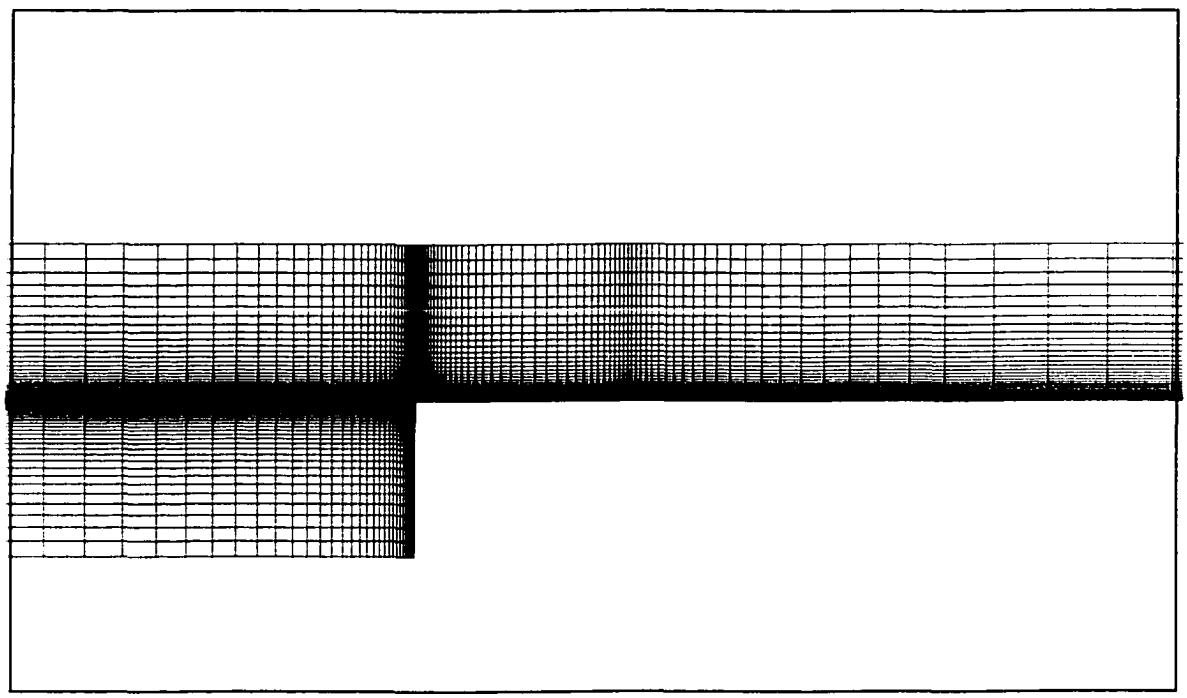

Figure 5.4: Schematic view of a typical grid array around the leading edge

held. The same condition was applied to E_x within two separation bubbles regions. D distance before the leading edge and also D distance before the trailing edge. Once the preliminary computations resulted in approximate sizes of the separation bubbles. the grid in the x direction was locally refined around the approximate stream wise locations of the boundaries of separation bubbles. This refinement provides a more accurate prediction of the length of the separation bubbles. The reattachment point downstream the leading edge, where wall shear stress vanishes, is calculated by linear interpolation from calculated wall shear stresses. For separation bubble downstream the trailing edge, a similar process is carried out for stream wise velocity distribution on the symmetry line passing through the middle of the boards.

5.1.4 Preliminary computations

After monitoring the effect of mass residue on the length of separation bubbles for different Reynolds numbers, a value of less than 0.012 percent of the total mass flux for a relatively fine grid of 228x44 was considered as a convergence criterion in this preliminary case. This grid array was used at the lowest Reynolds number of 8200 ($u_{inlet} = 1.5m/s$) for comparing the results of standard $k-\varepsilon$ turbulence model and hybrid discretization scheme with the results of low Reynolds number $k-\varepsilon$ turbulence model and QUICK discretization scheme. While QUICK scheme resulted in oscillations in the residues even after 8000 iterations, the velocity profile appeared stable and predicted longer recirculation zones- 33 percent longer for the one adjacent to the leading edge and 22.4 percent for the one after the trailing edge. The results show that the first point adjacent to the wall is in the laminar sublayer for the most sections of the upper wall as well as the trailing edge wall (y^+ was between 2.5 and 4, i.e., less than 11.2, the border of laminar sublayer and buffer layer). A second computation using RNG $k-\varepsilon$ turbulence model with hybrid discretization scheme predicted values of y^+ within the same range.

Effect of grid refinement

It is known that y^+ of the adjacent point to the wall has a significant effect on the prediction of wall shear stress as well as the dimension-less heat transfer from the wall. y^+ has a distribution over the the wall which reaches an asymptotic value. y^+_{as}. Different grid sizes in the y-direction were used along with the standard $k-\varepsilon$ turbulence model and the hybrid scheme to study the effect of $\frac{\Delta y_{min}}{D}$ at the lowest Reynolds number of 8200 on $\frac{x_R}{D}$, $\frac{l_d}{D}$ and y^+_{as} of the horizontal wall. Table 1 provides the results of this investigation. Comparison of results for an array of 168x60 with

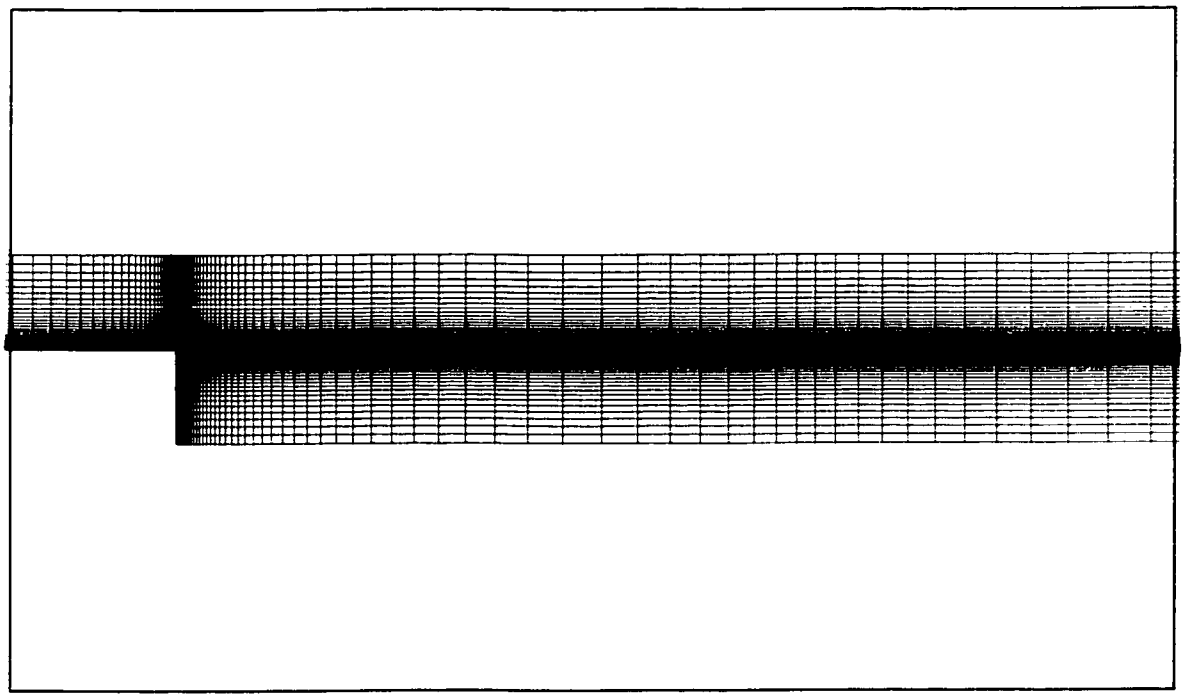

Figure 5.5: Schematic view of a typical grid array around the trailing edge

those of 160x55 showed a difference of about 2.5 percent in $\frac{x_R}{D}$ and less than 0.5 percent in $\frac{l_d}{D}$. The array of 168x60 with $\frac{\Delta y_{min}}{D} = 0.3$ percent resulted in y_{as}^+=1.2.

Coarser grids in the y-direction were then used until the condition of $y_{as}^+ > 11.2$. for the first point near the wall, was reached. When this happened, the corresponding grid of 16 vertical points resulted in $\frac{\Delta y_{min}}{D} = 4.3$ percent. Previous computations showed the following predictions for the dimension-less height of the separation bubble adjacent to the leading edge ($\frac{y_R}{D}$): 4.1 percent from low Re $k-\varepsilon$ turbulence model with the QUICK scheme, and 2.5 percent from the standard $k-\varepsilon$ turbulence model with the hybrid scheme. Comparing these values with $\frac{\Delta y_{min}}{D} = 4.3$ and noticing such low values of y_{as}^+ for the grid independency of $\frac{x_R}{D}$ in the case of using high Reynolds number turbulence models, we draw the conclusion that using such a coarse grid, which satisfies the condition of $y_{as}^+ > 11.2$, a high Reynolds number turbulence model

$N_i * N_J$	N_t	$\frac{x_R}{D}$	$\frac{l_d}{D}$	y^+_{as} of first point	$\frac{\Delta y_{min}}{D}$ percent
140*16	1612	0.2164	2.097	11.3	4.37
140*20	2130	0.2602	2.173	8.9	3.14
150*30	3424	0.2571	2.222	5.3	1.57
155*44	4686	0.2662	2.223	3.3	0.87
160*55	5994	0.2558	2.212	2.0	0.51
168*60	7530	0.2493	2.203	1.2	0.30

Table 5.1: Results of length of separation bubbles and other parameters for Re=8200

cannot resolve the flow inside the separation bubble. Therefore, the low Re $k-\varepsilon$ turbulence model must be used.

5.1.5 Results and discussions

For low Reynolds number $k-\varepsilon$ turbulence models, non-logarithmic wall treatment velocity profiles should be used with finer grids. Thus, the grids were refined near the walls according to the previous results for different Reynolds numbers to provide a reasonable y^+ near the wall (of order of one). A bounded QUICK scheme (CCCT) was also used to provide the superior accuracy of QUICK scheme and reduce the instability of the standard formulation of this scheme. Some of the results of this study are compared with the result of standard $k-\varepsilon$ turbulence model and hybrid discretization scheme in Figures 5.6 to 5.12.

Figures 5.7 to 5.10 compare the dimension-less stream wise velocity component ($\frac{u}{u_{ref}}$) at four locations after the leading edge. The difference between the results of two methods, even at $\frac{x}{D}=7$, can be observed, while the trend remains consistent. Velocity profile inside the separation bubble after the trailing edge (Figure 5.11) also

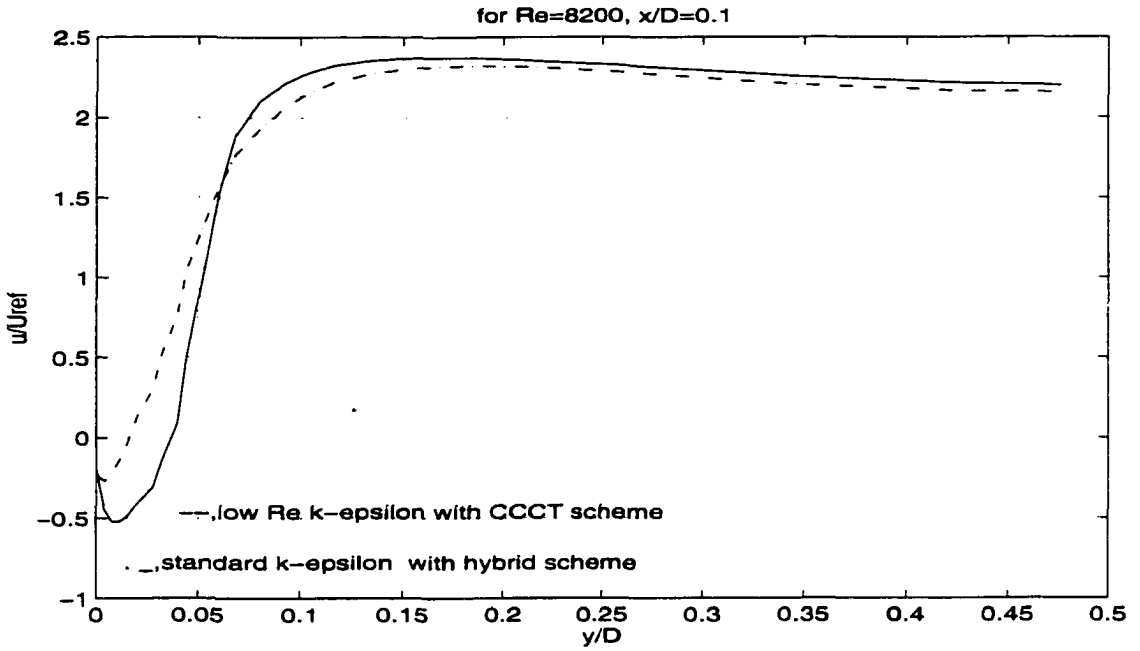

Figure 5.6: Dimensionless u velocity at the top of the boards after the leading edge for the Kho's geometry at Re=8200

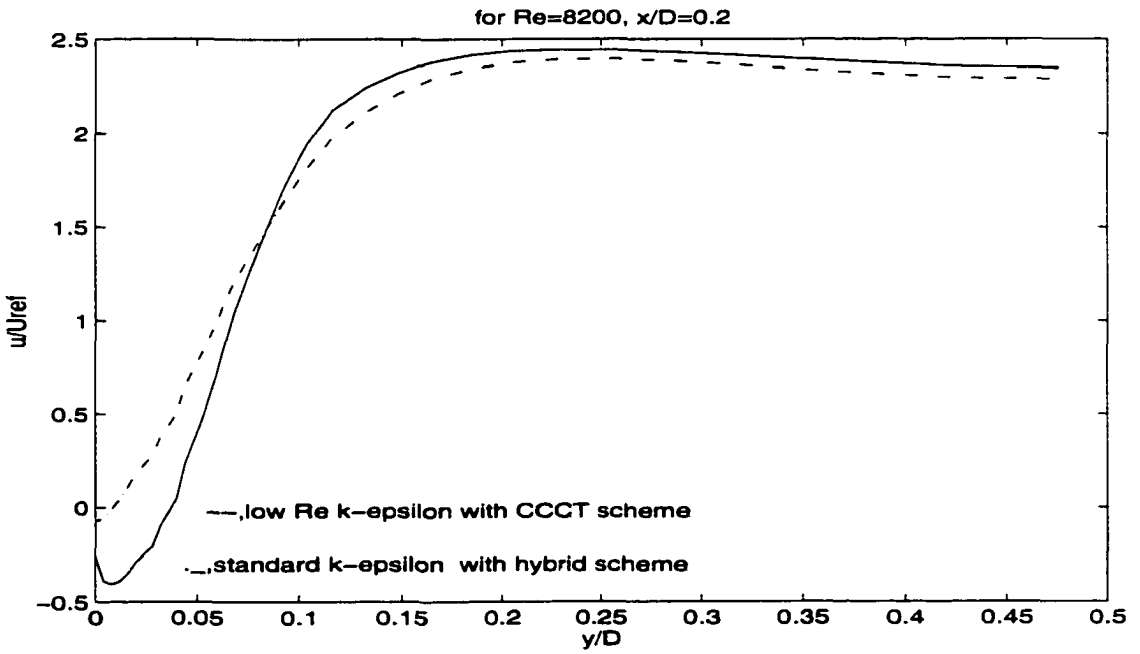

Figure 5.7: Dimensionless u velocity at the top of the boards (D=boards height and width =100mm)

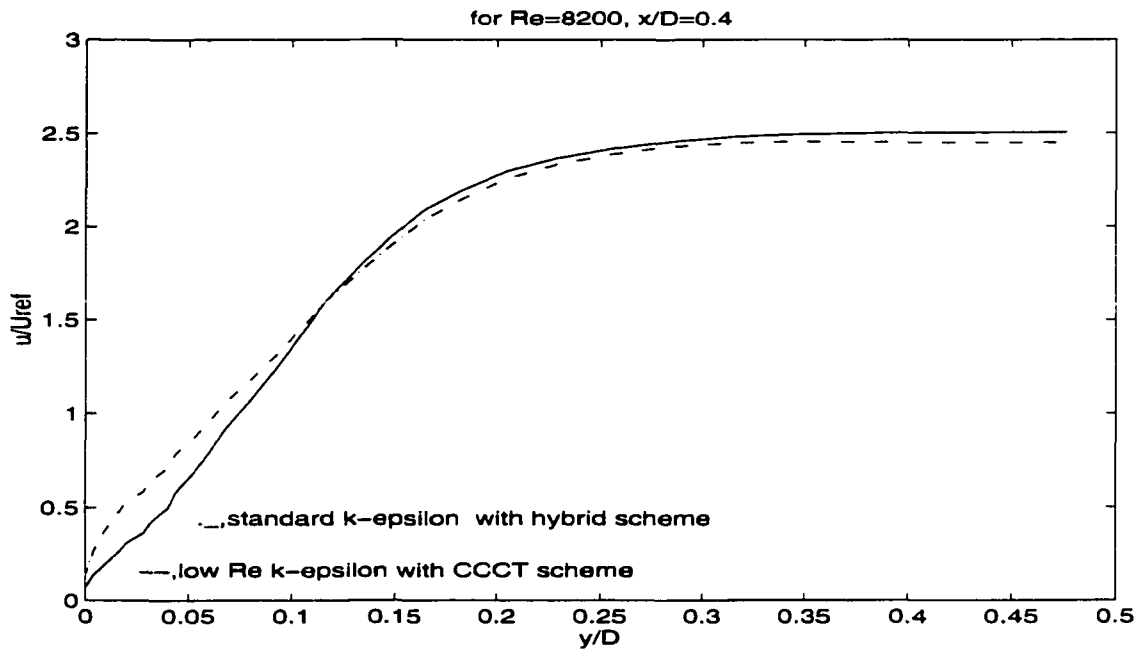

Figure 5.8: Dimensionless u velocity at the top of the boards

shows the same behaviour. From the velocity profiles inside the separation bubbles, it is predicted that combination of $k-\varepsilon$ model and the hybrid scheme will result in shorter stream wise length of separation bubbles. This phenomena is related to the hybrid scheme.

Figure 5.11 shows the $\frac{u}{u_{ref}}$ profile along the board's centre line, after the trailing edge. The dimension-less wall shear stress distribution in the channel is presented in Figure 5.12. From Figures 5.11 and 5.12, the length of the separation bubbles at the up- and down-streams are computed to be about 75 and 24 percent shorter using the combination of $k-\varepsilon$ model and the hybrid scheme than those from the other combination. This phenomena is related to the hybrid scheme. It was concluded that because of having some grids in the laminar sublayer for Re=8200, the high Reynolds number models cannot predict the wall shear stress accurately. In fact combining the standard $k-\varepsilon$ model and the hybrid scheme resulted in 155 percent larger asymptotic

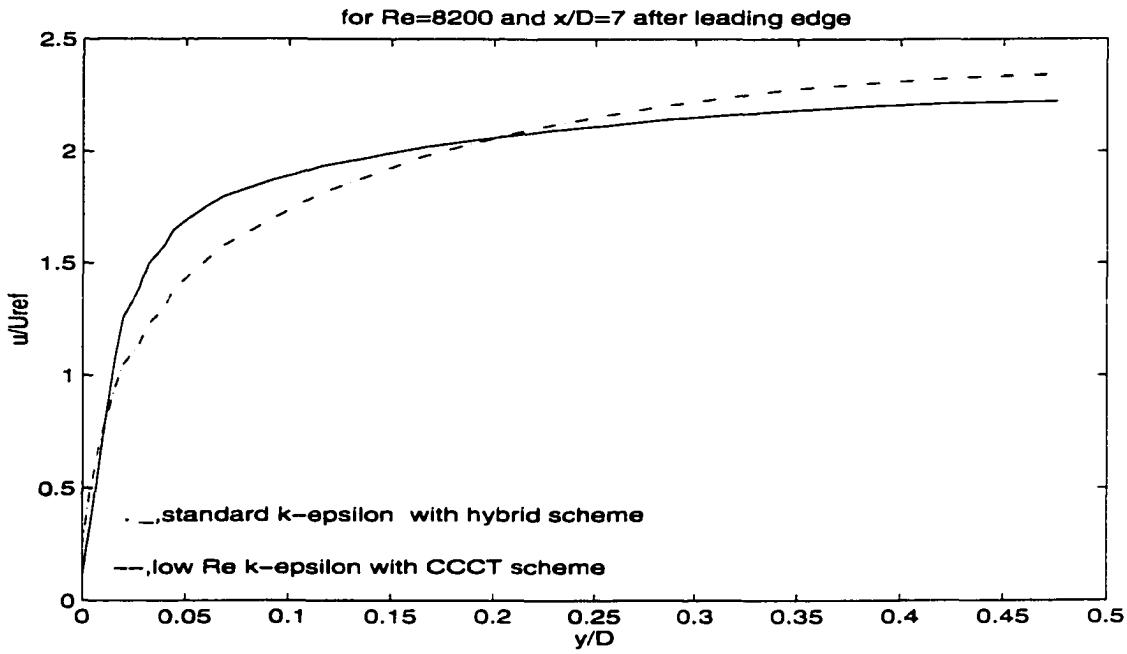

Figure 5.9: Dimensionless u velocity at the top of the boards

values for the wall shear stress than the other combination. Using the analogy between the momentum and heat/mass transfer, one can see that the high Reynolds number models will over predict the convective heat/mass transfer coefficients. This is one of the reasons behind some unsuccessful attempts in earlier numerical studies.

Using the low Re $k-\varepsilon$ turbulence model with QUICK scheme and an array of 265x60 points, computations were performed for three different Reynolds numbers (8200, 13600, and 19100), based on the mean velocity and hydraulic diameter. The values of local Nu_x versus dimension-less distance from the leading edge are presented in Figures 5.13 to 5.15 together with the measured values reported by Kho *et al.*[29]. The experimental trends are well born out by the computed values which are within 10 to 15 percent of measured values. Langrish *et al.*[30,31] have also employed the analogy between the heat/mass and momentum transfer and solved the Navier-Stokes equations using the standard high Re $k-\varepsilon$ model without the contribution of the

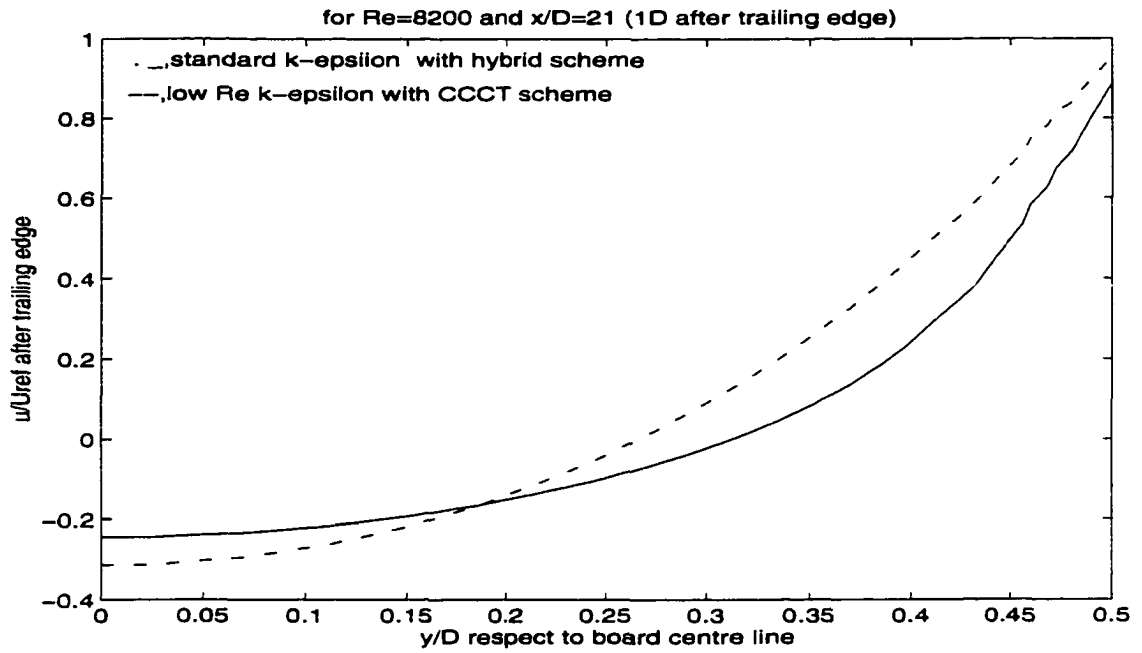

Figure 5.10: Dimensionless u velocity 1D (=100mm) after the trailing edge

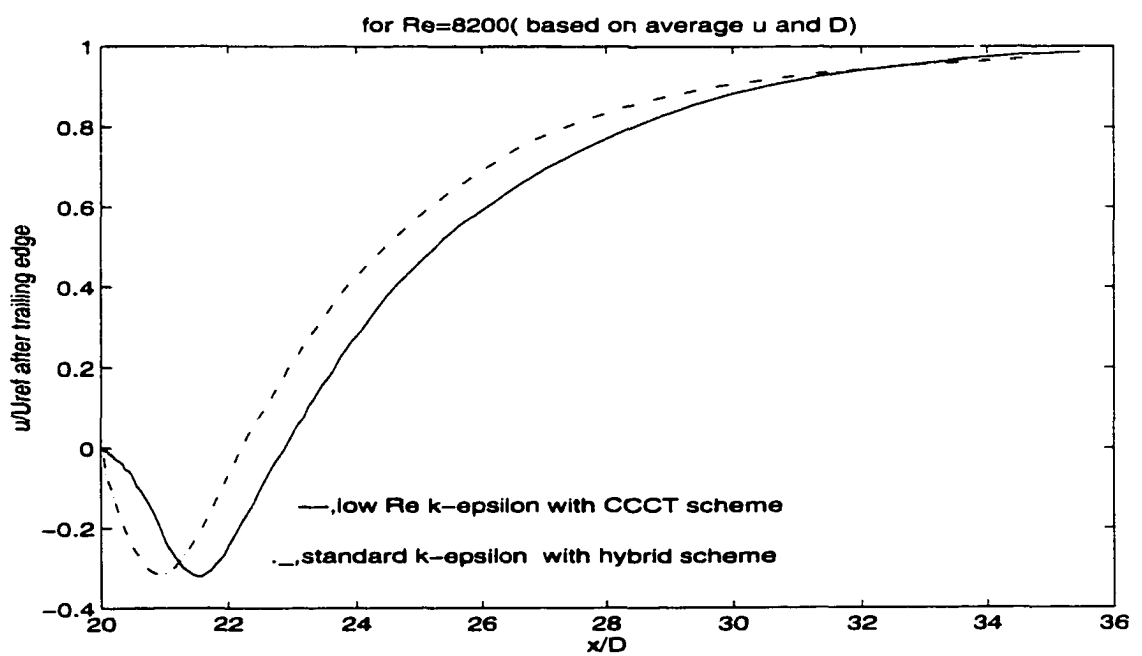

Figure 5.11: Dimensionless u velocity along the centre line after the trailing edge

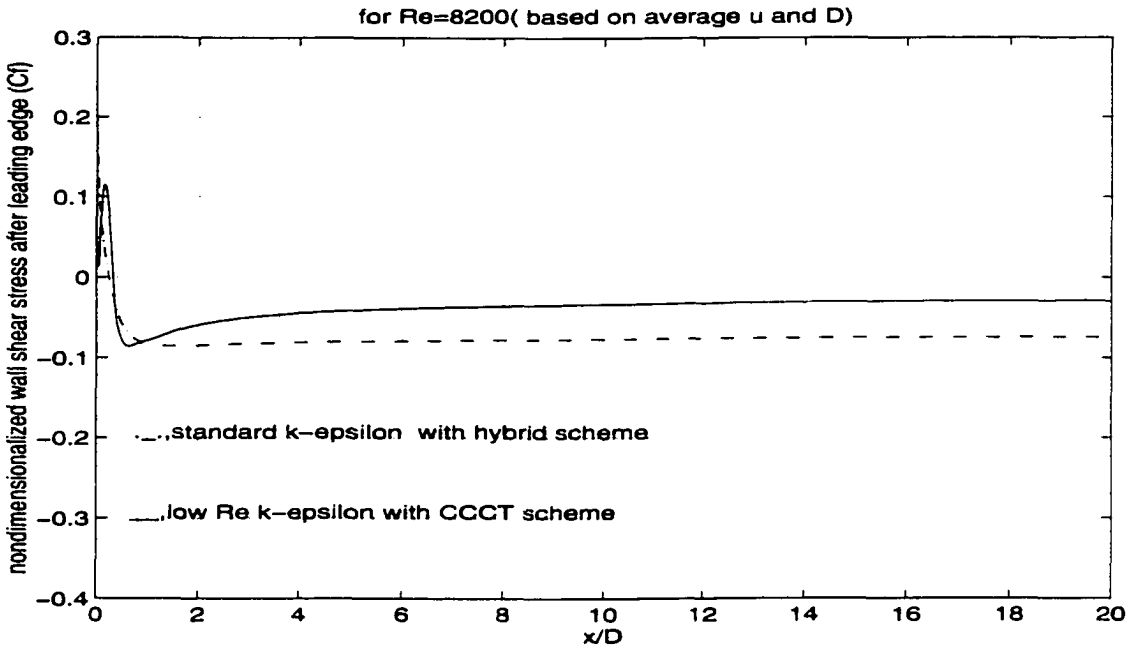

Figure 5.12: Local dimension-less wall shear stress after the leading edge for the Kho's geometry at Re=8200

energy equation. Their results could not reach the desired accuracy.

5.2 Numerical computations of surface coefficients over a commercial stack plank geometry (Li's case)

Li[52] experimentally investigated the effect of side gaps on the drying process of western hemlock lumber in a laboratory kiln. In her set up, each row of lumber contained seven 105x105 mm boards. The thickness of sticker was $s = 19$ mm which provided a blockage ratio of 84.7%.

Numerical simulations were carried out for Li's set up using the low Re $k - \varepsilon$

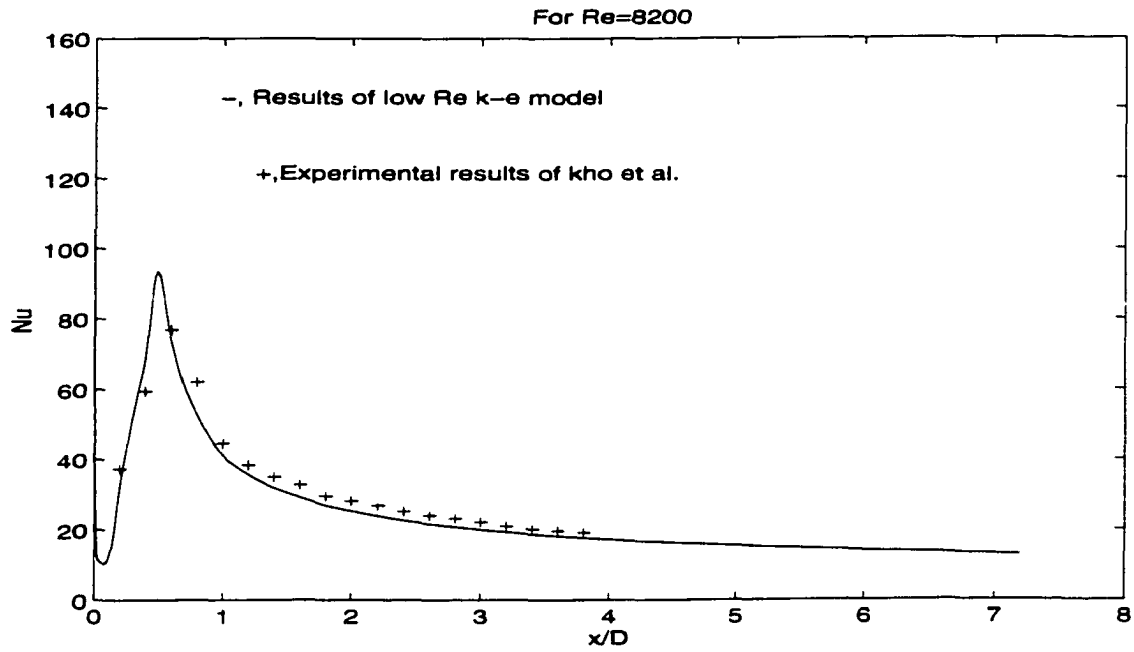

Figure 5.13: Local Nu number after the leading edge for the Kho's geometry at Re=8200

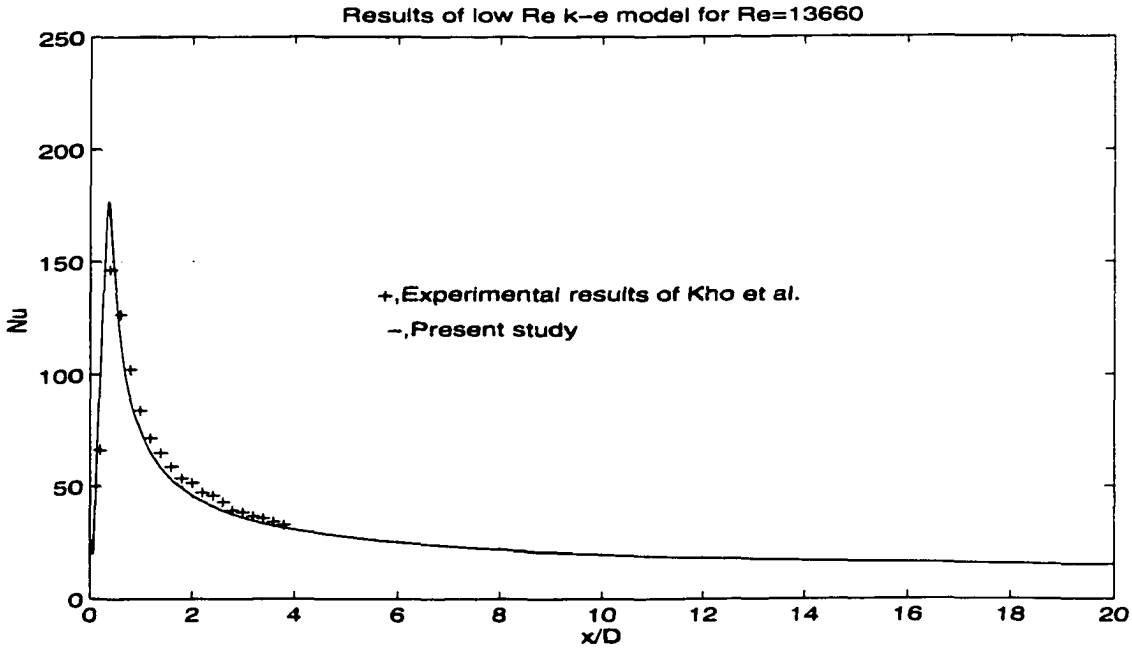

Figure 5.14: Local Nu number after the leading edge for the Kho's geometry at Re=13600

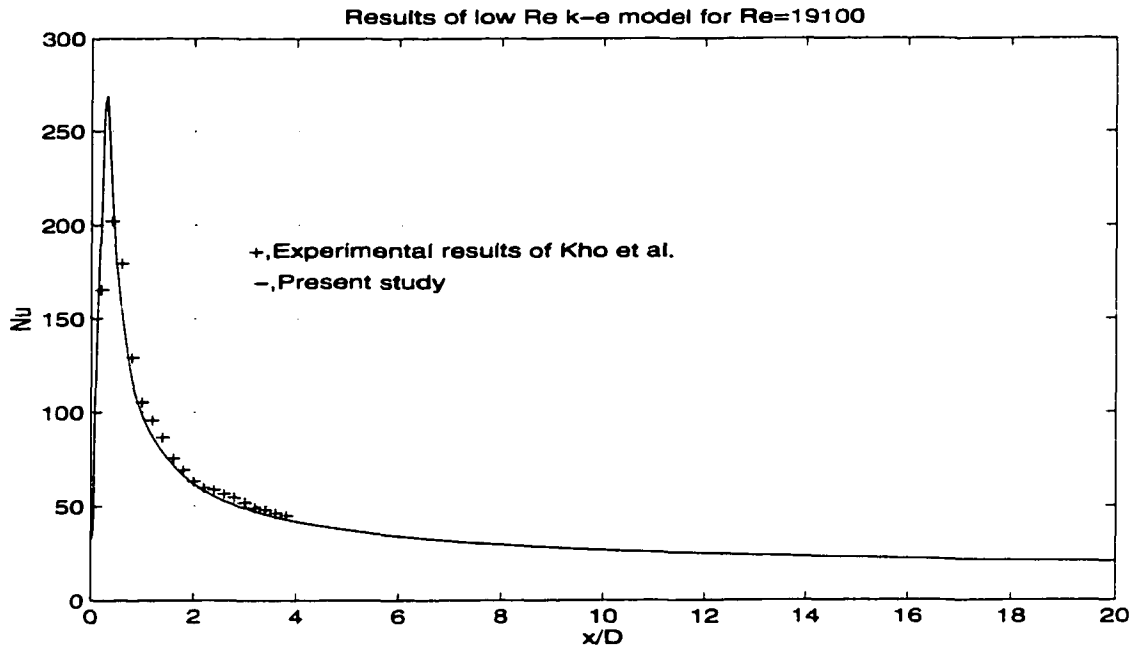

Figure 5.15: Local Nu number after the leading edge for the Kho's geometry at Re=19100

model and CCCT scheme at $u_{centre} = 2.54$ (u_{centre} is the velocity at the centre line of the sticker thickness). The temperature of the inlet air and the boards surfaces were taken as $54.4°C$ and $22.6°C$, respectively. Based on the average air velocity and hydraulic diameter of duct ($2s$), the Re number is 4400. A procedure similar to that used in the Kho's geometry was followed for determining the boundary conditions and mesh generation.

5.2.1 Preliminary computations

Computations were first performed for the case with no side gaps to determine the locations of inlet and outlet boundaries. For $l_u > 45s$ and $l_d > 40s$ the grid independency of the flow field features (lengths of separation bubbles after leading and trailing edges) was observed. Then the effect of average side gap of 1.5 mm, due to

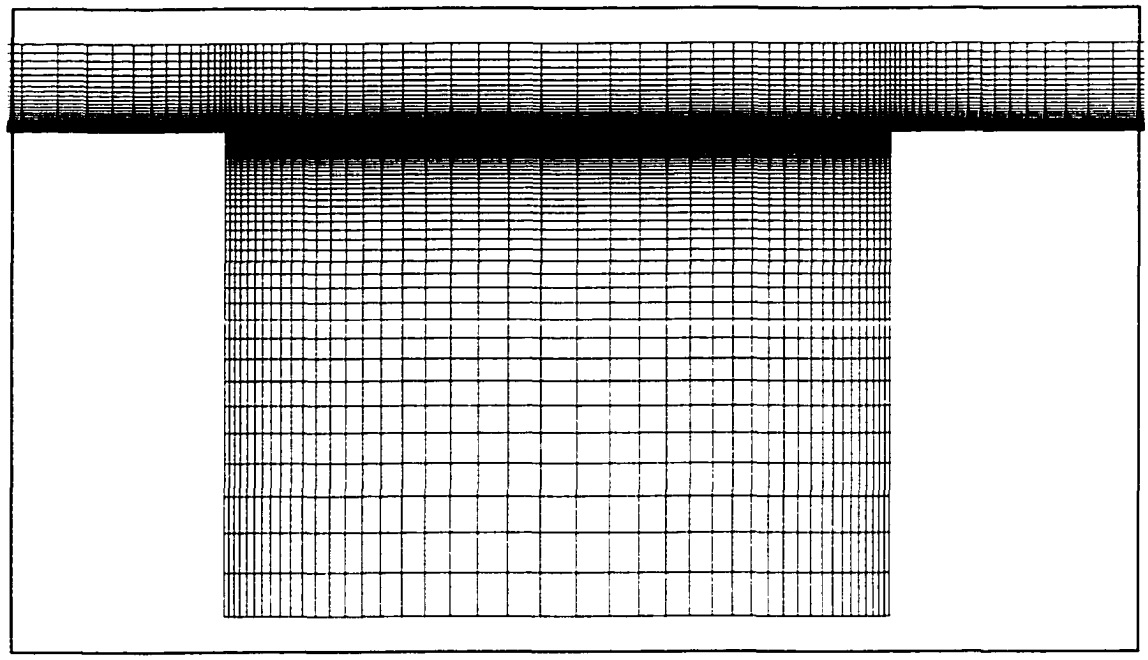

Figure 5.16: Schematic view of a typical grid array around the side gap

1.1 mm average shrinkage of boards during drying, and 0.4 mm standard deviation of board width, was investigated. A proper grid refinement adjacent to the leading and trailing edges of each board was performed in order to better resolve the flow and heat/mass transfer around the edges and inside the gaps. Over refinement in gap area caused an instability in the numerical procedure due to very small values of turbulence parameters initiated from small velocity components and their perturbations near the vertical walls. A typical grid array around the gap is shown in Figure 5.16.

5.2.2 Effect of irregularities due to shrinkage and sawing

The results of local Nu number versus dimension-less horizontal distance for this case are compared in Figure 5.17 with the results of the case without side gaps. A sharp increase in Nu_x is observed after each gap. After that, an asymptotic behaviour is seen apart from the slight increase in the last 2-3 points of each board. The maximum

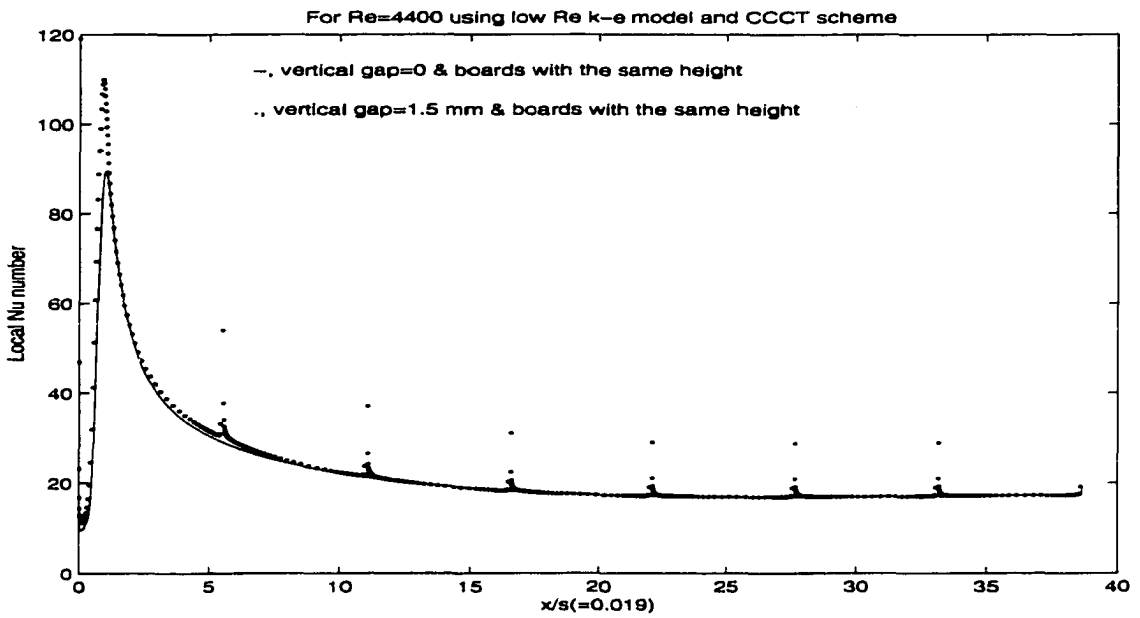

Figure 5.17: Comparison of the distribution of local Nu number for the Li's geometry having vertical side gap (due to shrinkage and sawing) with the case without side gap at Re=4400

value of local Nu number on the first board occurs at $\frac{x}{s} = 0.96$ for the case with side gaps of 1.5 mm and at $\frac{x}{s} = 1.03$ for the case of no side gaps.

The effect of irregularity in board heights due to sawing was taken into account by considering the second board to be taller than the others. The height difference was taken equal to the standard deviation of the average board height (0.4mm). Figure 5.18 compares this case, shown by (-) sign, with the case without such irregularity, represented by (.) sign. Comparison of these curves shows that their main differences are on the second, third, and fourth boards and at the end of the first board. At the end of the first board, flow gradually "senses" the stagnation effect of the vertical surface of the second taller board causing a decrease in the flow velocity as well as the Nu number. On the second board a decrease in the curve of the taller board is observed. Then on the start of the third board, a sharp decrease in curve appears. This is due to separation from the trailing edge of the second board which is taller

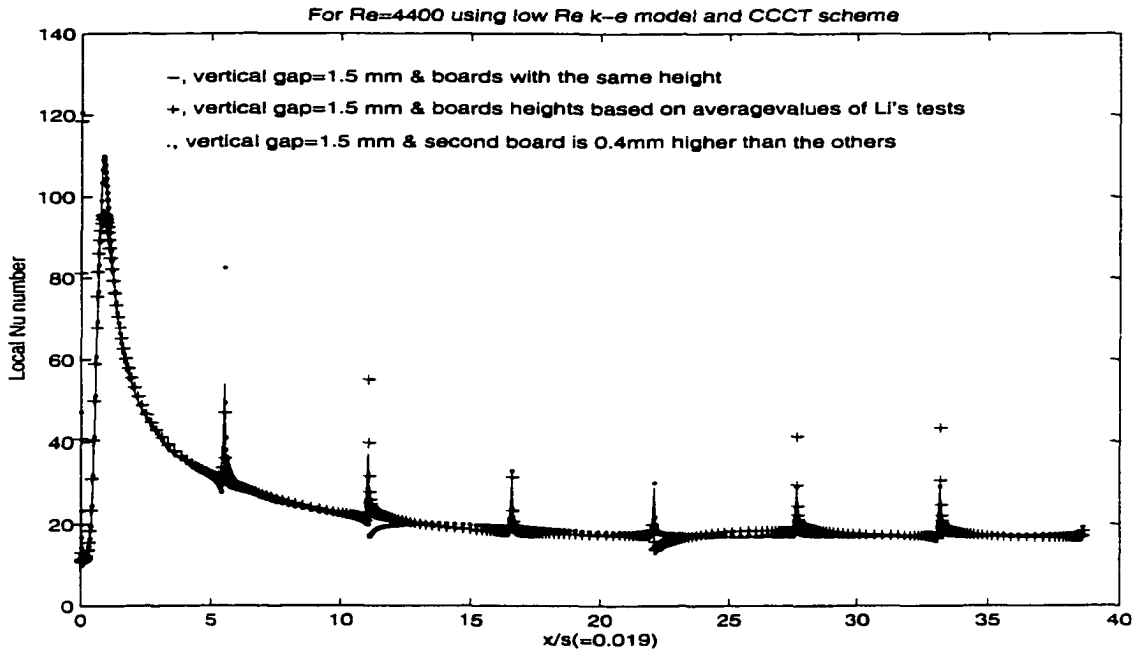

Figure 5.18: Comparison of the distribution of local Nu number for the Li's geometry with different boards heights at Re=4400

than the next board. At the beginning of the third board the main flow is away from the board surface and gradually reattaches to its surface resulting in the asymptotic increasing trend. Also, another case shown in this figure by (+) sign, was considered based on the average height of the boards during the drying period (average of the dry and wet board thickness).

5.2.3 Effect of different gap sizes

Further computations were carried out for the boards with the same height but with different side gaps of g=11.5, 21.5, 31.5, 36.5, 41.5 and 51.5 mm. Local Nu number distributions on horizontal walls for these cases and the one for g=1.5 mm are compared in Figure 5.19. The results are the same for the first board in the stack. Except for the first two points at the beginning of each board, the results for various

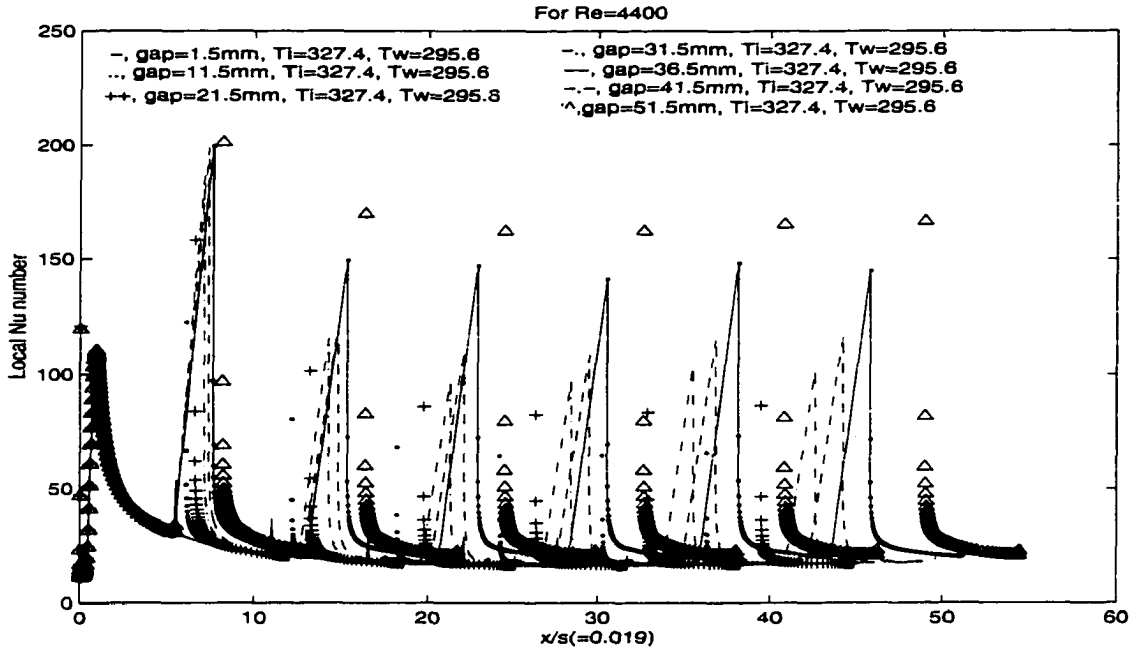

Figure 5.19: Comparison of the distribution of local Nu number for the Li's geometry with different vertical side gaps at Re=4400

gap sizes up to $g = 36.5mm$ are the same. A sudden increase in local Nu is observed by changing the gap size from $g = 36.5$ to $41.5mm$. For the larger gap sizes, the Nu disribution does not change.

Local Nu number on front vertical walls of the boards for different gap sizes are plotted in Figures 5.20 to 5.26. For the first board, the gap size has no effect. At the center of the board ($\frac{y}{D} = 0$) Nu is considerable (about 18) due to stagnation flow in this area and stays more or less the same in most of the wall. Close to the edge, it suddenly enhances as a result of entrance.

For the other boards, the trend is somewhat similar when $g < 41.5mm$ with this difference that at the center of the board Nu is almost zero. Increasing the gap size, enhances the slope of Nu and its value till a sudden increase is observed after $g = 36.5mm$. For larger gap sizes a considerable Nu value is seen after the center of

the board which is decreased till $\frac{y}{D} = 0.3$ and then follows the increasing trend. The Nu values are larger for the second board and almost the same after the third one.

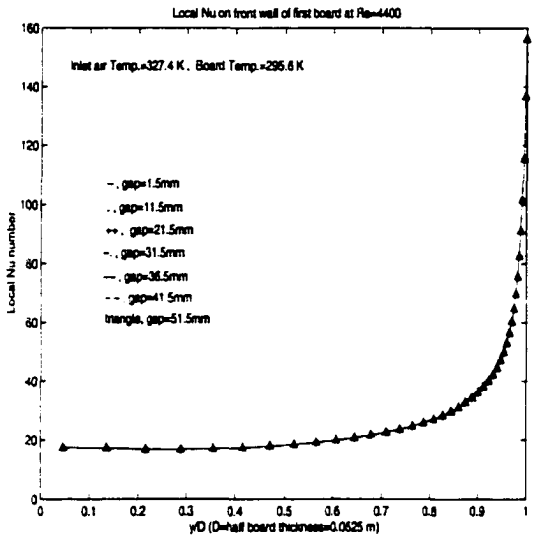

Figure 5.20: Local Nu number on front wall of the first board for the Li's geometry with different side gaps at Re=4400

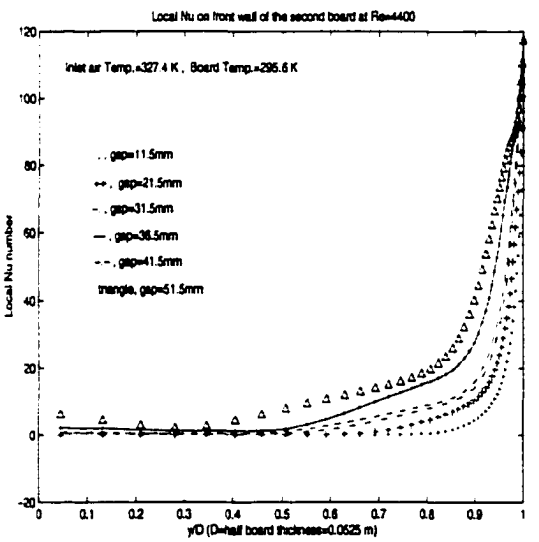

Figure 5.21: Local Nu number on front wall of the second board for the Li's geometry with different side gaps at Re=4400

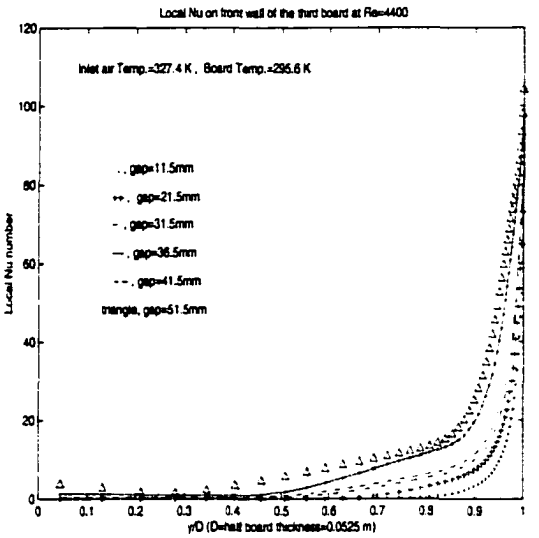

Figure 5.22: Local Nu number on front wall of the third board for the Li's geometry with different side gaps at Re=4400

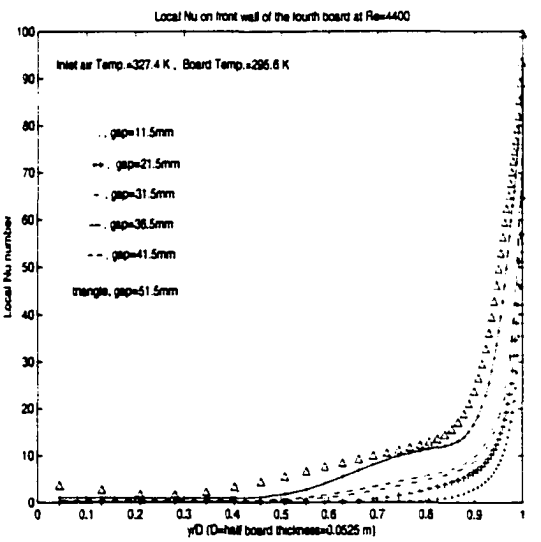

Figure 5.23: Local Nu number on front wall of the fourth board for the Li's geometry with different side gaps at Re=4400

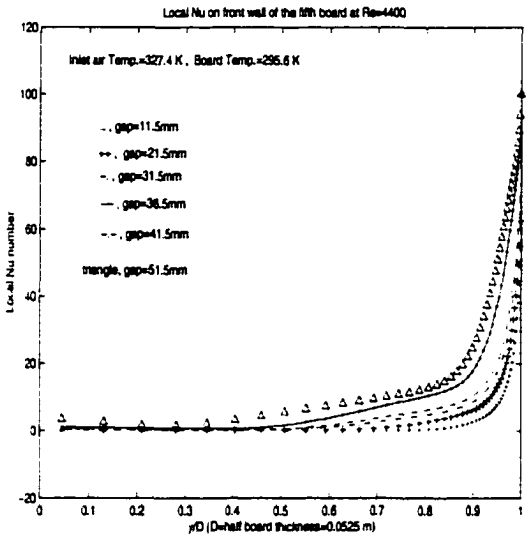

Figure 5.24: Local Nu number on front wall of the fifth board for the Li's geometry with different side gaps at Re=4400

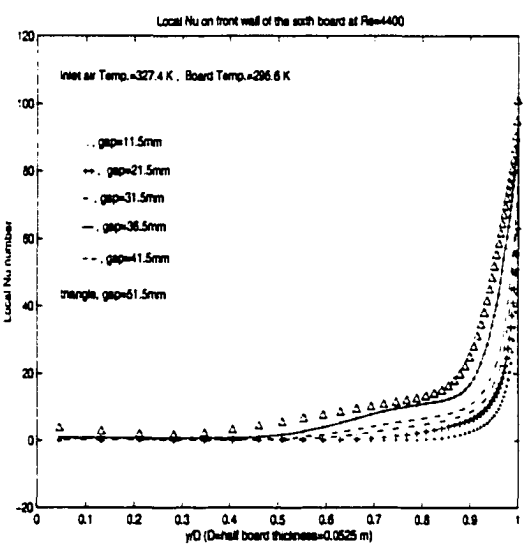

Figure 5.25: Local Nu number on front wall of the sixth board for the Li's geometry with different side gaps at Re=4400

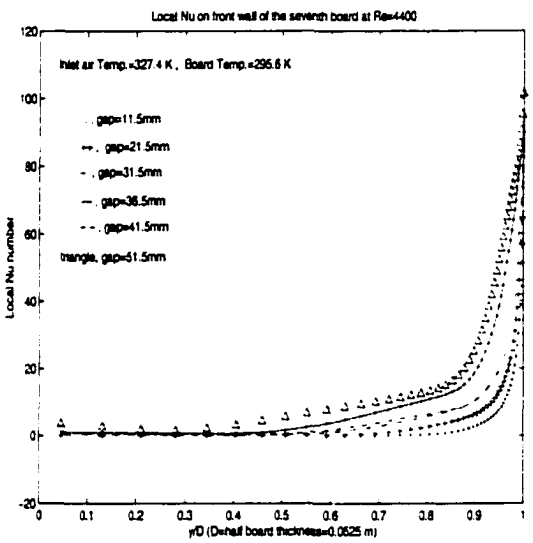

Figure 5.26: Local Nu number on front wall of the seventh board for the Li's geometry with different side gaps at Re=4400

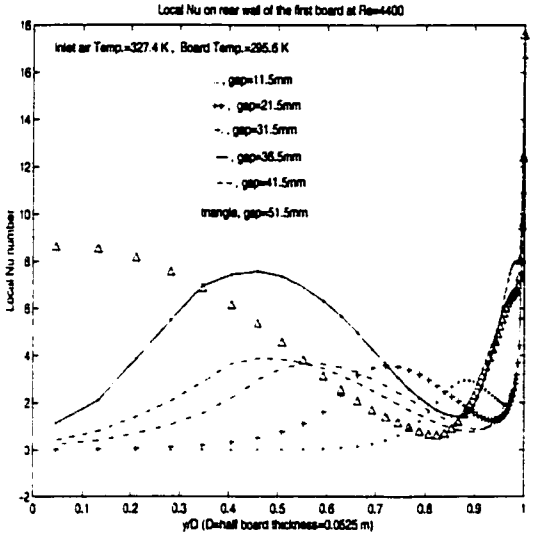

Figure 5.27: Local Nu number on rear wall of the first board for the Li's geometry with different side gaps at Re=4400

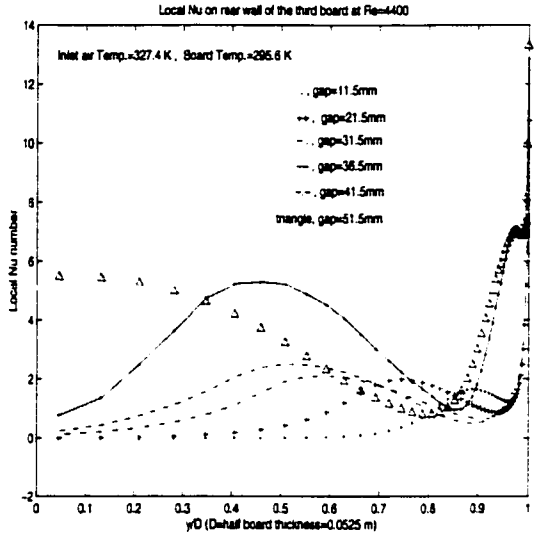

Figure 5.29: Local Nu number on rear wall of the third board for the Li's geometry with different side gaps at Re=4400

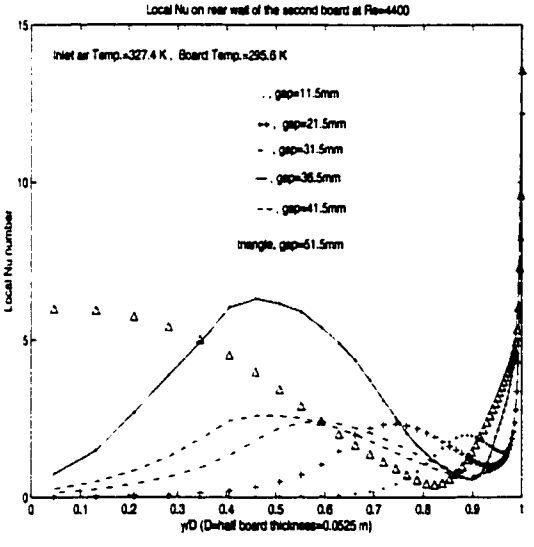

Figure 5.28: Local Nu number on rear wall of the second board for the Li's geometry with different side gaps at Re=4400

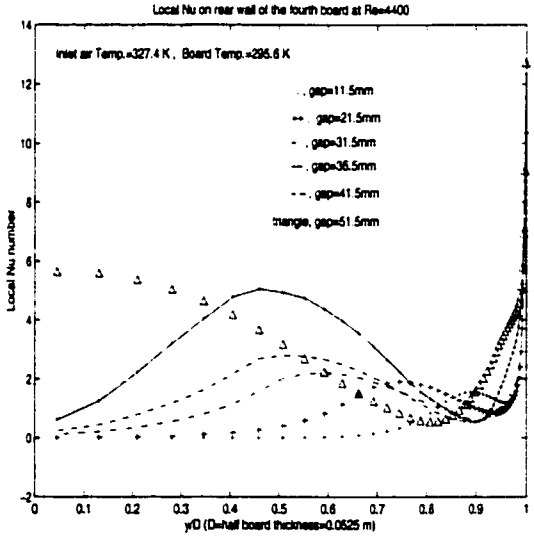

Figure 5.30: Local Nu number on rear wall of the fourth board for the Li's geometry with different side gaps at Re=4400

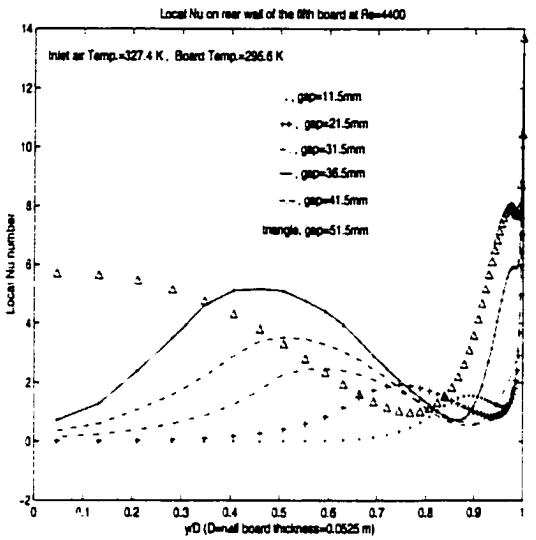

Figure 5.31: Local Nu number on rear wall of the fifth board for the Li's geometry with different side gaps at Re=4400

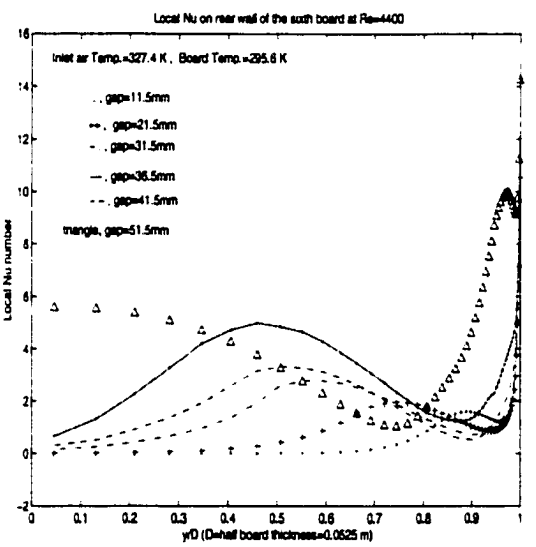

Figure 5.32: Local Nu number on rear wall of the sixth board for the Li's geometry with different side gaps at Re=4400

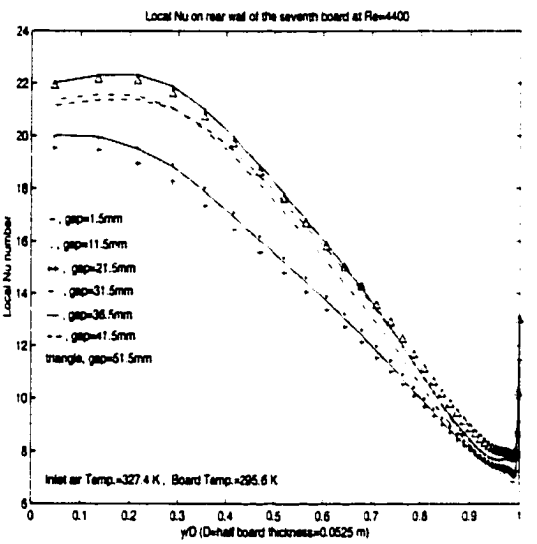

Figure 5.33: Local Nu number on rear wall of the seventh board for the Li's geometry with different side gaps at Re=4400

Figures 5.27 to 5.33 show the local Nu on rear walls of the boards. As a result of the large recirculation after the last board, the behaviour of Nu on rear wall of the seventh board is different than the others. Here, Nu is considerable around the board center and decreases with height to one third of its initial value till very close to the edge ($\frac{y}{D} = 0.98$) that suddenly gains some of its loss due to main stream influence. A sudden increase in local Nu is observed when the gap size is changed from 31.5 mm to 36.5 mm. For larger gap sizes, an slight increase in Nu around $\frac{y}{D} = 0.1$ to 0.2 happens due to interaction of small vortices at the back with the main one. A second smaller increase in Nu is distinguished when the gap size is increased from 36.5 mm to 41.5 mm. Further enhancements of the gap size do not change the Nu distribution significantly.

For the other boards, the gap size has a more considerable effect on Nu distributions. For $g < 41.5mm$, Nu is very small at board center and increases to a local maximum followed by a local minimum and a sudden increase around the edge to an absolute maximum value. By enhancing the gap size, the location of local maximum and minimum moves toward the center of the board accompanied by an increase in average Nu. Here like the horizontal walls, altering the gap size from 36.5 to 41.5 mm causes a sudden increase in local Nu. The average Nu remains the same by changing the gap size to 51.5 mm while the location of local maximum moves towards the center and for some boards a second local maximum appears close to the edge.

Also the comparison of total heat transfer to boards is presented in Table 5.2. Total heat transfer from air to the boards slowly increases with increasing the gap sizes up to g=36.5 mm (the case of $g = 36.5mm$ shows 10.7 percent increase relative to $g = 1.5mm$ case). This is due to heat transfer increase from the vertical edges of the boards. Here the gain in heat transfer due to enhancing the gap drops from 1040 W/m at $g = 11.5mm$ to 840 at $g = 21.5mm$. A sudden increase of 15.6 percent

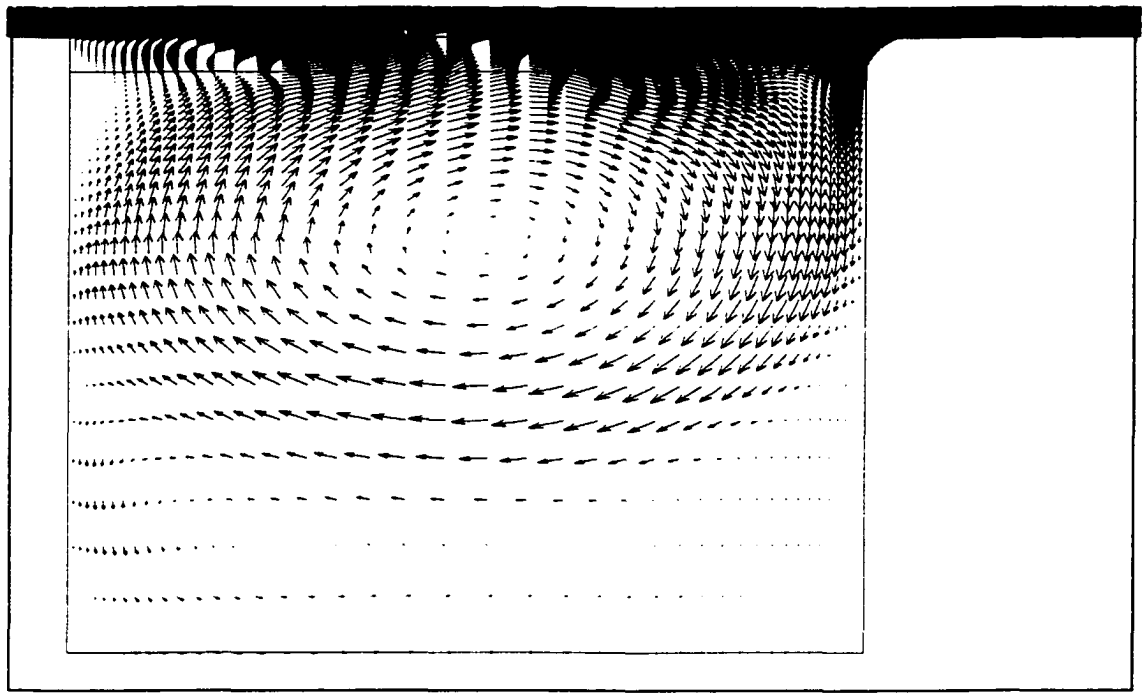

Figure 5.34: Velocity vectors inside the gap of g=41.5 mm at Re=4400

in the total heat transfer mostly due to a similar increase in the local Nu number distribution is observed by going from the gap size of $g = 36.5$ to $g = 41.5mm$ resulting in a jump in $\frac{\Delta Q}{\Delta g}$ to 10080 W/m. Any further increase in the gap size did not affect the distribution of the local Nu number on horizontal walls while a smaller enhancement was observed in the total heat transfer and $\frac{\Delta Q}{\Delta g}$ due to changes in Nu on vertical walls. On the other hand, one can therefore suggest that the gap size after which no significant increase in the total heat transfer, Nusselt number and $\frac{\Delta Q}{\Delta g}$ was observed may be taken as the optimum gap for drying of a stack of wood planks, namely for Re=4400, $g_{opt} = 41.5$ mm.

Velocity vectors in the gap area for the case of g=41.5 mm are shown in Figure 5.34. Above conclusions may be justified by the following reasoning. Study of the flow field inside the gap area shows that the size of vortex inside the gap increases

boards height condition	gap size g (mm)	total heat transfer,$\dot{Q}(W)$	$\frac{\dot{Q}-\dot{Q}^*_{1.5}}{\dot{Q}^*_{1.5}} \times 100$ (%)	$\frac{\Delta\dot{Q}}{\Delta g}$ ($\frac{W}{m}$)
the same	0	312.4	-	
the same*	1.5	322.5	3.23 relative to g=0	-
only 2nd board 0.4 mm taller	1.5	325.1	0.8	-
average heights of Li's test	1.5	326.9	1.4	-
the same	11.5	332.9	3.2	1040
the same	21.5	341.3	5.8	840
the same	31.5	351.2	8.9	990
the same	36.5	357.0	10.7	1160
the same	41.5	407.4	26.3	10080
the same	51.5	428.4	32.8	2100

Table 5.2: Comparison of the results of total heat transfer to 7 boards for different cases at Re_{D_h}=4400 (heat transfer rates are for unit length of lumber)

with the gap size after g=1.5 mm. This enhances the heat transfer from the vertical edges of the boards. Gradually, smaller vortices develop in the corner regions by further increases in gap sizes. It is thought that the presence of these vortices and their interactions may be responsible for the sudden increase in the local Nu number distributions on horizontal walls and other changes of Nu on vertical faces.

Drying time comparisons

To investigate the influence of the gap size on total heat/mass transfer, the following calculations were carried out.

Let V_l be the total volume of lumber to be dried, q_l be the heat/mass to be transfered per unit volume of lumber. Assuming the average rate of heat/mass transfer per each stack array as $\dot{Q}$ and n_{st} the number of stacks per kiln, the total time of kiln

working, t, will be:

$$t = \frac{q_l V_l}{\dot{Q} n_{st}} \quad , \tag{5.1}$$

where:

$$n_{st} = \frac{V_{kiln-eff}}{V_{stack}} \quad , \tag{5.2}$$

and $V_{kiln-eff}$ and V_{stack} are effective volume of kiln and stack volume, respectively. Therefore:

$$t = \frac{q_l V_l V_{stack}}{\dot{Q} V_{kiln-eff}} \; . \tag{5.3}$$

For a specific kiln used for drying a certain amount of lumber, the dependency of t will become:

$$t \propto \frac{V_{stack}}{\dot{Q}} \; . \tag{5.4}$$

If the parameters of the stack set up, except the gap size, remain unchanged, then:

$$t \propto \frac{l_{stack}}{\dot{Q}} \quad , \tag{5.5}$$

where l_{stack} is the length of each stack. Letting the distance between two adjacent stacks be 100 mm, l_{stack} can be calculated by:

$$(l_{stack})_{g=1.5} = (7 \times 103.5) + (6 \times 1.5) + 100 = 833.5 \; mm \; . \tag{5.6}$$

Now the difference in t using different gap sizes can be compared with the $g = 1.5$ mm case. Table 5.3 compares the calculated differences in time t with respect to $g = 1.5$ mm, using the above method. The Table shows that increasing the gap size up to $g = 36.5$ mm increases the total drying time up to 13.1%. But using the optimum gap size of 41.5 mm only causes 1% increases in the total drying time of a given amount of lumber. The cost of enhancement in the total drying time is due to reloading the

gap size g (mm)	stack length l_{stack} (mm)	% increase in t relative to g=1.5 mm case
11.5	893.5	3.85
21.5	953.5	8.1
31.5	1013.5	11.66
36.5	1043.5	13.1
41.5	1073.5	1.95
51.5	1133.5	2.38

Table 5.3: Comparison of the results of total time of drying for different cases at Re_{D_h}=4400

kiln, more energy consumption, manpower and utilities. The above calculations show that if the optimum gap size is used this extra cost is less than the extra income due to the better quality of the lumber and less degradation due to more uniform drying of boards. Another conclusion is that total drying time in addition to percentage of increase in total heat transfer ($\frac{\dot{Q}-\dot{Q}^*_{1.5}}{\dot{Q}^*_{1.5}} \times 100$) and $\frac{\Delta \dot{Q}}{\Delta g}$ can be used to decide about the optimum gap size and its effect on the total cost of drying.

5.2.4 Effect of Re number

Similar computations were also carried out for Re=8800 and 13200 (u_{centre} = 5.08 and 7.62 m/s, respectively). Since the local Nu distribution does not change significantly after the fourth board, only four boards in the stream-wise direction were considered. The results for horizontal wallls are presented in Figures 5.35 and 5.36. The trend in the beginning of the first board is slightly different from the Re=4400 case by having two local maximums inside the separation zone on top of the first board instead of one observed for Re=4400. In these high Re number cases, the changes in the total heat transfer from the boards become more sensitive to changes in the gap size.

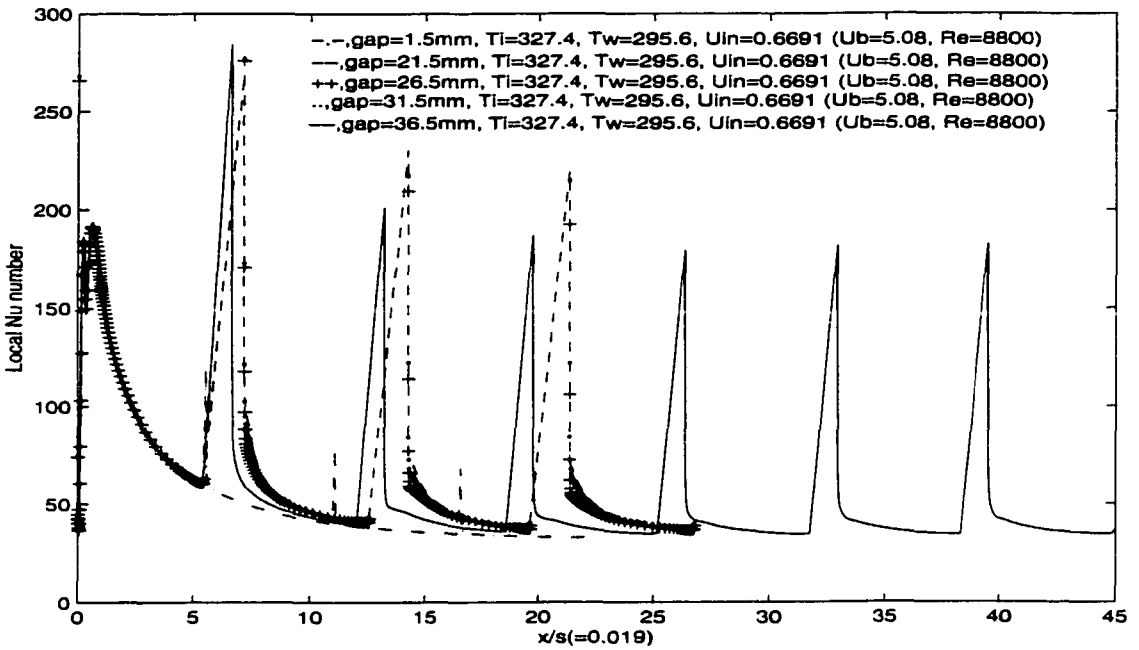

Figure 5.35: Comparison of the distribution of local Nu number for the Li's geometry with different vertical side gaps at Re=8800

This is due to higher air velocities observed in the main duct and their propagation effects resulting from higher degree of turbulence. Here, even before sudden change in the local Nu number starts (at g = 21.5 and 16.5mm for Re=8800 and 13200. respectively), the local Nu number on horizontal walls is enhanced by increasing the gap size. At Re=8800 and 13200, the sudden change phenomena which started at g = 21.5 mm and 16.5 mm, continues up to g = 26.5mm and 21.5 mm, repectively.

Figures 5.37 to 5.40 show the local Nu on front walls of the first, second, third and last boards at Re=8800, respectively. The same distributions for Re=13200 are plotted in Figures 5.41 to 5.44. Nu numbers at each location increase with Re number. On the first board, unlike the Re=4400 case, Nu has a larger value at the center of the board followed by a small drop. Only a small increase in Nu distribution happens if Re is changed from 8800 to 13200 keeping the gap size 21.5mm. The absolute

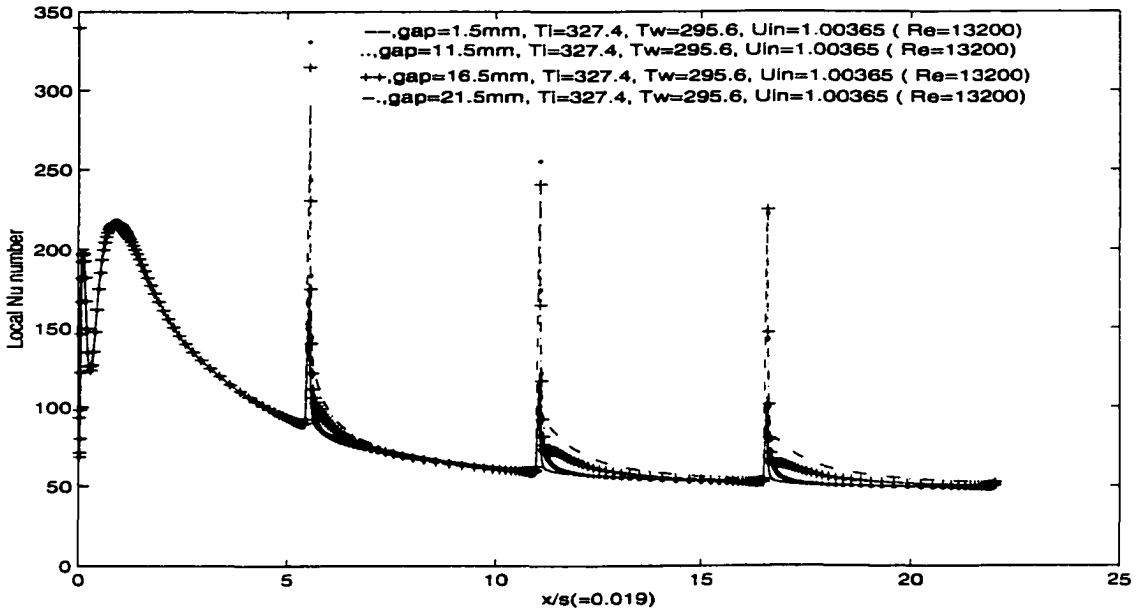

Figure 5.36: Comparison of the distribution of local Nu number for the Li's geometry with different vertical side gaps at Re=13200

maximum at the edge ($\frac{y}{D} = 1$) is almost the same at all Re numbers.

Nu distributions on rear walls of the boards are shown for Re=8800 in Figures 5.45 to 5.48 and for Re=13200 in Figures 5.49 to 5.52. At g = 21.5mm. increasing the Re number cause an increase in Nu distribution. However, Re number does not affect the trend and locations of local maximum for inside the gaps. On the back of the last board, the trend is totally different from Re=4400 case. It starts with a small value (12-13) followed by an increase to a local maximum. The location of this maximium moves upward by increasing the Re number showing a larger recirculation zone at the back.

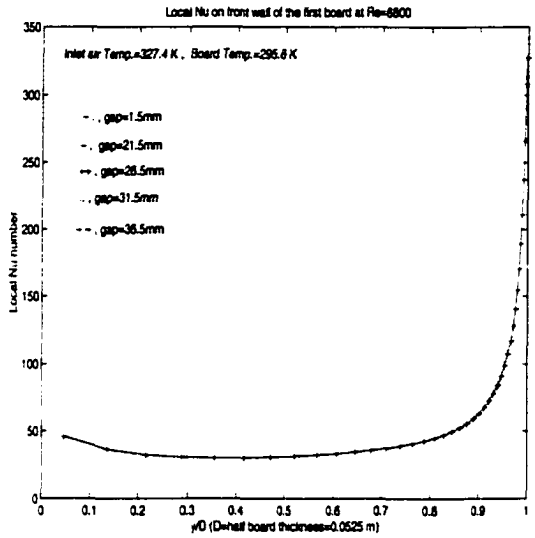

Figure 5.37: Local Nu number on front wall of the first board for the Li's geometry with different side gaps at Re=8800

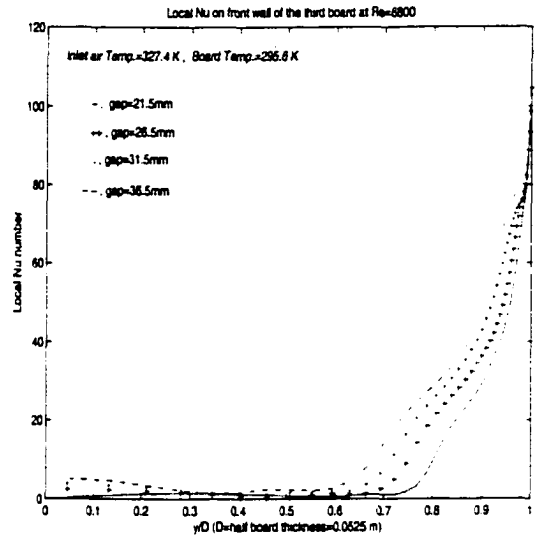

Figure 5.39: Local Nu number on front wall of the third board for the Li's geometry with different side gaps at Re=8800

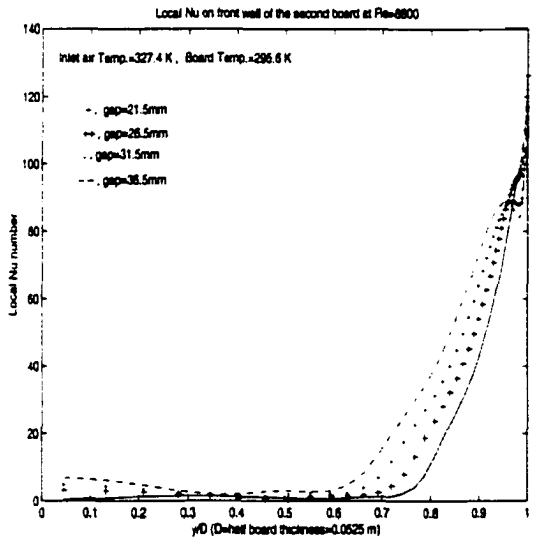

Figure 5.38: Local Nu number on front wall of the second board for the Li's geometry with different side gaps at Re=8800

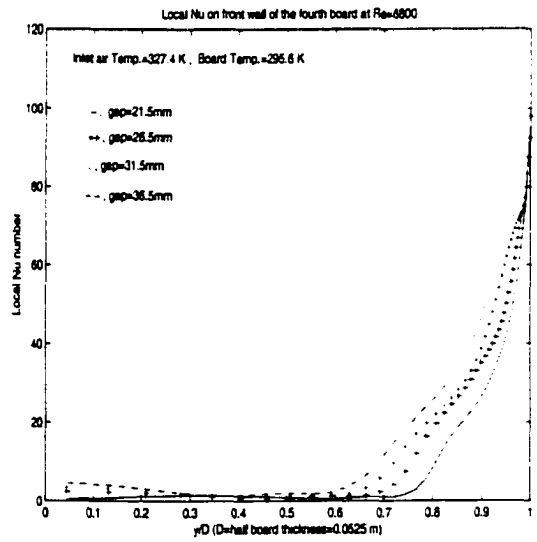

Figure 5.40: Local Nu number on front wall of the last board for the Li's geometry with different side gaps at Re=8800

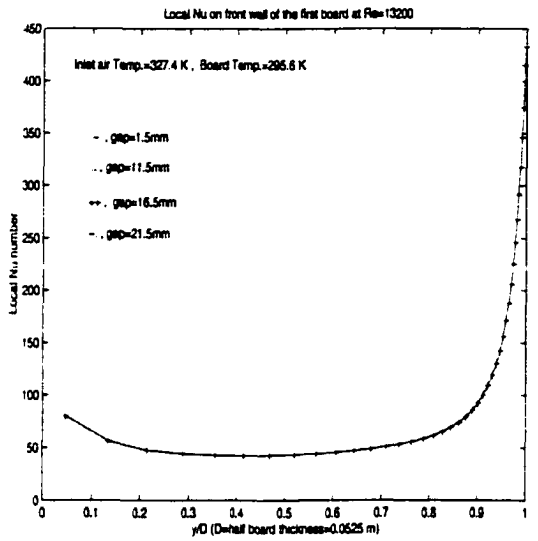

Figure 5.41: Local Nu number on front wall of the first board for the Li's geometry with different side gaps at Re=13200

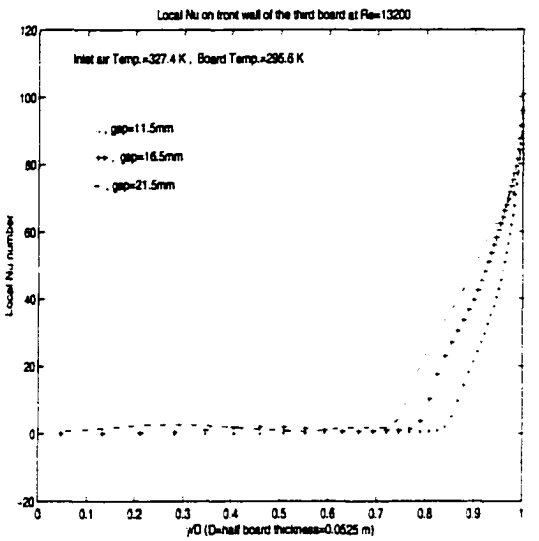

Figure 5.43: Local Nu number on front wall of the third board for the Li's geometry with different side gaps at Re=13200

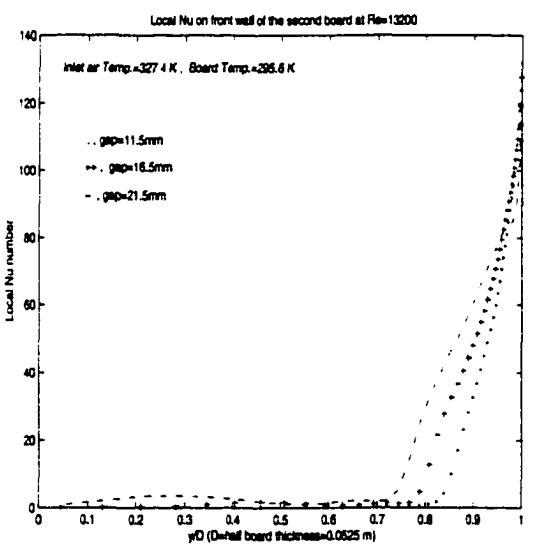

Figure 5.42: Local Nu number on front wall of the second board for the Li's geometry with different side gaps at Re=13200

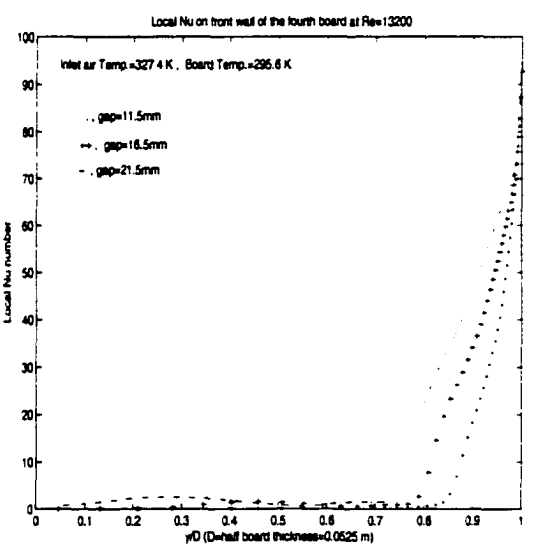

Figure 5.44: Local Nu number on front wall of the last board for the Li's geometry with different side gaps at Re=13200

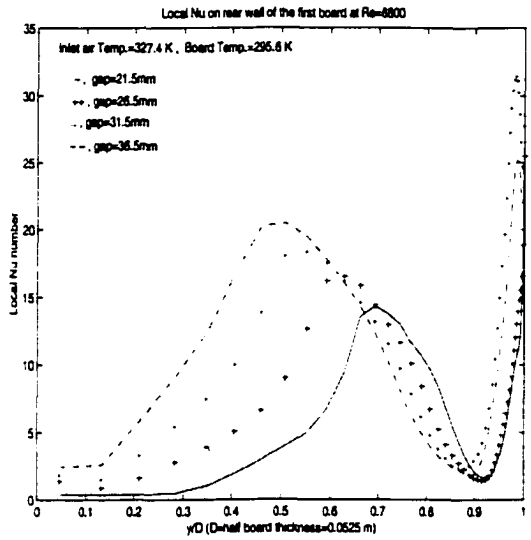

Figure 5.45: Local Nu number on rear wall of the first board for the Li's geometry with different side gaps at Re=8800

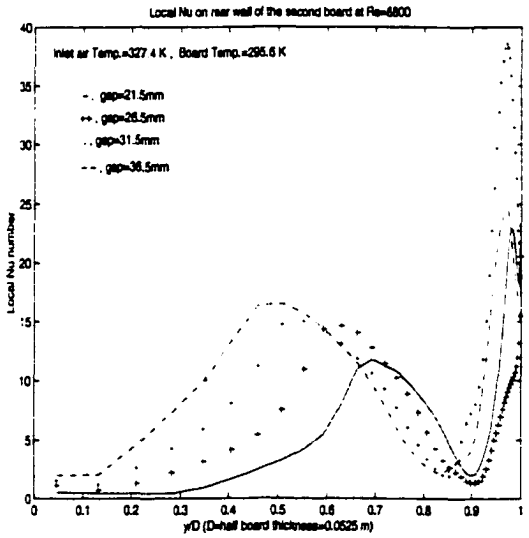

Figure 5.46: Local Nu number on rear wall of the second board for the Li's geometry with different side gaps at Re=8800

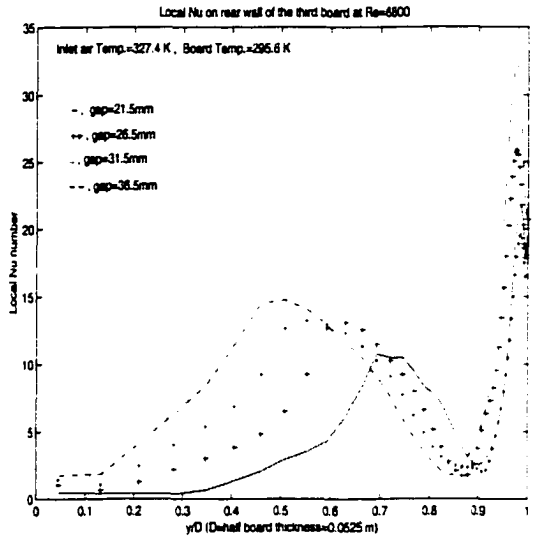

Figure 5.47: Local Nu number on rear wall of the third board for the Li's geometry with different side gaps at Re=8800

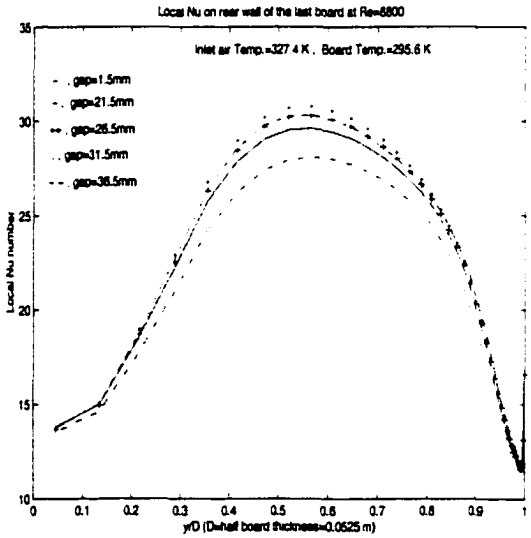

Figure 5.48: Local Nu number on rear wall of the fourth board for the Li's geometry with different side gaps at Re=8800

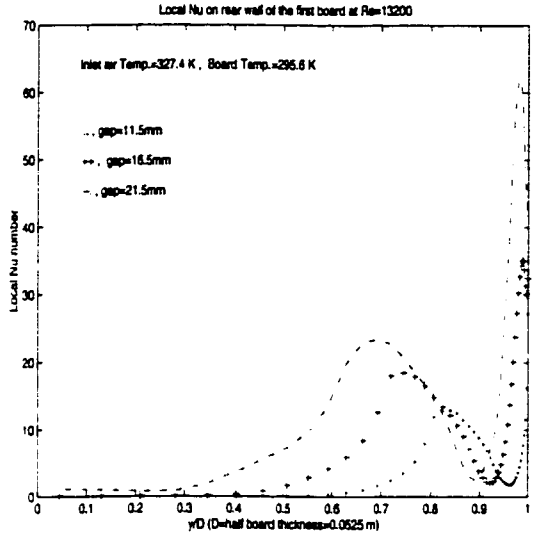

Figure 5.49: Local Nu number on rear wall of the first board for the Li's geometry with different side gaps at Re=13200

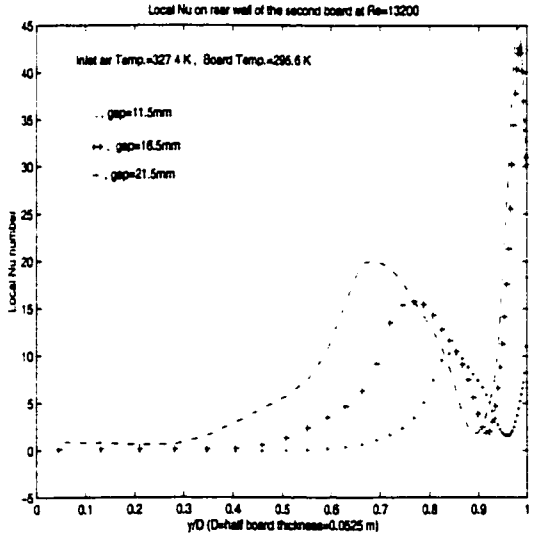

Figure 5.50: Local Nu number on rear wall of the second board for the Li's geometry with different side gaps at Re=13200

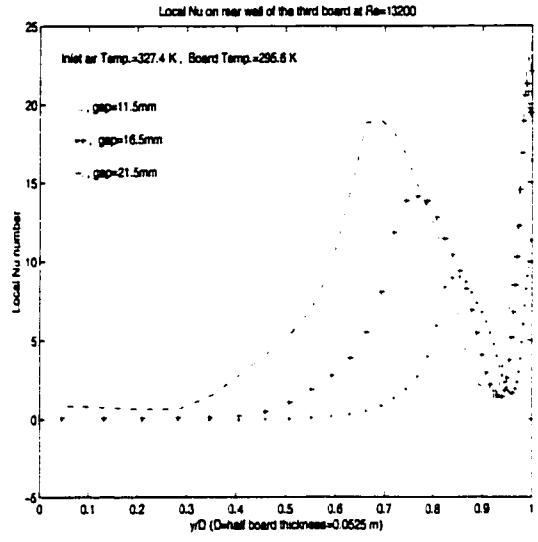

Figure 5.51: Local Nu number on rear wall of the third board for the Li's geometry with different side gaps at Re=13200

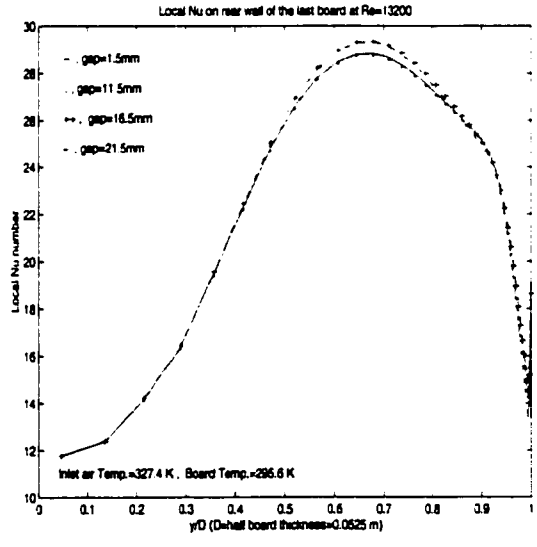

Figure 5.52: Local Nu number on rear wall of the fourth board for the Li's geometry with different side gaps at Re=13200

gap size g (mm)	total heat transfer,$\dot{Q}(W)$	$\frac{\dot{Q}-\dot{Q}_{1.5}}{\dot{Q}_{1.5}} \times 100$ %	$\frac{\Delta\dot{Q}}{\Delta g}$ $\frac{W}{m}$	$\frac{t-t_{1.5}}{t_{1.5}} \times 100$ %
1.5	686.0	-	-	-
21.5	741.4	8.1	2770	+5.8
26.5	830.3	21.0	17780	-2.5
31.5	865.0	26.1	6940	-3.6
36.5	894.4	30.4	5880	-4.0

Table 5.4: Comparison of the results of total heat transfer to 7 boards for different cases at Re_{D_h}=8800 (heat transfer rates are for unit length of lumber)

Tables 5.4 and 5.5 compare the results of total heat transfer and drying time as well as $\frac{\Delta\dot{Q}}{\Delta g}$ at different gap sizes for Re=8800 and 13200, respectively. For Re=8800, we saw that Nu number distributions do not change significantly for $g > 26.5$ mm. Here also the maximum $\frac{\Delta\dot{Q}}{\Delta g}$ happens at this gap size. Total drying time at this condition is estimated to be 2.5% less than the without extra gap case (g=1.5mm). This is an important finding that at higher Re numbers the extra gap size can reduce the total drying time. Based on the above discussions $g = 26.5$mm can be considered as the optimum gap size for Re=8800. Another important finding is that for Re=8800 and $g_{opt} = 26.5$mm, the total heat transfer is more than double the Re=4400 case at its optimum gap size of 41.5 mm.

At Re=13200, the sudden increase in Nu distributios, total heat transfer and $\frac{\Delta\dot{Q}}{\Delta g}$ is first observed at $g = 16.5$mm accompanied by a sudden drop in total drying time. But the gains are more considerable at $g = 21.5$mm making it the optimum gap choice. Such a gap reduces the total drying time 1.8 percent compared to $g = 1.5$mm and triples the total heat transfer compared to the optimum choice at Re=4400.

gap size g (mm)	total heat transfer,$\dot{Q}(W)$	$\frac{\dot{Q}-\dot{Q}_{1.5}}{\dot{Q}_{1.5}} \times 100$ %	$\frac{\Delta\dot{Q}}{\Delta g}$ $\frac{W}{m}$	$\frac{t-t_{1.5}}{t_{1.5}} \times 100$ %
1.5	1046.1	-	-	-
11.5	1086.1	3.8	4000	+3.3
16.5	1145.3	9.5	11840	+1.2
21.5	1218.8	16.5	14700	-1.8

Table 5.5: Comparison of the results of total heat transfer to 7 boards for different cases at Re_{D_h}=13200 (heat transfer rates are for unit length of lumber)

5.2.5 Effect of inlet and wall temperature/moisture content

It was emphasized in Chapters 2 and 3 that using the mean temperature/moisture content instead of the inlet variables leads to incorrect disributions of surface coefficients. To show such a claim better, the distribution of mean temperature for g=21.5 mm at Re=8800 is plotted against the dimensionless length across the stack in Figure 5.53. The temperature difference between the air and board surface is $31.8°K$ at the inlet and $16.7°K$ at the stack exit. If the inlet conditions were used instead of the mean values, the surface coefficient would have been predicted 47 percent less at the exit and the closeness between the assymptotic values of surface coefficients for the third to seventh boards would have not be observed. This advantage is one of the contributions of the present work. Now the next question is whether the changes in the board surface and inlet air temperature have any effect on the surface coefficients.

The effect of the inlet and wall temperature/moisture content was studied by a series of similar computations with different combinations at Re=4400. First, the wall temperature and air inlet temperature were interchanged in order to observe the effect of heat/mass transfer direction and subsequent changes in the stream-wise

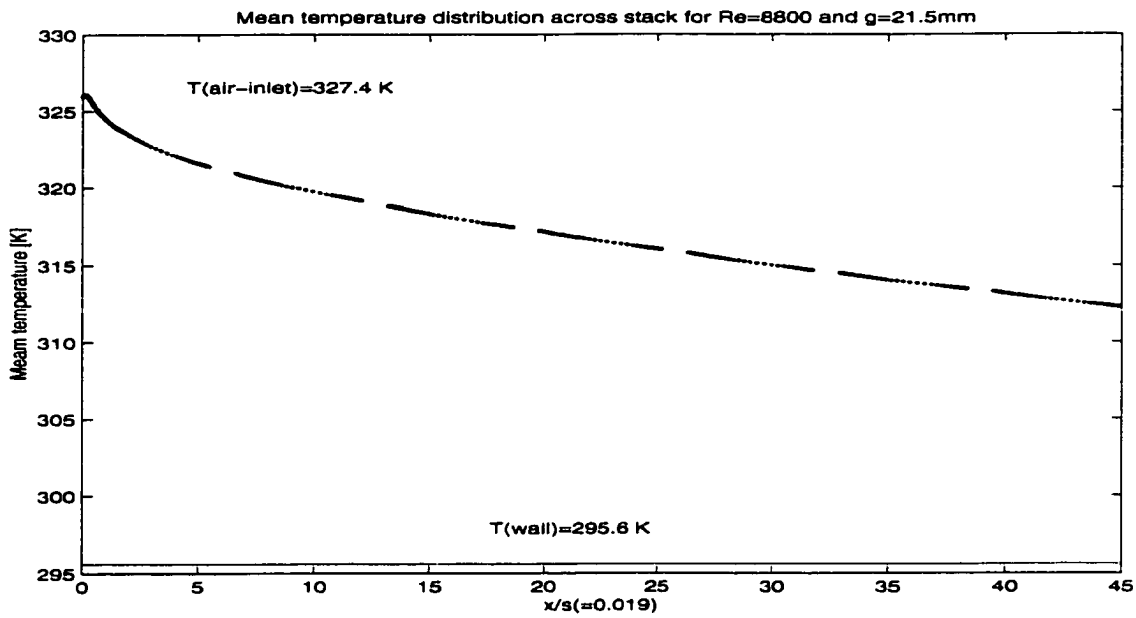

Figure 5.53: Mean temperature distribution across stack for Re=8800 and g=21.5mm

distribution of mean temperature on local and total heat transfer and optimum gap size. The results of the local Nu number are presented in Figure 5.54. Neither of these parameters showed any change.

Then for the numerical procedure, the temperature of different boards in a row were set differently based on the total heat transfer to each board. The computations were carried out for the optimum gap size (g=41.5 mm) and the case just before the optimum size (g=36.5 mm). The results are shown in Figure 5.55.

It can be seen that the wall temperature/moisture content does not have any significant effect on the local Nu and the optimum gap size. This is due to having air Prandtl numbers of about 0.7 and its slight changes with temperature in the kiln temperature range. Based on experimentally suggested equations for internal gas flows[71], usually Nu changes with Pr^n (n=-0.34 to -0.19). Therefore, one can conclude that the local Nu/Sh number distribution for step wise wall temperatures/moisture content can be used for the unsteady case when the wall conditions

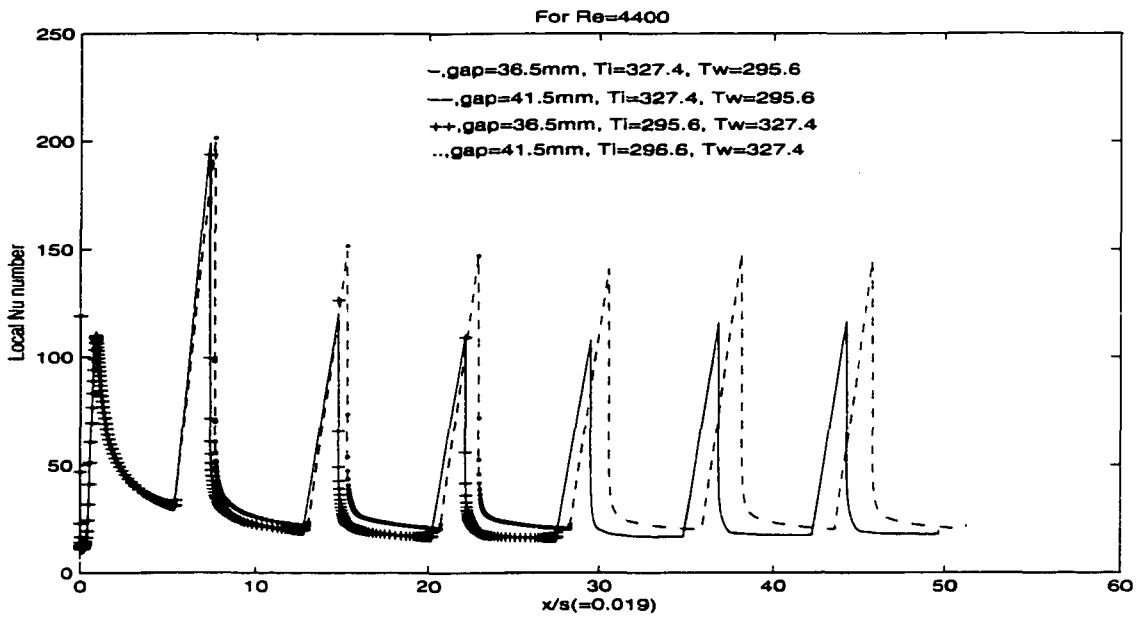

Figure 5.54: Comparison of the distribution of local Nu number for the Li's geometry with two different inlet and wall temperatures at Re=4400

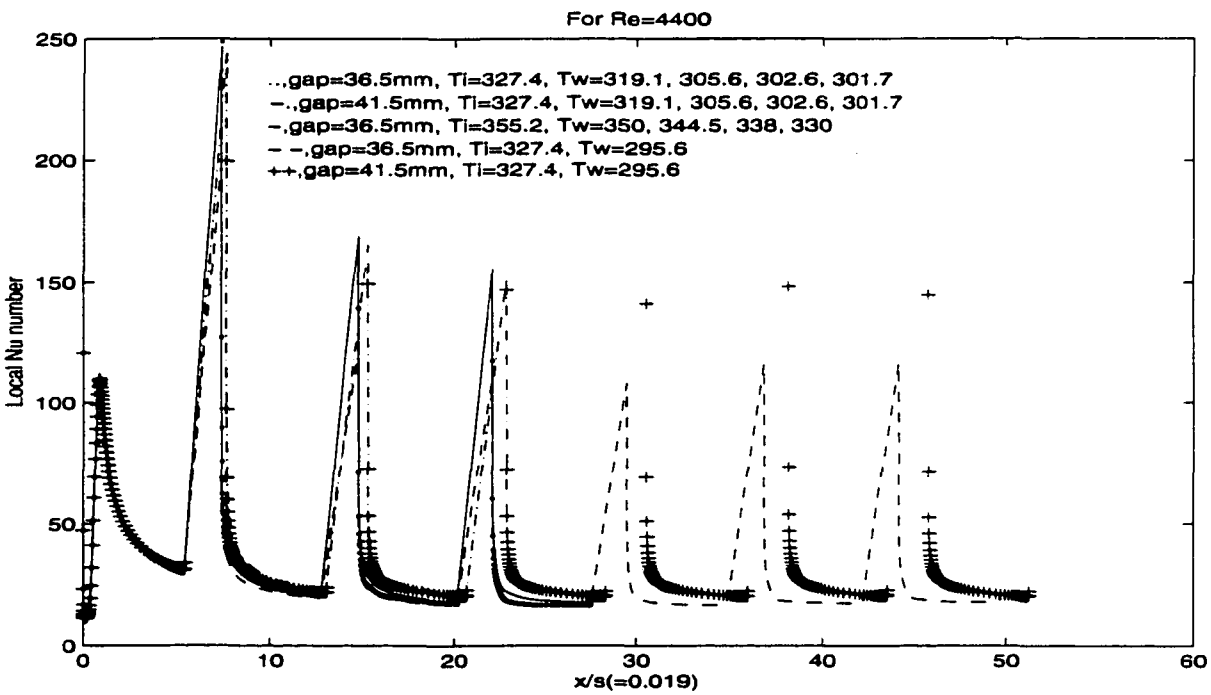

Figure 5.55: Comparison of the distribution of local Nu number for the Li's geometry with different inlet and wall temperatures at Re=4400

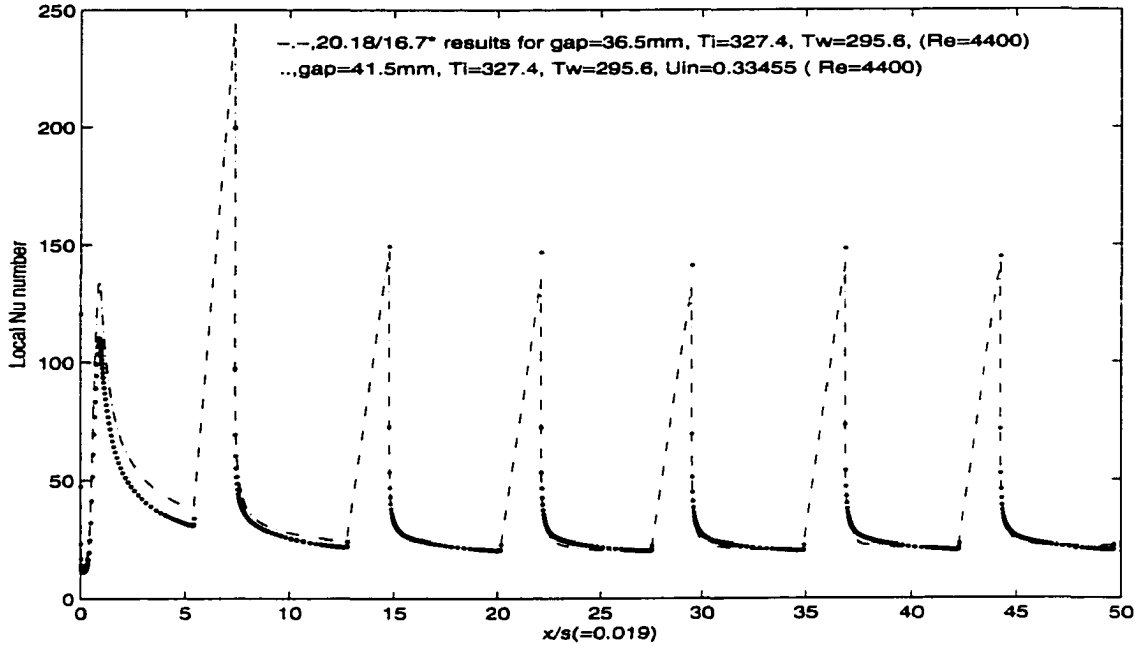

Figure 5.56: Comparison of the distribution of local Nu number for the Li's geometry with g=36.5 and 41.5 mm at Re=4400

are changing with time and space.

5.2.6 Similarities at different Re numbers

Further study of the local Nu number distributions for the cases before and after the jump phenomena shows that they have similar patterns after the second board while they are almost the same in the first board. Figures 5.56 and 5.57 show that for different Re numbers the local Nu distributions before and after the jump can be related by a multlipication factor (ratio of asymptotic values of local Nu numbers). Figure 5.58 shows that the same relation can be established between the Nu distributions of two Re numbers just before the jump at each Re. Figure 5.59 also demonstrates such a relation between the distributions of optimum gap size cases at two Re numbers of 4400 and 8800.

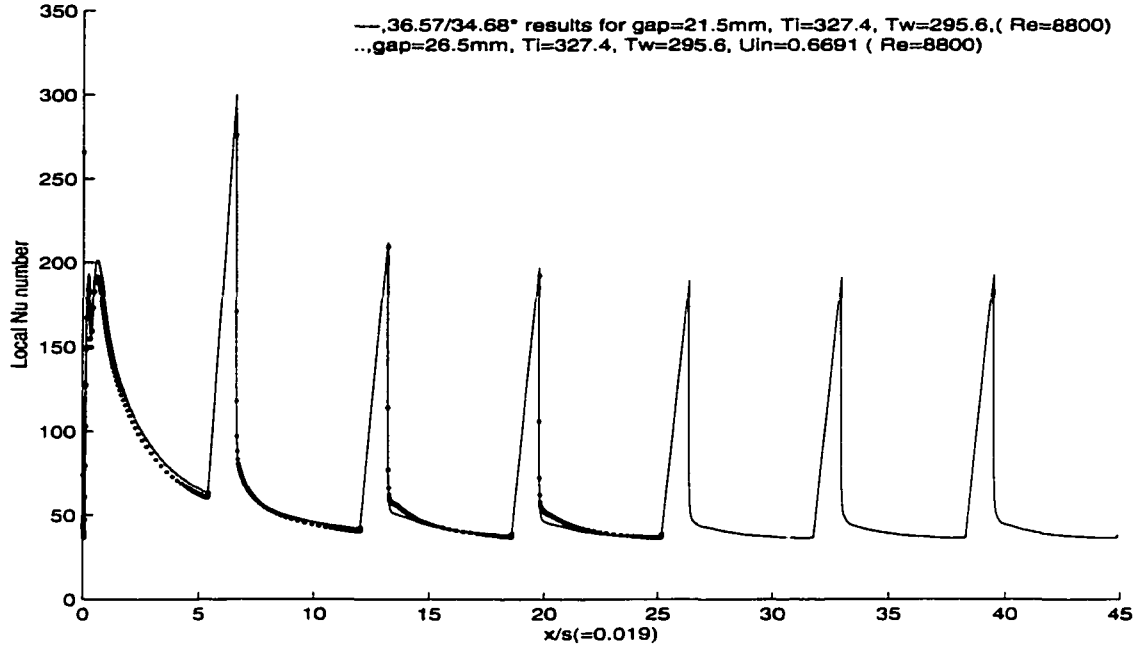

Figure 5.57: Comparison of the distribution of local Nu number for the Li's geometry with g=21.5 and 26.5 mm at Re=8800

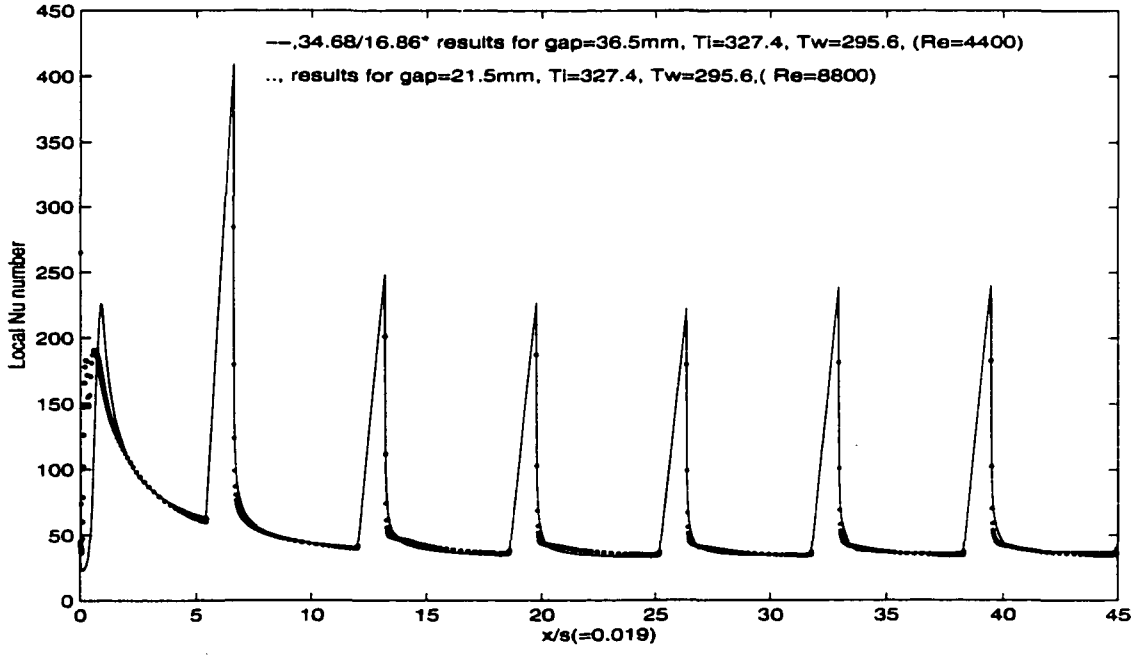

Figure 5.58: Comparison of the distribution of local Nu number just before optimum gap size (g=36.5 at Re=4400 and g=21.5 mm at Re=8800)

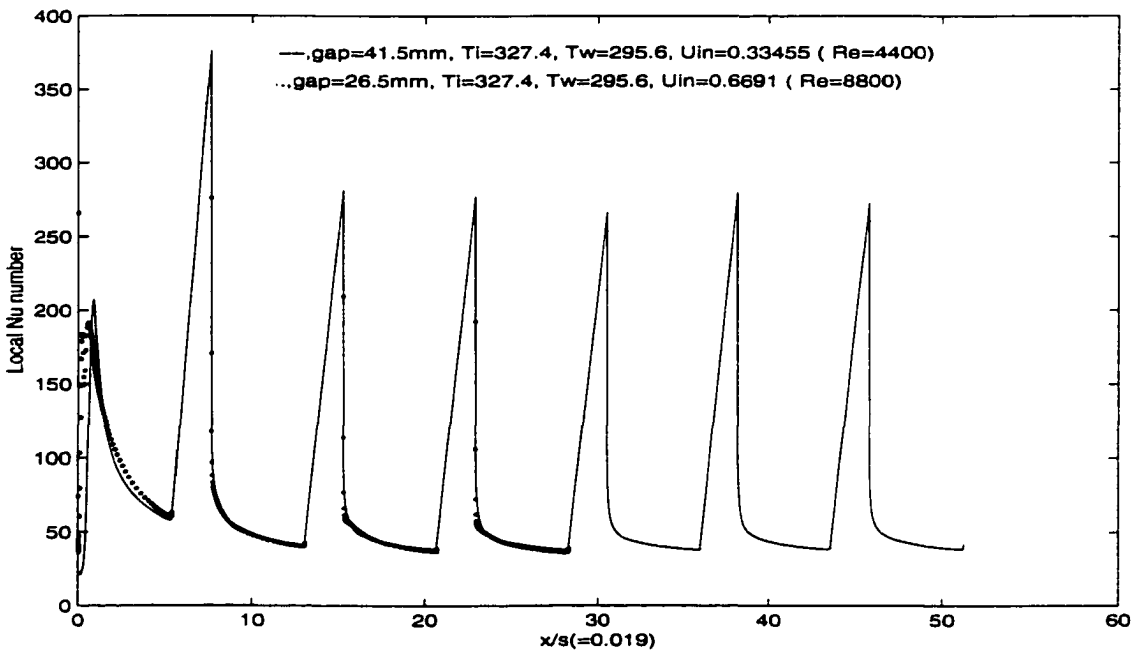

Figure 5.59: Comparison of the distribution of local Nu number for the optimum gap size (g=41.5 at Re=4400 and g=26.5 mm at Re=8800)

Chapter 6

One dimensional numerical simulation of drying process

6.1 Introduction

With the model developed in chapter 4 and the surface coefficients obtained in chapter 5, we are able to predict the temperature and moisture content in lumber drying more accurately. The governing equations developed in the previous section are two dimensional, unsteady, parabolic and non-linear because of the varying coefficients. They can only be solved numerically. As it was mentioned earlier, since wood drying is a relatively slow process, the coefficients D_X, D_T, λ_{eff}, λ_X, $(\rho C_p)_{eff}$ and other properties of different phases generally do not change very rapidly with time. Therefore, the coefficients are evaluated using values from previous time step. This makes the linearization of the system of equation and its discretization possible. In order to have better accuracy, at the beginning of any change in the drying air conditions. smaller values of time steps, Δt, are used. Later, Δt can be increased up to a cer-

tain level which guarantees the stability and physically meaningful results. In the mass transport equation, terms are linearized with respect to moisture content and will be solved for moisture content in each time step. In the energy equation, the linearization is carried out with respect to the temperature.

As mentioned earlier, wood drying can generally be treated as a two dimensional problem. However, when the changes in the thickness direction are large compared with those in the other dirctions, a one dimensional analysis will provide a good approximation. The further approximation for drying a stack is to investigate the drying of an individual board with average properties of the stack. This is a useful tool when the changes in the average moisture content of the stack is the important parameter of study. In such a case, the effect of changes in different parameters of the model on the trend of results can be investigated faster due to less compuatational resources and CPU time required.

6.2 One dimensional modelling

The moisture and heat transport are considered through a one dimensional model in the $y-$direction. For discretization of the heat and mass balance equations, the forward difference scheme is applied for the time derivative term in a time step. The fully implicit method is implemented for space derivative terms of the parameter to be solved (T in energy balance and X in mass balance). The space derivatives of the other parameter (T in mass balance and X in energy balance) is considered explicitly. Non-uniform grids are used with clustering near the surface when gradients of variables are larger.

The computational domain consists of half of the board thickness. Therefore, there are three types of nodes in one dimensional analysis, namely: internal, surface

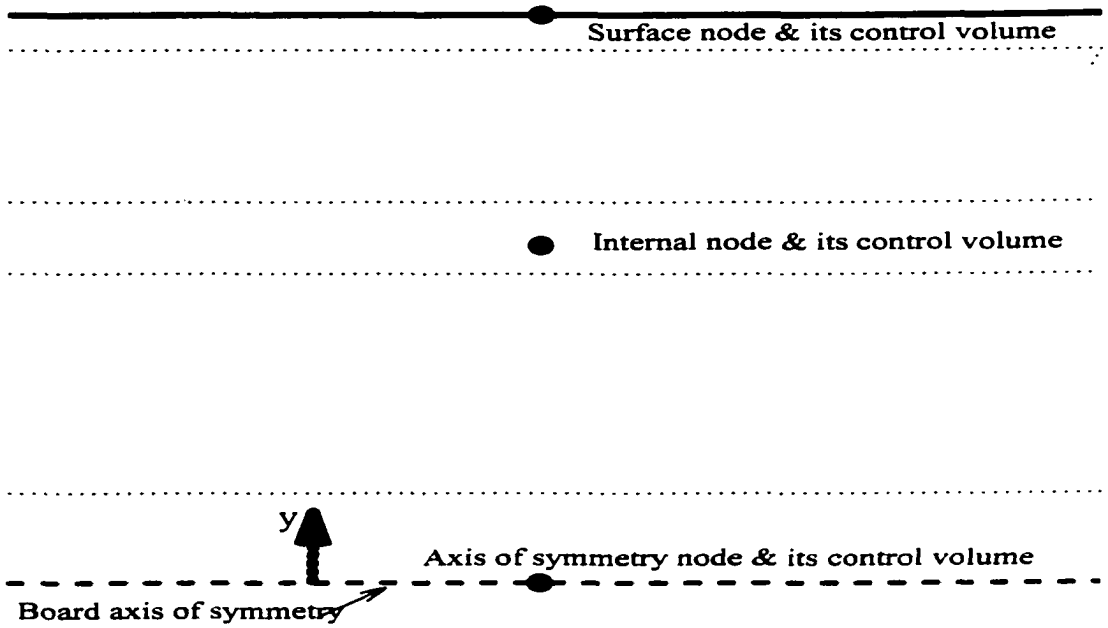

Figure 6.1: Schematic view of different node types in one dimensional case and their control volumes

and axis of symmetry. Figure 6.1 shows these points schematically.

A control volume surrounding an internal node is shown in Figure 6.2. The finite volume approach derives the differencing equations by considering the mass/energy storage and net flux of mass/heat transfer over such a finite volume. In the grid system, the scalar variables are referred to the grid points while the fluxes are calculated at the faces of these scalar cells. The fluxes of heat and mass transfer at the boundaries of each control volume are considered based on the gradients between two adjacent points. This provide a second order accurate space derivative representation (like central differencing). For accuracy of fluxes at the faces of the control volumes, Patankar[53] suggested the usage of the harmonic average instead of the weighted average since it better represents the physical reality across the discontinuities that

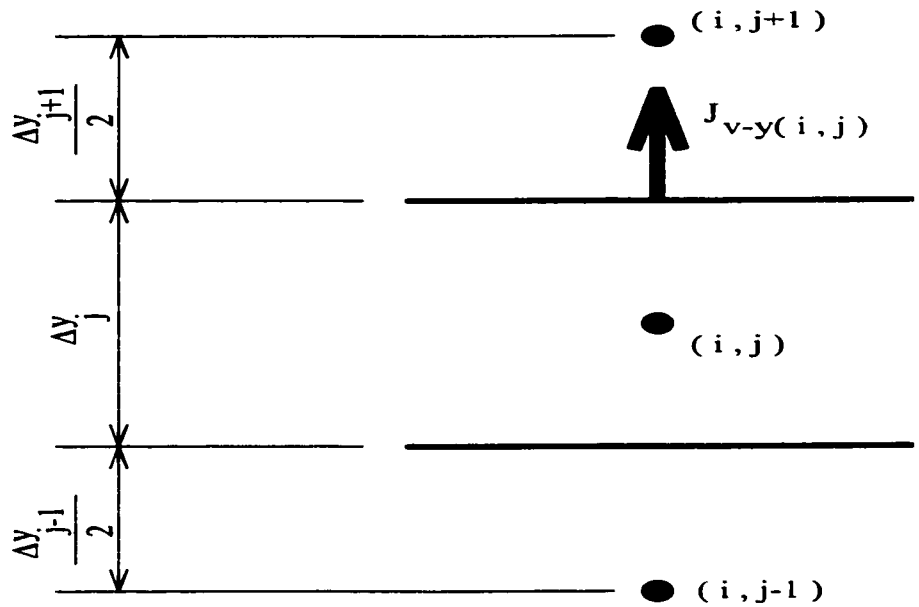

Figure 6.2: Configuration of internal node control volume and the surrounding nodes

may occur within the material. Therefore:

$$\frac{\Delta y_j + \Delta y_{j+1}}{\Phi_{(i,j+\frac{1}{2})}} = \frac{\Delta y_{j+1}}{\Phi_{(i,j+1)}} + \frac{\Delta y_j}{\Phi_{(i,j)}} \quad . \tag{6.1}$$

where Φ is one of the coefficients of D_X, D_T, λ_{eff}, λ_X, and $(\rho C_p)_{eff}$.

6.2.1 Internal nodes

The discretized form of the mass balance for an internal node is:

$$\rho_d \frac{X^{n+1}_{(i,j)} - X^n_{(i,j)}}{\Delta t} \Delta y_j = D_{X(i,j+\frac{1}{2})} \frac{X^{n+1}_{(i,j+1)} - X^{n+1}_{(i,j)}}{\delta y_j}$$
$$- D_{X(i,j-\frac{1}{2})} \frac{X^{n+1}_{(i,j)} - X^{n+1}_{(i,j-1)}}{\delta y_{j-1}} + D_{T(i,j+\frac{1}{2})} \frac{T^*_{(i,j+1)} - T^*_{(i,j)}}{\delta y_j} - D_{T(i,j-\frac{1}{2})} \frac{T^*_{(i,j)} - T^*_{(i,j-1)}}{\delta y_{j-1}} \tag{6.2}$$

where:

$$\delta y_j = 0.5(\Delta y_j + \Delta y_{j+1}) \quad , \tag{6.3}$$

$$T^*_{(i,j)} = 0.5(T^k_{(i,j)} + T^n_{(i,j)}) \ . \tag{6.4}$$

Here $T^k_{(i,j)}$ is the latest value obtained for $T^{n+1}_{(i,j)}$ from the last outer iteration.

Similarly, the discretization of the energy balance for an internal control volume yields:

$$\begin{aligned}(\rho C_p)_{eff(i,j)} \frac{T^{n+1}_{(i,j)} - T^n_{(i,j)}}{\Delta t} \Delta y_j = \lambda_{eff(i,j+\frac{1}{2})} \frac{T^{n+1}_{(i,j+1)} - T^{n+1}_{(i,j)}}{\delta y_j} \\ -\lambda_{eff(i,j-\frac{1}{2})} \frac{T^{n+1}_{(i,j)} - T^{n+1}_{(i,j-1)}}{\delta y_{j-1}} + \lambda_{X(i,j+\frac{1}{2})} \frac{X^*_{(i,j+1)} - X^*_{(i,j)}}{\delta y_j} \\ -\lambda_{X(i,j-\frac{1}{2})} \frac{X^*_{(i,j)} - X^*_{(i,j-1)}}{\delta y_{j-1}} \ ,\end{aligned} \tag{6.5}$$

with a similar definition for $X^*_{(i,j)}$ and $X^k_{(i,j)}$:

$$X^*_{(i,j)} = 0.5(X^k_{(i,j)} + X^n_{(i,j)}) \ , \tag{6.6}$$

The equations for heat and mass balance for an internal node can be rewritten as:

$$a_{X,j} X^{n+1}_{(i,j-1)} + b_{X,j} X^{n+1}_{(i,j)} + c_{X,j} X^{n+1}_{(i,j+1)} = d_{X,j} \ , \tag{6.7}$$

$$a_{T,j} T^{n+1}_{(i,j-1)} + b_{T,j} T^{n+1}_{(i,j)} + c_{T,j} T^{n+1}_{(i,j+1)} = d_{T,j} \ , \tag{6.8}$$

where:

$$a_{X,j} = -\Delta t \frac{D_{X(i,j-\frac{1}{2})}}{\delta y_{j-1}} \ , \tag{6.9}$$

$$b_{X,j} = \rho_d \Delta y_j + \Delta t \left(\frac{D_{X(i,j+\frac{1}{2})}}{\delta y_j} + \frac{D_{X(i,j-\frac{1}{2})}}{\delta y_{j-1}}\right) \ , \tag{6.10}$$

$$c_{X,j} = -\Delta t \frac{D_{X(i,j+\frac{1}{2})}}{\delta y_j} \ , \tag{6.11}$$

$$d_{X,j} = \rho_d \Delta y_j X^n_{(i,j)} + \Delta t[D_{T(i,j+\frac{1}{2})} \frac{T^*_{(i,j+1)} - T^*_{(i,j)}}{\delta y_j} - D_{T(i,j-\frac{1}{2})} \frac{T^*_{(i,j)} - T^*_{(i,j-1)}}{\delta y_{j-1}}] \quad (6.12)$$

$$a_{T,j} = -\Delta t \frac{\lambda_{eff(i,j-\frac{1}{2})}}{\delta y_{j-1}} \quad , \quad (6.13)$$

$$b_{T,j} = (\rho C_p)_{eff(i,j)} \Delta y_j + \Delta t(\frac{\lambda_{eff(i,j+\frac{1}{2})}}{\delta y_j} + \frac{\lambda_{eff(i,j-\frac{1}{2})}}{\delta y_{j-1}}) \quad , \quad (6.14)$$

$$c_{T,j} = -\Delta t \frac{\lambda_{eff(i,j+\frac{1}{2})}}{\delta y_j} \quad , \quad (6.15)$$

$$d_{T,j} = (\rho C_p)_{eff(i,j)} \Delta t y_j T^n_{(i,j)} + \Delta t[\lambda_{X(i,j+\frac{1}{2})} \frac{X^*_{(i,j+1)} - X^*_{(i,j)}}{\delta y_j} - \lambda_{X(i,j-\frac{1}{2})} \frac{X^*_{(i,j)} - X^*_{(i,j-1)}}{\delta y_{j-1}}] \quad , \quad (6.16)$$

6.2.2 Surface node

The discretized form of the mass balance for a surface node is:

$$\rho_d \frac{X^{n+1}_{(i,j)} - X^n_{(i,j)}}{\Delta t} \frac{\Delta y_j}{2} = -D_{X(i,j-\frac{1}{2})} \frac{X^{n+1}_{(i,j)} - X^{n+1}_{(i,j-1)}}{\delta y_{j-1}} - D_{T(i,j-\frac{1}{2})} \frac{T^*_{(i,j)} - T^*_{(i,j-1)}}{\delta y_{j-1}} - h_m \epsilon_{(i,j)} \rho_{v(i,j)} (X^{n+1}_{(i,j)} - X_{eq-air}) \; . \quad (6.17)$$

Similarly, the discretized energy balance for a surface node yields:

$$(\rho C_p)_{eff(i,j)} \frac{T^{n+1}_{(i,j)} - T^n_{(i,j)}}{\Delta t} \Delta y_j = -\lambda_{eff(i,j-\frac{1}{2})} \frac{T^{n+1}_{(i,j)} - T^{n+1}_{(i,j-1)}}{\delta y_{j-1}} - \lambda_{X(i,j-\frac{1}{2})} \frac{X^*_{(i,j)} - X^*_{(i,j-1)}}{\delta y_{j-1}} - h_{v^{n+1}_{(i,j)}} h_m \epsilon_{(i,j)} \rho_{v(i,j)} (X^*_{(i,j)} - X_{eq-air}) - h(T^{n+1}_{(i,j)} - T_{db-air}) \quad , \quad (6.18)$$

where T_{db-air} is the dry bulb temperature of drying air; h_m and h are convective mass and heat transfer coefficients; and $h_{v(i,j)}$, the enthalpy of water vapor can be related to temperature of the surface at different time steps as:

$$h_{v(i,j)}^{n+1} = h_{v(i,j)}^{n} + C_{p-v(i,j)}(T_{(i,j)}^{n+1} - T_{(i,j)}^{n}) \ . \tag{6.19}$$

Here, the $C_{p-v(i,j)}$ is a function of $T_{(i,j)}^{n}$. The rearrangement of equations like the format for internal nodes yields $c_{X,j} = 0$, $c_{T,j} = 0$ and:

$$a_{X,j} = -\Delta t \frac{D_{X(i,j-\frac{1}{2})}}{\delta y_{j-1}} \quad , \tag{6.20}$$

$$b_{X,j} = \rho_d \frac{\Delta y_j}{2} + \Delta t \frac{D_{X(i,j-\frac{1}{2})}}{\delta y_{j-1}} + h_m \epsilon_{(i,j)} \rho_{v(i,j)} \quad . \tag{6.21}$$

$$d_{X,j} = \rho_d \frac{\Delta y_j}{2} X_{(i,j)}^{n} - \Delta t D_{T(i,j-\frac{1}{2})} \frac{T_{(i,j)}^{*} - T_{(i,j-1)}^{*}}{\delta y_{j-1}} + h_m \epsilon_{(i,j)} \rho_{v(i,j)} X_{eq-air} \quad . \tag{6.22}$$

$$a_{T,j} = -\Delta t \frac{\lambda_{eff(i,j-\frac{1}{2})}}{\delta y_{j-1}} \quad . \tag{6.23}$$

$$b_{T,j} = (\rho C_p)_{eff(i,j)} \frac{\Delta y_j}{2} + \Delta t \frac{\lambda_{eff(i,j-\frac{1}{2})}}{\delta y_{j-1}} + h_m \Delta t \epsilon_{(i,j)} \rho_{v(i,j)} (X_{(i,j)}^{n+1} - X_{eq-air}) C_{p-v(i,j)} + h \Delta t \quad . \tag{6.24}$$

$$d_{T,j} = (\rho C_p)_{eff(i,j)} \frac{\Delta y_j}{2} T_{(i,j)}^{n} - \Delta t \lambda_{X(i,j-\frac{1}{2})} \frac{X_{(i,j)}^{*} - X_{(i,j-1)}^{*}}{\delta y_{j-1}}] + h_m \Delta t \epsilon_{(i,j)} \rho_{v(i,j)} (X_{(i,j)}^{n+1} (C_{p-v(i,j)} T_{(i,j)}^{n} - h_{v(i,j)}^{n}) + h \Delta t T_{db-air} \ . \tag{6.25}$$

6.2.3 Node on axis of symmetry

The discretization of the mass balance for the control volume surrounding a node on axis of symmetry yields:

$$\rho_d \frac{X^{n+1}_{(i,j)} - X^{n}_{(i,j)}}{\Delta t} \frac{\Delta y_j}{2} = -D_{X(i,j+\frac{1}{2})} \frac{X^{n+1}_{(i,j)} - X^{n+1}_{(i,j+1)}}{\delta y_j} - D_{T(i,j+\frac{1}{2})} \frac{T^{*}_{(i,j)} - T^{*}_{(i,j+1)}}{\delta y_j} \quad (6.26)$$

Also the balance of energy for such a control volume results in:

$$(\rho C_p)_{eff(i,j)} \frac{T^{n+1}_{(i,j)} - T^{n}_{(i,j)}}{\Delta t} \Delta y_j = -\lambda_{eff(i,j+\frac{1}{2})} \frac{T^{n+1}_{(i,j)} - T^{n+1}_{(i,j+1)}}{\delta y_j} - \lambda_{X(i,j+\frac{1}{2})} \frac{X^{*}_{(i,j)} - X^{*}_{(i,j+1)}}{\delta y_j} . \quad (6.27)$$

After rearranging the above equations in the format of Eqns. 6.7 and 6.8, it is observed that $a_{X,j} = 0$, $a_{T,j} = 0$ and

$$c_{X,j} = -\Delta t \frac{D_{X(i,j+\frac{1}{2})}}{\delta y_j} \quad , \quad (6.28)$$

$$b_{X,j} = \rho_d \frac{\Delta y_j}{2} + \Delta t \frac{D_{X(i,j+\frac{1}{2})}}{\delta y_j} \quad . \quad (6.29)$$

$$d_{X,j} = \rho_d \frac{\Delta y_j}{2} X^{n}_{(i,j)} - \Delta t D_{T(i,j+\frac{1}{2})} \frac{T^{*}_{(i,j)} - T^{*}_{(i,j+1)}}{\delta y_j} \quad . \quad (6.30)$$

$$c_{T,j} = -\Delta t \frac{\lambda_{eff(i,j+\frac{1}{2})}}{\delta y_j} \quad , \quad (6.31)$$

$$b_{T,j} = (\rho C_p)_{eff(i,j)} \frac{\Delta y_j}{2} + \Delta t \frac{\lambda_{eff(i,j+\frac{1}{2})}}{\delta y_j} \quad , \quad (6.32)$$

$$d_{T,j} = (\rho C_p)_{eff(i,j)} \frac{\Delta y_j}{2} T^{n}_{(i,j)} - \Delta t \lambda_{X(i,j+\frac{1}{2})} \frac{X^{*}_{(i,j)} - X^{*}_{(i,j+1)}}{\delta y_j}] . \quad (6.33)$$

6.2.4 1D solution procedure

Figure 6.3 shows the flow chart of the program written for the one dimensional problem. The set of discretized mass transport and heat transfer equations are solved separately. The TDMA(*Three Diagonal Matrix Algorithm*) is used for each set. The solution of both sets is continued in an outer loop until required convergence is attained. First the old values of all parameters are used for the first outer iteration. At the end of each outer iteration the values of T^*'s and X^*'s are updated based on the last obtained values for T^{n+1}'s and X^{n+1}'s. This will cause less oscillations and CPU time. The convergence criterion is based on two values:

a) the maximum of difference between newly obtained and last iteration values at each point, and

b) summation of all the above differences at all nodes.

When changes in moisture content at any node during a time step is more than a certain limit, the time step,Δt, is halved after solving the field and the calculations are repeated for the whole domain using the new Δt. This usually happens when the moisture content of a point is greater than X_{FSP} in the last time step and suddenly drops below X_{FSP} during the time interval.

6.2.5 Benchmark case

The combined experimental and numerical work of Stanish *et. al.*[19] was considered as the benchmark case for the present model. Stanish *et. al.* studied the drying of 5 × 15 cm Southern Pine specimen assuming a one dimensional model with a fully developed air flow between parallel plates. There are a few reasons for selecting [19] as a benchmark case in the present work. First, a fully developed flow has a well known relationship for its surface coefficients (see Rohsenow and Hartnett[71]). The

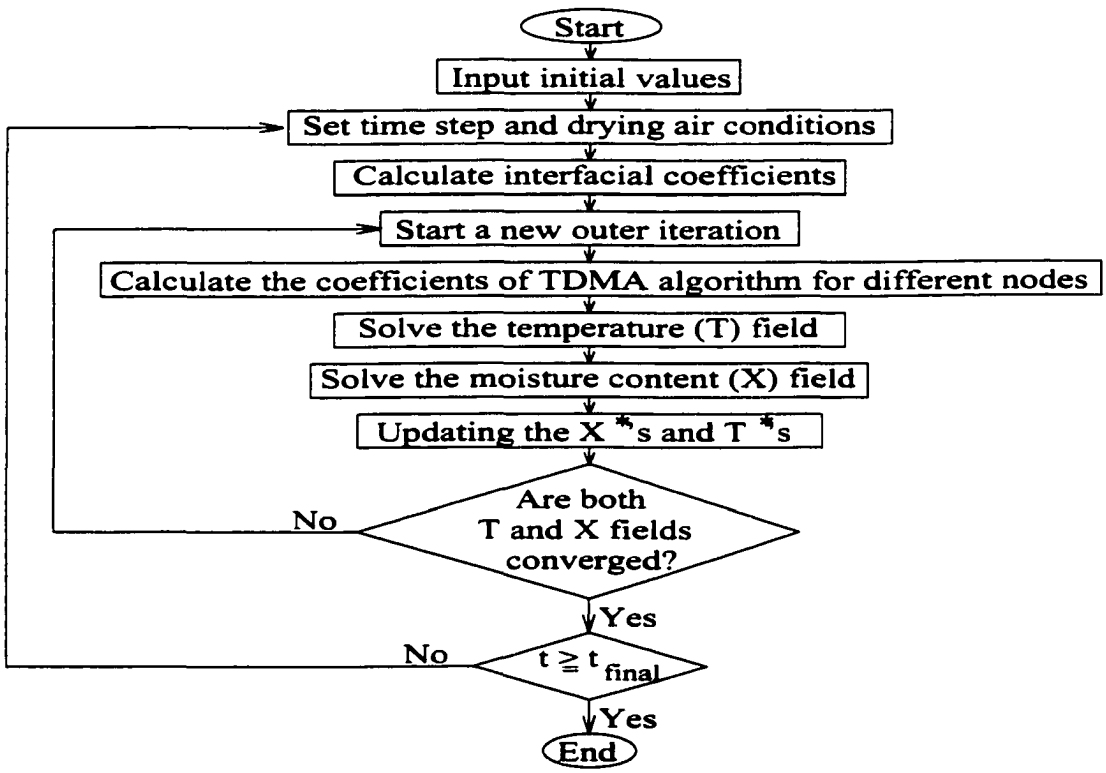

Figure 6.3: Flow chart of the Fortran program for one dimensional modelling

second reason for choosing this case is that almost all the well performed models mentioned in the review article of Kamke and Vanek[37] are based on the model of Stanish *et. al.*[19]. Although the model suggested in [19] has some similarities in approach to the present model, there are a few major differences. Since [19] took into account the differences in total gas phase (water vapor and air) pressure inside the wood and subsequently the contribution of air in the wood, they had to solve the air density variations inside the wood in addition to moisture content and temperature fields. This resulted in a complicated set of three coupled differential equations to be solved simultaneously. This is a very difficult task in two dimensions. Another major difference is the usage of constant values for the bound water diffusion coefficient. Simplified relationships used for physical properties of water phases, the usage of the multiplier factor $(1-\epsilon)$ in calculating the flux of bound water, and their expression of the surface boundary condition in terms of air/water vapor pressure instead of moisture content constitute other main differences between the work of Stanish *et. al.* and the current model.

In one of the drying tests performed by Stanish *et. al.*, the velocity, dry- and wet-bulb temperatures of the dring air were 7 m/s, $75^oC(348^oK)$ and $55^oC(328^oK)$, respectively. Based on the mentioned air velocity, they assumed the heat transfer coefficient (h) to be $58W/m^2/^oK$ using the formulation of Rohsenow and Hartnett[71] for flow between parallel plates. The dry wood density of the specimen was 420 Kg/m^3. The other coefficients used in their model are:

$K_g^d = 5.0 \times 10^{-15}m^2$, the permeabilty of dry wood for gas,

$K_{ls} = 5.0 \times 10^{-16}m^2$,

$\alpha = 0.05$,

$D_b = 3.0 \times 10^{-13}Kg/m^3/s$,

$S_{min} = 0.1.$

For the present simulations a total grid array of 40 with expansion factor of 1.1 has been used. The unknowns of the present model were considered with trial and error until a good fit with experimental data for average moisture content versus time was attained. In addition to a closer fit, one of the criteria for such a good fit was the slope of the numerical results in the most of drying time especially the final stages. Fitting the simulation results to the data yielded the following set of model parameters:

$S_T = 8000(^oC),$

$K_{ls} = 1.5 \times 10^{-16} m^2,$

$\alpha = 0.014,$

$D_\mu = 0.4 Kg/m^3/s,$

$S_{min} = 0.02555.$

Figure 6.4 shows the comparison between time dependent distribution of average moisture content of the present work and experimental and numerical data of Stanish *et. al.*[19]. As can be seen, the present model performs better than the Stanish's model. Figure 6.5 shows the moisture content profile at different times. The simulation model predicts that the wood surface dries very rapidly. When free water exists at some parts of the board, a change in the trend of moisture content profile around the Fiber Saturation Point ($FSP \simeq 0.24 - 0.28$) can be observed. Around this area the curvature of the moisture content profile tends to be upward, unlike the rest of the curve. This is where free water movement cease to exist due to ($S < S_{min}$) and bound water diffusion starts to increase.

The variation of temperature at the board center line is plotted in Figure 6.6 from which it can be seen that the temperature difference between locations inside the

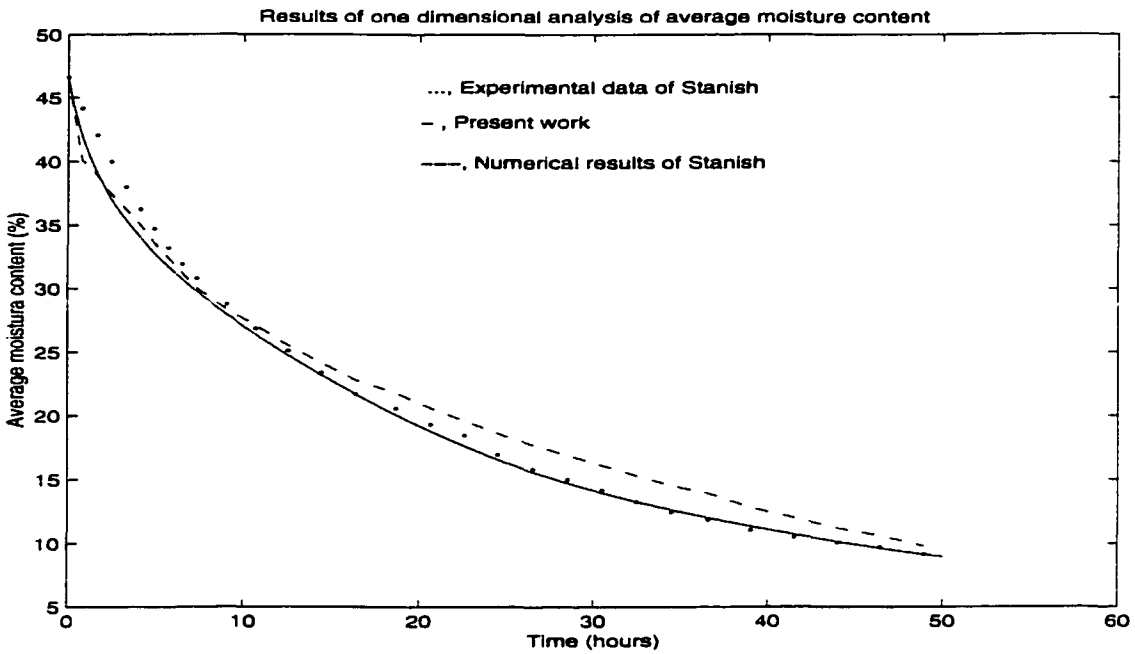

Figure 6.4: Time dependent average moisture content of a single board (Stanish test 1), $h = 58W/m^2/^oK$

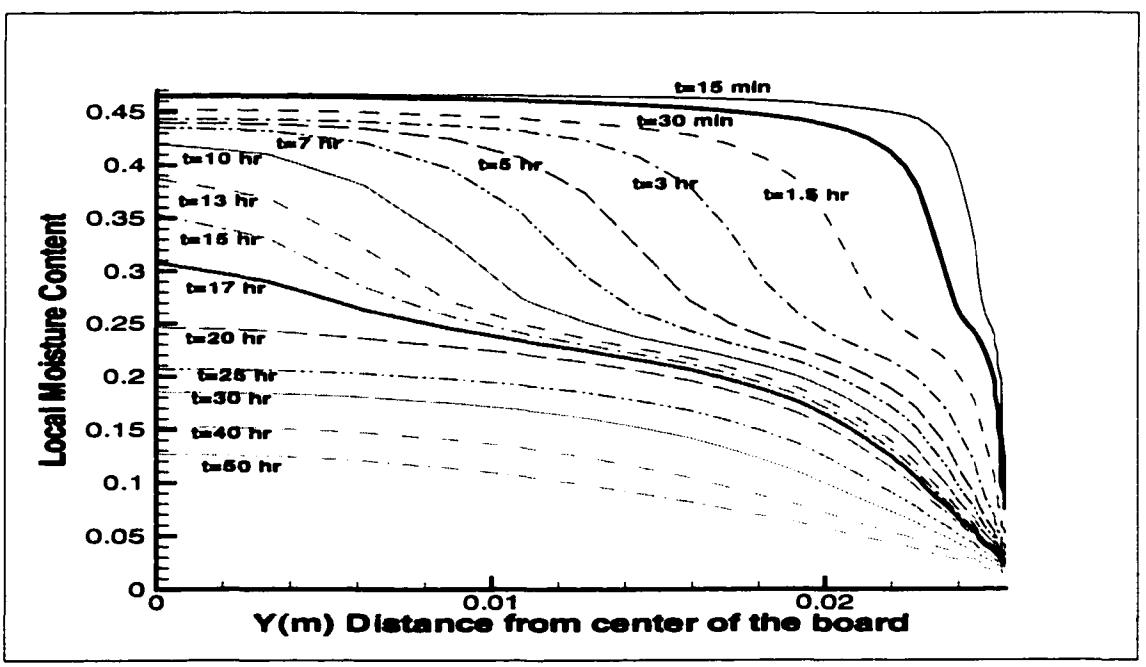

Figure 6.5: Time dependent local moisture content of a single board (Stanish test 1), $h = 58W/m^2/^oK$

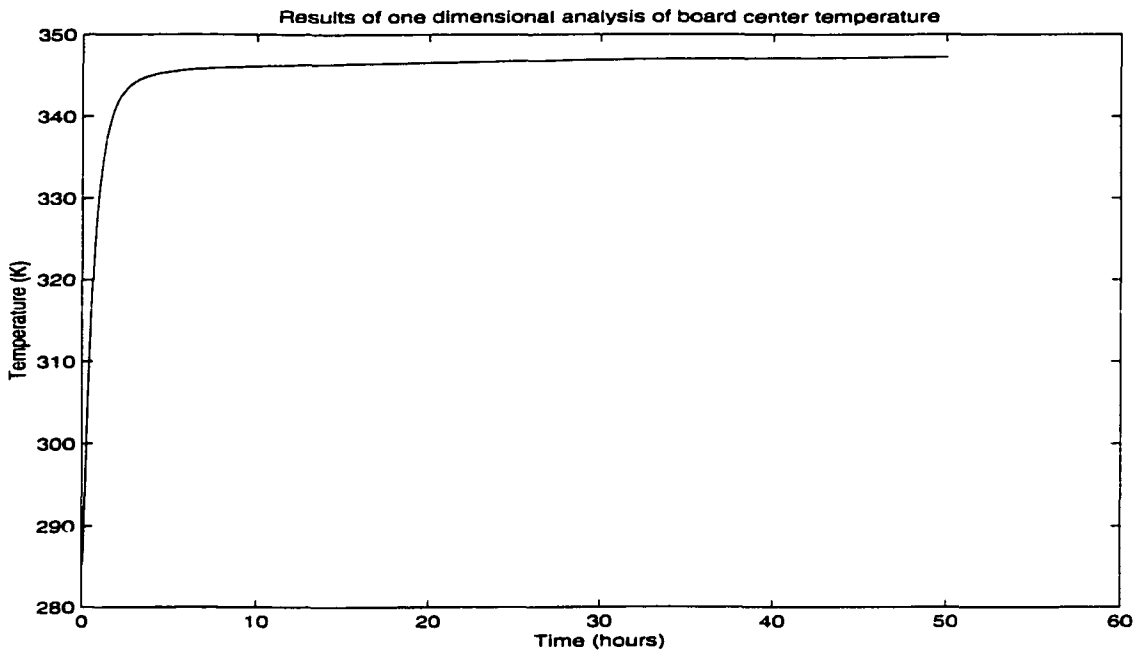

Figure 6.6: Time dependent temperature at the board center line (Stanish test 1). $h = 58W/m^2/^oK$

board becomes less than a few degrees after 5 hours of drying.

6.2.6 Further model verification

One of the aspects of the model verification is to compare experimental data of drying under different conditions using the model unknown values obtained from the base data. Experimental and numerical data from drying of a different pine specimen performed by Stanish *et. al.* are compared with the results of the present model in Figure 6.7. All model parameters were the same as the ones listed above, except the surface coefficients ($h = 87W/m^2/^oK$) due to change of the air velocity. The results of the present model are in reasonably good agreement with experiments particularly in later stages of the drying period. In addition, one can say that the overall performance of the present model is also better than those of the literature.

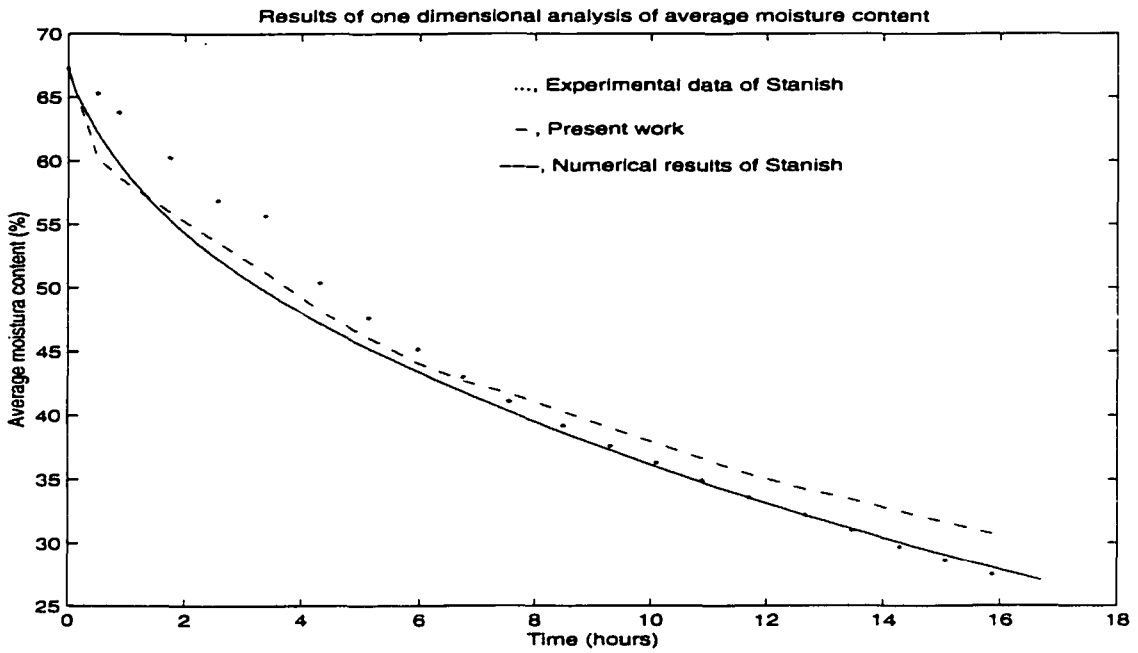

Figure 6.7: Time dependent average moisture content of a single board (Stanish test 2), $h = 87W/m^2/^oK$

6.2.7 Sensitivity study of the model unknown parameters

Expressions of the mathematical model discretized here are very complex in respect to the parameters to be determined for specific species. A sensitivity analysis provide a better understanding of the effects of these parameters and will help to optimize the unknowns and assess the reliability of the model. For the sensitivity analysis, the selected parameter was varied at different values while the other parameters were kept unchanged. Differences in the average moisture content and center temperature due to the variation of the parameter were observed.

Effect of K_{ls} and S_{min}

K_{ls} and S_{min} appear in the calculation of the flux of free water. K_{ls} is the permeability of solid when the voids are completely filled by liquid (fully saturated).

S_{min} is the minimum saturation required for free water migration. Below S_{min}, the permeability,K_{ls}, and therefore J_f is set to zero. Stanish [19] defined the effective permeability of free water, K_l, as:

$$K_l = K_{ls}\{1 - cos[\frac{\pi}{2}.\frac{S - S_{min}}{1 - S_{min}}]\} \ . \tag{6.34}$$

From this formulation, it is understood that $J_f \propto K_{ls}$. But the dependency of J_f on S_{min} is yet to be examined. First, we define:

$$\zeta = S_{min} \quad , \tag{6.35}$$

$$\gamma = \frac{\pi}{2}.\frac{S - S_{min}}{1 - S_{min}} \ . \tag{6.36}$$

For simplicity we assume the second term on the left hand side of Eq. 6.36 is defined as:

$$f(\zeta) = 1 - cos(\gamma) \ . \tag{6.37}$$

The implementation of the Maclaurin expansion of $f(\zeta)$ yields:

$$f(\zeta) = f(\zeta_0) + (\zeta - \zeta_0)f'(\zeta_0) \quad , \tag{6.38}$$

where, since $(\zeta - \zeta_0) < 1$, the higher order derivative terms are neglected. Now using the chain rule we write:

$$f'(\zeta) = \frac{\partial f}{\partial \gamma}\frac{\partial \gamma}{\partial \zeta} \ . \tag{6.39}$$

Using Eqs. 6.35-6.37 and 6.39 in Eq. 6.38, we obtain:

$$1 - cos[\frac{\pi}{2}.\frac{S - S_{min}}{1 - S_{min}}] = 1 - cos[\frac{\pi}{2}.\frac{S - S_{min-0}}{1 - S_{min-0}}]$$
$$+\frac{\pi}{2}(S_{min} - S_{min-0})\frac{S - 1 - 2S_{min-0}}{(1 - S_{min-0})^2}sin[\frac{\pi}{2}.\frac{S - S_{min-0}}{1 - S_{min-0}}] \ . \tag{6.40}$$

Since γ is small, we assume $sin(\gamma) \simeq \gamma$. Using Eq. 6.40 in Eq.6.34, K_l is obtained as:

$$K_l = K_{l0}[1 + \frac{\pi^2}{4}(S_{min} - S_{min-0})\frac{(S - 1 - 2S_{min-0})(S - S_{min-0})}{(1 - S_{min-0})^3}] \quad . \tag{6.41}$$

Using the values of $S_{min-0} = 0.02555$, $X_{max} \simeq 1.5$ and $X_{FSP} \simeq 0.28$, then for a moisture content of $X = 0.45$, we obtain $S \simeq 0.1557$. Now if we set $S_{min} = 0.038325$ (1.5 times the initial value), then:

$$K_l = K_{l0}[1 - 0.004] \quad , \tag{6.42}$$

which means 0.4% reduction in the permeability. If we assume that the moisture content and saturation at that point are $X = 0.3715$ and $S = 0.07$, K_l will be reduced by 0.15%. Therefore, changes in S_{min} do not cause significant changes in the effective permeability. Figure 6.8 shows the the effect of changes in S_{min} on the moisture content. These changes shown in Figure 6.8 seem much more than we expected it to be related to K_l. The reason for this is the following: if $S_{min} = 0.038325$ it means that for $X < 0.3268$ we impose $J_f = 0$ while when $S_{min-0} = 0.02555$, for $X < 0.3111$ this is imposed in the modelling. Therefore, the real effect of S_{min} is in setting the X_{min} for which J_f has a non-zero value and its effect on K_l is negligible. Figures 6.8 and 6.9 show the effect of $\pm 50\%$ change in S_{min} on average moisture content, X_{av}, and board center temperature. This effect, as can be seen in Figure 6.8 , consists of a major shift in the time dependent X_{av} curve. The change in the slope of X_{av} is quite considerable between 2 and 30 hours after the start of drying while at the final and initial stages, its difference is less. This is due to having local moisture contents above limits required for $(S > S_{min-0})$ condition at the beginning and below the values for $(S < S_{min-new})$ condition after 30 hours. The effect on board center temperature is almost nil.

Figure 6.10 and 6.11 plot the effect of K_{ls}. The changes in K_{ls} cause the same trend of shifting X_{av} as was seen for S_{min} in the opposite direction. The increase in

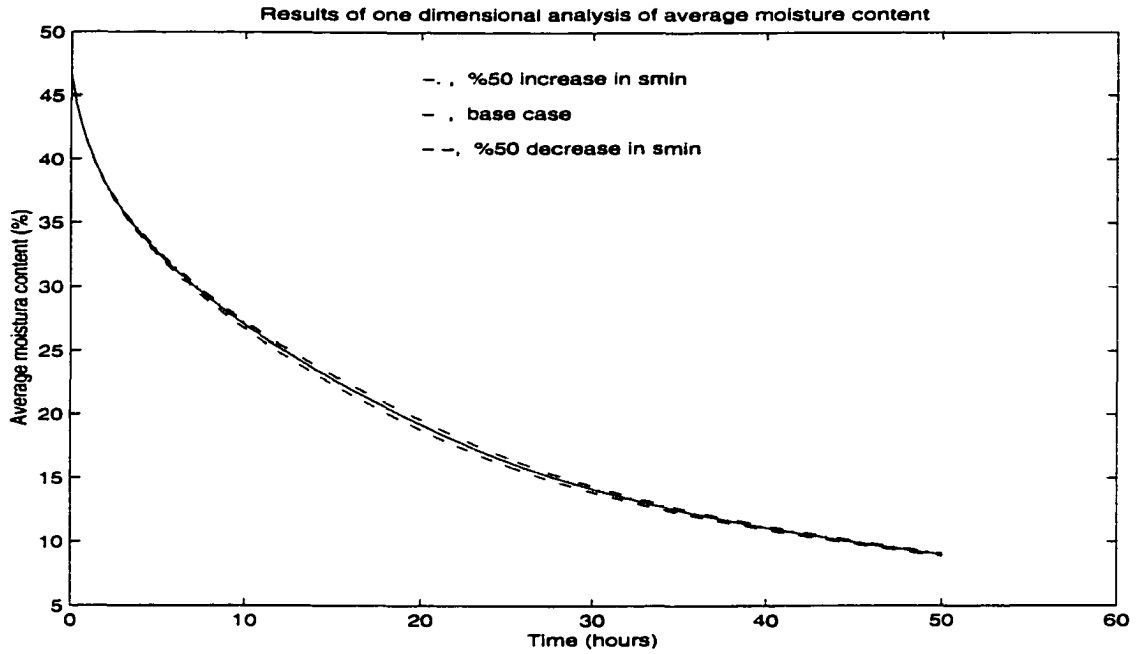

Figure 6.8: Sensitivity of time dependent average moisture content to S_{min}

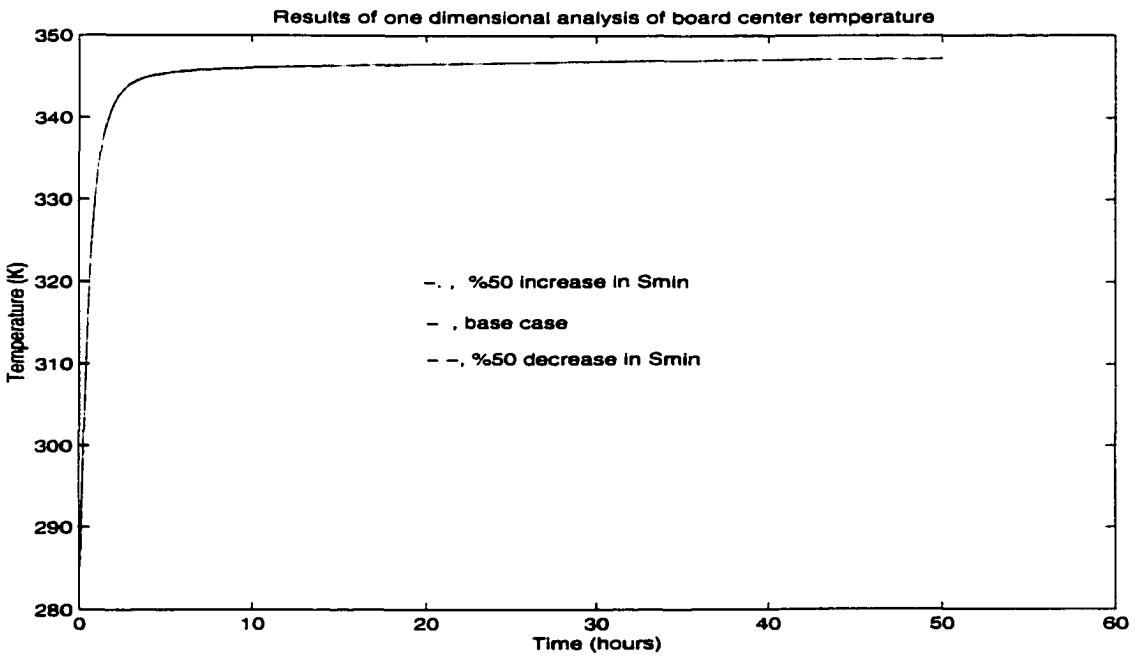

Figure 6.9: Sensitivity of time dependent board center temperature to S_{min}

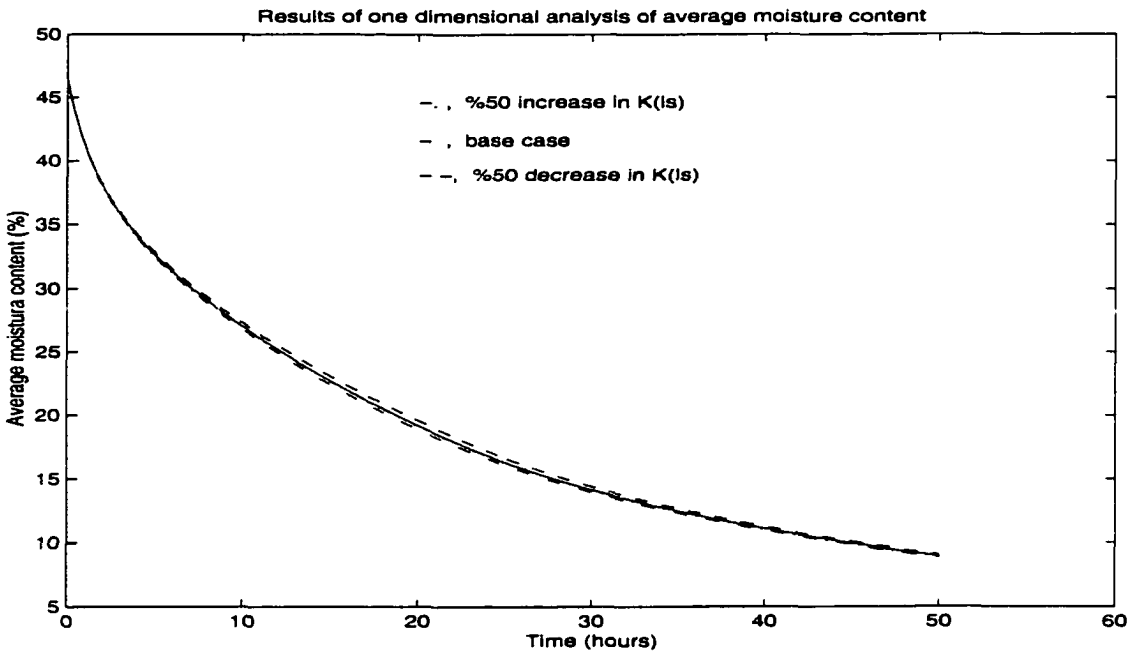

Figure 6.10: Sensitivity of time dependent average moisture content to K_{ls}

K_{ls} shifts the X_{av} curve upward but reduces its curvature in the midway. The slow changes in the slope decay as time passes by and free water phase vanishes in the most of the board thickness. Here, like the S_{min} case, the center temperature is not affected, and the effect of 50% increase in K_{ls} is less than a 50% decrease in it.

Effect of D_μ and S_T

In Chapter 4 the following equation was proposed for bound water diffusion coefficient:

$$D_b = D_\mu exp[40(\frac{\rho_b}{\rho_d} - X_{FSP}) - \frac{S_T}{T})] \ . \tag{6.43}$$

As mentioned earlier, such a relationship performs better both above and below FSP and mathematically closer to behavior of wood structure. We expect that any change in D_μ will change D_b linearly, but the effect of S_T is more complicated. As can be observed in Figure 6.12, D_μ has a considerable effect on time dependent X_{av}. 50%

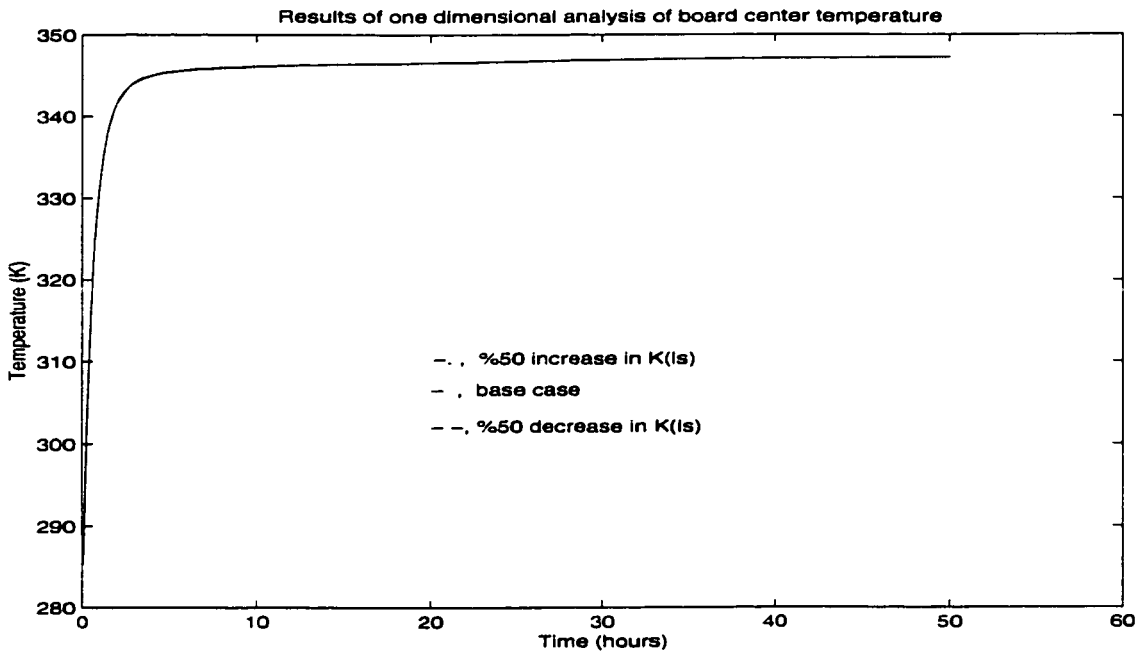

Figure 6.11: Sensitivity of time dependent board center temperature to K_{ls}

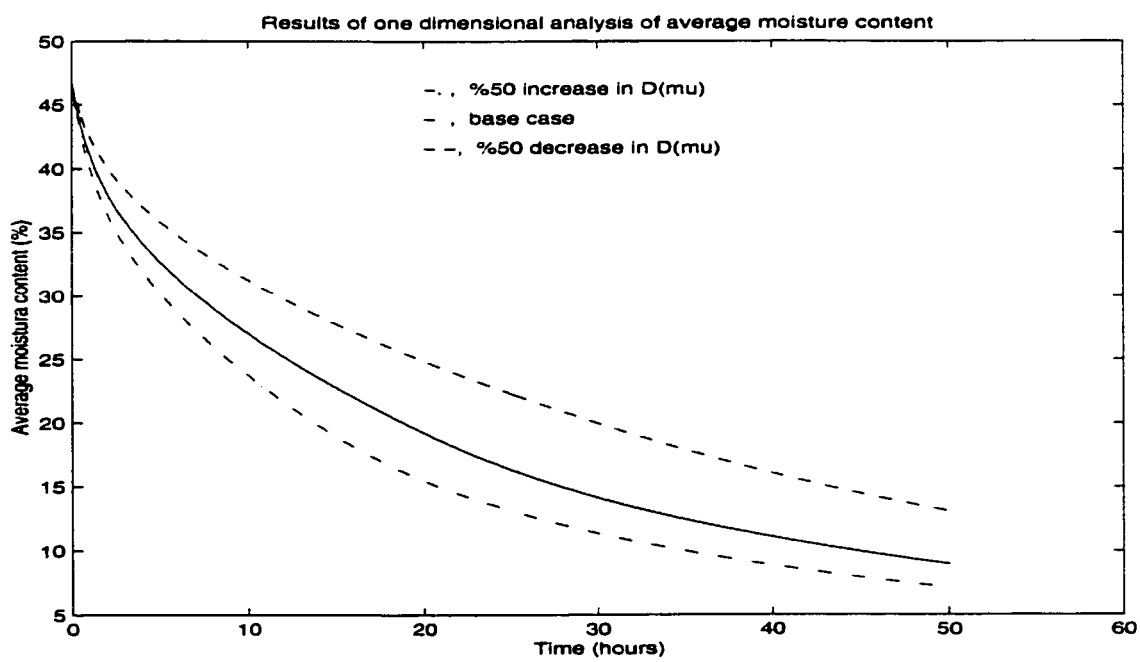

Figure 6.12: Sensitivity of time dependent average moisture content to D_μ

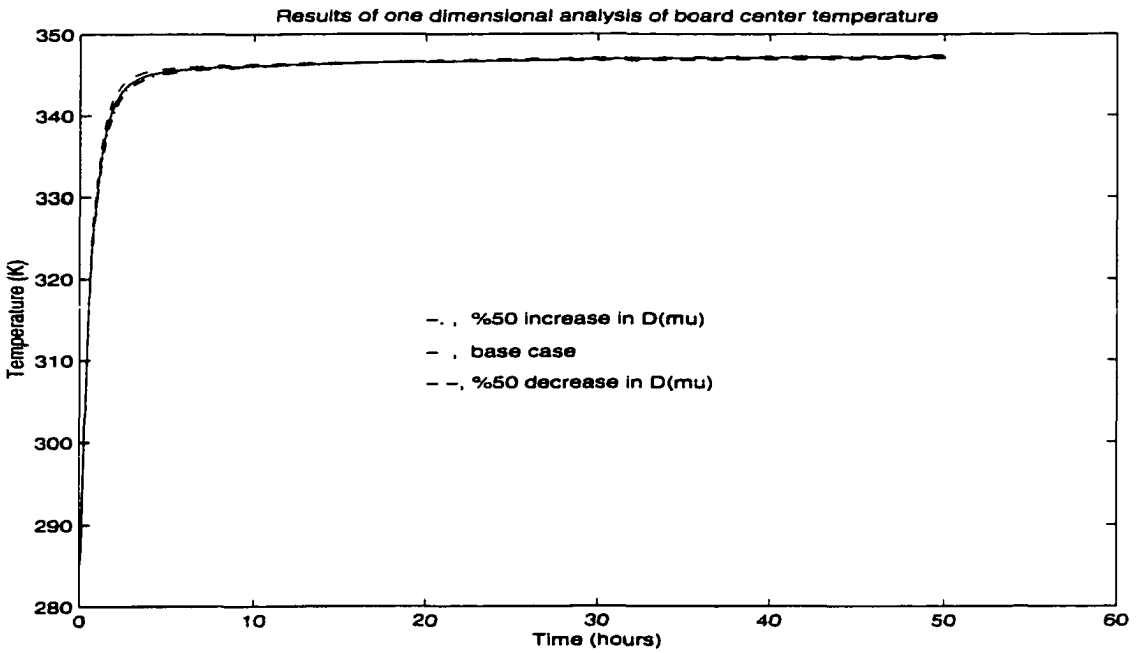

Figure 6.13: Sensitivity of time dependent board center temperature to D_μ

decrease in D_μ decreases the change in X_{av} with time (drying rate), and shifts its curve upward more than twice as much as +50% change moves it downward. Also the decrease in D_μ causes considerable decrease in the curvature of the X_{av} plot.

Figures 6.12 and 6.13 show that ±50% changes in D_μ have almost no effect in the initial stages of drying when bound water is not the dominant phase. From Figure 6.13, it can be noted that a -50% change in D_μ causes up to $2°C$ rise in board center temperature after 2 to 3 hours of drying. Then its effect drops and is less than $0.5°C$ after 7 hours of drying. The difference with respect to the base case stays almost the same after 30 hours.

Figures 6.14 and 6.15 represent the effect of ±50% changes in S_T on X_{av} and board center temperature. Figures 6.16 and 6.17 present similar curves for ±10% changes in S_T. Any increase in S_T will decrease D_μ due to the nature of $exp(\frac{-S_T}{T})$ term. As can be seen from Figures 6.14 and 6.16, such an effect will lower the drying

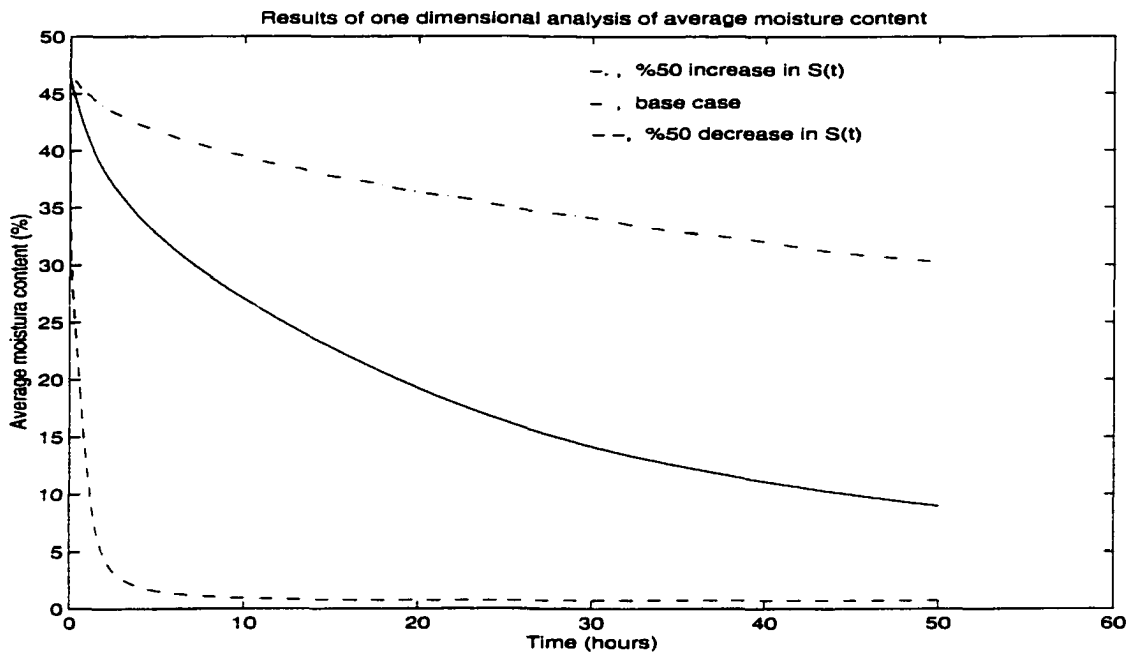

Figure 6.14: Effect of $\pm 50\%$ change in S_T on time dependent average moisture content

rate as well as the curvature of X_{av} versus time. In the extreme case of $+50\%$ change, the bound water diffusion is weakened to such a level that causes a sort of instable solution observed (see Figures 6.14 and 6.15) in the form of small oscillations about the expected solution. -50% change also dries out the board very fast as shown in Figure 6.14. This also causes slower changes in center temperature during initial stages, and a final higher temperature closer to the air temperature. This means a smaller initial effective conductivity at lower temperatures and a larger conductivity at higher final temperatures. The effect of $\pm 10\%$ changes in S_T plotted in Figure 6.17 show better such a trend, due to a stable solution while the effect of $+10\%$ change is considerably less than that of the -10%.

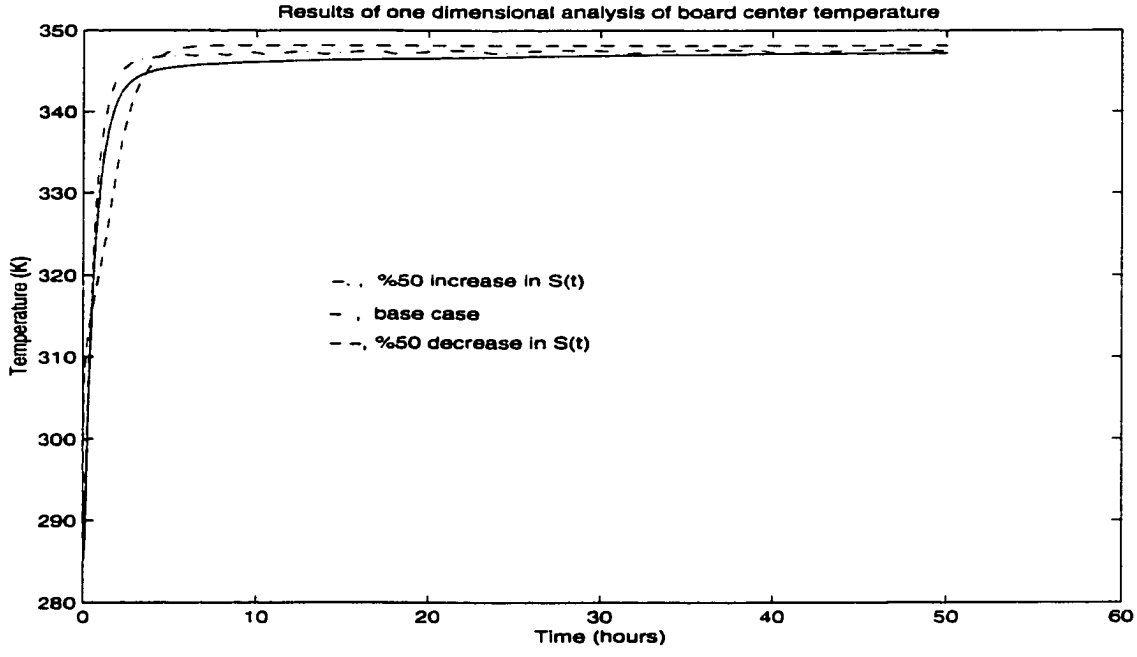

Figure 6.15: Effect of $\pm 50\%$ change in S_T on time dependent board center temperature

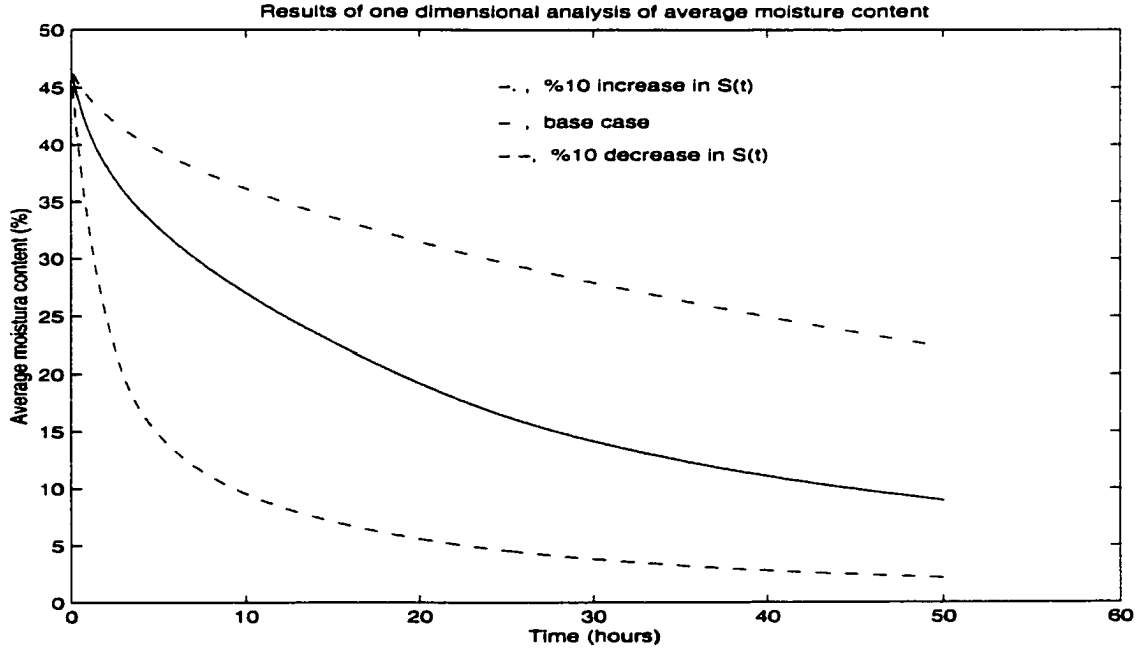

Figure 6.16: Effect of $\pm 10\%$ change in S_T on time dependent average moisture content

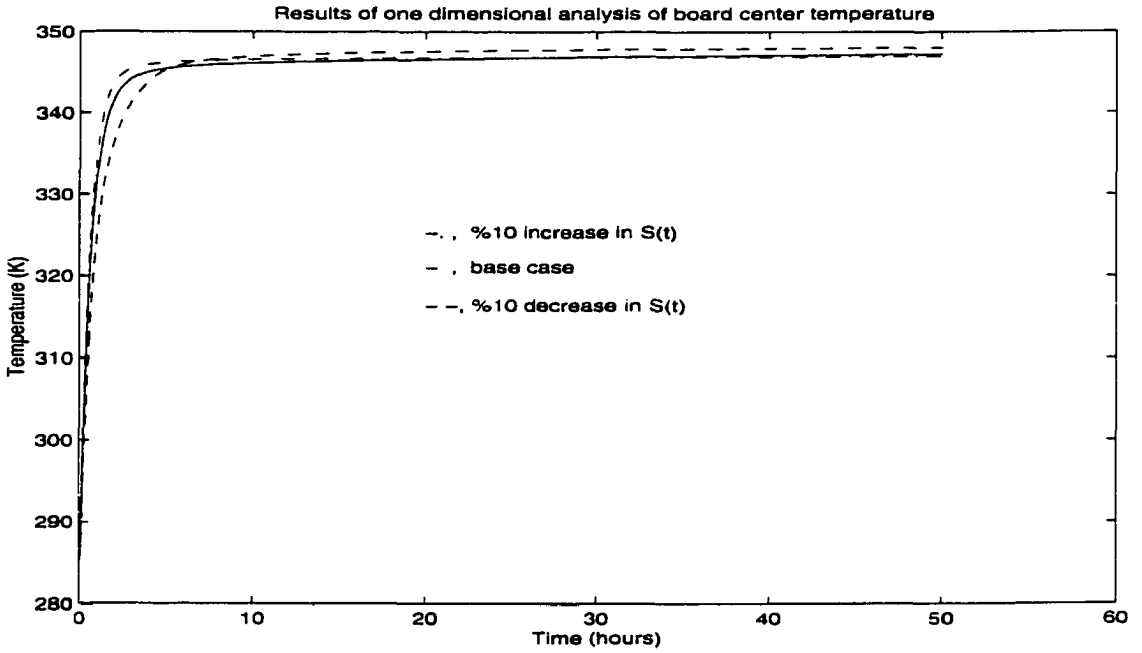

Figure 6.17: Effect of $\pm 10\%$ change in S_T on time dependent board center temperature

Effect of α

α is the only unknown of the model related to water vapor phase. The effect of changes in α is shown in Figures 6.18 and 6.19. Effect of α is negligible up to 3 hours of drying due to small amount of water vapor exist and move inside the board. With temperature rising everywhere as time increases, more moisture evaporates. This means that with 50% higher values for α, more water vaporizes and moves resulting in much faster rate of drying as can be seen in Figure 6.18. Also the temperature at board center rises by 1^oC in Figure 6.19 due to -50% change in α. At final stages of drying, most moisture inside the wood consists of water vapor. Thus the effect of α on the slope of time dependent X_{av} at final stages of drying has a major role in minimizing the model parameters.

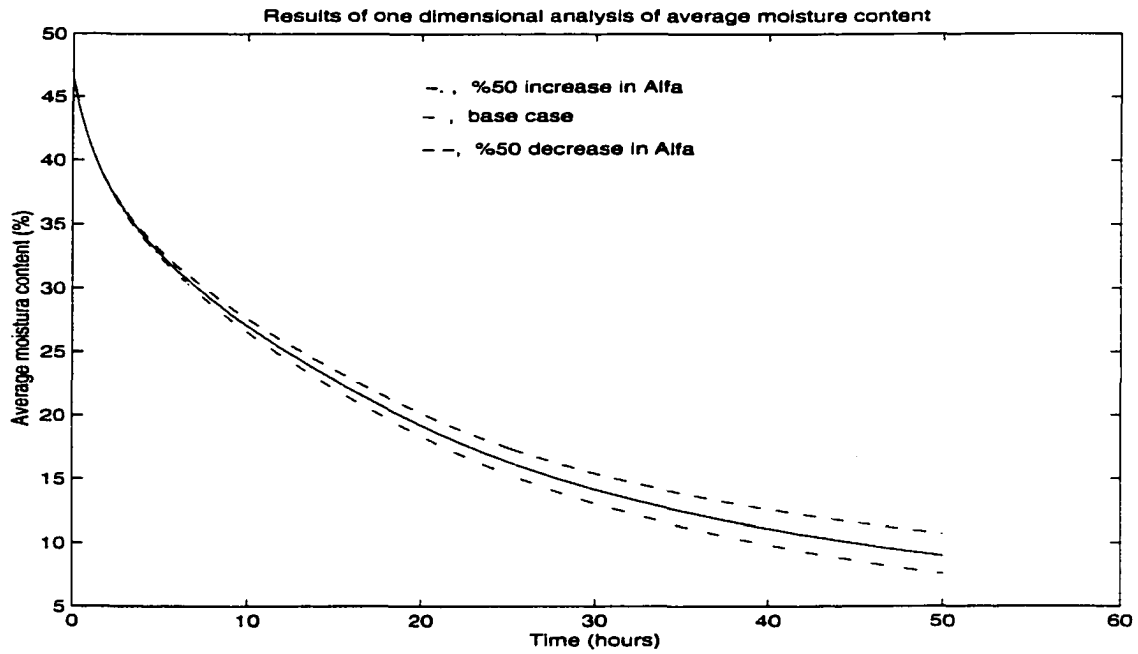

Figure 6.18: Sensitivity of time dependent average moisture content to α

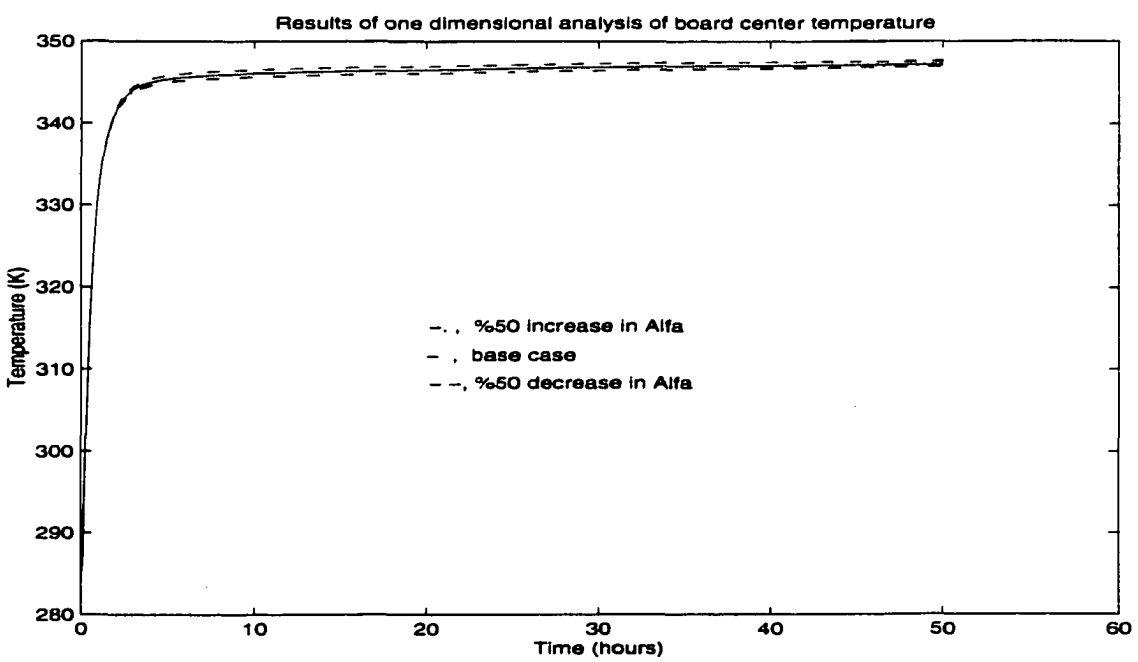

Figure 6.19: Sensitivity of time dependent board center temperature to α

Chapter 7

Two dimensional simulation of kiln drying

A two dimensional model is developed for drying of a stack. In the present numerical model (similar to the experiments of Li[52]), the stack considered here consists of 42 boards stacked in 6 rows (see Figure 5.1). The kiln used in experiments provides uniform inlet air flow for the stack, making possible to consider the fluid flow and Nu distributions the same for all rows. Thus, only one row is considered in the simulations. For each board of the row, the average characteristics (ρ_d and initial moisture content) of the boards in the related column is considered. Here, the mass and heat transport equations are linearized with respect to moisture content and temperature, respectively. Similar to our one dimensional model, the coefficients are evaluated using the values of the last time step. The computational domain is chosen as half of each board thickness due to symmetry. There are nine types of nodes as shown in Figure 7.1 schematically.

During the discretization of the mass balance equation, two methods can be implemented for space derivatives: *ADI* (Alternating Direction Implicit) and Fully

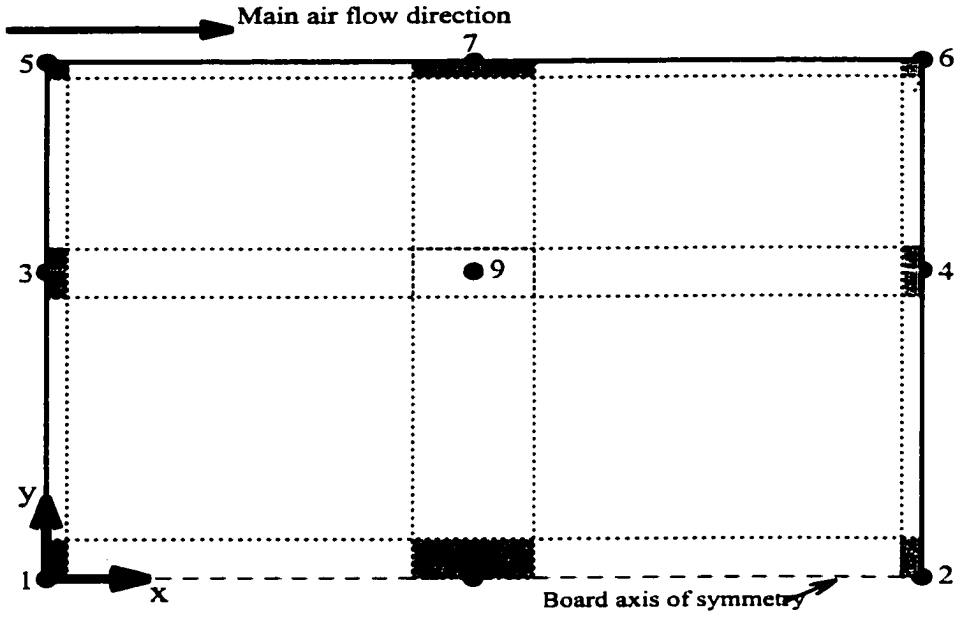

Figure 7.1: Schematic view of different node types in two dimensional case and their control volumes

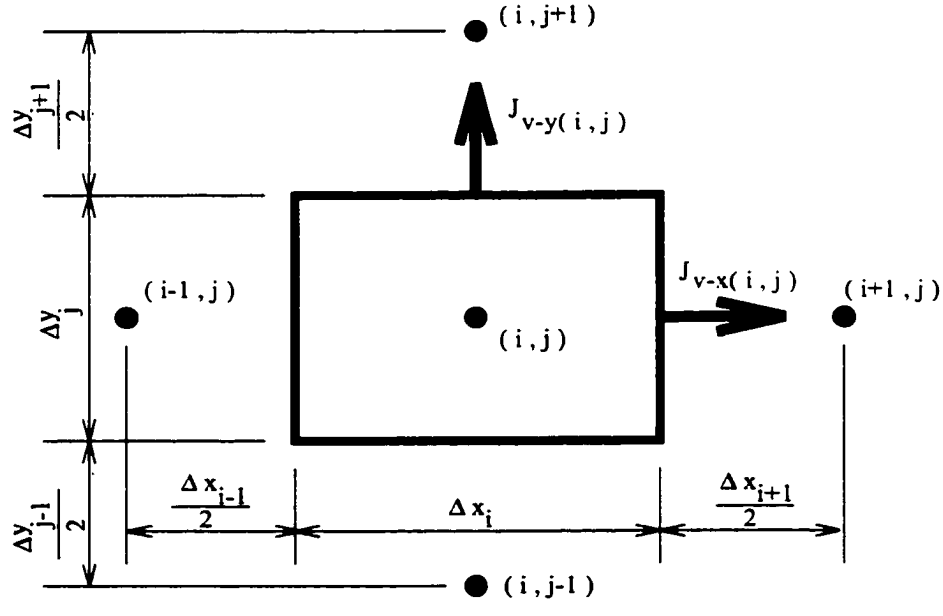

Figure 7.2: Configuration of internal node control volume and the surrounding nodes

Implicit. ADI is an approximation to the Crank-Nicolson method. In this technique, the total time step is divided into two equal half time steps. In each half time step, the forward difference approach is applied for time derivative terms. In the first half time step, the space derivative terms are considered explicitly in one direction (e.g. $x-$direction), and implicitly in the other (e.g. $y-$direction). Solving such a set of discretized equations results in the moisture content values at time $n+\frac{1}{2}$, $X^{n+\frac{1}{2}}$'s. The similar procedure is used for the second half time step, except that in this case the explicit procedure is applied in the $y-$direction to the $X^{n+\frac{1}{2}}$'s and the implicit procedure is used in the $x-$direction to X^{n+1}'s. The set of mass transfer equations for each direction in each half time step is solved using the TDMA algorithm. Since solving the one dimensionalized equations in each half time step is very straight forward and easy, the ADI method is much faster than iterative methods used in two dimensional analysis.

The fully implicit method requires only one time step. The time derivative is discretized using forward scheme and for the space derivatives the fully implicit scheme is applied. Different degrees of implicity can be used in evaluating the space derivatives, but the fully implicit case is less prone to instability in non-linear transfer equations.

For the heat transfer equation, the fully implicit method is applied due to growing instability observed in the temperature field when other methods, such as ADI, are implemented. For the present work the *Chebichev* acceleration technique of the *SOR* (Successive Over Relaxation) method[72] has been modified further to achieve the stability and faster convergence of the results. Figure 7.3 illustrates the structure of the Fortran program written for the two dimensional model.

The discretized form of the equations for internal and some boundary nodes are presented next. Due to similarities and to save space, some details are omitted.

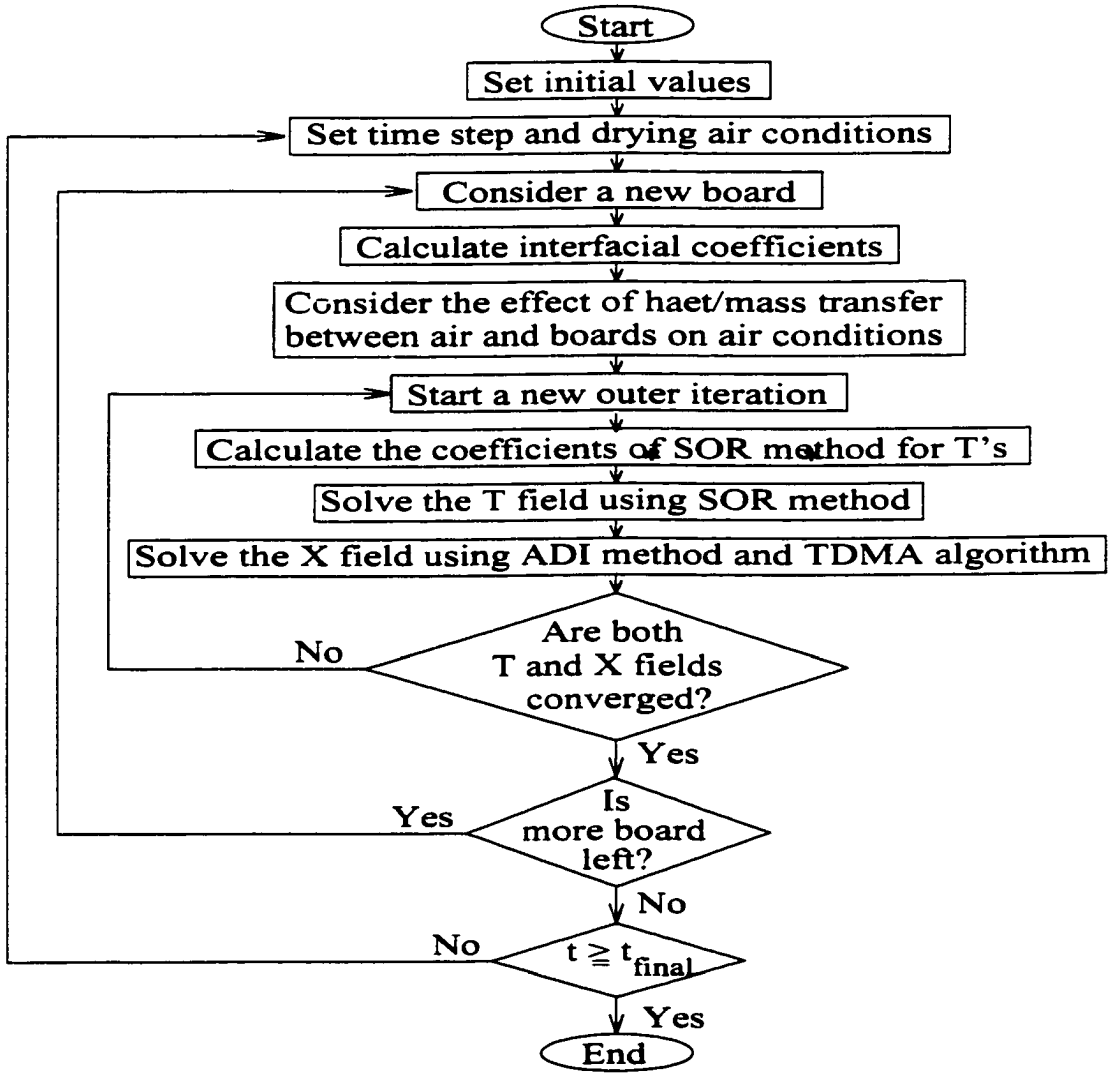

Figure 7.3: Flow chart of the Fortran program for two dimensional modelling

7.1 Discretization for internal nodes

The discretized form of the mass balance for an internal node in the first half time step, using the ADI method, is:

$$\rho_d \Delta y_j \Delta x_i \frac{X^{n+\frac{1}{2}}_{(i,j)} - X^{n}_{(i,j)}}{\frac{\Delta t}{2}} =$$
$$\Delta x_i [D_{X(i,j+\frac{1}{2})} \frac{X^{n+\frac{1}{2}}_{(i,j+1)} - X^{n+\frac{1}{2}}_{(i,j)}}{\delta y_j} - D_{X(i,j-\frac{1}{2})} \frac{X^{n+\frac{1}{2}}_{(i,j)} - X^{n+\frac{1}{2}}_{(i,j-1)}}{\delta y_{j-1}}]$$
$$+\Delta x_i [D_{T(i,j+\frac{1}{2})} \frac{T^{*}_{(i,j+1)} - T^{*}_{(i,j)}}{\delta y_j} - D_{T(i,j-\frac{1}{2})} \frac{T^{*}_{(i,j)} - T^{*}_{(i,j-1)}}{\delta y_{j-1}}]$$
$$+\Delta y_j [D_{X(i+\frac{1}{2},j)} \frac{X^{n}_{(i+1,j)} - X^{n}_{(i,j)}}{\delta x_i} - D_{X(i-\frac{1}{2},j)} \frac{X^{n}_{(i,j)} - X^{n}_{(i-1,j)}}{\delta x_{i-1}}]$$
$$+\Delta y_j [D_{T(i+\frac{1}{2},j)} \frac{T^{*}_{(i+1,j)} - T^{*}_{(i,j)}}{\delta x_i} - D_{T(i-\frac{1}{2},j)} \frac{T^{*}_{(i,j)} - T^{*}_{(i-1,j)}}{\delta x_{i-1}}] \quad . \tag{7.1}$$

where:

$$\delta x_i = 0.5(\Delta x_i + \Delta x_{i+1}) \quad , \tag{7.2}$$

$$T^{*}_{(i,j)} = T^{n}_{(i,j)} \; . \tag{7.3}$$

This equation for the second half time step can be written as:

$$\rho_d \Delta y_j \Delta x_i \frac{X^{n+1}_{(i,j)} - X^{n+\frac{1}{2}}_{(i,j)}}{\frac{\Delta t}{2}} =$$
$$\Delta x_i [D_{X(i,j+\frac{1}{2})} \frac{X^{n+\frac{1}{2}}_{(i,j+1)} - X^{n+\frac{1}{2}}_{(i,j)}}{\delta y_j} - D_{X(i,j-\frac{1}{2})} \frac{X^{n+\frac{1}{2}}_{(i,j)} - X^{n+\frac{1}{2}}_{(i,j-1)}}{\delta y_{j-1}}]$$
$$+\Delta x_i [D_{T(i,j+\frac{1}{2})} \frac{T^{*}_{(i,j+1)} - T^{*}_{(i,j)}}{\delta y_j} - D_{T(i,j-\frac{1}{2})} \frac{T^{*}_{(i,j)} - T^{*}_{(i,j-1)}}{\delta y_{j-1}}]$$
$$+\Delta y_j [D_{X(i+\frac{1}{2},j)} \frac{X^{n+1}_{(i+1,j)} - X^{n+1}_{(i,j)}}{\delta x_i} - D_{X(i-\frac{1}{2},j)} \frac{X^{n+1}_{(i,j)} - X^{n+1}_{(i-1,j)}}{\delta x_{i-1}}]$$
$$+\Delta y_j [D_{T(i+\frac{1}{2},j)} \frac{T^{*}_{(i+1,j)} - T^{*}_{(i,j)}}{\delta x_i} - D_{T(i-\frac{1}{2},j)} \frac{T^{*}_{(i,j)} - T^{*}_{(i-1,j)}}{\delta x_{i-1}}] \; . \tag{7.4}$$

The discretization of the energy balance for an internal control volume using the fully implicit method yields:

$$(\rho C_p)_{eff(i,j)}\Delta y_j \Delta x_i \frac{T^{n+1}_{(i,j)} - T^{n}_{(i,j)}}{\Delta t} =$$
$$\Delta x_i[\lambda_{eff(i,j+\frac{1}{2})}\frac{T^{n+1}_{(i,j+1)} - T^{n+1}_{(i,j)}}{\delta y_j} - \lambda_{eff(i,j-\frac{1}{2})}\frac{T^{n+1}_{(i,j)} - T^{n+1}_{(i,j-1)}}{\delta y_{j-1}}]$$
$$+\Delta x_i[\lambda_{X(i,j+\frac{1}{2})}\frac{X^{*}_{(i,j+1)} - X^{*}_{(i,j)}}{\delta y_j} - \lambda_{X(i,j-\frac{1}{2})}\frac{X^{*}_{(i,j)} - X^{*}_{(i,j-1)}}{\delta y_{j-1}}]$$
$$+\Delta y_j[\lambda_{eff(i+\frac{1}{2},j)}\frac{T^{n+1}_{(i+1,j)} - T^{n+1}_{(i,j)}}{\delta x_i} - \lambda_{eff(i-\frac{1}{2},j)}\frac{T^{n+1}_{(i,j)} - T^{n+1}_{(i-1,j)}}{\delta x_{i-1}}]$$
$$+\Delta y_j[\lambda_{X(i+\frac{1}{2},j)}\frac{X^{*}_{(i+1,j)} - X^{*}_{(i,j)}}{\delta x_i} - \lambda_{X(i-\frac{1}{2},j)}\frac{X^{*}_{(i,j)} - X^{*}_{(i-1,j)}}{\delta x_{i-1}}] \quad . \tag{7.5}$$

where $X^{*}_{(i,j)} = X^{n}_{(i,j)}$. During the computations, it was observed that this type of slection of X^{*} causes faster convergence and changing it to X^{n+1} did not show any change in the results since moisture content changes very slowly with time.

Rerarranging the discretized mass equation in each half time step in a similar format for the one dimensional case of TDMA algorithm results in:

$$a_{X,j}X^{n+\frac{1}{2}}_{(i,j-1)} + b_{X,j}X^{n+\frac{1}{2}}_{(i,j)} + c_{X,j}X^{n+\frac{1}{2}}_{(i,j+1)} = d_{X,j} \quad . \tag{7.6}$$

$$a_{X,i}X^{n+1}_{(i-1,j)} + b_{X,i}X^{n+1}_{(i,j)} + c_{X,i}X^{n+1}_{(i+1,j)} = d_{X,i} \quad . \tag{7.7}$$

where

$$a_{X,j} = -\Delta x_i \frac{\Delta t}{2}\frac{D_{X(i,j-\frac{1}{2})}}{\delta y_{j-1}} \quad , \tag{7.8}$$

$$b_{X,j} = \Delta x_i[\rho_d \Delta y_j + \frac{\Delta t}{2}(\frac{D_{X(i,j+\frac{1}{2})}}{\delta y_j} + \frac{D_{X(i,j-\frac{1}{2})}}{\delta y_{j-1}})] \quad , \tag{7.9}$$

$$c_{X,j} = -\Delta x_i \frac{\Delta t}{2}\frac{D_{X(i,j+\frac{1}{2})}}{\delta y_j} \quad , \tag{7.10}$$

$$
\begin{aligned}
d_{X,j} &= \rho_d \Delta x_i \Delta y_j . X^n_{(i,j)} \\
&+ \frac{\Delta t}{2} \Delta x_i [D_{T(i,j+\frac{1}{2})} \frac{T^*_{(i,j+1)} - T^*_{(i,j)}}{\delta y_j} - D_{T(i,j-\frac{1}{2})} \frac{T^*_{(i,j)} - T^*_{(i,j-1)}}{\delta y_{j-1}}] \\
&+ \Delta y_j \frac{\Delta t}{2} [D_{X(i+\frac{1}{2},j)} \frac{X^n_{(i+1,j)} - X^n_{(i,j)}}{\delta x_i} - D_{X(i-\frac{1}{2},j)} \frac{X^n_{(i,j)} - X^n_{(i-1,j)}}{\delta x_{i-1}}] \\
&+ \Delta y_j \frac{\Delta t}{2} [D_{T(i+\frac{1}{2},j)} \frac{T^*_{(i+1,j)} - T^*_{(i,j)}}{\delta x_i} - D_{T(i-\frac{1}{2},j)} \frac{T^*_{(i,j)} - T^*_{(i-1,j)}}{\delta x_{i-1}}] \quad , \qquad (7.11)
\end{aligned}
$$

and

$$
a_{X,i} = -\Delta y_j \frac{\Delta t}{2} \frac{D_{X(i-\frac{1}{2},j)}}{\delta x_{i-1}} \quad , \qquad (7.12)
$$

$$
b_{X,i} = \Delta y_j [\rho_d \Delta x_i + \frac{\Delta t}{2} (\frac{D_{X(i+\frac{1}{2},j)}}{\delta x_i} + \frac{D_{X(i-\frac{1}{2},j)}}{\delta x_{i-1}})] \quad . \qquad (7.13)
$$

$$
c_{X,i} = -\Delta y_j \frac{\Delta t}{2} \frac{D_{X(i+\frac{1}{2},j)}}{\delta x_i} \quad , \qquad (7.14)
$$

$$
\begin{aligned}
d_{X,i} &= \rho_d \Delta x_i \Delta y_j . X^{n+\frac{1}{2}}_{(i,j)} \\
&+ \frac{\Delta t}{2} \Delta x_i [D_{T(i,j+\frac{1}{2})} \frac{T^*_{(i,j+1)} - T^*_{(i,j)}}{\delta y_j} - D_{T(i,j-\frac{1}{2})} \frac{T^*_{(i,j)} - T^*_{(i,j-1)}}{\delta y_{j-1}}] \\
&+ \Delta x_i \frac{\Delta t}{2} [D_{X(i,j+\frac{1}{2})} \frac{X^{n+\frac{1}{2}}_{(i,j+1)} - X^{n+\frac{1}{2}}_{(i,j)}}{\delta y_j} - D_{X(i,j-\frac{1}{2})} \frac{X^{n+\frac{1}{2}}_{(i,j)} - X^{n+\frac{1}{2}}_{(i,j-1)}}{\delta y_{j-1}}] \\
&+ \Delta y_j \frac{\Delta t}{2} [D_{T(i+\frac{1}{2},j)} \frac{T^*_{(i+1,j)} - T^*_{(i,j)}}{\delta x_i} - D_{T(i-\frac{1}{2},j)} \frac{T^*_{(i,j)} - T^*_{(i-1,j)}}{\delta x_{i-1}}] . \qquad (7.15)
\end{aligned}
$$

In order to solve the heat transfer equation by SOR method, this equation is rewritten in the following format:

$$
a_{(i,j)} T^{n+1}_{(i+1,j)} + b_{(i,j)} T^{n+1}_{(i-1,j)} + c_{(i,j)} T^{n+1}_{(i,j+1)} + d_{(i,j)} T^{n+1}_{(i,j-1)} + e_{(i,j)} T^{n+1}_{(i,j)} = f_{(i,j)} \quad . \qquad (7.16)
$$

where:

$$
a_{(i,j)} = -\Delta t \Delta y_j \frac{\lambda_{eff(i+\frac{1}{2},j)}}{\delta x_i} \quad , \qquad (7.17)
$$

$$b_{(i,j)} = -\Delta t \Delta y_j \frac{\lambda_{eff(i-\frac{1}{2},j)}}{\delta x_{i-1}} \quad , \tag{7.18}$$

$$c_{(i,j)} = -\Delta t \Delta x_i \frac{\lambda_{eff(i,j+\frac{1}{2})}}{\delta y_j} \quad , \tag{7.19}$$

$$d_{(i,j)} = -\Delta t \Delta x_i \frac{\lambda_{eff(i,j-\frac{1}{2})}}{\delta y_{j-1}} \quad , \tag{7.20}$$

$$\begin{aligned} e_{(i,j)} = (\rho C_p)_{eff(i,j)} \Delta x_i \Delta y_j + \Delta t \Delta y_j \left(\frac{\lambda_{eff(i+\frac{1}{2},j)}}{\delta x_i} + \frac{\lambda_{eff(i-\frac{1}{2},j)}}{\delta x_{i-1}}\right) \\ + \Delta t \Delta x_i \left(\frac{\lambda_{eff(i,j+\frac{1}{2})}}{\delta y_j} + \frac{\lambda_{eff(i,j-\frac{1}{2})}}{\delta y_{j-1}}\right) \quad . \end{aligned} \tag{7.21}$$

$$\begin{aligned} f_{(i,j)} = (\rho C_p)_{eff(i,j)} \Delta x_i \Delta y_j T^n_{(i,j)} \\ + \Delta t \Delta x_i \left[\lambda_{X(i,j+\frac{1}{2})} \frac{X^*_{(i,j+1)} - X^*_{(i,j)}}{\delta y_j} - \lambda_{X(i,j-\frac{1}{2})} \frac{X^*_{(i,j)} - X^*_{(i,j-1)}}{\delta y_{j-1}}\right] \\ + \Delta t \Delta y_j \left[\lambda_{X(i+\frac{1}{2},j)} \frac{X^*_{(i+1,j)} - X^*_{(i,j)}}{\delta x_i} - \lambda_{X(i-\frac{1}{2},j)} \frac{X^*_{(i,j)} - X^*_{(i-1,j)}}{\delta x_{i-1}}\right] . \end{aligned} \tag{7.22}$$

7.2 Treatment of boundary nodes

Since most boundary nodes are dealt with in a similar way, the discretized equations for type 1 of Figure 7.1 is discussed here. This node is located on the front vertical surface and the right hand side of axis of symmetry. Implementing the ADI method to the mass balance during the first half time step for a control volume surrounding this point yields:

$$\begin{aligned} \rho_d \frac{\Delta y_j}{2} \frac{\Delta x_i}{2} \frac{X^{n+\frac{1}{2}}_{(i,j)} - X^n_{(i,j)}}{\frac{\Delta t}{2}} = -h_m \frac{\Delta y_j}{2} \epsilon_{(i,j)} \rho_{v(i,j)} (X^n_{(i,j)} - X_{eq-air}) \\ + \frac{\Delta x_i}{2} \left[D_{X(i,j+\frac{1}{2})} \frac{X^{n+\frac{1}{2}}_{(i,j+1)} - X^{n+\frac{1}{2}}_{(i,j)}}{\delta y_j} + D_{T(i,j+\frac{1}{2})} \frac{T^*_{(i,j+1)} - T^*_{(i,j)}}{\delta y_j}\right] \\ + \frac{\Delta y_j}{2} \left[D_{X(i+\frac{1}{2},j)} \frac{X^n_{(i+1,j)} - X^n_{(i,j)}}{\delta x_i} + D_{T(i+\frac{1}{2},j)} \frac{T^*_{(i+1,j)} - T^*_{(i,j)}}{\delta x_i}\right] . \end{aligned} \tag{7.23}$$

The discretized form of mass balance for the second half time step is:

$$\rho_d \frac{\Delta y_j}{2}\frac{\Delta x_i}{2}\frac{X_{(i,j)}^{n+1} - X_{(i,j)}^{n+\frac{1}{2}}}{\frac{\Delta t}{2}} = -h_m \frac{\Delta y_j}{2}\epsilon_{(i,j)}\rho_{v(i,j)}(X_{(i,j)}^{n+1} - X_{eq-air})$$
$$+\frac{\Delta x_i}{2}[D_{X(i,j+\frac{1}{2})}\frac{X_{(i,j+1)}^{n+\frac{1}{2}} - X_{(i,j)}^{n+\frac{1}{2}}}{\delta y_j} + D_{T(i,j+\frac{1}{2})}\frac{T_{(i,j+1)}^{*} - T_{(i,j)}^{*}}{\delta y_j}]$$
$$+\frac{\Delta y_j}{2}[D_{X(i+\frac{1}{2},j)}\frac{X_{(i+1,j)}^{n+1} - X_{(i,j)}^{n+1}}{\delta x_i} + D_{T(i+\frac{1}{2},j)}\frac{T_{(i+1,j)}^{*} - T_{(i,j)}^{*}}{\delta x_i}] \ . \qquad (7.24)$$

The balance of energy for the same control volume, using the fully implicit method. can be written as:

$$(\rho C_p)_{eff(i,j)}\frac{\Delta y_j}{2}\frac{\Delta x_i}{2}\frac{T_{(i,j)}^{n+1} - T_{(i,j)}^{n}}{\Delta t} =$$
$$-h_m \frac{\Delta y_j}{2}h_{v(i,j)}^{n+1}\epsilon_{(i,j)}\rho_{v(i,j)}(X_{(i,j)}^{*} - X_{eq-air}) - h\frac{\Delta y_j}{2}(T_{(i,j)}^{n+1} - T_{db-air})$$
$$+\frac{\Delta x_i}{2}[\lambda_{eff(i,j+\frac{1}{2})}\frac{T_{(i,j+1)}^{n+1} - T_{(i,j)}^{n+1}}{\delta y_j} + \lambda_{X(i,j+\frac{1}{2})}\frac{X_{(i,j+1)}^{*} - X_{(i,j)}^{*}}{\delta y_j}]$$
$$+\frac{\Delta y_j}{2}[\lambda_{eff(i+\frac{1}{2},j)}\frac{T_{(i+1,j)}^{n+1} - T_{(i,j)}^{n+1}}{\delta x_i} + \lambda_{X(i+\frac{1}{2},j)}\frac{X_{(i+1,j)}^{*} - X_{(i,j)}^{*}}{\delta x_i}] \ . \qquad (7.25)$$

Here, like the one dimensional case we use the following relationship for $h_{v(i,j)}$. the enthalpy of water vapor:

$$h_{v(i,j)}^{n+1} = h_{v(i,j)}^{n} + C_{p-v(i,j)}(T_{(i,j)}^{n+1} - T_{(i,j)}^{n}) \ . \qquad (7.26)$$

The rearrangement of the mass balance equations in the TDMA format for internal node yields $a_{X,j} = 0$, $a_{X,i} = 0$ and:

$$b_{X,j} = \Delta x_i[\rho_d \Delta y_j + \Delta t\frac{D_{X(i,j+\frac{1}{2})}}{\delta y_j}] \quad , \qquad (7.27)$$

$$c_{X,j} = -\Delta x_i \Delta t\frac{D_{X(i,j+\frac{1}{2})}}{\delta y_j} \quad , \qquad (7.28)$$

$$d_{X,j} = \rho_d \Delta x_i \Delta y_j X^n_{(i,j)} + \Delta t \Delta x_i D_{T(i,j+\frac{1}{2})} \frac{T^*_{(i,j+1)} - T^*_{(i,j)}}{\delta y_j}$$
$$- h_m \Delta y_j \Delta t \epsilon_{(i,j)} \rho_{v(i,j)} (X^n_{(i,j)} - X_{eq-air})$$
$$+ \Delta y_j \Delta t [D_{X(i+\frac{1}{2},j)} \frac{X^n_{(i+1,j)} - X^n_{(i,j)}}{\delta x_i} + D_{T(i+\frac{1}{2},j)} \frac{T^*_{(i+1,j)} - T^*_{(i,j)}}{\delta x_i}] \quad , \tag{7.29}$$

and:

$$b_{X,i} = \Delta y_j [\rho_d \Delta x_i + \Delta t (\frac{D_{X(i+\frac{1}{2},j)}}{\delta x_i} + h_m \epsilon_{(i,j)} \rho_{v(i,j)})] \quad , \tag{7.30}$$

$$c_{X,i} = -\Delta y_j \Delta t \frac{D_{X(i+\frac{1}{2},j)}}{\delta x_i} \quad , \tag{7.31}$$

$$d_{X,i} = \rho_d \Delta x_i \Delta y_j X^{n+\frac{1}{2}}_{(i,j)}$$
$$+ \Delta t \Delta x_i [D_{T(i,j+\frac{1}{2})} \frac{T^*_{(i,j+1)} - T^*_{(i,j)}}{\delta y_j} + D_{X(i,j+\frac{1}{2})} \frac{X^{n+\frac{1}{2}}_{(i,j+1)} - X^{n+\frac{1}{2}}_{(i,j)}}{\delta y_j}]$$
$$+ \Delta y_j \Delta t [D_{T(i+\frac{1}{2},j)} \frac{T^*_{(i+1,j)} - T^*_{(i,j)}}{\delta x_i} + h_m \epsilon_{(i,j)} \rho_{v(i,j)} X_{eq-air}] \, . \tag{7.32}$$

Writing the balance of energy in the format used for SOR solver results in $b_{(i,j)} = 0$, $d_{(i,j)} = 0$, and:

$$a_{(i,j)} = -\Delta t \Delta y_j \frac{\lambda_{eff(i+\frac{1}{2},j)}}{\delta x_i} \quad , \tag{7.33}$$

$$c_{(i,j)} = -\Delta t \Delta x_i \frac{\lambda_{eff(i,j+\frac{1}{2})}}{\delta y_j} \quad , \tag{7.34}$$

$$e_{(i,j)} = (\rho C_p)_{eff(i,j)} \Delta x_i \frac{\Delta y_j}{2} + h \Delta t \Delta y_j$$
$$+ \Delta t \Delta y_j C_{p-v(i,j)} h_m \epsilon_{(i,j)} \rho_{v(i,j)} (X^*_{(i,j)} - X_{eq-air})$$
$$+ \Delta t (\Delta y_j \frac{\lambda_{eff(i+\frac{1}{2},j)}}{\delta x_i} + \Delta x_i \frac{\lambda_{eff(i,j+\frac{1}{2})}}{\delta y_j}) \quad , \tag{7.35}$$

$$f_{(i,j)} = (\rho C_p)_{eff(i,j)} \Delta x_i \frac{\Delta y_j}{2} T^n_{(i,j)} + h \Delta t \Delta y_j T_{db-air}$$
$$- \Delta t \Delta y_j h_m \epsilon_{(i,j)} \rho_{v(i,j)} (X^*_{(i,j)} - X_{eq-air}) (h^n_{v(i,j)} - C_{p-v} T^n_{(i,j)})$$
$$+ \Delta t (\Delta x_i \lambda_{X(i,j+\frac{1}{2})} \frac{X^*_{(i,j+1)} - X^*_{(i,j)}}{\delta y_j} + \Delta y_j \lambda_{X(i+\frac{1}{2},j)} \frac{X^*_{(i+1,j)} - X^*_{(i,j)}}{\delta x_i}) \, . \tag{7.36}$$

7.3 Changes in drying air condition inside the stack due to heat and mass transfer

Due to heat transfer from air to the boards, the air temperature decreases streamwise inside the stack. Also the migration of moisture from boards increases the absolute humidity, ω, of air along the main flow direction. These two mechanisms cause an increase in air relative humidity, R_h, and decrease of X_{eq-air}. This might lead to saturation of drying air with water (air relative humidity becomes %100). In order to consider the above facts, the heat and mass balance for a control volume extended between the stack inlet and any position in the stack should be written. Such a control volume is shown in Figure 7.4 . $\Delta\dot{Q}$ and $\Delta\dot{m}_v$ are heat and mass transfered between planks and drying air up to station x, respectively. Also $\dot{m}_t$, $\dot{m}_v$ and $\dot{m}_{air}$ represent the total mass flux of moist air, water vapor exist in air and dry air, respectively. Therefore:

$$\dot{m}_t = \dot{m}_v + \dot{m}_{air} \ . \tag{7.37}$$

ω is defined as:

$$\omega = \frac{\dot{m}_v}{\dot{m}_{air}} = \frac{\dot{m}_t - \dot{m}_{air}}{\dot{m}_{air}} \ . \tag{7.38}$$

The balance of mass and energy for the mentioned control volume yields:

$$\Delta\dot{m}_v = \int_0^x d\dot{m}_v = \int_0^x h_m \epsilon_{(i,j)} \rho_{v(i,j)} [X^*_{(i,j)} - X_{eq-air}].dl \quad , \tag{7.39}$$

$$\Delta\dot{Q} = \int_0^x d\dot{Q} = \int_0^x h[T_{(i,j)} - T_{db-air}].dl + \int_0^x h_{v(i,j)} h_m \epsilon_{(i,j)} \rho_{v(i,j)} [X^*_{(i,j)} - X_{eq-air}].dl \quad , \tag{7.40}$$

where dl is the length of control volume exposed to drying air. The above integrations can be calculated using computational techniques. The air dry-bulb temperature at

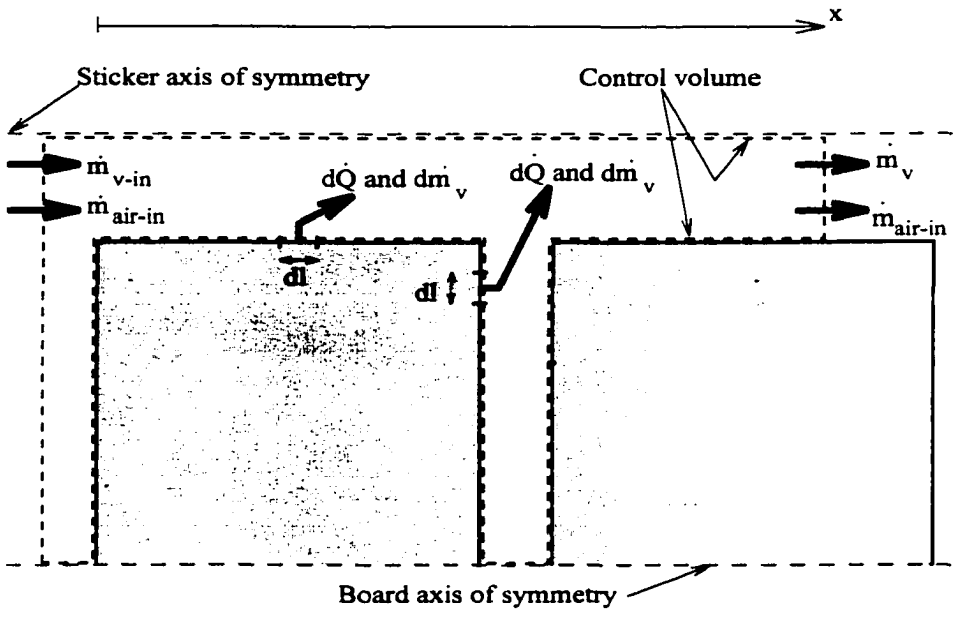

Figure 7.4: Schematic view of control volume used for considering the effect of heat/mass transfer between air and boards

station x, based on the definition of mean temperature, can be written as:

$$T_{db} = T_{db-in} + \frac{\Delta \dot{Q}}{\dot{m}_t C_{P-air}} \,. \tag{7.41}$$

The relative humidity of moist air, R_h, at any location is related to P_{atm}, the atmospheric pressure, as[73]:

$$R_h = \frac{\omega P_{atm}}{P_{sv(T_{db})}(0.62198 + \omega)} \quad , \tag{7.42}$$

where $P_{sv(T_{db})}$ is the saturated vapor pressure of water vapor at dry-bulb temperature. Knowing R_h and T_{db}, the X_{eq-air} can be calculated using the relationships mentioned in Chapter 4. When we obtain $R_h > 1$ (saturation), its value is considered 1 and the corrected ω, $\Delta \dot{m}_v$, $\Delta \dot{Q}$, T_{db} and X_{eq-air} are obtained by back substitution and trial and error.

7.4 Solution procedure for the two dimensional case

The discretized equations for heat and mass transfer are solved separately and the solution process is continued through an outer iteration until convergence (see the flow chart of the program in Figure 7.3). The drying air conditions are updated at the end of each time step. The program has two different versions for solving the mass transfer equation using the ADI or Fully Implicit methods. As was mentioned earlier, the ADI version uses the TDMA algorithm for solving the moisture content field in each half time step. The SOR algorithm with Chebyshev acceleration technique is adopted and modified to solve the equations discretized using fully implicit method. The program uses this solver for temperature field as well as for fully implicit version of the mass transfer.

7.4.1 Chebyshev acceleration version of SOR method

For the SOR method, we define the residue of the equation as:

$$\begin{aligned}\xi_{(i,j)} = a_{(i,j)}T^{n+1}_{(i+1,j)} + b_{(i,j)}T^{n+1}_{(i-1,j)} + c_{(i,j)}T^{n+1}_{(i,j+1)} \\ +d_{(i,j)}T^{n+1}_{(i,j-1)} + e_{(i,j)}T^{n+1}_{(i,j)} - f_{(i,j)} \ .\end{aligned} \tag{7.43}$$

The formulation for the new parameter, e.g. $T^{new}_{(i,j)}$, in this iterative method is:

$$T^{new}_{(i,j)} = T^{old}_{(i,j)} - \Omega\frac{\xi_{(i,j)}}{e_{(i,j)}} \ . \tag{7.44}$$

The convergence criterion for terminating the iteratin is related to maximum of the norm of the residual. The optimal choice for Ω is given by (see [72]):

$$\Omega_{optimal} = \frac{2}{1+\sqrt{1-\rho^2_{Jacobi}}} \ . \tag{7.45}$$

ρ_{Jacobi}, the spectral radius of the Jacobi iteration, for a rectangular uniform $J \times L$ grid, is:

$$\rho_{Jacobi} = \frac{cos\frac{\pi}{J} + (\frac{\Delta x}{\Delta y})^2 cos\frac{\pi}{L}}{1 + (\frac{\Delta x}{\Delta y})^2} \quad . \tag{7.46}$$

Usually the asymptotic rate of convergence in SOR is not attained until the J^{th} iterations. The error often grows by a factor of 20 before convergence is achieved. The Ω defined above is the optimum asymptotic relaxation parameter, but it is not necessarily a good initial choice. In SOR with Chebyshev acceleration, odd-even ordering is used and Ω is changed at each half sweep according to the following formulation:

$$\begin{aligned} \Omega^0 &= 1 \quad , \\ \Omega^{\frac{1}{2}} &= \frac{1}{1 - 0.5\rho^2_{Jacobi}} \quad , \\ \Omega^{k+\frac{1}{2}} &= \frac{1}{1 - 0.25\rho^2_{Jacobi}\Omega^k}, k = \frac{1}{2}, 1, ..., \infty \quad , \\ \Omega^{\infty} &\rightarrow \Omega_{optimal} \quad . \end{aligned} \tag{7.47}$$

By this type of formulation, the norm of error for $T_{(i,j)}$ always decreases with each iteration. The other modification is the changing the start location of sweeping from one corner to the opposite corner of the domain after a certain number of iterations. This was done to reduce the difference between values at different points when a one dimensional case is solved using the two dimensional approach. In such a case, in the direction with no change, all the calculated values should be the same. Without this modification, there is a tendency for the small errors to grow and cause instability.

Time duration[hr]	Dry-bulb temperature[^oC]	Wet-bulb temperature[^oC]	X_{eq} %	Relative humidity%
12	54	49	12.1	75
48	$54 + \frac{28}{48}(t-12)$	$49 + \frac{5}{48}(t-12)$	$3.3 \leq X_{eq} \leq 12.1$	$26 \leq R_h \leq 75$
($X_{av} \geq 13\%$)	82	54	3.3	26
2.333	$82 - \frac{16.9}{2.3}(t-t_c)$	$54 + \frac{7}{2.3}(t-t_c)$	$3.3 \leq X_{eq} \leq 13.7$	$26_h \leq 82$
21.85	65.1	61	13.7	82

Table 7.1: Drying air schedule used in present work (Li[52])

7.5 Process of obtaining the model unknowns

In modelling of the conventional kiln drying of western hemlock, certain unknown parameters are required to achieve the desired performance for different gap sizes and drying air conditions (temperature, relative humidity and velocity). Several sets of experimental data of Li[52] have been considered for adjaustments of the model parameters. Two of these are runs number 7 and 10 of [52], which have the specifications of Re=4400, g=1.5 mm and Re=8800, g=21.5 mm. Table 7.1 shows the time schedule of wet- and dry-bulb temperature, relative humidity and equilbrium moisture content of drying air at the inlet of kiln used in the present study as well as Li's tests. In this schedule, the third stage is the longest one. This stage is continued until a preset stack average moisture content, here 13 percent, is achieved. The final stage of the drying schedule is the *conditioning* followed after a transition stage. During the conditioning process a moist air with a larger equilibrium moisture content than the preset one and close to the desired X_{eq} for the final product is sent through the stack. The main purpose of this process is to increase the moisture content of the board surface already over dried.

For the stack array with g=1.5 mm since the effect of side gaps is not significant,

a one dimensional analysis for seven individual boards of a row, similar to the process of Chapter 6 was performed. In this case, first the average Nu number of each board was obtained using the results of Chapter 5. The effect of heat/mass transfer from the front wall of the first board and the rear wall of the last board were taken into account. This was carried out by adding the percentage of the total heat transfer from each board through these faces, to the averege surface coefficients of the related board. Then the model unknowns were changed, starting with values obtained for pine, until a close fit between the computed time dependent average moisture content and experimental data was achieved.

Later, the information obtained through the one dimensional analysis for the unknown parameters of the model are used as initial guesses for the two dimensional analysis. Here the grid array of 76×40 for each board was used for all simulations. The grids were uiform in the x direction. In the $y-$ direction, grids have an expansion factor of 1.1 allowing smaller control volume sizes closer to horizontal faces of the boards. The convergence criterion for temperature field at each board, solved by the SOR method, was set as:

$$S_{err} < 10^{-13} \sum_{i,j} |\xi_{(i,j)}|_{initial} \quad , \tag{7.48}$$

where:

$$S_{err} = \sum_{i,j} |\xi_{(i,j)}| \quad , \tag{7.49}$$

S_{err} is the summation of all the errors at different points which was defined already in Section 7.4.

The computaions were carried out for several sets of parameters until the best fit between results and experiments was attained. The final set of coefficients used for the two dimensional simulation of the drying process of hemlock in the present work are:

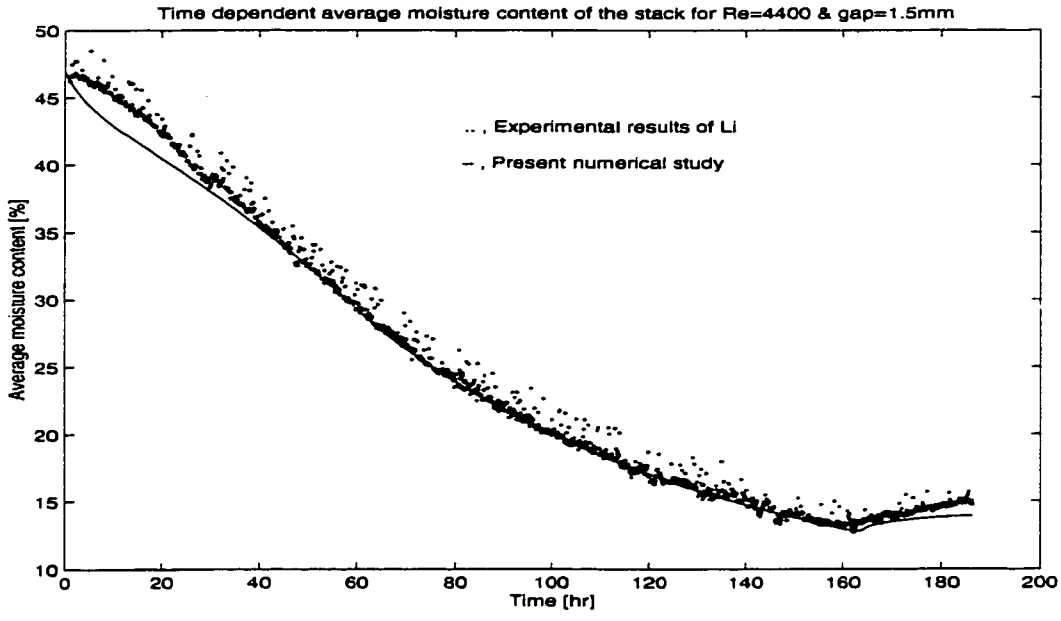

Figure 7.5: Time dependent stack average moisture content of the Li's geometry for g=1.5 mm at Re=4400

$S_T = 6500(^oC)$,

$K_{ls} = 1.1 \times 10^{-16} m^2$,

$\alpha = 0.0075$,

$D_\mu = 0.0041 Kg/m^3/s$,

$S_{min} = 0.028$.

Results for the average moisture content in these two cases are compared with the experimental data in Figures 7.5 and 7.6. The experimental trend is well produced. considering the dispersion of the data, shown completely in Figure 7.5 as an example. The moisture content is reasonably predicted by the model, particularly during the final conditioning process. This is a major contribution of the present work.

The average temperature at the center of boards is plotted against Li's test findings for Re=4400 and g=1.5 in Figure 7.7. Li reported that the difference between

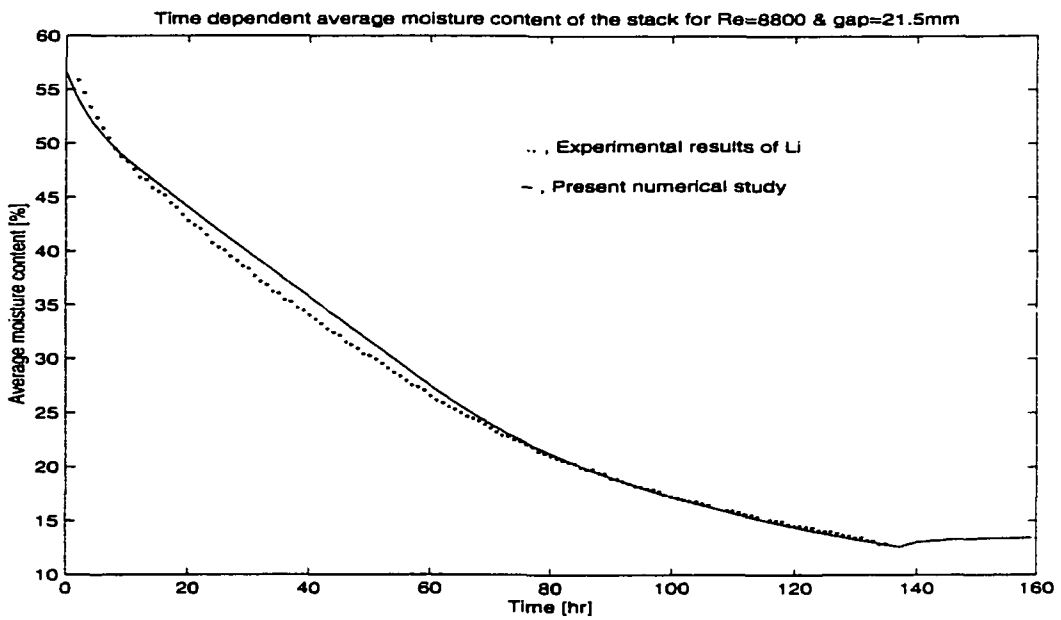

Figure 7.6: Time dependent stack average moisture content of the Li's geometry for g=21.5 mm at Re=8800

temperature at the center of different boards is small in most of the drying time. Therefore, the average value is a good parameter to study the performance of the model in predicting the tempearture across the stack. As it is observed in this Figure, the results are in good agreement with experiments.

7.6 Validation of the model

Validation of the model is carried out by comparing the numerical results with the experimental data of Li for Re=4400, g=21.5mm and Re=8800, g=1.5 mm. The numerical simulation results for the time dependent stack average moisture content are plotted along with the experimental data in Figures 7.8 and 7.9. As can be seen, the numerical model predicts the drying process in both cases.

Li performed different cuts in vertical, horizontal and central locations of the

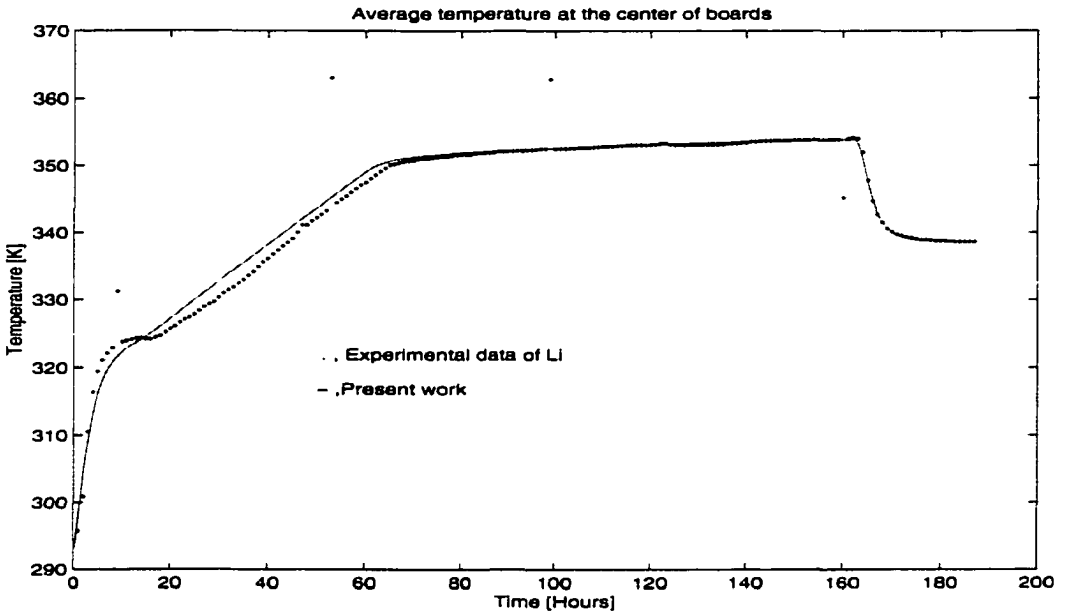

Figure 7.7: Average temperature at the center of the boards of the Li's geometry for g=1.5 mm at Re=4400

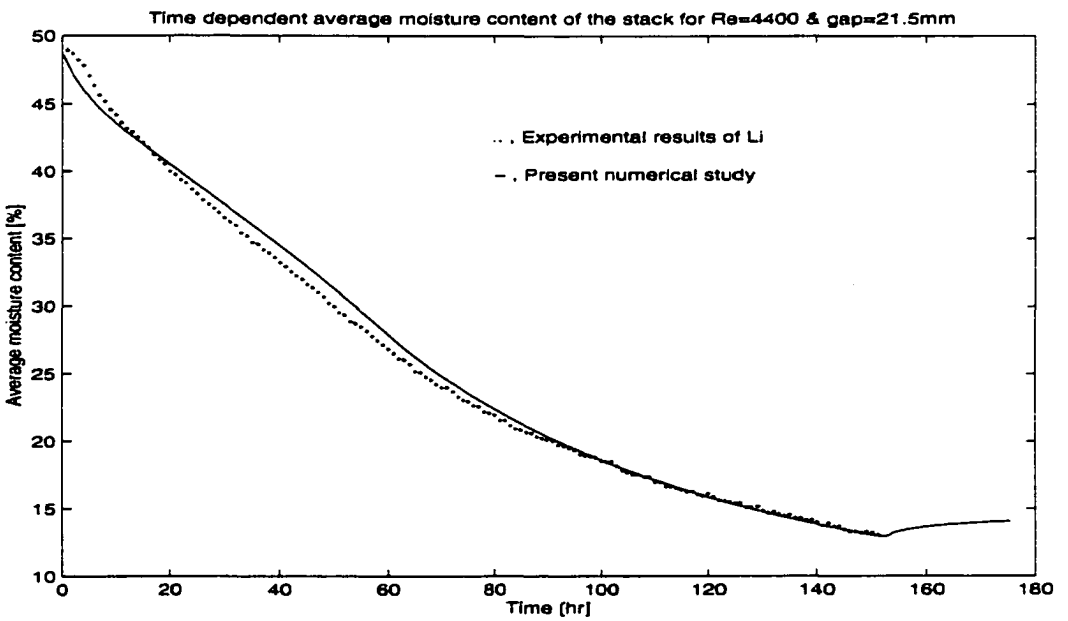

Figure 7.8: Time dependent stack average moisture content of the Li's geometry for g=21.5 mm at Re=4400

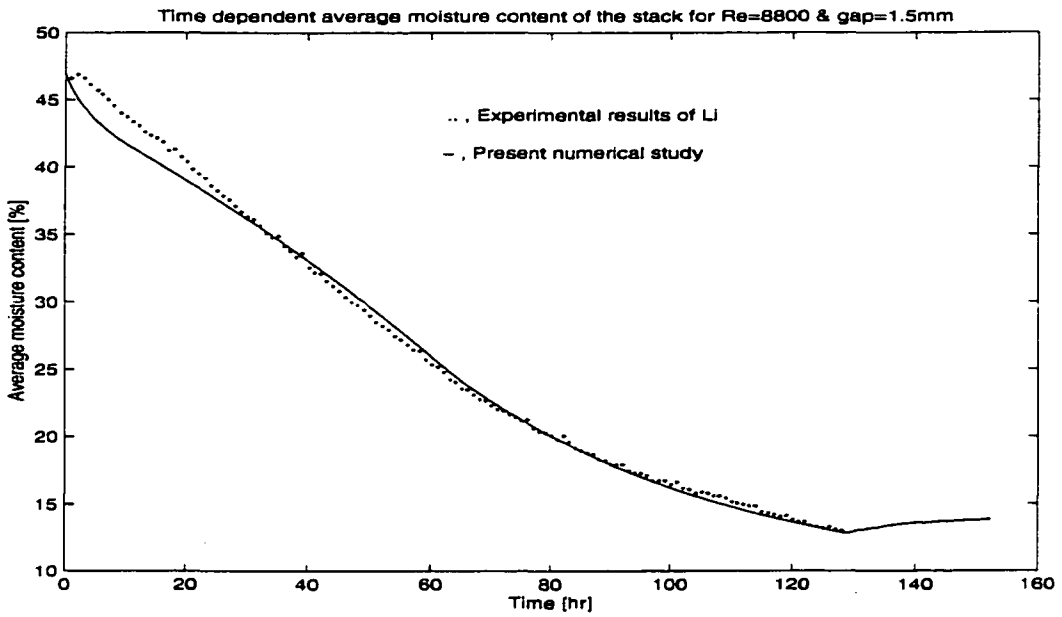

Figure 7.9: Time dependent stack average moisture content of the Li's geometry for g=1.5 mm at Re=8800

final product to investigate the distribution of local moisture contents at different locations of each board. In Figures 7.10 and 7.11, the data for the fourth boards of the row are compared with our numerical results for the drying conditions of Re=4400, g=21.5mm. The computed final average moisture content of the fourth board is 15.6% compared to the reported 16.7% of Li. Keeping this fact and the dispersion of experimental data in mind, the trend and values of the experimental data for moisture content of different cuts are well predicted. Thus, it can be concluded that the present model has shown a good performance in predicting the local and average moisture contents as well as the temperature field.

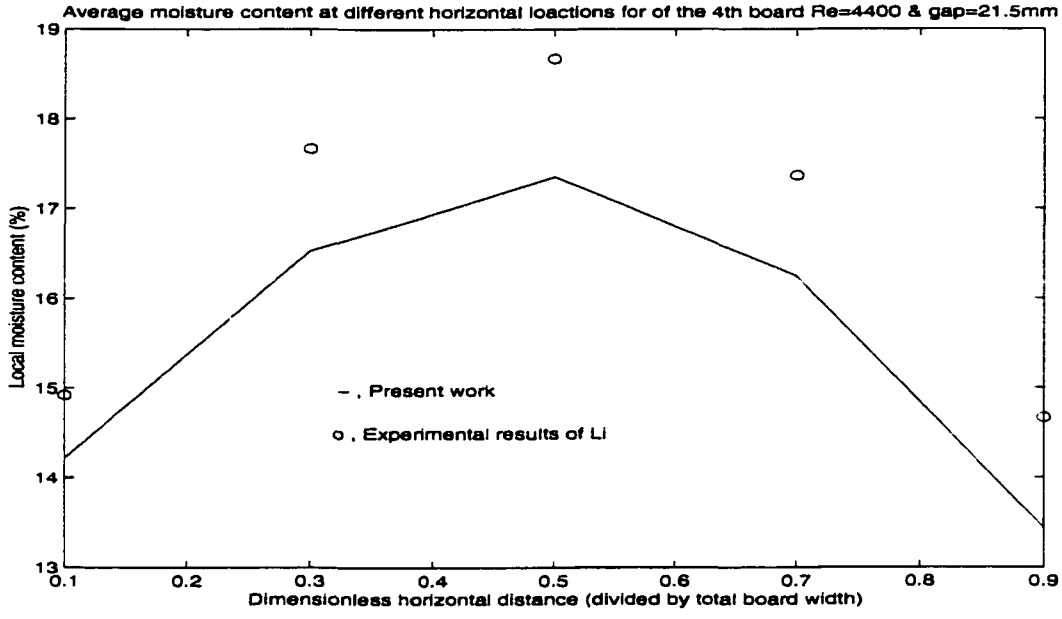

Figure 7.10: Distribution of local moisture content in horizontal direction of the forth board of the Li's geometry for g=21.5 mm at Re=4400

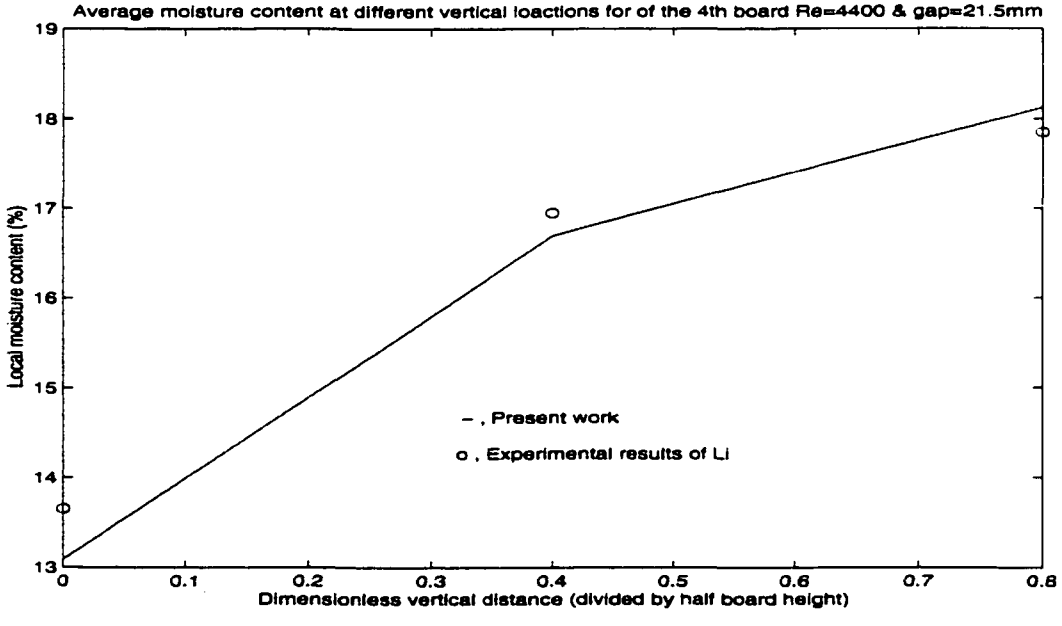

Figure 7.11: Distribution of local moisture content in vertical direction of the forth board of the Li's geometry for g=21.5 mm at Re=4400

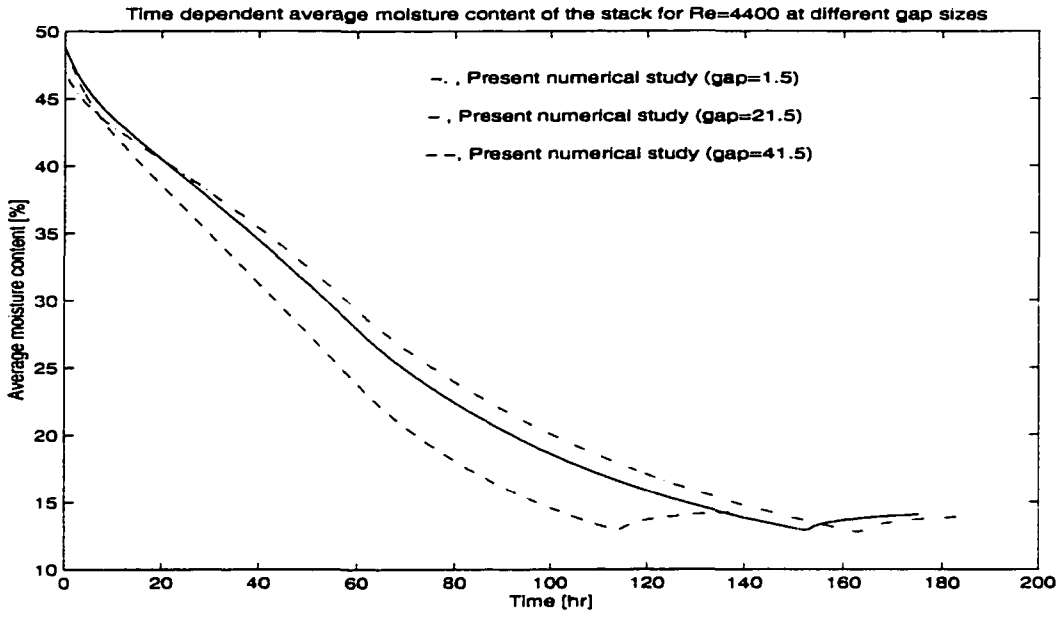

Figure 7.12: Time dependent stack average moisture content of the Li's geometry for different gaps at Re=4400

7.7 Effects of the optimum gap size on drying curves

Program runs were performed for optimum gap sizes of g=41.5 mm and 26.5 mm at Re=4400 and 8800, respectively. In one set of computations, the same initial conditions of boards(ρ_s and initial moisture contents) for the case of g=21.5 mm were used. Plotted in Figures 7.12 and 7.13 are the comparisons of these computations for time dependent stack average moisture content with those of the case of g=21.5 mm. The conditioning time period is the same in all cases (21.85 hours). It can be understood that using the optimum gap size decreases the drying time 21.9 and 6.2 percent compared with the case of g=21.5 mm at Re=4400 and 8800, respectively.

Similar computations were repeated using the initial conditions of the case of g=1.5 mm at each Re number. Figures 7.14 and 7.15 compares the drying curves

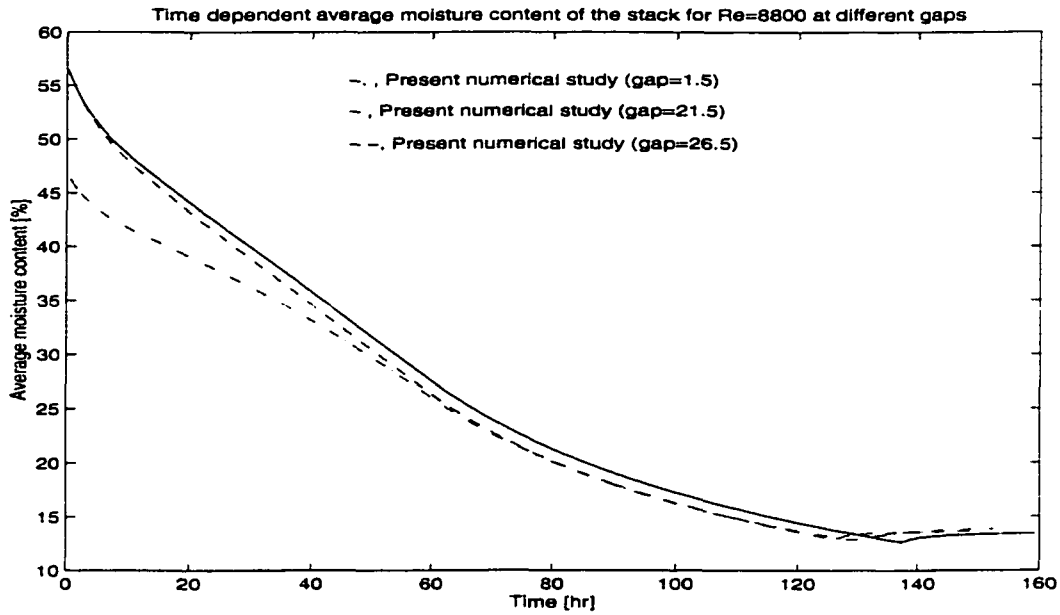

Figure 7.13: Time dependent stack average moisture content of the Li's geometry for different gap sizes at Re=8800

of such runs for optimum gap sizes with the case of g=1.5 mm at two different Re numbers of 4400 and 8800. According to these Figures, the optimum gap size reduces the drying time 27.0 and 11.6 percent in comparison with no side gap cases at Re=4400 and 8800, respectively.

Figures 7.16 and 7.17 show the distribution of moisture content across the fourth board at different times for Re=4400 when gap sizes are $g = 1.5mm$ and $g_{opt} = 41.5mm$. As can be seen in these Figures, the distribution of moisture content around the surfaces of the final product is more uniform when the stack array has the optimum gap size. This will result in a lower possibility of some defects due to a corresponding reduction in internal stresses. The same conclusion can be drawn for possibility of these defects during the whole period of drying.

Another case which was not investigated by Li is the one with $u_{center} = 7.62m/s$ or Re=13200. The initial conditions of the case of g=21.5 mm at Re=8800 was

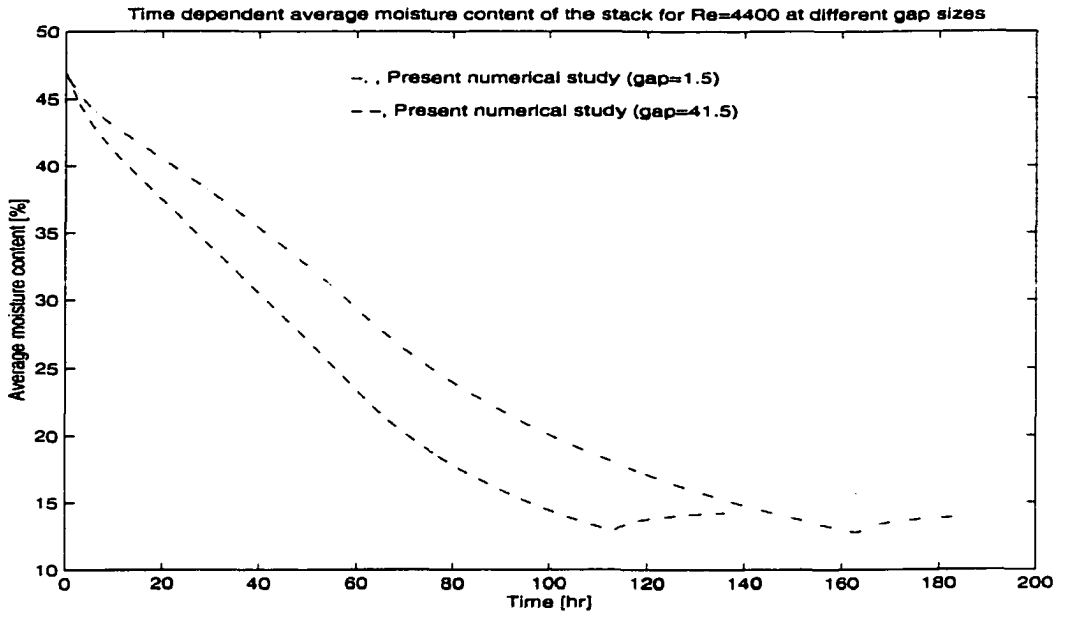

Figure 7.14: Time dependent stack average moisture content of the Li's geometry for different gaps at Re=4400

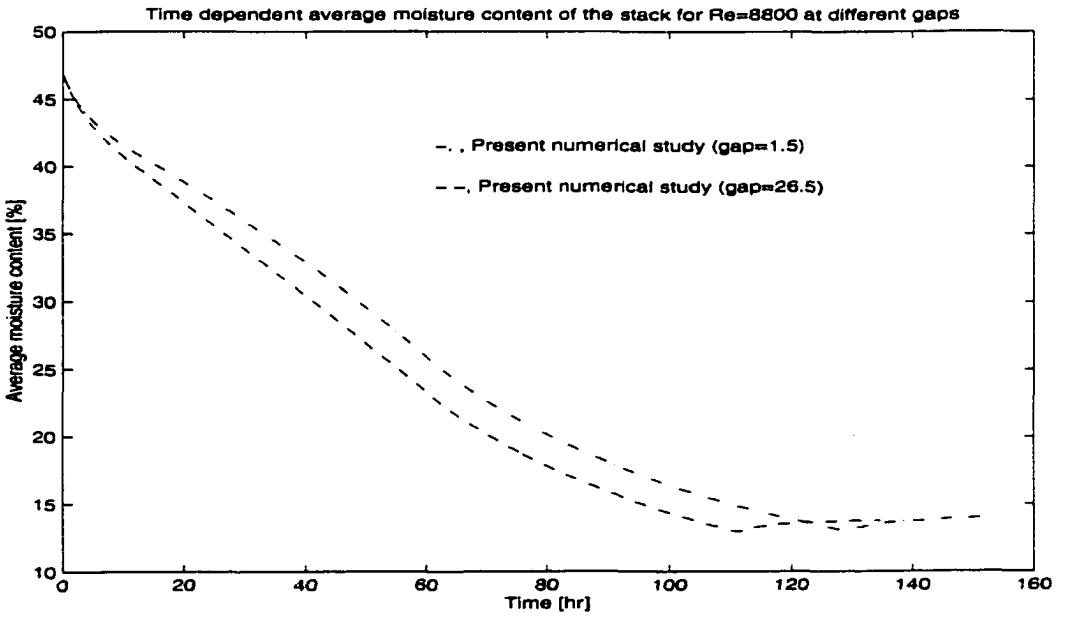

Figure 7.15: Time dependent stack average moisture content of the Li's geometry for different gap sizes at Re=8800

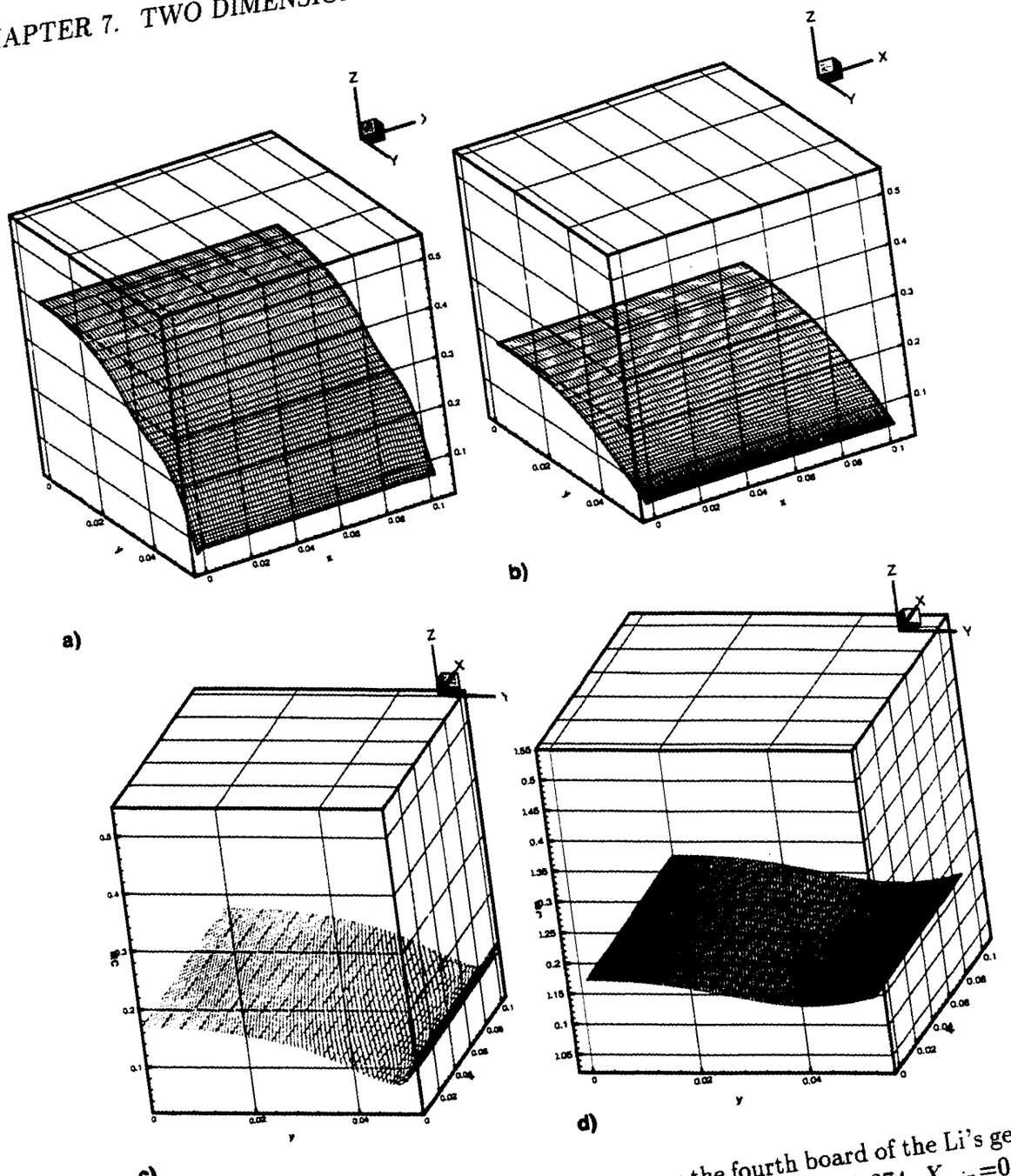

Figure 7.16: Distribution of moisture content across the fourth board of the Li's geometry at different times for Re=4400 and g=1.5mm; a=60hr (X_{max}=0.374, X_{min}=0.05), b=end of 3rd stage (X_{max}=0.17, X_{min}=0.039), c=end of 4th stage (X_{max}=0.169, X_{min}=0.072), d=end of conditioning (X_{max}=0.163, X_{min}=0.12)

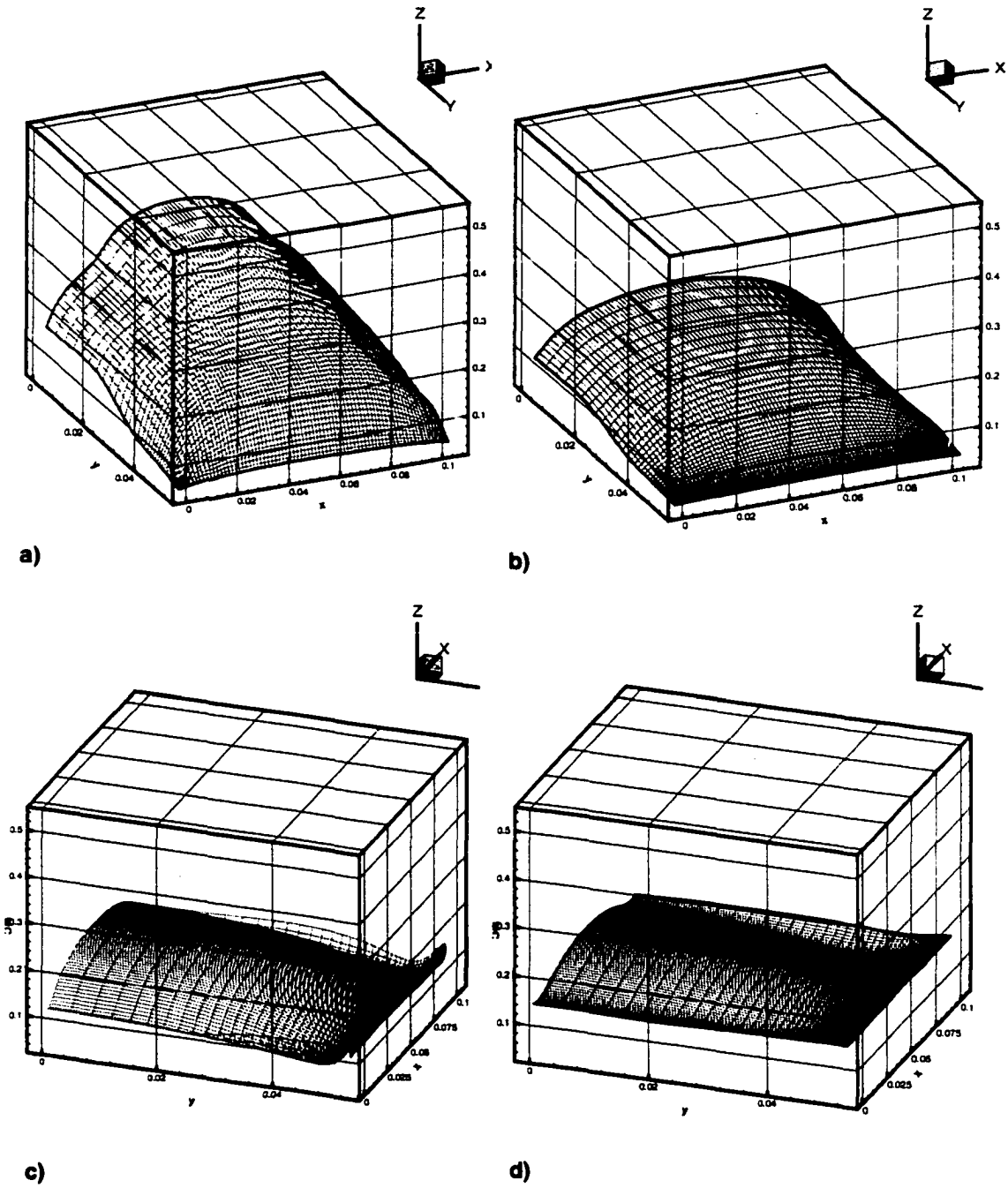

Figure 7.17: Distribution of moisture content across the fourth board of the Li's geometry at different times for Re=4400 and g=41.5mm; a=60hr (X_{max}=0.349, X_{min}=0.036), b=end of 3rd stage(X_{max}=0.183 ,X_{min}=0.035), c=end of 4th stage(X_{max}=0.182, X_{min}=0.052), d=end of conditioning(X_{max}=0.174, X_{min}=0.108)

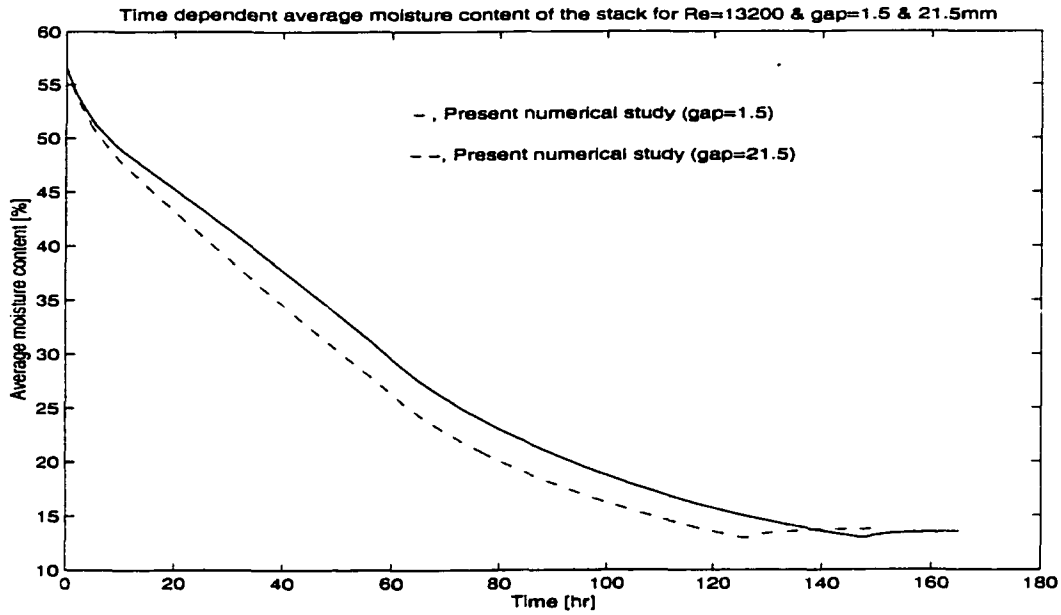

Figure 7.18: Time dependent stack average moisture content of the Li's geometry for different gap sizes at Re=13200

used for modelling of drying subjected to $g = 1.5mm$ and $g_{opt} = 21.5mm$ conditions at Re=13200. The drying curves are compared with each other in Figure 7.18. It demonstrates that the optimum gap size decreases the total drying time 12.8 percent.

7.8 Effects of the optimum gap size on uniformity of products

In drying of a stack, the ideal desired condition for dried products is that the products will have a uniform final local moisture content every where in the planks. Such an ideal case will result in best quality final products. This means: uniform strain (shrinkage); zero degraded and over dried product; and no need for redrying the under dried boards. One can imagine that in such a case:

a) the average moisture content of all the boards in a row are the same,

b) the standard and average deviation of each board, std_i and ad_i, as well as its average value of moisture content gradient are zero. The latter parameter can be defined as:

$$|\nabla X|_{av} = \frac{\sum[(\frac{\partial X}{\partial x})^2 + (\frac{\partial X}{\partial y})^2]^{1/2}\Delta x.\Delta y}{\sum \Delta x.\Delta y} . \tag{7.50}$$

The above mentioned three $non - uniformity$ parameters are time dependent and can be normalized if we divide them by the average moisture content of the related board. Plotted in Figures 7.19 to 7.24 are the absolute and normalized distributions of the non-uniformity parameters of each board versus the average moisture content of the same board when Re=4400 and g=1.5 mm. Also shown in Figure 7.25 is the time dependent standard deviation of boards for this case. All absolute graphs predict a sudden increase in nonuniformity of all the boards during the first stage of drying followed by another increase in the second stage. The maximum happens during the second stage of drying (between 42 to 52 hours) when we have the fastest rate of drying. During the third stage, which is the longest one and when the driest air is used, the non-uniformity drops. At the end of this stage, two groups are distinct. The first and last board are over-dried and their curves are close to each other for moisture contents less than 16 %. The same closeness is observed for the plots of the five middle boards when their X_{av} is less than 26 %. Also the last and first boards have the largest maximum non-uniformities. During the transition period between the third stage and the final conditioning stage, air becomes cooler and moister. Here, the average moisture content of boards continues decreasing for about half an hour then increases. The absolute non-uniformity drops suddenly during the final conditioning section when the moisture content enhances. While each of the products has much less non-uniformity than before the conditioning, the difference between the final average moisture contents of boards is quite considerable (3.8 % between the maximum and

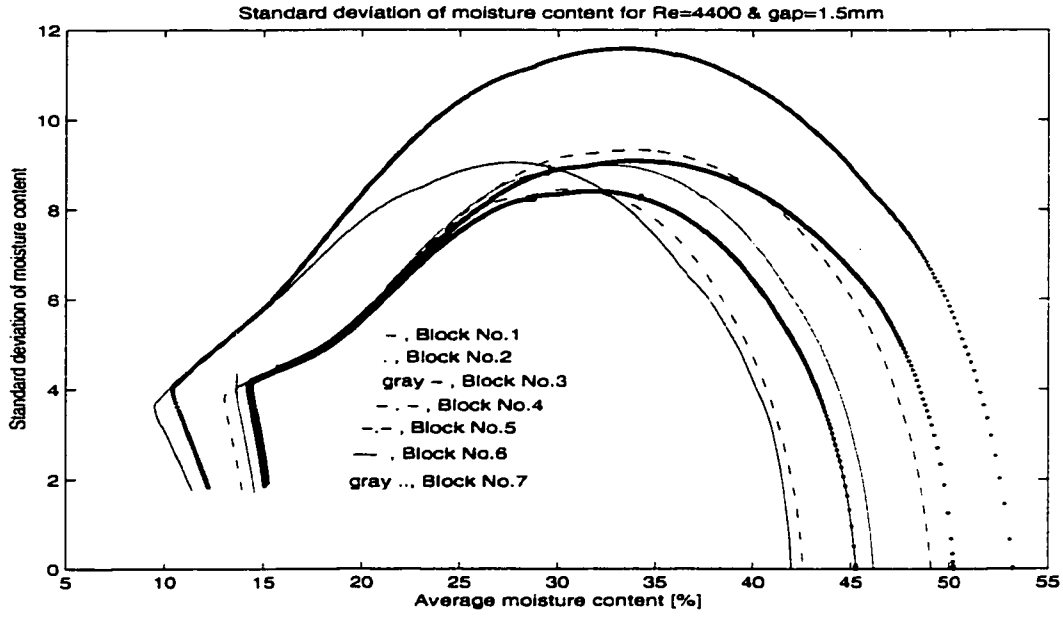

Figure 7.19: Standard deviation of moisture content for the Li's geometry for g=1.5mm at Re=4400

minimum).

The difference between the two groups is more clear in the normalized plots. Here, the maximum occurs during the third stage followed by a local minimum at the end of this stage. The transition period usually enhances the normalized non-uniformity while it drops during the main conditioning process.

Since the absolute standard deviation curve versus X_{av} of the boards represents the non-uniformity better, we continue our discussion with such plots. In Figures 7.26 and 7.27, the mentioned distribution is plotted at Re=4400 for two side gaps of 21.5 and $g_{opt} = 41.5mm$. Also Figure 7.28 present a similar plot when $g_{opt} = 41.5mm$ and initial conditions are the same as those of the case of g=1.5mm. These plots show that the optimum gap size provides the closest conditions of the boards to each other both before and after conditioning (less than 1.4% difference between maximum and minimum final X_{av}). In order to get a better overall view, the summation of the

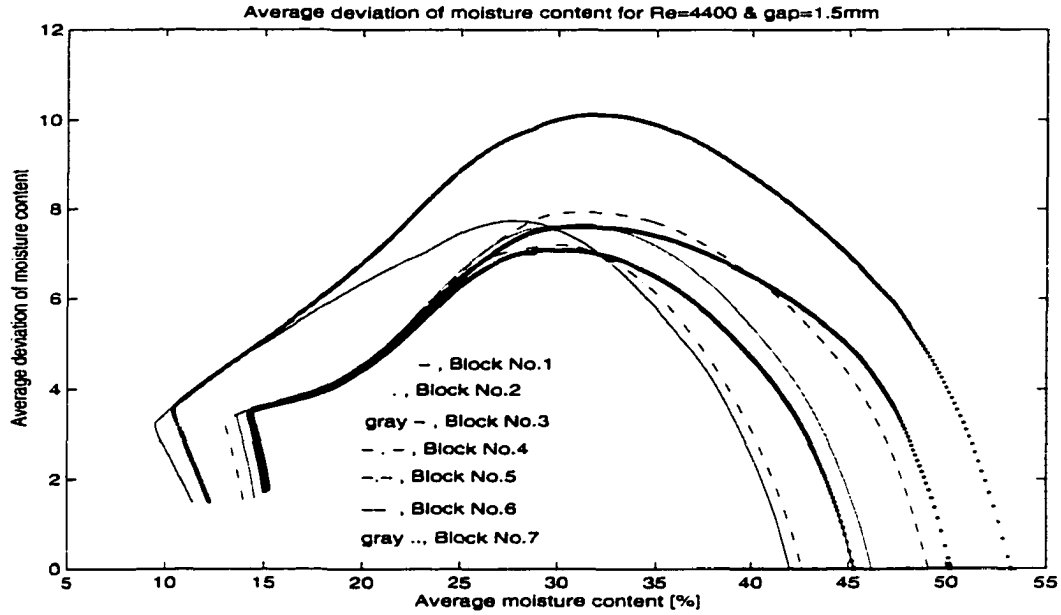

Figure 7.20: Average deviation of moisture content for g=1.5mm at Re=4400

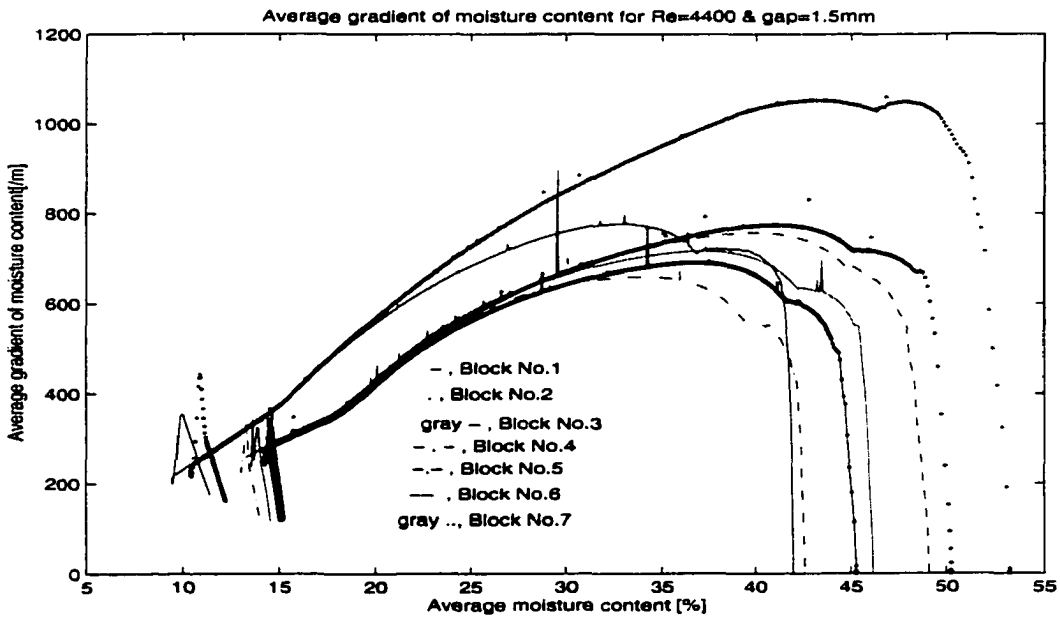

Figure 7.21: Average gradient of moisture content for g=1.5mm at Re=4400

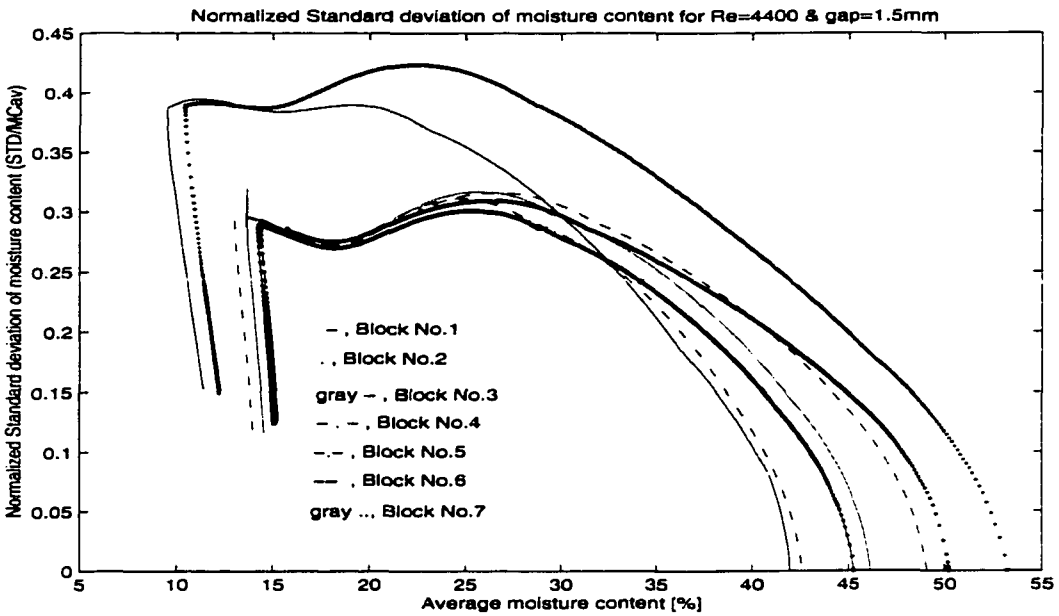

Figure 7.22: Normalized Standard deviation of moisture content at Re=4400

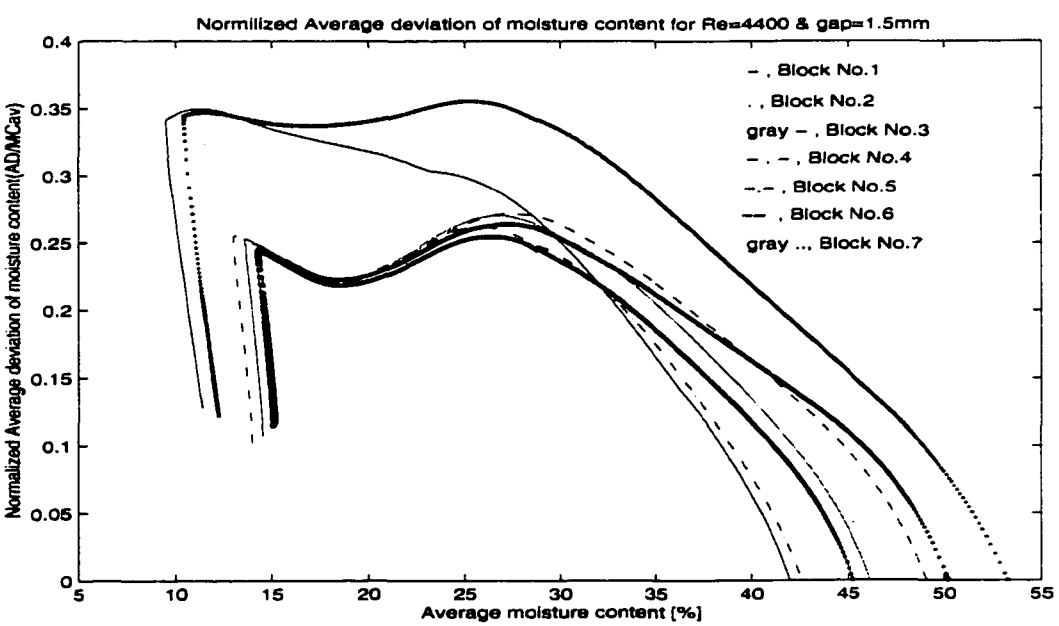

Figure 7.23: Normalized average deviation of moisture content for g=1.5mm at Re=4400

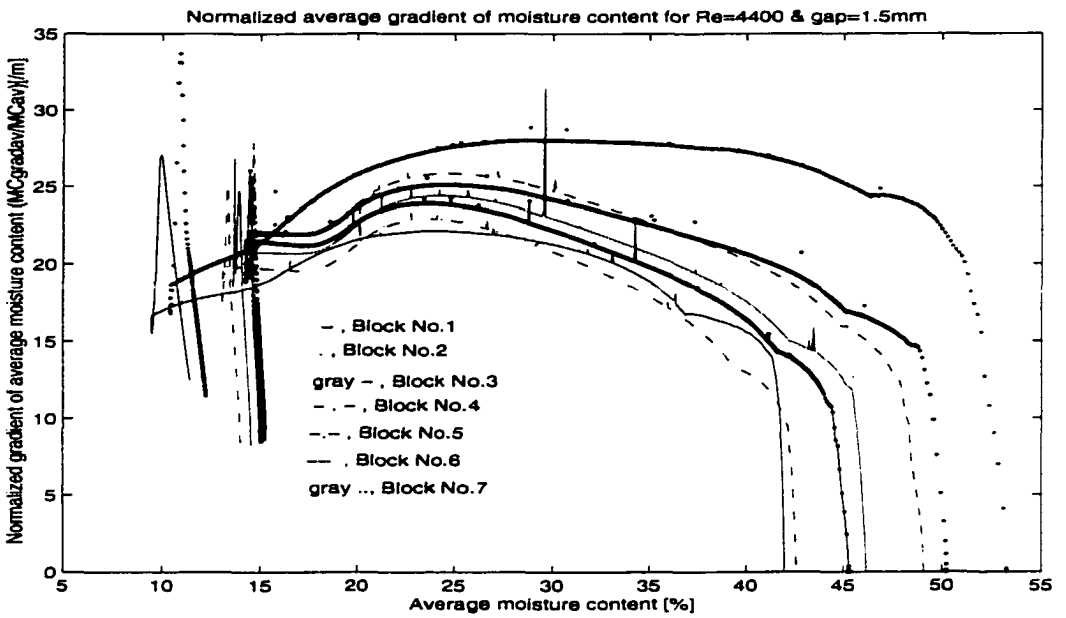

Figure 7.24: Normalized average garadient of moisture content for g=1.5mm at Re=4400

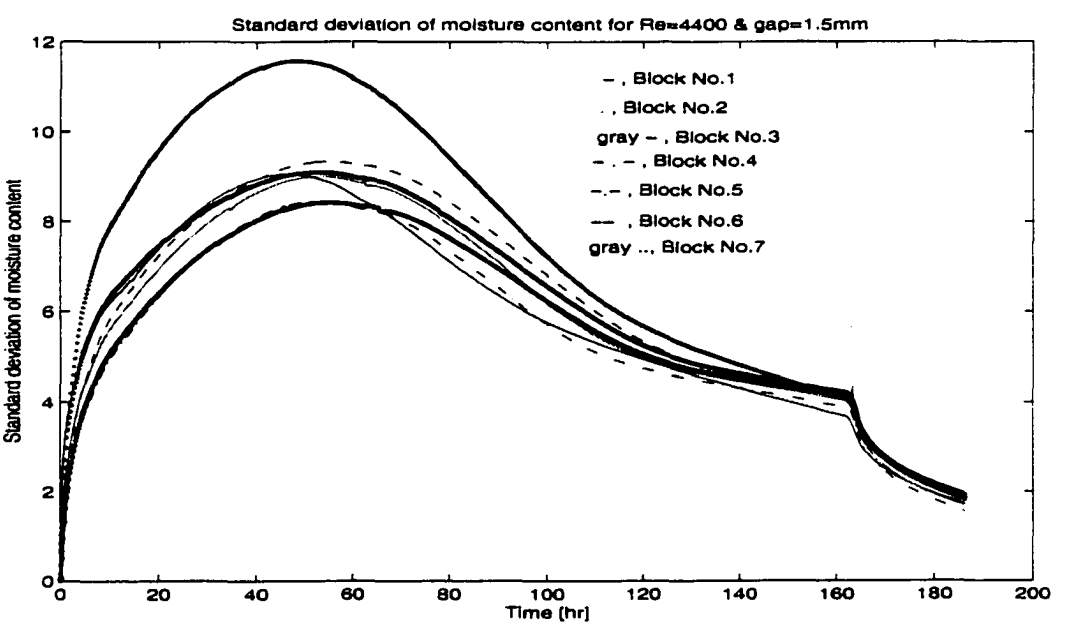

Figure 7.25: Time dependent Standard deviation of moisture content for g=1.5mm at Re=4400

standard deviations of all boards can be plotted against the X_{av} of the whole stack. Such curves are presented in Figure 7.29 and 7.30. In the first figure, only the initial conditions of g=21.5 and g=41.5 are the same. Here, the total standard deviation has a smaller maximum when the optimum gap size is used. However, its value is larger before the conditioning. Conditioning reduces the difference between the standard deviation of the optimum gap case and the g=1.5 mm case, and at the end of drying the former has slightly more standard deviation. This is due to having more drying from all surfaces of the boards for the optimum gap size compared to the g=1.5mm case. By looking at this trend one cannot judge that the g=41.5 mm case is less uniform at the end since most of the non-uniformity is referred to differences between the boards. If we want to obtain the same final total standard deviation for the g=41.5 case, the conditioning stage should be 1.4 hours longer. This extra time, if we insist on its requirement, is much less than 50.22 hours difference between the two total drying times.

A series of similar plots are presented in Figures 7.31 to 7.33 for Re=8800 at two gap sizes of g=1.5mm and $g_{opt} = 26.5mm$. Plotted in Figures 7.34 to 7.36 are the similar distributions for Re=13200 when gap sizes are 1.5 and $g_{opt} = 21.5mm$. From these figures and the ones for Re=8800 and Re=4400, it can be concluded that the optimum gap size reduces the difference between the final average moisture content of different boards of the row before and after the conditioning. By using the optimum gap size instead of g=1.5 mm, the difference between the maximum and minimum final X_{av} is reduced from 3.57% to 1.37% and from 3.0% to 1.9% for Re=8800 and 13200, respectively. This provides a better distribution of the final average moisture content and reduces the amount of boards over- or under-dried. We observed that the non-uniformity curves for the first and last board when there is no extra gap are close. This shows that reversing the air flow as a remedy is not that much effective

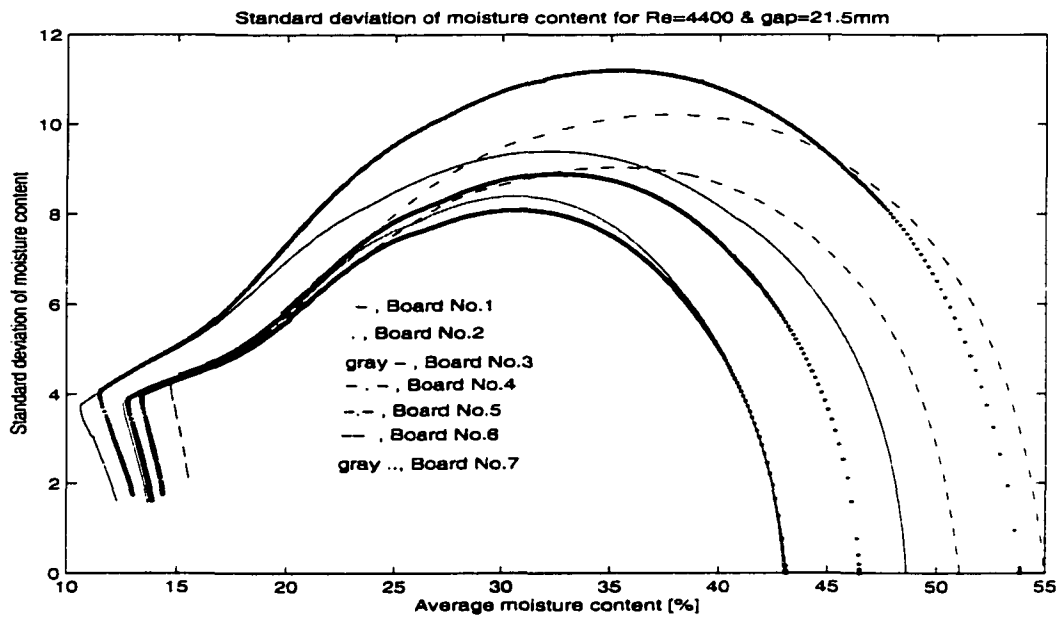

Figure 7.26: Standard deviation of moisture content for the Li's geometry for g=21.5mm at Re=4400

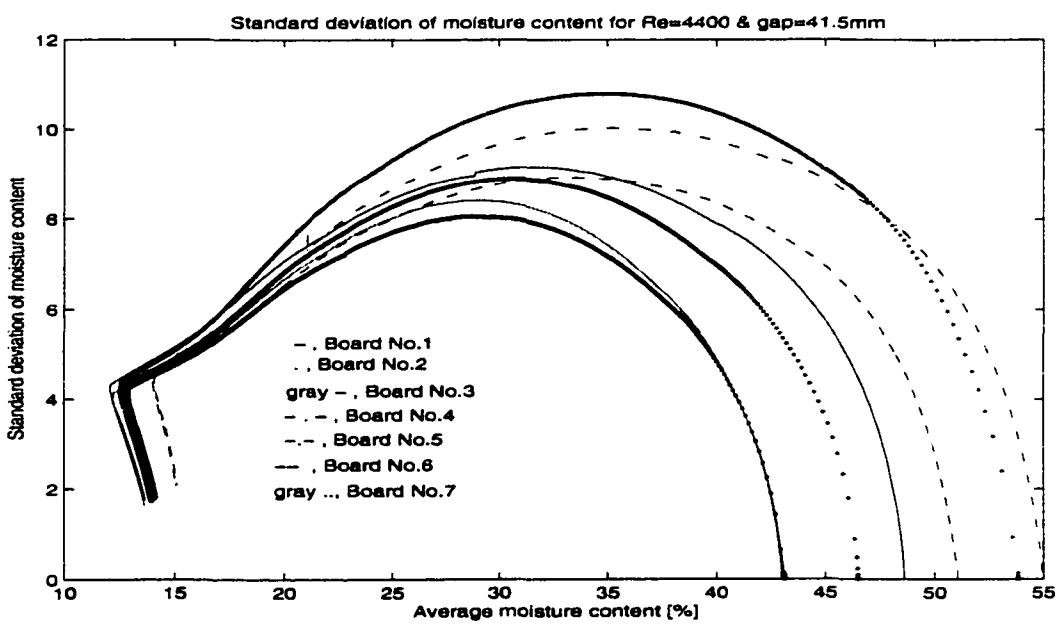

Figure 7.27: Standard deviation of moisture content for g=41.5mm at Re=4400 (initial values the same as those of g=21.5mm case)

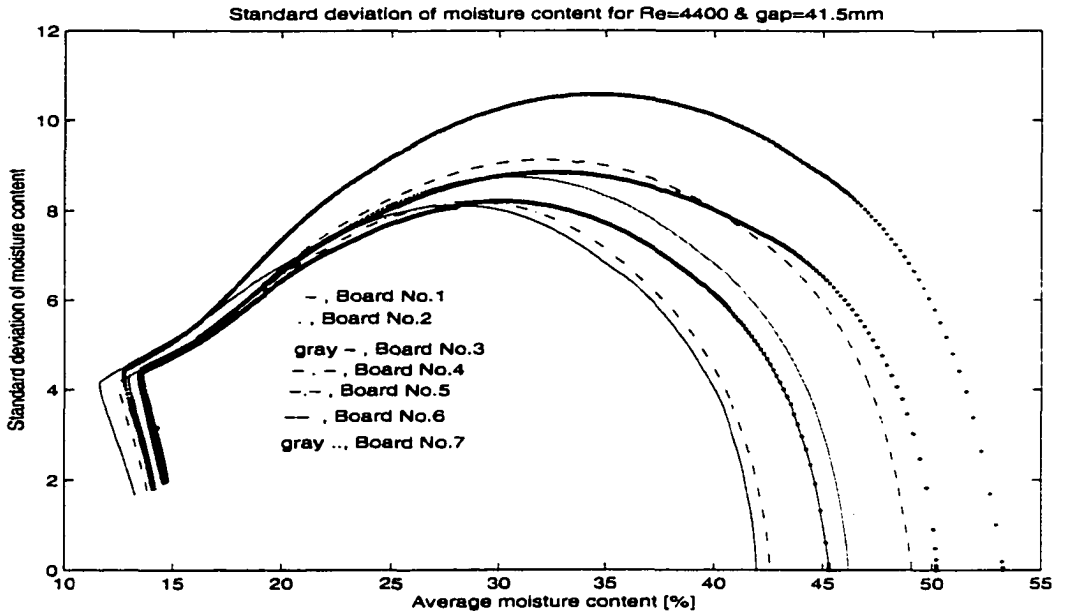

Figure 7.28: Standard deviation of moisture content for g=41.5mm at Re=4400(initial values the same as those of g=1.5mm case)

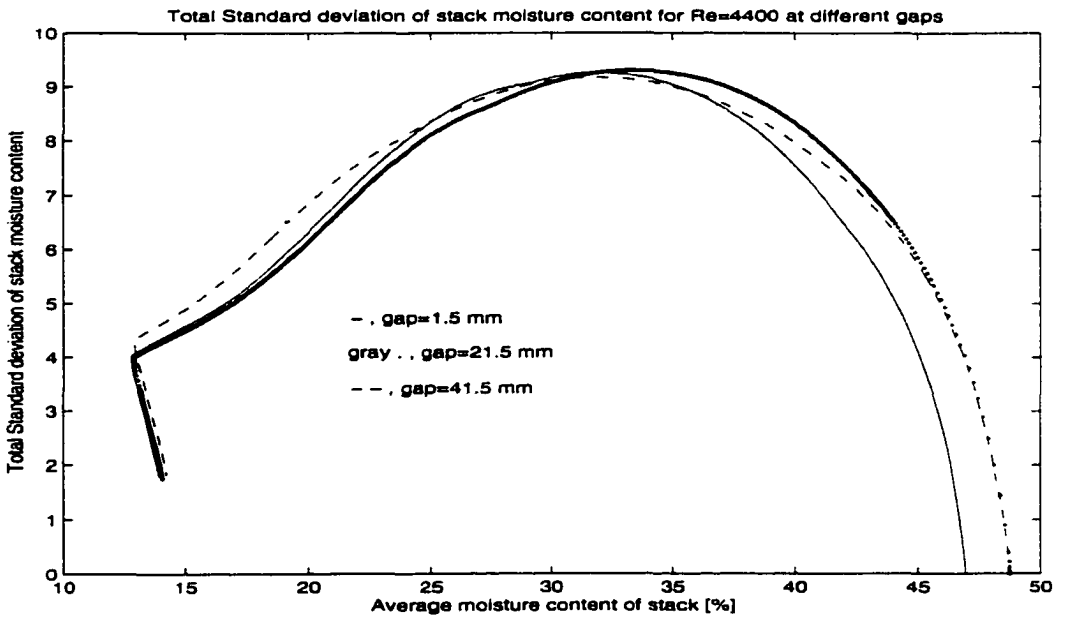

Figure 7.29: Total standard deviation of moisture content for the Li's geometry at Re=4400

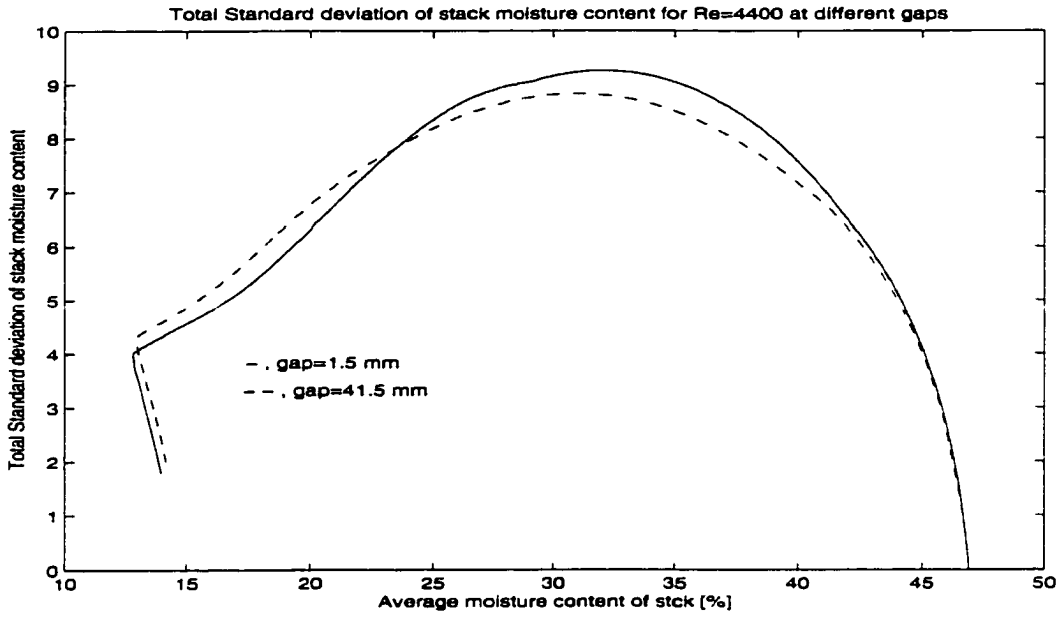

Figure 7.30: Total standard deviation of moisture content for the Li's geometry at Re=4400

when the length of stack is not too long, and cannot reduce the difference between the middle boards and this group. The alternative should be applying the side gap for all stacks besides reversing the air flow when a couple of stacks are put beside each other.

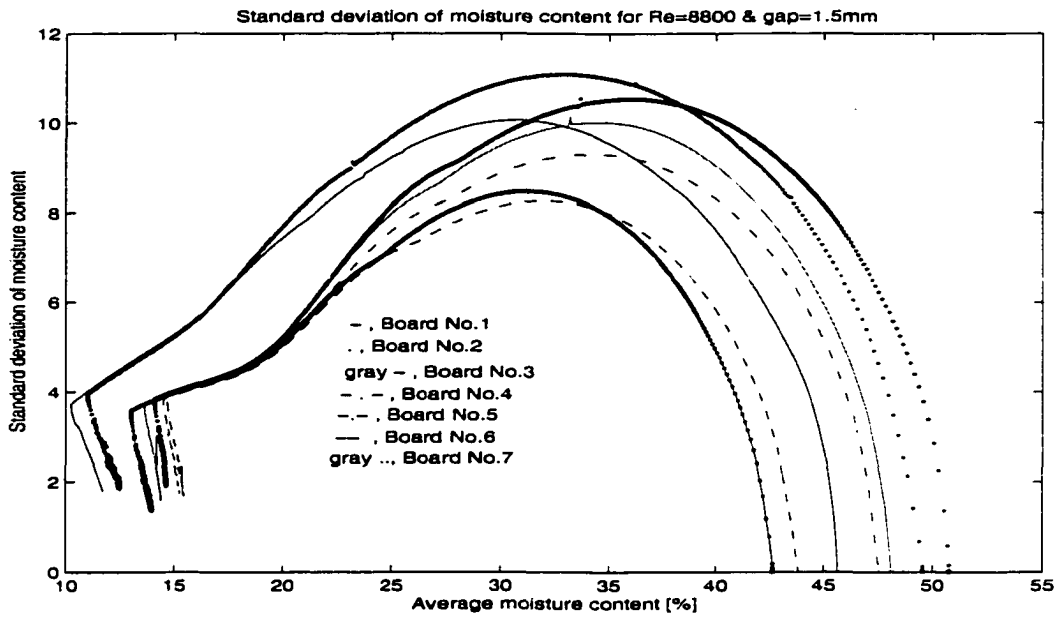

Figure 7.31: Standard deviation of moisture content for the Li's geometry for g=1.5mm at Re=8800

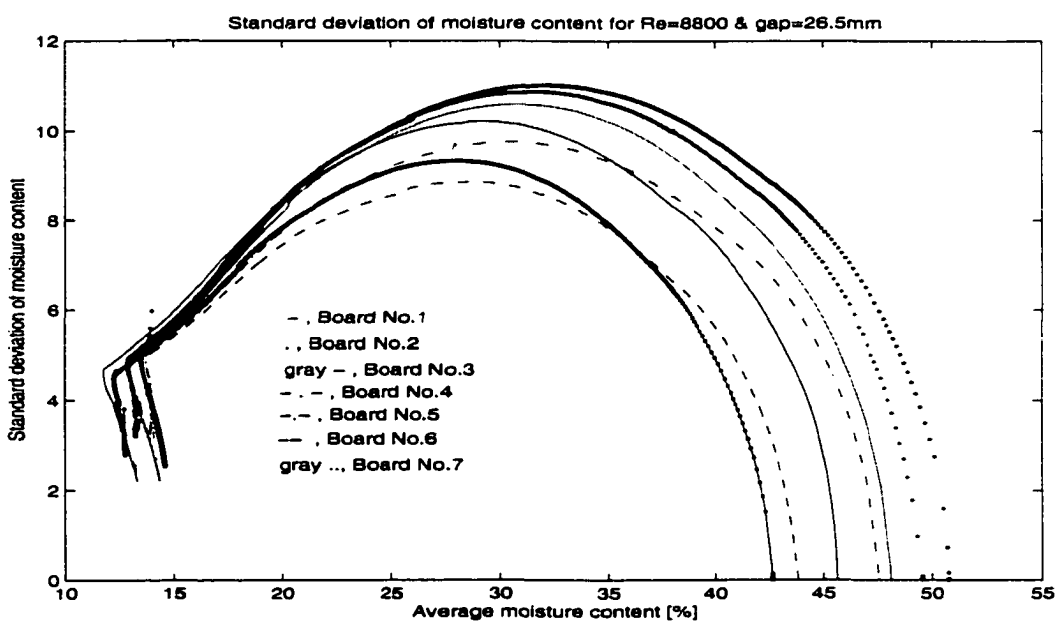

Figure 7.32: Standard deviation of moisture content for g=26.5mm at Re=8800

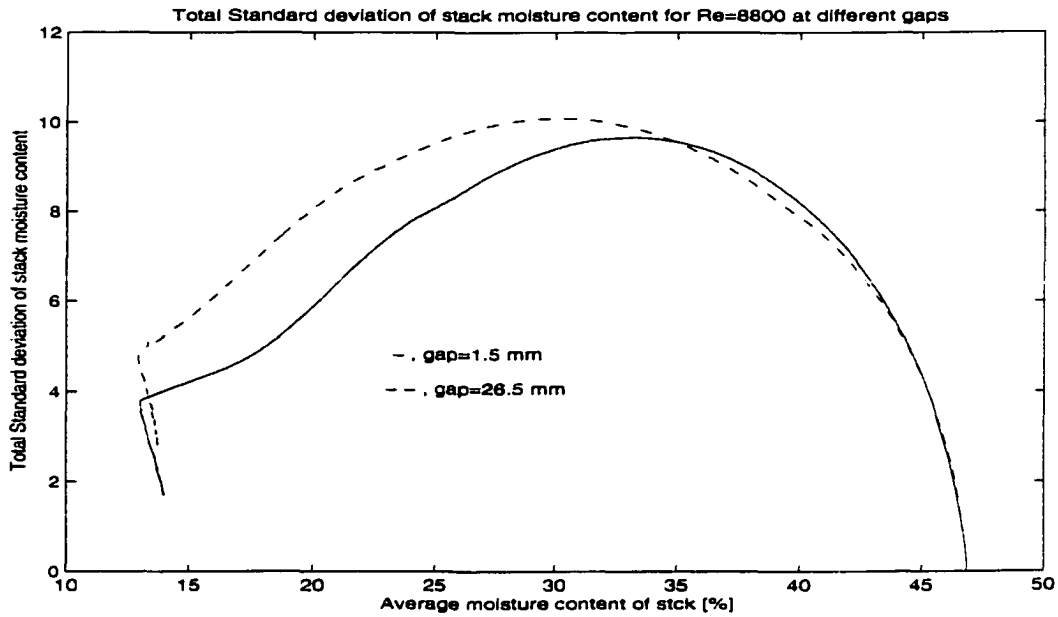

Figure 7.33: Total standard deviation of moisture content at Re=8800

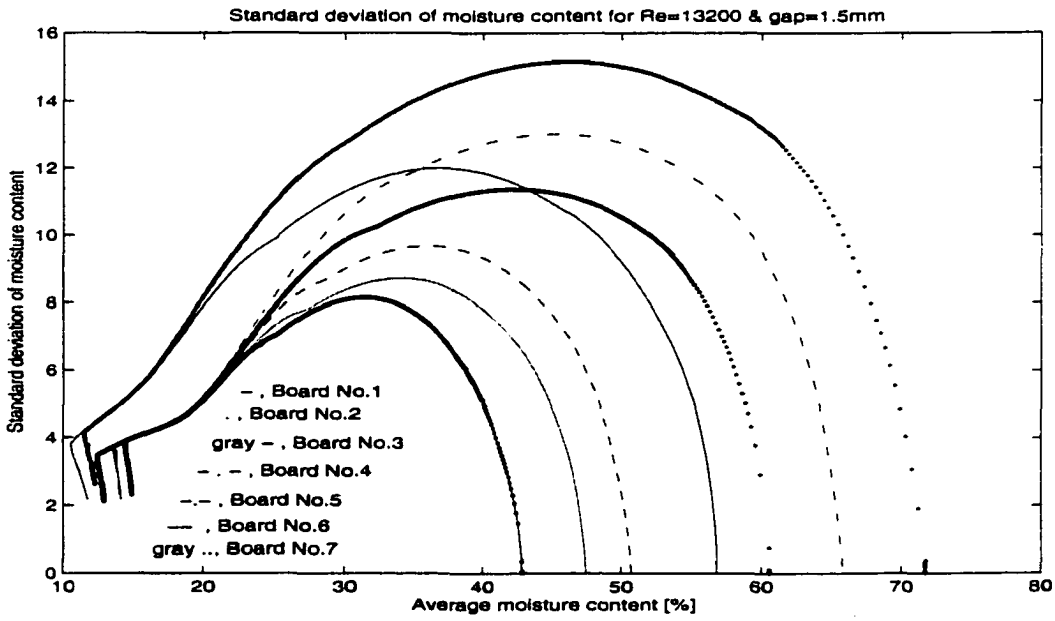

Figure 7.34: Standard deviation of moisture content for g=1.5mm at Re=13200 (initial values the same as those of Run 13 of Li)

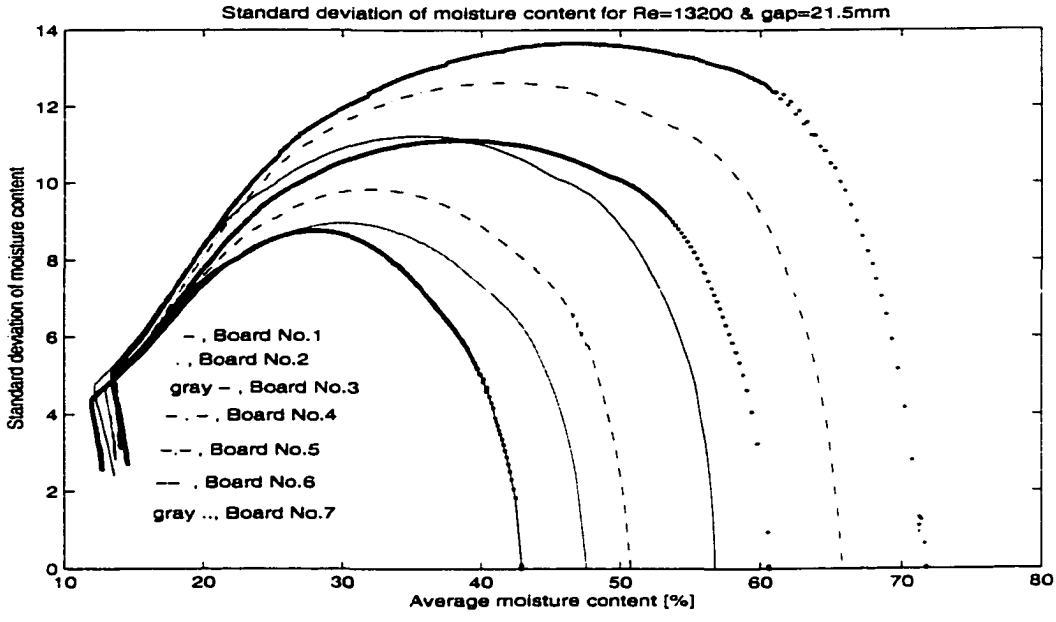

Figure 7.35: Standard deviation of moisture content for g=21.5mm at Re=13200(initial values the same as those of Run 13 of Li)

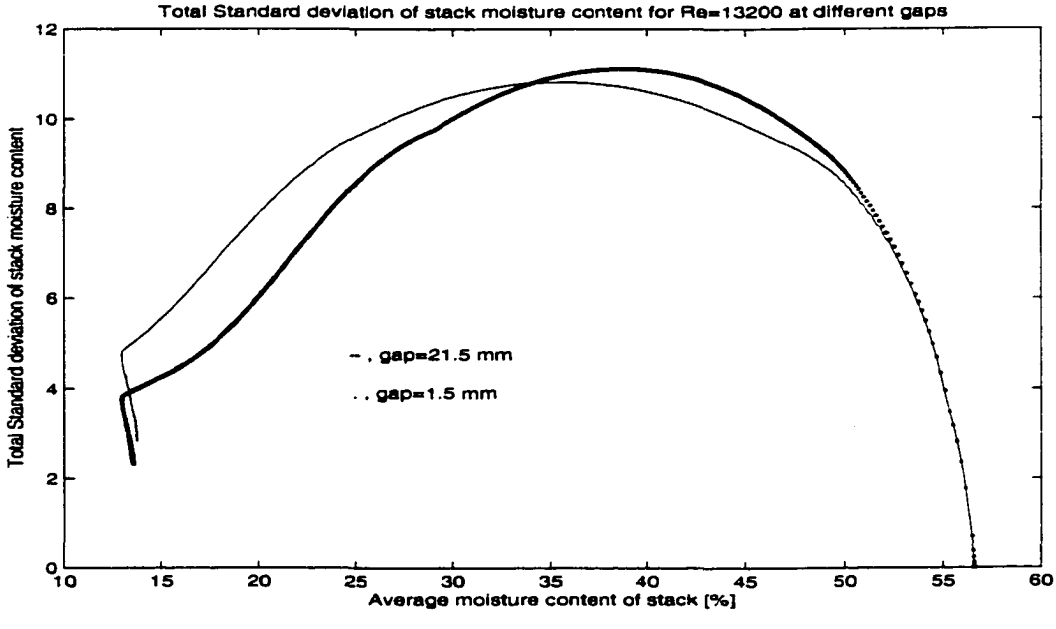

Figure 7.36: Total standard deviation of moisture content at Re=13200(initial values the same as those of Run 13 of Li)

Chapter 8

Simple diffusion case

It has been observed that heat transfer during wood drying occurs much faster than mass transfer and the wood reaches thermal equilibrium with surrounding air within few hours while drying takes days. Therefore, in spite of the complexity of equations 4.3 and 4.5 (for numerical procedure), the total mass transfer in wood can be modelled as a diffusion process with a diffusion coefficient as a function of the moisture content and temperature. Simpson and Liu[14] determined the surface emission and mass diffusion coefficients of aspen from experimental data of sorption and desorption over a range of moisture content. The method was applied only for an individual wood slab with constant external boundary conditions and not a stack of boards. They proposed the following relationship for mass diffusion coefficient:

$$D = A_1.exp(\frac{B_1}{T}).exp(B_2X) \ . \tag{8.1}$$

Thus, instead of equation 4.3, we will use the following equation for the total mass flux, **J**, in equation 4.5:

$$\mathbf{J} = D(X,T)\nabla X \ . \tag{8.2}$$

The assumption of a constant diffusion coefficient, when the drying air temperature is constant, has been used for an individual slab subjected to the external boundary layer air flow, by Simpson[49]. They proposed the following equations for $D_{av}(\frac{cm^2}{s})$, constant diffusion coefficient, and $S_{av}(\frac{cm}{s})$, constant surface coefficient:

$$D_{av} = \frac{-0.165(\frac{a}{2})^2}{0.701(\frac{dt}{dE})_{t(0.5)} + 2.05t_{0.5}} \quad . \tag{8.3}$$

$$S_{av} = \frac{0.701 D_{av}}{(\frac{a}{2})[\frac{D_{av}t_{0.5}}{(\frac{a}{2})^2} - 0.196]} \quad , \tag{8.4}$$

where $E = \frac{X - X_i}{X_f - X_i}$ and X_i is the initial moisture content and X_f is the final moisture content if desorption continues for a long time, e.g., equilibrium moisture content of drying air. $t_{0.5}$ is the time required for half the desorption to occur in seconds (time to reach the $\frac{X_i + X_f}{2}$). $(\frac{dt}{dE})_{t(0.5)}$ is the inverse of the slope of the dimensionless X curve versus time computed at $t_{0.5}$, and a is the board thickness in centimeters.

Present work

An attempt to apply the above method to the experimental data of Li[52] for time dependent average moisture content of a stack of hemlock during drying resulted in negative coefficients. Further investigations showed that the method cannot be applied to cases with non-constant air conditions.

Then the method was applied to part of the process which had constant air conditions ($T_{wb} = 54^0C, T_{db} = 82.2^0C$ which resulted in $X_f = 0.033$). These conditions were held between 61.53 and 162.17 hours after drying had started for a stack of planks without side gaps. Having $X_i = 0.3$ as the average initial moisture content of boards at the beginning of this period of drying, the $t_{0.5}$, D_{av} and S_{av} were obtained

successfully as:

$$t_{0.5} = 221003 \qquad (s) \tag{8.5}$$

$$D_{av} = 6.7456 \times 10^{-5} \qquad (\frac{cm^2}{s}) \tag{8.6}$$

$$S_{av} = 2.6116 \times 10^{-5} \quad (\frac{cm}{s}) \quad . \tag{8.7}$$

A Fortran program was written for solving the simple one dimensional diffusion case. The program used the implicit Crank-Nicholson method for discretization and the TDMA method for solving the equations. The obtained coefficients, in time steps of 30 seconds, and 21 grids in thickness direction were used in the present calculations of this Fortran program. Figure 8.1 shows the numerical results of average moisture content obtained by this method. They are in good agreement with experimental results. This is an interesting finding since the flow over a stack is an internal flow with separation at the inlet and outlet which provides complicated boundary conditions. These boundary conditions and the flow are quite different from the assumed external flow over an individual board of the original method with constant boundary conditions. This type of application has not appeared in the literature.

Based on the results of Chapter 5, the average heat transfer coefficient for this run is $h \simeq 15 \frac{W}{m^2 K}$. The average mass transfer coefficient can be calculated by:

$$h_m = \frac{D_{water-air} h}{\lambda_{air}} \quad , \tag{8.8}$$

where $D_{water-air} = 2.9886 \times 10^{-5} \frac{m^2}{s}$ and $\lambda_{air} = 2.6820 \times 10^{-2} \frac{W}{mK}$. These values result in, $h_m \simeq 0.0167 \frac{m}{s}$. The average effective surface coefficient applied to the determination of the moisture content in the model proposed in Chapter 4 and discretized in Eq. 6.17, is:

$$S_{av-eff} = \frac{h_m \epsilon_s^2 \rho_{sv} \psi_s}{\rho_d} \quad . \tag{8.9}$$

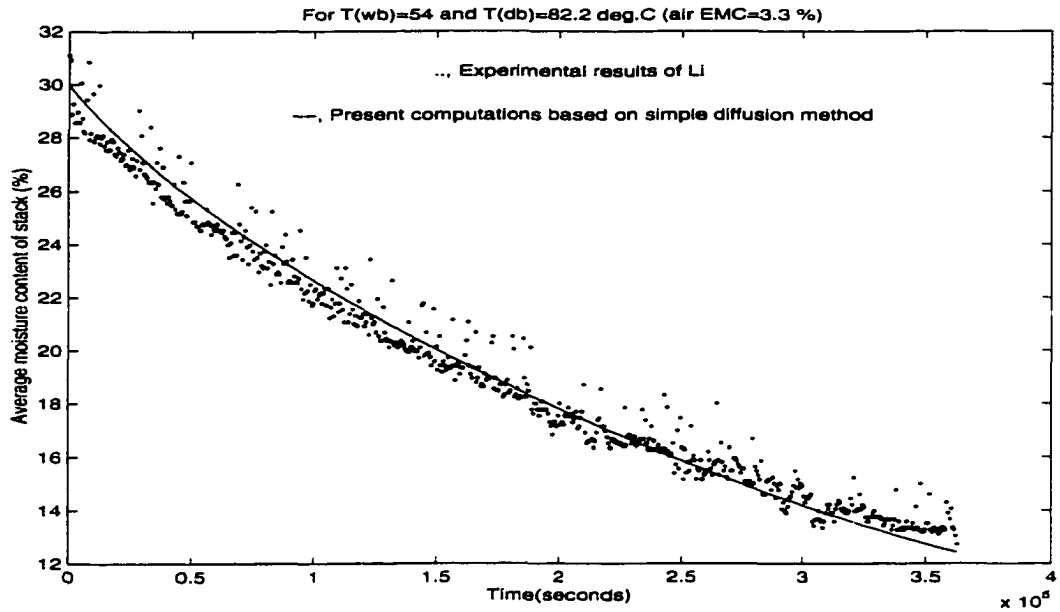

Figure 8.1: Comparison of the distribution of stack average moisture content as calculated by solving the simple diffusion equation with experimental results of Li[40] for Re=4400

The average dry wood density for this run was $\rho_d = 440\frac{kg}{m^3}$. The surface conditions are close to the drying air conditions, i.e. $T_s \simeq 355.15^oK$ and $X_s \simeq 0.033$. This results in $\epsilon_s \simeq 0.7067$, $\psi_s \simeq 0.2434$ and $\rho_{sv} \simeq 0.3150\frac{kg}{m^3}$. Therefore:

$$S_{av-eff} \simeq 1.4540 \times 10^{-4}(\frac{cm}{s}) \quad . \tag{8.10}$$

This implies that the average effective surface coefficient (S_{av-eff}) computed from solving the external heat/mass transfer equations in Chapter 5 is approximately 5.6 times larger than S_{av} of the simple diffusion analysis. The reason for the difference in these values could be due to the omission of the complexities of the moisture movement process. Such an assumption could lead to higher diffusion coefficients and lower surface coefficients in order to reach the same accuracy of results. The second reason is because of the definition of the above S_{av}, which is based on the constant inlet air conditions in the assumed external flow instead of the mean conditions used

in the real case of the duct flow. Since the air absorbs moisture from the wood surface, the mean concentration of water in the drying air increases in the stream wise direction. Therefore, the difference between the concentration of the surface and outside air in the external flow is larger than the difference between the surface and air mean concentrations with the same entrance conditions. This results in much lower S_{av} values for the external flow with the same inlet air conditions and total mass transfer.

Chapter 9

Conclusions

This thesis has focused on various aspects of the transport phenomena occuring during drying of a stack of wood planks. The objective was to provide accurate predictions through numerical simulation models towards an optimum drying process. The new findings of this study are summarized below.

The two-dimensional problem of drying a stack of 105 × 105 western hemlock planks, stated in Chapters 3 to 4, has been solved in Chapters 5 to 8. The effect of side gap on the drying process was studied. The problem consists of two major parts. The first part requires obtaining the surface coefficients on all faces of boards. Surface coefficients indicate the rate of heat and mass transfer between the board surfaces and the drying air. The importance of this section for the external air flow was brought to light in Chapter 5. The second part studies the drying process inside the wood and relates to the first part via wood surfaces. The study involves the behaviour of different phases of moisture inside the board. Solution to this part forms the main subject of Chapters 6 to 8.

In Chapter 5 a numerical procedure for finding the local distribution of surface

coefficients and the turbulent flow field was developed and validated for several air flow rates. This was the first successful attempt for obtaining the surface coefficient distributions on the horizontal faces of boards and the first published work for the same distribution on vertical faces. The procedure used relates the surface coefficients to the mean temperature (or concentration) and not to the inlet conditions which were mistakenly used in the literature. The present work investigated for the first time the effect of side gaps on the surface coefficients on both horizontal and vertical surfaces of different boards of stack at different air flows. Combinations of several parameters were analyzed to observe the gains in the external process due to such gaps. The analysis showed that there is an optimum gap size for each air velocity (Re number). It was also found that the suggested optimum gap size decreases when Re number increases and the rate of this decrease is less for higher Re numbers. The optimum gap size at higher Re numbers can also reduce the total time required for drying a certain amount of lumber after taking into account the loss of kiln loading capacity due to unused space of the gaps. The effect of air temperature and humidity on the distribution of surface coefficients was found to be negligible. Therefore, the optimum gap size can be considered only a function of the Re number and stack array. The other important point was the similarity between the distributions on the horizontal walls at different Re numbers and gap sizes with a multiplication factor of the ratio of their assymptotic values. This will help save time and reduce the number of required studies in selecting cases, and will also help to generalize the external process.

A new relationship for the bound water diffusion coefficient was proposed in Chapter 4 and validated in Chapter 6. This required the introduction of a new unknown parameter, related to the effect of temperature, for the specific wood species. A sensitivity analysis for the model unknown parameters was performed in Chapter 6. It was demonstrated that the effect of this new parameter on the predictions of

moisture content and temperature was much more significant than those of the other unknown parameters. Comparing with another numerical models, it was shown that this relationship for bound water diffusion coefficient incorporates the effects of local temperature and moisture content into the diffusion process better. Other reasons for a better performance are the following. The type of the governing equations and other sub-models used in this work provide a better implementation of the effect of different phases contributions to mass and energy balance at each control volume. They also facilitate the contributions of gradients of moisture content and temperature on each other. Usage of wood porosity in the mass transfer boundary condition at the surfaces brings the surface resistance to mass transfer into consideration.

An algorithm capable of solving the governing coupled two-dimensional mass and heat transfer equations has been developed in Chapter 7. The modifications to SOR iterative solver, developed in this work, increased its accuracy and lowered the chances of oscillatory and non-physical results. The comparison of the numerical results with experiments showed that the model is able to predict the local and average moisture content as well as the temperature field with a good accuracy. The program calculates and saves the transfer parameters at the boundaries of the control volumes as well as at their centers. This makes it possible to implement the effects of anisotropy to the program in the future works. The other advantage of the program is that it considers and calculates the changes in the drying air temperature and humidity across the stack. This is due to heat and mass transfer between the planks and the drying air which lowers its drying capability downstream. Considering such effects, makes the program capable of predicting the effect of reversing air flow in the stack in future investigations. Several parameters were calculated to study the non-uniformity of the planks during drying. These include: standard and average deviation as well as the average gradient of the moisture content of each board. It was proposed that

the above parameters (or their normalized values with average moisture content) can be plotted against the average moisture content of each board to judge about the uniformity occuring during the drying process. The plots distinguished two groups of boards when planks are laid in one stack and any row contains seven boards without side gap. The first and last board are over-dried at the end. Based on the trends of the parameters, the standard deviation (Std) has been chosen as the parameter to predict the uniformity. Distributions of Std showed that when the optimum gap size is used, the difference between the maximum and minimum final average moisture content becomes less than halved compared to the case with no gap.

A successful one dimensional diffusion analysis was presented in Chapter 8 to study an aspect of the drying process. The average diffusion and surface coefficients were determined from the experimental data of stack average moisture content based on a recently proposed method. This method was originally proposed for a single board and this new type of application for a stack has not appeared in the literature. The study showed that this method is capable of predicting the drying process when there is no side gap, and the temperature and humidity of the drying air are kept constant for a long period, and change stepwise. Several sets of experimental data are needed to obtain the average coefficients for different drying air conditions (temperature, humidity and velocity) and initial wood parameters (dry wood density and moisture content). Therefore, such a simple one-dimensional model is inadequate for studying the effects of the side gaps and air velocity, and a comrehensive method, such as prescribed in previous chapters of this thesis, is neccessary. However, such a simple method can be useful if the coefficients are extracted for many different combinations of air condition and wood from experiments and when an approximation for the distribution of avarege moisture content of the stack with time is needed.

9.1 Future work

The effect of the geometrical parameters of the stack array on the distribution of surface coefficients at different Re numbers can be studied more thoroughly. The dimension-less numbers such as the gap-thickness ratio, g/t (t is the board thickness); the gap-sticker ratio, g/s (s is the sticker thickness); baord aspect ratio, W/t (W is the board width), can be examined.

Extensive experiments can be arranged to measure the time dependent local moisture content and strain in different directions at various locations of the boards such as: surface, center, etc. Comparisons of moisture content data with numerical results will improve the accuracy of the model unknowns and performance of the model. The strain data should be linked to moisture content data to establish new theories for their relationships. Lack of such strong and validated theories has slowed down the very much demanded analysis of stress and strain during drying.

References

[1] Dincer, I. and Dost, S., 1993, "On the Energy Resources of Canada," *Int. Journal of Energy Resources*, Vol.10, pp.461-476.

[2] Siau, J., 1984, "*Transport Processes in Wood*," *Springer Verlag*, Berlin, p.131 and 240.

[3] "*Canada Year Book*," 1995, p.254.

[4] Tuttle, F., 1925, "A Mathematical Theory of the Drying of Wood." *J. Franflin Inst.*, 200, pp. 609-614.

[5] Newman , A.B., 1931, "The Drying of Porous Solids: Diffusion Calculations." *Transactions of the AIChE*, Vol.27, pp.310-333.

[6] Choong, E. T., 1963, "Movement of Moisture through a Softwood in the Hygroscopic Range," *For. Prod. Jour.*, Nov., pp. 489- 498.

[7] Stamm, A. J., 1963, "Permeability of Wood to Fluids," *Forest Products Journal.* Nov., pp.503-507.

[8] Comstock, G.L., 1965, "Longitudinal Permeability of Green Eastern Hemlock," *Forest Products Journal*, 15(10), pp.441-449.

[9] Spolek, G.A., and Plumb, O.A., 1981, "Capillary Pressure in Softwoods," *Wood Sci. Tech.*, Vol.15, pp.189-199.

[10] Plumb, O. A., Brown, C.A. and Olmstead, B.A., 1984, "Experimental Measurements of Heat and Mass Transfer During Convective Drying of Southern Pine," *Wood Sci. Tech.*, 18, pp.187-204.

[11] Siau, J., 1992, "Non-isothermal Diffusion Model Based on Irreversible Thermodynamics," *Wood Sci. Tech.*, 26, pp. 325-328.

[12] Dincer, I., and Dost, S., 1995, "An Analytical Model for Moisture Diffusion in Solid Objects During Drying," *Drying Tech.*, Vol.13(2), pp.425-435.

[13] Josserand, D.A., Taverdet, J.L., and Vergnaud, J.M., 1988, "Modelling the Absorption and Desorption of Moisture by Wood in an Atmosphere of Constant and Programmed Relative Humidity," *Wood Sci. Tech.*, Vol.22, pp.299-310.

[14] Simpson, W. T. and Liu, J.Y., 1991, "Dependence of the Water Vapor Diffusion Coefficient of Aspen on Moisture Content," *Wood Sci. Tech.*, Vol.26, pp.9-21.

[15] Dincer, I., and Dost, S., 1996, "Determination of Moisture Diffusivities and Moisture Transfer coefficients for Wooden Slabs Subject to Drying," *Wood Sci. Tech.*, Vol.30, pp.245-251.

[16] Mounji, H., Bouzon, J., and Vergnaud, J.M., 1991, "Modelling the Process of Absorption and Desorption of Water in Two Dimensions (Traverse) in a Square Wood Beam," *Wood Sci. Tech.*, Vol.26, pp.23-37.

[17] El Kouali, M., Bouzon, J., and Vergnaud, J.M., 1992, "Process of Absorption and Desorption of Water in a Wood Board, with Three Dimensional Transport Beyond the FSP," *Wood Sci. Tech.*, Vol.26, pp.307-321.

[18] Kayihan, F., 1982, "Simultaneous Heat and Mass Transfer with Local Three-Phase Equilibrium in Wood Drying," *Proceedings 3rd Int. Drying Symp.*, Birmingham, pp.123-134.

[19] Stanish, M.A., Schajer, G.S., and Kayihan, F., 1986, "A Mathematical Model of Drying for Hygroscopic Porous Media," *AIChE Journal*, Vol.32, No. 8, pp.1301-1311.

[20] Mitchel, P. and Bigbee,K., 1989, "Drying Variables Affecting Drying Rate and Moisture Content Distribution in Western Hemlock," *Proceedings of the 5th Western Dry Kiln Association Meeting*, Seattle,pp 13-26.

[21] Avramidis, S., Englezos, P., and Papathanasiou, T., 1992, "Dynamic Non-isothermal Transport in Hygroscopic Porous Media: Moisture Diffusion in Wood," *AIChE Journal*, Vol.38, No. 8, pp.1279-1287.

[22] Cloutier, A., Fortin, Y. and Dhatt, P., 1992, "A Wood Drying Finite Element Model Based on the Water Potential Concept," *Drying Tech.*, 10(5), pp.1151-1181.

[23] Collignan, A., Nadeau, J.P. and Puiggali, J., 1993, "Description and Analysis of Timber Drying Kinetics," *Drying Tech.*, 11(3), pp. 489-506.

[24] Puiggali, J., Nadeau, J.P. and Sales, C., 1993, "Assessment of Timber Drying Schedules by Evaluation of Damage Risks," *Drying Tech.*, 11(3), pp. 507-524.

[25] Liu, J., Avramidis, S., and Ellis, S., 1994, "Simulation of Heat and Moisture Transfer in Wood During Drying under Constant Ambient Conditions," *Holzforschung*, Vol.48, No. 3, pp.236-240.

[26] Hernandez, J. M., and Puiggali, J. R., 1994, "Simulation of Drying of Coniferous Wood Using Various Processes," *Int. Chem. Engg.*, Vol.34, No. 3, pp.339-350.

[27] Avramidis, S., and Hatzikiriakos, S., 1995, "Convective Heat and Mass Transfer in Non-isothermal Moisture Desorption," *Holzforschung*, Vol.49, No. 2, pp.163-167.

[28] Pang, S., Keey, R.B., and Langrish, T., 1995, "Airflow Reversals in High Temperature Kiln Drying: Drying of a Single Board," *New Zealand Journal of Forestry Sci.* Vol.24, No. 1, pp. 83-103.

[29] Kho, P.C.S., Keey, R.B. and Walker, J.C.F., 1989, "The Effect of Minor Board Irregularities and Air Flow on the Drying Rate of Softwood Timber in Kilns," *Proceedings of the Third International Wood Drying Symposium*, Seattle,pp 150-157.

[30] Langrish, T., Kho, P.C.S., Keey, R.B. and Walker, J.C.F., 1992, "Experimental Measurement and Numerical Simulation of Local Mass Transfer Coefficient in Timber Kilns," *Drying Tech.* Vol.10(3), pp. 753-781.

[31] Langrish, T., Kho, P.C.S., Keey,R.B. and Walker,J.C.F., 1993, "Time Dependent Flow in Arrays of Timber Boards: Flow Visualization, Mass Transfer and Numerical Simulation," *Chemical Eng. Sci.*, Vol.48, No.12, pp.2211-2223.

[32] Turner, I. W., 1996, "A Two Dimensional Orthotropic Model for Simulating Wood Drying Processes," *Appl. Math. Modelling* Vol.20(1), pp. 60-81.

[33] Pang, S., Keey, R.B., Walker, J.C.F., and Langrish, T., 1994, "Airflow Reversals in High Temperature Kiln Drying of Pinus Radiata Boards: Drying of a Stack of Boards," *New Zealand Journal of Forestry Sci.*, Vol.24, No. 1, pp. 104-119.

[34] Keey, R.B., 1978, "Introduction to Industrial Drying Operations," *Pergamon Press*, Oxford, P. 376.

[35] Gong, L., Plumb, O. A., 1994, "The Effect of Heterogeneity on Wood Drying. I. Model Development and Predictions," *Drying Tech.* Vol.12(8), pp. 1983-2001.

[36] Gong, L., Plumb, O. A., 1994, "The Effect of Heterogeneity on Wood Drying. II. Experimental Results," *Drying Tech.* Vol.12(8), pp. 2003-2026.

[37] Kamke, F. A., and M. Vanek, 1994, "Comparison of wood drying models," *4th International IUFRO wood drying conference*, Rotorua, New Zealand, pp. 1-17.

[38] Sutherland, J. W., Turner, I, and Northway, R. L., 1992, "A Theoretical and Experimental Investigation of the Convective Drying of Australian Pinus Radiata

Timber," *3rd International IUFRO Wood Drying Conference*, Vienna, Austria, pp. 145-155.

[39] Salin, J. G., 1990, "Simulation of the Timber Drying Process, Prediction of Moisture and Quality Changes," PhD thesis, Abo Akademi, Abo, Finland.

[40] Ranta-Maunus, A., 1994, "Computation of Moisture Transport and Drying Stresses by a 2-D FE-Programme," *4th International IUFRO Wood Drying Conference*, Rotorua, New Zealand, pp. 187-194.

[41] Vogel, R., 1989, "Modellierung des Warme- und Stofftransportes und des Mechanischen Spannungsfeldes bei der Trocknung Fester Korper am Beispeil der Schnittholztrocknung," PhD dissertation, Technische Universitat Dersden, Germany.

[42] Akulich, P V; Militzer, K-E., 1998, "Simulation of Nonisothermal Moisture Transfer and Stresses in Wood in Drying," *Journal of Engineering Physics and Thermophysics*, Vol.71, No.3, pp.398-406.

[43] Tarasiewicz, S, Leger, F., 1998, "Modeling Simulation and Control of the Wood Drying Process. I. A Set of PDE's as an Internet Model," *Drying Tech.*, 16(6), pp.1075-1084.

[44] Tarasiewicz, S, Ding, F., Leger, F, 1998, "Modeling Simulation and Control of the Wood Drying Process. II. Variable Control Structure," *Drying Tech.*, 16(6), pp.1085-1100.

[45] Tarasiewicz, S, Kucukada, K., Point, N., 1998, "Modeling Simulation and Control of the Wood Drying Process. III. Programming and Computer Solutions," *Drying Tech.*, 16(6), pp.1101-1118.

[46] Bai, G., and Garrahan, P., 1984, "The Temperature and Moisture Content in Lumber During Pre-heating and Drying," *Wood Sci. Tech.*, Vol.18, pp.121-135.

[47] Plumb, O.A., Brown, C.A., and Olmstead, B.A., 1984, "Experimental Measurements of Heat and Mass Transfer During Convective Drying of Southern Pine," *Wood Sci. Tech.*, Vol.18, pp.187-204.

[48] Rice, W.R., and Young, R.L., 1991, "One- and Two-Dimensional Moisture Profiles in Red Oak," *Wood and Fiber Sci.*, Vol.23, No.3, pp.328-341.

[49] Simpson, W.T., 1993, "Determination and Use of Moisture Diffusion Coefficient to Characterize Drying of Northern Red Oak," *Wood Sci. Tech.*, Vol.27, pp.409-420.

[50] Soderstrom, O., and Salin, J. G., 1993, "On Determination of Surface Emission Factors in Wood Drying," *Holzforschung*, Vol.47, No. 5, pp.391-397.

[51] Salin, J. G., 1996,"Prediction of Heat and Mass Transfer Coefficients for Individual Boards: a Review," *4th International IUFRO Wood Drying Conference*, Univ. of Laval, Quebec, pp. 49-58.

[52] Li, M., 1996, "A Study on the Effects of Air Gaps, Air Velocities and Fan Revolutions on the Drying Characteristics of Western Hemlock Baby Squares," M.Sc. Thesis, Faculty of Forestry, The University of British Columbia.

[53] Patankar, S. V., 1980, "*Numerical Heat Transfer and Fluid Flow*," Hemishpere.

[54] "*British Columbia Forest Industry Fact Book*," 1995, Council of Forest Industries of British Columbia, Vancouver, Canada, p.74 and 150.

[55] "*Widman's World Wood Review*," 1995, Widman Associates Inc., June, p.8.

[56] Avramidis, S., and Mackay, J.F.G., 1988, "Development of Kiln Schedules for 4-inch by 4-inch Pacific Coast Hemlock," *Forest Prod. J.*, Vol.38, No. 9, pp.45-48.

[57] Simpson, W.T., and Rosen, H. N., 1981, "Equilibrium Moisture Content of Wood at High Temperature," *Wood and Fiber*, Vol.13, No.3, pp.150-158.

[58] Salin, J-G., 1996, "Mass Transfer from Wooden Surfaces and Internal Moisture Nonequilibrium," *Drying Tech.* Vol.14(10), pp. 2213-2224.

[59] Li, M., Avramidis, S., Oliveira, L. and Hartley, I. D., 1997, "The Effect of Vertical Air Gaps, Air Velocities and Fan Revolutions on the Drying Characteristics of Thick Pacific Coast Hemlock Lumber," *Holzforschung*, Vol.51, No. 4, pp.381-389.

[60] Reynolds, O., 1895, "On the Dynamical Theory of Incompressible Viscous Fluids and the Determination of the Criterion and Internal Moisture Nonequilibrium," *Philosophical Transactions of the Royal Society of London, Series A* Vol.186, pp. 123-164.

[61] Kays, W. M., 1988, "Convective Heat and Mass Transfer," McGraw-Hill, p. 243 and 263.

[62] Hanjalic, K., 1994, "Advanced Turbulence Closure Models: A Review of Current Status and Future Prospects," *Int. Journal of Heat and Fluid Flow*, Vol.15, pp.178-203.

[63] Bousinesq, J., 1877, "Theorie de l'ecoulement tourbilant," *Memoiers Presentes par Divers Savants a l'academie des Sciences de l'Institute de France*, Tome XXIII, Paris, France, pp.46-50.

[64] Tennekes, H. and Lumley, J. L., 1972, "*A First Course in Turbulence*, The MIT Press, Cambrideg, MA.

[65] Launder, B. E. and Spalding, D. B., 1974, "The Numerical Computation of Turbulent Flows," *Computer Methods Applied Mechanics Engineering*,Vol.3, pp.269-289.

[66] White, F. M., 1991, "*Viscous Fluid Flow*," McGraw-Hill, New York.

[67] Launder, B. E. and Sharma, B. I., 1974, "Application of the Energy Dissipation Model of Turbulence to the Calculation of Flow Near a Spinning Disk," *Letters in Heat and Mass Transfer*,Vol.1, pp.131-138.

[68] Courant, R., Isaacson, E. and Rees, M., 1952, "On the Solution of Non-Linear Hyperbolic Differential Equations by Finite differences," *Comm. Pure Appl. Math.*,Vol.5, p.243.

[69] Alderton, J. H. and Wilkes, N.S., 1988, "Some Applications of New Finite Difference Schemes for Fluid Flow Problems," *AERE-R*13324.

[70] Djilali, N. , Gartshore, I.S., and Salcudean, M., 1991, "Turbulent Flow Around a Bluff Rectangula Plate. Part II: Numerical Predictions," *ASME Journal of Fluids Engineering*, Vol.113, pp.60-66.

[71] Rohsenow, W.H., and Hartnet, J. P., 1991, *"Handbook of Heat Transfer,"* McGraw-Hill, New York.

[72] Press, W. H., Flannery, B.P., Teokolsky, S.A., and Vetterling, W. T.. 1992. *"Numerical Recipes,"* Cambridge University Press, pp. 866-870.

[73] American Society of Heating, Refrigerating and Air-Conditioning Engineers. 1989, *"ASHRAE Handbook, Fundamentals,"* Pergamon Press, pp. 5.1-6.16.

[74] Grigull, U., Straub, J. and Schiebener, P., 1990, *"Steam Tables in SI-units."* Springer, Berlin.

Appendix A

Dry wood densities

The raw data of expriments of Li[52] have been used to obtain the dry wood density of each individual board. Then the average density of the boards in a column is used for each board in a row, namely boards 1 to 7. Tables A.1 to A.4 provide the dry wood densities of each board in a row for four runs of Li with different Re numbers and side gap sizes.

Board No.	1	2	3	4	5	6	7
$\rho_d[\frac{kg}{m^3}]$	450	470	431	421	460	438	408

Table A.1: Wood dry density used for boards of a row in Run No.7 of Li Re_{D_h}=4400, g=1.5 mm

Board No.	1	2	3	4	5	6	7
$\rho_d[\frac{kg}{m^3}]$	456	430	411	435	442	469	401

Table A.2: Wood dry density used for boards of a row in Run No.14 of Li Re_{D_h}=4400. g=21.5 mm

Board No.	1	2	3	4	5	6	7
$\rho_d[\frac{kg}{m^3}]$	358	359	346	395	348	413	355

Table A.3: Wood dry density used for boards of a row in Run No.10 of Li Re_{D_h}=8800. g=1.5 mm

Board No.	1	2	3	4	5	6	7
$\rho_d[\frac{kg}{m^3}]$	417	429	447	391	406	422	399

Table A.4: Wood dry density used for boards of a row in Run No.13 of Li Re_{D_h}=8800. g=21.5 mm

Appendix B

Computer program for two-dimensional drying

The following program is written for the two-dimensional drying of western hemlock. For the surface coefficients on horizontal and vertical faces of the boards, equations were obtained by curve fitting the best equation to the numerical results of Chapter 5. This has been performed using a commercial software called "Table Curve 2D".

For the physical properties of liquid water and water vapor, polynomials have been curve fitted to the steam tables of [74] to provide accuracy of better than 0.3 percent.

For one dimensional drying, the ADI formulation in the first half time step is only used and some changes, like doubling the time step, has been made in order to solve for points number 9,8,7 of Figure 7.1, instead of the whole domain.

```
C ** COPYRIGHT** AHMAD HASHEMI ESFAHANIAN, 1999
C ** THIS PROGRAM MAY NOT BE USED, COPIED, ALTERED OR REPRODUCED IN ANY
C  COMPUTER LANGUAGE OR OTHER WAYS WITHOUT THE EXPRESS WRITTEN CONSENT
C   OF THE AUTHOR

C  THIS PROGRAM IS FOR SOLVING THE DRYING OF STACK LUMBER x
C234567890123456781012345678901234567890123456789012345678901234567890
```

```
 DOUBLE PRECISION PSV,PV,SAI,DTSAI,DXSAI,ROW,RNUL,XFSP,ROSV
DOUBLE PRECISION amaxertv,amaxerxv,sumtv,sumxv,smin,skl,alfa
DOUBLE PRECISION dmu,ros,vtin,twin,tdin,wss,ww1,ww2,win
DOUBLE PRECISION wsd,emu,fiin,patm,pvin,xin,cvin,roain,rovin
DOUBLE PRECISION time,dt,epsd,xmax,rjac,SAM0,SHAH,FIINNEW
DOUBLE PRECISION sumt,sumX,amaxert,amaxerX,xav,PSVTD,MR,WINNEW
DOUBLE PRECISION ROTIN,TMIN,TMVIN,AMAIRIN
DOUBLE PRECISION T1(0:80,0:80,7),X1(0:80,0:80,7),T(0:80,0:80,7)
DOUBLE PRECISION XH(0:80,0:80,7)
DOUBLE PRECISION CX(0:80,0:80,7),TV(0:80,0:80,7)

DOUBLE PRECISION XX(80),YY(80),RX(80),RY(80),DX(80),DY(80)
   & ,TM(80,7),AVX(7)

DOUBLE PRECISION VX(80,80,3),VT(80,80,3)

DOUBLE PRECISION H1(80,80,3),DH(80,80,3),
   & U(80,80,4),DU(80,80,4),
   & RO(80,80,4),EPS(80,80),T1P(0:80,0:80,7),X1P(0:80,0:80,7)

    DOUBLE PRECISION AMBDA(80,80),BX(80,7),ROMV(80,7),XEQ(80,7)
   & ,FII(80,7),BY(80,7,2)

DOUBLE PRECISION A(80),B(80),C(80),D(80),E(80),G(80),H(80)
DOUBLE PRECISION BQY(80,7,2),TIN(7),AMVIN(7),AMTIN(7),BQX(80,7)
DOUBLE PRECISION XH0M,TH0M,X0M,T0M,XHM,XM0,TM0,T1M,X1M
DOUBLE PRECISION RODUP(80,80,4),RODU(80,80)

DOUBLE PRECISION SVXY(80,80),SVTY(80,80),SVXX(80,80),
   & GYT(80,80),GYX(80,80),GXT(80,80),GXX(80,80),SVTX(80,80)

DOUBLE PRECISION VIRCONDX(80,80),VIRCONDY(80,80),EE(80,80)
   & ,FF(80,80),AA(80,80),BB(80,80),CC(80,80),DD(80,80)
   & ,HYVXGX(80,80),HXVXGX(80,80),VIRCOND(80,80),HHVXY(80,80),
   & HHVXX(80,80),HHVX(80,80),HHVT(80,80),SVT(80,80),SVX(80,80)

c DOUBLE PRECISION AAX(80,80),BBX(80,80),CCX(80,80),DDX(80,80)
c    & ,FFX(80,80),EEX(80,80)

DOUBLE PRECISION TAD,TSTD
   & ,AD(7),STD(7),GRADYX(80,80,7),ADMAX(7),GRADXX(80,80,7)
   & ,XGRAD(80,80,7),GRADYXMAX(7),AVGRADYX(7),AX,AY,CXMAX(7)
   & ,GRADXXMAX(7),AVGRADXX(7),XGRADAV(7),XGRADMAX(7),CXMIN(7)

INTEGER NX,NY,I,J,K,NITOUT,NTIM,NX1,NX2,NY1,NY2
   & ,IMAX,JMAX,NMAX,NITINX,NFIFLAG(80,7),IFIFLAG,IPRINT,JPRINT

INTEGER JGRADMAX(7),JGY(7),IGY(7),JGX(7),IGX(7),IADMAX(7),
   & JADMAX(7),IXMAX(7),JXMAX(7),IXMIN(7),JXMIN(7),IGRADMAX(7)
   & ,NP1TIM,NP2TIM,NP4TIM,NP5TIM,N1TIM,NM1TIM,NM2TIM,NM4TIM,NM5TIM
   & ,N2TIM,N4TIM,N5TIM

C ASSIGNING THE CONVERGENCE CRITERION
     PARAMETER (AMAXERTV=1.D-3,AMAXERXV=5.D-7,SUMTV=1.D-2,
   & SUMXV=1.D-6)

PARAMETER (SMIN=0.028D0,SKL=1.1D-16,ALFA=0.0075D0,
   & DMU=0.0041D0)

OPEN(UNIT=8,FILE='dev1r10.ot')
OPEN(UNIT=1,FILE='mctemp1r10.out')
OPEN(UNIT=2,FILE='mctemp2r10.out')
OPEN(UNIT=3,FILE='mctemp3r10.out')
OPEN(UNIT=4,FILE='mctemp4r10.out')
OPEN(UNIT=5,FILE='mctemp5r10.out')
OPEN(UNIT=9,FILE='mctemp6r10.out')
OPEN(UNIT=7,FILE='mctemp7r10.out')
      WRITE(1,*) 'Variables= j,i,x,y,Temperature(K),MC,MC-GRADIENT'
      WRITE(2,*) 'Variables= j,i,x,y,Temperature(K),MC,MC-GRADIENT'
      WRITE(3,*) 'Variables= j,i,x,y,Temperature(K),MC,MC-GRADIENT'
      WRITE(4,*) 'Variables= j,i,x,y,Temperature(K),MC,MC-GRADIENT'
      WRITE(5,*) 'Variables= j,i,x,y,Temperature(K),MC,MC-GRADIENT'
      WRITE(9,*) 'Variables= j,i,x,y,Temperature(K),MC,MC-GRADIENT'
      WRITE(7,*) 'Variables= j,i,x,y,Temperature(K),MC,MC-GRADIENT'
WRITE(8,*)'%SMIN=',SMIN,' SKL=',SKL,' ALFA=',ALFA,'%DMU=',DMU

WRITE(8,*)'%NTIM   time    xav    ,TAD,    TSTD,  xav(1)
   &    xav(2)   xav(3)   xav(4)   xav(5)   xav(6)   xav(7)
   &          (STD(K),K=1,7)
   &          ,(AD(K),K=1,7),
   &          (ADMAX(K),K=1,7),
```

```
     &           (XGRADAV(K),K=1,7),
     &           (XGRADMAX(K),K=1,7)
     &           ,(AVGRADXX(K),K=1,7)
     &          ,(GRADXXMAX(K),K=1,7),
     &           (AVGRADYX(K),K=1,7)
     &          ,(GRADYXMAX(K),K=1,7),
     & (CXMAX(K),K=1,7)
     &          ,(CXMIN(K),K=1,7),
     &  (CX(IGRADMAX(K),JGRADMAX(K),K),K=1,7),
     &       (CX(IGX(K),JGX(K),K),K=1,7)
     &        ,(CX(IGY(K),JGY(K),K),K=1,7),
     & (XX(IGRADMAX(K)),K=1,7),
     &  ,(YY(JGRADMAX(K)),K=1,7),   (XX(IGX(K)),K=1,7),
     &  (YY(JGX(K)),K=1,7),
     &   (XX(IGY(K)),K=1,7),   (YY(JGY(K)),K=1,7),
     &  (XX(IXMAX(K)),K=1,7),
     &  (YY(JXMAX(K)),K=1,7),
     &  (XX(IXMIN(K)),K=1,7)   ,(YY(JXMIN(K)),K=1,7),'

NY1=76
NX1=76
NY2=76
NX2=76

C  ASSIGNING THE INLET AIR CONDITIONS
VTIN=0.0207421D0
TWIN=48.99D0+273.15D0
TDIN=327.4D0

C=== ASSIGNING THE INITIAL VALUES FOR RUN10 OF LI, RE=8600, G=1.5 MM
 DO 45 K=1,7

   IF(K.EQ.1)THEN
     DO 20 I=1,NX1
 BQX(I,K)=0.D0
 BX(I,K)=0.D0
 TM(I,K)=TDIN
 DO 20 J=1,NY1
   CX(I,J,K)=0.4563548243D0
   T(I,J,K)=293.15D0
20      CONTINUE
  END IF

  IF(K.EQ.2)THEN
    DO 22 I=1,NX1
BQX(I,K)=0.D0
BX(I,K)=0.D0
TM(I,K)=TDIN
  DO 22 J=1,NY1
    CX(I,J,K)=0.5077487336D0
    T(I,J,K)=293.15D0
22      CONTINUE
 END IF

 IF(K.EQ.3)THEN
   DO 24 I=1,NX1
BQX(I,K)=0.D0
BX(I,K)=0.D0
TM(I,K)=TDIN
 DO 24 J=1,NY1
   CX(I,J,K)=0.481341386D0
   T(I,J,K)=293.15D0
24     CONTINUE
 END IF

 IF(K.EQ.4)THEN
   DO 26 I=1,NX1
     BQX(I,K)=0.D0
     BX(I,K)=0.D0
     TM(I,K)=TDIN
     DO 26 J=1,NY1
 CX(I,J,K)=0.4756910157D0
 T(I,J,K)=293.15D0
26      CONTINUE
  END IF

  IF(K.EQ.5)THEN
    DO 28 I=1,NX1
BQX(I,K)=0.D0
BX(I,K)=0.D0
TM(I,K)=TDIN
```

```
  DO 28 J=1,NY1
    CX(I,J,K)=0.4265398935D0
    T(I,J,K)=293.15D0
 28   CONTINUE
      END IF

      IF(K.EQ.6)THEN
  DO 30 I=1,NX1
    BQX(I,K)=0.D0
    BX(I,K)=0.D0
    TM(I,K)=TDIN
    DO 30 J=1,NY1
CX(I,J,K)=0.4383420436D0
T(I,J,K)=293.15D0
 30     CONTINUE
  END IF

  IF(K.EQ.7)THEN
    DO 32 I=1,NX1
BQX(I,K)=0.D0
BX(I,K)=0.D0
TM(I,K)=TDIN
DO 32 J=1,NY1
  CX(I,J,K)=0.495548D0
  T(I,J,K)=293.15D0
 32 CONTINUE
    END IF
 45 CONTINUE

 DO 52 K=1,7

    DO 50 J=1,NY1
      BQY(J,K,1)=0.D0
      BQY(J,K,2)=0.D0
      BY(J,K,1)=0.D0
      BY(J,K,2)=0.D0
        DO 50 I=1,NX1
    RO(I,J,4)=ROS
50     CONTINUE

 52  CONTINUE

56  FORMAT(80(F15.9))
57 FORMAT(I5,F14.4,80(F14.10))
58 FORMAT(I5,1X,80(F10.3))

  NTIM=0
TIME=0.0D0
DT=0.1D0/1.1D0

CALL GRIDY(YY,DY,RY,NY)

C ********************************************************
C ************** STARTING A NEW TIME STEP **************

100 NTIM=NTIM+1

IF(TIME.LE.20.0D0)DT=1.1D0*DT
IF(TIME.LT.2000.0D0.AND.TIME.GT.20.0D0)DT=1.05D0*DT
IF(TIME.LT.8000.0D0.AND.TIME.GT.2000.D0)DT=1.1D0*DT
IF(TIME.LE.9000.0D0.AND.DT.GE.300.0D0)DT=300.0D0
IF(TIME.GT.1.0D0.AND.DT.GE.0.1D0*TIME)DT=0.1D0*TIME
IF(TIME.GT.9000.0)DT=1.05*DT
IF(TIME.LT.43200.0D0.AND.TIME+DT.GT.43200.0D0)DT=43200.0D0-TIME
IF(TIME.LT.43200.0D0.AND.DT.GT.100.0D0)DT=100.0D0
IF(TIME.LT.43200.0D0.AND.TIME.GT.31000.0D0.AND.DT.GT.60.0D0)DT=60.0D0

IF(TIME.LT.461220.0D0.AND.TIME+DT.GT.461220.0D0)
   & DT=461220.0D0-TIME

IF(ABS(TIME-DT).LE.461220.0D0.AND.TIME+DT.GE.461220.0D0
   & .AND.DT.LT.5.0D0)DT=5.0D0

IF(TIME.LE.80000.0D0.AND.DT.GE.100.0D0)DT=100.0D0
IF(DT.GT.150.0D0)DT=150.0D0

TIME=DT+TIME

C **********ASSIGNING THE INLET AIR CONDITIONS ************
IF(TIME.GE.43200.0D0.AND.TIME.LE.216000.0D0)THEN
```

```
TWIN=48.99D0+273.15D0+(53.97D0-48.99D0)/(216000.0D0-43200.0D0)*
   & (TIME-43200.0D0)

TDIN=54.02D0+273.15D0+(81.96D0-54.02D0)/(216000.0D0-43200.0D0)*
   & (TIME-43200.0D0)
END IF

IF(TIME.GE.216000.0D0.AND.TIME.LT.461220.0D0)THEN
TWIN=53.97D0+273.15D0
TDIN=81.96D0+273.15D0
END IF

IF(TIME.GT.461220.0D0.AND.TIME.LT.469620.0D0)THEN
 TWIN=53.97D0+273.15D0+(60.98D0-53.97D0)/(552540.0D0-544140.0D0)*
   & (TIME-461220.0D0)

 TDIN=81.96D0+273.15D0+(65.13D0-81.96D0)/(552540.0D0-544140.0D0)*
   & (TIME-461220.0D0)
END IF

IF(TIME.GE.469620.0D0)THEN
TWIN=60.98D0+273.15D0
TDIN=65.13D0+273.15D0
END IF



WSS=0.62198D0*PSV(TWIN)/(101325.0D0-PSV(TWIN))
WW1=(3151.37015D0-2.381D0*TWIN)*WSS+TWIN-TDIN
WW2=3151.37015D0+1.805D0*TDIN-4.186D0*TWIN
WIN=WW1/WW2
WSD=0.62198D0*PSV(TDIN)/(101325.0D0-PSV(TDIN))
EMU=WIN/WSD
FIIN=EMU/(1.0D0-(1.0D0-EMU)*PSV(TDIN)/101325.0D0)
PATM=101325.0D0
     PSVTD=PSV(TDIN)
     MR=18.01528D0/28.9645D0
      FIINNEW=WIN*PATM/PSVTD/(MR+WIN)
 FIIN=(FIINNEW+FIIN)/2.0D0
5  PVIN=FIIN*PSVTD

     ROTIN=MR*PATM*(1.0D0+WIN)*28.9654D0/(8314.41D0*TDIN)
    &       /(MR+WIN)

     CVIN=WIN/(1.0D0+WIN)
     ROVIN=ROTIN*CVIN
     TMIN=ROTIN*VTIN
     TMVIN=ROVIN*VTIN
     AMAIRIN=TMIN-TMVIN
     WINNEW=TMVIN/AMAIRIN
      FIINNEW=WIN*PATM/PSVTD/(MR+WIN)

       IF(ABS(WINNEW-WIN)/WINNEW.GT.0.02D0.AND.
    &    ABS(FIINNEW-FIIN)/FIINNEW.GT.0.02D0)THEN

   WIN=WINNEW
   FIIN=FIINNEW
   GO TO 5
 END IF
 6      CONTINUE
C*************************
IF(IFIFLAG.NE.1)THEN
  DO 25 K=1,7
    AMVIN(K)=ROVIN*VTIN
    AMTIN(K)=AMVIN(k)/CVIN
    TIN(K)=TDIN

    DO 25 I=1,80
ROMV(I,K)=ROVIN
TM(I,K)=TDIN
FII(I,K)=FIIN
 25     CONTINUE
END IF
C ********************************************************
C ***********START SOLVING FOR A NEW BOARD ******************
K=0
120 K=K+1

C  CALLING THE CORRECT MESH GENARATION FOR EACH BOARD AT EACH TIME STEP
 IF(K.EQ.1)THEN
   CALL GRIDX1(XX,DX,RX,NX)
```

```
 END IF

 IF(K.NE.1)THEN
   CALL GRIDX2(XX,DX,RX,NX)
 END IF
C *********ASSIGNING THE VALUES FOR SURFACE COEFFICIENTS
CALL BQXYCAL(BX,BY,BQX,BQY,K,NX,NY,XX,YY)

 185 NITOUT=0

IMAX=NX+1
JMAX=NY+1
 C  ********* SETTING THE AVERAGE ROS FOR EACH BOARD ***********
IF(K.EQ.1)ROS=358.015384D0
IF(K.EQ.2)ROS=358.8973191D0
IF(K.EQ.3)ROS=346.2378746D0
IF(K.EQ.4)ROS=395.0738574D0
IF(K.EQ.5)ROS=348.3127815D0
IF(K.EQ.6)ROS=413.060263D0
IF(K.EQ.7)ROS=355.6120802D0
C*****************************************************
C  COMPUTING THE VALUES FOR INITIAL TEMPERATURE OF THE NEW TIME STEP
CALL UHCAL(U,H1,DU,DH,T,K,NX,NY)

CALL ROEPCAL(RO,EPS,EPSD,CX,T,K,NX,NY,ROS,AMBDA,XMAX,U,H1
    & ,DU,DH)

CALL VTXCAL(VX,VT,RO,T,CX,NX,NY,K,SMIN,XMAX,ALFA,DMU,SKL,EPS
    & ,ROS)

C  ASSIGNING THE N'S COEF. VALUES FOR (N+1/2)'S FOR STARTING THE ITERATIONS
DO 200 I=1,NX
DO 200 J=1,NY
T1P(I,J,K)=T(I,J,K)
T1(I,J,K)=T(I,J,K)
X1P(I,J,K)=CX(I,J,K)
X1(I,J,K)=CX(I,J,K)
200 CONTINUE

C** CALCULATING TM,FII & XEQ (TEMPERATURE, RELATIVE HUMIDITY & EQULIBRIUM MOISTURE CONTENT OF AIR)**
  CALL CALXEQ(XEQ,TM,FII,NX)

C ********* UPDATING TM,XEQ & FII BASED ON HEAT & MASS TRANSFER ******
CALL XTAIRUPDATENEW2(CX,ROMV,TDIN,TWIN,VTIN,NX,NY,BY,BX
    & ,DX,DY,EPS,AMTIN,AMVIN,T,H1,BQY,TIN,TM,BQX,FIIN,XEQ
    & ,FII,NFIFLAG,WIN,IFIFLAG)

C ********** START A NEW OUTER ITERATION  *********************************
250 NITOUT=NITOUT+1

C THESE TWO SENTENCES ARE CALLED FOR ONE DIMENSIONAL CASE
c  CALL CXVCAL(CXV,X1,CX,NX,NY,K)
C CALL CALXEQ(XEQ,TM,FII,NX)
C*****************************************************************

C       ******* START ENERGY EQUATION ******

    IF(NITOUT.EQ.1)THEN

C THIS IS CALLED FOR ONE DIMENSIONAL CASE
c 1D CALL TVCAL(TV,T1,T,NX,NY,K)
CALL CALRODU(RODUP,RODU,RO,DU,NX,NY,DX,DY)

CALL CALSVTXXY(VT,VX,DX,DY,DT,NX,NY,SVT,SVX,
    & SVTX,SVTY,SVXX,SVXY)

CALL CALVIRCOND2(H1,VT,VX,AMBDA,VIRCOND,VIRCONDX,
    & VIRCONDY,HHVX,HHVT,HHVXX,HHVXY,DX,DY,NX,NY,DT)

CALL CALHVXGX(HXVXGX,HYVXGX,HHVXX,HHVXY,CX,DX,DY,NX,NY,DT,K)
c 1D CALL CALHVXGX(HXVXGX,HYVXGX,HHVXX,HHVXY,CXV,DX,DY,NX,NY,DT,K)

CALL CALABCD(VIRCONDX,VIRCONDY,AA,BB,CC,DD,NX,NY)


C*********************************

   CALL CALEFNEW(VIRCONDX,VIRCONDY,EE,FF,T,T,CX,CX,RODU,EPS,
    & BY,BX,XEQ,TM,BQY,BQX,DH,DX,DY,NX,NY,K,DT,H1,HXVXGX,HYVXGX,
    & NFIFLAG)
```

```
      CALL sor(aa,bb,cc,dd,ee,ff,t1,IMAX,jmax,rjac,K,NMAX)
C*****************************************************************
CALL CALXGRADXT(GXT,GXX,T1,X1,NX,NY,K)
CALL CALYGRADXT(GYT,GYX,T1,X1,NX,NY,K)
PRINT *,'Nmax=',Nmax
C*************************************************************
C  **** *******  START MASS EQUATION  **************************
CALL TVCAL(TV,T,T,NX,NY,K)

C ********** START A NEW INNER ITERATION FOR X'S ********************
NITINX=0
260 NITINX=NITINX+1
C*************************************************************

C *** SETTING THE COEFFICIENTS FOR ADI METHOD
DO 3000 I=1,NX
A(1)=0.0D0
C(NY)=0.0D0
H(NY)=0.0D0
C ** ASSIGNING ZERO TO ALL VALUES
B(1)=0.0D0
C(1)=0.0D0
D(1)=0.0D0
E(1)=0.0D0
G(1)=0.0D0
H(1)=0.0D0

A(NY)=0.0D0
B(NY)=0.0D0
D(NY)=0.0D0
E(NY)=0.0D0
G(NY)=0.0D0
C ----------  FOR BOUNDARY POINTS NO. 2 & 6
IF(I.EQ.NX)THEN
J=1
C(J)=SVXY(I,J)

D(J)=SVXX(I-1,J)*(CX(I,J,k)-CX(I-1,J,k))-SVTY(I,J)*
   & (TV(I,J+1,k)-TV(I,J,k))+SVTX(I-1,J)*(TV(I,J,k)-TV(I-1,J,k))

X0M=CX(I,1,K)
T0M=T(I,1.K)

SAM0=DY(J)*BY(J,K,2)*DT*SAI(X0M,T0M)*ROSV(T0M)*EPS(I,J)**2
   &  *(X0M-XEQ(I,K))

    IF(NFIFLAG(I,K).EQ.1)SAM0=0.0D0
B(1)=-1.0D0*C(1)+DX(I)*DY(1)*ROS
D(1)=D(1)+CX(I,1,k)*DX(I)*DY(1)*ROS-SAM0

J=NY
D(J)=SVXX(I-1,J)*(CX(I,J,k)-CX(I-1,J,k))+SVTY(I,J-1)*
   & (TV(I,J,k)-TV(I,J-1,k))+SVTX(I-1,J)*(TV(I,J,k)-TV(I-1,J,k))

A(J)=SVXY(I,J-1)
XH0M=CX(NX,NY,K)
TH0M=T(NX,NY,K)

SAM0=DY(J)*BY(J,K,2)*DT*SAI(XH0M,TH0M)*
   & ROSV(TH0M)*EPS(I,J)**2*(XH0M-XEQ(I,K))

    IF(NFIFLAG(I,K).EQ.1)SAM0=0.0D0

SHAH=DX(I)*BX(I,K)*DT*SAI(XH0M,TH0M)*ROSV(TH0M)*EPS(I,J)**2
    IF(NFIFLAG(I,K).EQ.1)SHAH=0.0D0
B(NY)=-1.0D0*A(NY)+DX(I)*DY(NY)*ROS+SHAH
D(J)=D(J)+CX(I,J,k)*DX(I)*DY(J)*ROS+SHAH*XEQ(I,K)-SAM0

END IF
C ----------  FOR BOUNDARY POINTS NO. 7 & 8
IF(I.LT.NX.AND.I.GT.1)THEN

J=1
C(J)=SVXY(I,J)

D(J)=0.5D0*SVXX(I-1,J)*(CX(I,J,k)-CX(I-1,J,k))-SVTY(I,J)*
   & (TV(I,J+1,k)-TV(I,J,k))+0.5D0*SVTX(I-1,J)*(TV(I,J,k)
   & -TV(I-1,J,k))-0.5D0*SVXX(I,J)*(CX(I+1,J,k)-CX(I,J,k))
   & -0.5D0*SVTX(I,J)*(TV(I+1,J,k)-TV(I,J,k))

X0M=CX(I,1,K)
```

```
T0M=T(I,1,K)
B(1)=-1.0D0*C(1)+DX(I)*DY(1)*ROS
D(1)=D(1)+CX(I,1,k)*DX(I)*DY(1)*ROS

J=NY
D(J)=0.5D0*SVXX(I-1,J)*(CX(I,J,k)-CX(I-1,J,k))+SVTY(I,J-1)*
   & (TV(I,J,k)-TV(I,J-1,k))+0.5D0*SVTX(I-1,J)*(TV(I,J,k)
   & -TV(I-1,J,k))-0.5D0*SVXX(I,J)*(CX(I+1,J,k)-CX(I,J,k))
   & -0.5D0*SVTX(I,J)*(TV(I+1,J,k)-TV(I,J,k))


A(J)=SVXY(I,J-1)
XH0M=CX(I,NY,K)
TH0M=T(I,NY,K)
SHAH=DX(I)*BX(I,K)*DT*SAI(XH0M,TH0M)*ROSV(TH0M)*EPS(I,J)**2
     IF(NFIFLAG(I,K).EQ.1)SHAH=0.0D0

B(NY)=-1.0D0*A(NY)+DY(NY)*DX(I)*ROS+SHAH
D(J)=D(J)+CX(I,J,k)*DX(I)*DY(J)*ROS+SHAH*XEQ(I,K)

END IF
C ————————  FOR BOUNDARY POINTS NO. 1 & 5
IF(I.EQ.1)THEN
J=1
C(J)=SVXY(I,J)

D(J)=-1.0D0*SVTY(I,J)*(TV(I,J+1,k)-TV(I,J,k))
   & -SVXX(I,J)*(CX(I+1,J,k)-CX(I,J,k))
   & -SVTX(I,J)*(TV(I+1,J,k)-TV(I,J,k))

X0M=CX(I,1,K)
T0M=T(I,1,K)

SAM0=DY(J)*BY(J,K,1)*DT*SAI(X0M,T0M)*ROSV(T0M)*EPS(I,J)**2
   & *(X0M-XEQ(I,K))

     IF(NFIFLAG(I,K).EQ.1)SAM0=0.0D0

B(1)=-1.0D0*C(1)+DX(I)*DY(1)*ROS
D(1)=D(1)+CX(I,1,k)*DX(I)*DY(1)*ROS-SAM0

J=NY
D(J)=SVTY(I,J-1)*(TV(I,J,k)-TV(I,J-1,k))
   & -SVXX(I,J)*(CX(I+1,J,k)-CX(I,J,k))
   & -SVTX(I,J)*(TV(I+1,J,k)-TV(I,J,k))

A(J)=SVXY(I,J-1)
XH0M=CX(I,NY,K)
TH0M=T(I,NY,K)

SAM0=DY(J)*BY(J,K,1)*DT*SAI(XH0M,TH0M)*
   & ROSV(TH0M)*EPS(I,J)**2*(XH0M-XEQ(I,K))

     IF(NFIFLAG(I,K).EQ.1)SAM0=0.0D0

SHAH=DX(I)*BX(I,K)*DT*SAI(XH0M,TH0M)*ROSV(TH0M)*EPS(I,J)**2

     IF(NFIFLAG(I,K).EQ.1)SHAH=0.0D0
B(NY)=-1.0D0*A(NY)+DX(I)*DY(NY)*ROS+SHAH
D(J)=D(J)+CX(I,J,k)*DX(I)*DY(J)*ROS+SHAH*XEQ(I,K)-SAM0

END IF
C ————————————————
G(1)=D(1)/B(1)
H(1)=C(1)/B(1)

DO 2900 J=2,NY-1
A(J)=0.0
B(J)=0.0
C(J)=0.0
D(J)=0.0
E(J)=0.0
G(J)=0.0
H(J)=0.0
C ————————  FOR GENERAL SURFACE POINT NO. 4
IF(I.EQ.NX)THEN
A(J)=0.5D0*SVXY(I,J-1)

C(J)=0.5D0*SVXY(I,J)

D(J)=SVXX(I-1,J)*(CX(I,J,k)-CX(I-1,J,k))-0.5D0*SVTY(I,J)*
```

```
     & (TV(I,J+1,k)-TV(I,J,k))+SVTX(I-1,J)*(TV(I,J,k)
     & -TV(I-1,J,k))+0.5D0*SVTY(I,J-1)*(TV(I,J,k)-TV(I,J-1,k))

X0M=CX(I,J,K)
T0M=T(I,J,K)

SAM0=DY(J)*BY(J,K,2)*DT*SAI(X0M,T0M)*ROSV(T0M)*EPS(I,J)**2
     & *(X0M-XEQ(I,K))

      IF(NFIFLAG(I,K).EQ.1)SAM0=0.0D0
B(J)=-1.0D0*(A(J)+C(J))+DX(I)*DY(J)*ROS
D(J)=D(J)+CX(I,J,k)*DX(I)*DY(J)*ROS-SAM0
END IF

C ————————  FOR GENERAL INTERNAL POINT NO. 9

IF(I.LT.NX.AND.I.GT.1)THEN

A(J)=0.5D0*SVXY(I,J-1)
C(J)=0.5D0*SVXY(I,J)

D(J)=0.5D0*SVXX(I-1,J)*(CX(I,J,k)-CX(I-1,J,k))-0.5D0*SVTY(I,J)
     & *(TV(I,J+1,k)-TV(I,J,k))+0.5D0*SVTX(I-1,J)*(TV(I,J,k)
     & -TV(I-1,J,k))-0.5D0*SVXX(I,J)*(CX(I+1,J,k)-CX(I,J,k))
     & -0.5D0*SVTX(I,J)*(TV(I+1,J,k)-TV(I,J,k))
     & +0.5D0*SVTY(I,J-1)*(TV(I,J,k)-TV(I,J-1,k))

B(J)=-1.0D0*(A(J)+C(J))+DX(I)*DY(J)*ROS
D(J)=D(J)+CX(I,J,k)*DX(I)*DY(J)*ROS

END IF

C ————————  FOR GENERAL SURFACE POINT NO. 3
IF(I.EQ.1)THEN

A(J)=0.5D0*SVXY(I,J-1)
C(J)=0.5D0*SVXY(I,J)

D(J)=0.5D0*SVTY(I,J-1)*(TV(I,J,k)-TV(I,J-1,k))-0.5*SVTY(I,J)
     & *(TV(I,J+1,k)-TV(I,J,k))-SVXX(I,J)*(CX(I+1,J,k)
     & -CX(I,J,k))-SVTX(I,J)*(TV(I+1,J,k)-TV(I,J,k))

X1M=XH(I,J,K)
X0M=CX(I,J,K)
T0M=T(I,J,K)

SAM0=DY(J)*BY(J,K,1)*DT*SAI(X0M,T0M)*ROSV(T0M)*EPS(I,J)**2
     & *(X0M-XEQ(I,K))

      IF(NFIFLAG(I,K).EQ.1)SAM0=0.0D0
B(J)=-1.0D0*(A(J)+C(J))+DX(I)*DY(J)*ROS
D(J)=D(J)+CX(I,J,k)*DX(I)*DY(J)*ROS-SAM0
END IF
C ————————————————————
  E(J)=B(J)-A(J)*H(J-1)
  H(J)=C(J)/E(J)
  G(J)=(D(J)-A(J)*G(J-1))/E(J)
2900    CONTINUE
E(NY)=B(NY)-A(NY)*H(NY-1)
G(NY)=(D(NY)-A(NY)*G(NY-1))/E(NY)
XH(I,NY,K)=G(NY)
IF(XH(I,NY,K).GT.XMAX)XH(I,NY,K)=XMAX
IF(XH(I,NY,K).LT.0.03D0)XH(I,NY,K)=0.03D0


        DO 2920 J=NY-1,1,-1
XH(I,J,K)=G(J)-H(J)*XH(I,J+1,K)
IF(XH(I,J,K).GT.XMAX)XH(I,J,K)=XMAX
IF(XH(I,J,K).LT.0.03D0)XH(I,J,K)=0.03D0
2920    CONTINUE

3000    CONTINUE


C*****************************************************************

CALL CALXGRADXT(GXT,GXX,T1,XH,NX,NY,K)
CALL CALYGRADXT(GYT,GYX,T1,XH,NX,NY,K)
C*****************************************************************
C*****************************************************************
```

```
c ***** START MASS EQUATION IN 2nd HALF TIME********

C *** SETTING THE COEFFICIENTS
DO 1000 J=NY,1,-1
A(1)=0.0D0
C(NX)=0.0D0
H(NX)=0.0D0

C ASSIGNING ZERO VALUES FOR STARTING THE COMPUTATIONS
B(1)=0.0D0
D(1)=0.0D0
C(1)=0.0D0
E(1)=0.0D0
G(1)=0.0D0
H(1)=0.0D0

A(NX)=0.0D0
B(NX)=0.0D0
D(NX)=0.0D0
E(NX)=0.0D0
G(NX)=0.0D0

C ————————  FOR CORNER POINTS NO. 5 & 6

IF(J.EQ.NY)THEN

I=1
C(I)=SVXX(I,J)
D(I)=SVXY(I,J-1)*(XH(I,J,k)-XH(I,J-1,k))-SVTX(I,J)
    &  *(TV(I+1,J,k)-TV(I,J,k))+SVTY(I,J-1)*(TV(I,J,k)-TV(I,J-1,k))

X1M=X1(1,J,K)
X0M=XH(1,J,K)
XM0=CX(I,J,K)
TM0=T(I,J,K)

SHAH=DY(J)*BY(J,K,1)*DT*SAI(XM0,TM0)*
    & ROSV(TM0)*EPS(I,J)**2

     IF(NFIFLAG(I,K).EQ.1)SHAH=0.0D0

SAM0=DX(I)*BX(I,K)*DT*SAI(XM0,TM0)*ROSV(TM0)*EPS(I,J)**2*
    & (X0M-XEQ(I,K))

     IF(NFIFLAG(I,K).EQ.1)SAM0=0.0D0
B(I)=-1.0D0*C(I)+DX(I)*DY(J)*ROS+SHAH

D(I)=D(I)+XH(I,J,k)*DX(I)*DY(J)*ROS+SHAH*XEQ(I,K)-SAM0

I=NX
XH0M=XH(NX,J,K)

XM0=CX(I,J,K)
TM0=T(I,J,K)

A(NX)=SVXX(I-1,J)

D(I)=SVXY(I,J-1)*(XH(I,J,k)-XH(I,J-1,k))+SVTX(I-1,J)
    &  *(TV(I,J,k)-TV(I-1,J,k))+SVTY(I,J-1)*(TV(I,J,k)-TV(I,J-1,k))

SHAH=DY(J)*BY(J,K,2)*DT*SAI(XM0,TM0)*
    & ROSV(TM0)*EPS(I,J)**2

     IF(NFIFLAG(I,K).EQ.1)SHAH=0.0D0

SAM0=DX(I)*BX(I,K)*DT*SAI(XM0,TM0)*ROSV(TM0)*EPS(I,J)**2*
    & (XH0M-XEQ(I,K))

     IF(NFIFLAG(I,K).EQ.1)SAM0=0.0D0

B(NX)=-1.0D0*A(NX)+DX(NX)*DY(J)*ROS+SHAH

D(I)=D(I)+XH(I,J,k)*DX(I)*DY(J)*ROS+SHAH*XEQ(I,K)-SAM0
END IF

C ————————  FOR CORNER POINTS NO. 3 & 4

IF(J.LT.NY.AND.J.GT:1)THEN

I=1
C(I)=SVXX(I,J)
```

```
D(I)=0.5D0*SVXY(I,J-1)*(XH(I,J,k)-XH(I,J-1,k))-SVTX(I,J)
     &  *(TV(I+1,J,k)-TV(I,J,k))+0.5D0*SVTY(I,J-1)*(TV(I,J,k)
     & -TV(I,J-1,k))-0.5D0*SVXY(I,J)*(XH(I,J+1,k)-XH(I,J,k))
     & -0.5D0*SVTY(I,J)*(TV(I,J+1,k)-TV(I,J,k))

X1M=X1(1,J,K)
X0M=XH(1,J,K)
XM0=CX(I,J,K)
TM0=T(I,J,K)

SHAH=DY(J)*BY(J,K,1)*DT*SAI(XM0,TM0)*ROSV(TM0)*EPS(I,J)**2
      IF(NFIFLAG(I,K).EQ.1)SHAH=0.0D0

B(1)=-1.0D0*C(1)+DX(1)*DY(J)*ROS+SHAH
D(I)=D(I)+XH(I,J,k)*DX(I)*DY(J)*ROS+SHAH*XEQ(I,K)

I=NX
XHM=X1(NX,J,K)
XH0M=XH(NX,J,K)
XM0=CX(I,J,K)
TM0=T(I,J,K)
A(I)=SVXX(I-1,J)

D(I)=0.5D0*SVXY(I,J-1)*(XH(I,J,k)-XH(I,J-1,k))+SVTX(I-1,J)
     &  *(TV(I,J,k)-TV(I-1,J,k))+0.5D0*SVTY(I,J-1)*(TV(I,J,k)
     & -TV(I,J-1,k))-0.5D0*SVXY(I,J)*(XH(I,J+1.k)-XH(I,J,k))
     & -0.5D0*SVTY(I,J)*(TV(I,J+1,k)-TV(I,J,k))

SHAH=DY(J)*BY(J,K,2)*DT*SAI(XM0,TM0)*ROSV(TM0)*EPS(I,J)**2
      IF(NFIFLAG(I,K).EQ.1)SHAH=0.0D0

B(NX)=-1.0D0*A(NX)+DX(NX)*DY(J)*ROS+SHAH
D(I)=D(I)+XH(I,J,k)*DX(I)*DY(J)*ROS+SHAH*XEQ(I,K)
END IF
C ————————  FOR CORNER POINTS NO. 1 & 2

IF(J.EQ.1)THEN

I=1
C(I)=SVXX(I,J)

D(I)=-1.0D0*SVTX(I,J)*(TV(I+1,J,k)-TV(I,J,k))-SVXY(I,J)*
     & (XH(I,J+1,k)-XH(I,J,k))-SVTY(I,J)*(TV(I,J+1,k)-TV(I,J,k))

X1M=X1(1,J,K)
X0M=XH(1,J,K)

XM0=CX(I,J,K)
TM0=T(I,J,K)

SHAH=DY(J)*BY(J,K,1)*DT*SAI(XM0,TM0)*
     & ROSV(TM0)*EPS(I,J)**2

      IF(NFIFLAG(I,K).EQ.1)SHAH=0.0D0

B(1)=-1.0D0*C(1)+DX(1)*DY(J)*ROS+SHAH
D(1)=D(1)+XH(1,J,k)*DX(1)*DY(J)*ROS+SHAH*XEQ(I,K)

I=NX
A(I)=SVXX(I-1,J)

D(I)=SVTX(I-1,J)*(TV(I,J,k)-TV(I-1,J,k))-SVXY(I,J)*
     & (XH(I,J+1,k)-XH(I,J,k))-SVTY(I,J)*(TV(I,J+1,k)-TV(I,J,k))

XHM=X1(NX,J,K)
XH0M=XH(NX,J,K)
XM0=CX(I,J,K)
TM0=T(I,J,K)


SHAH=DY(J)*BY(J,K,2)*DT*SAI(XM0,TM0)*
     & ROSV(TM0)*EPS(I,J)**2

      IF(NFIFLAG(I,K).EQ.1)SHAH=0.0D0

B(NX)=-1.0D0*A(NX)+DX(NX)*DY(J)*ROS+SHAH
D(I)=D(I)+XH(I,J,k)*DX(I)*DY(J)*ROS+SHAH*XEQ(I,K)

END IF
C ————————————————
```

```
G(1)=D(1)/B(1)
H(1)=C(1)/B(1)

DO 900 I=2,NX-1
A(I)=0.0D0
B(I)=0.0D0
C(I)=0.0D0
D(I)=0.0D0
E(I)=0.0D0
G(I)=0.0D0
H(I)=0.0D0

C ————————— FOR GENERAL SURFACE POINT NO. 7
IF(J.EQ.NY)THEN

C(I)=0.5D0*SVXX(I,J)
A(I)=0.5D0*SVXX(I-1,J)

D(I)=SVXY(I,J-1)*(XH(I,J,k)-XH(I,J-1,k))-0.5D0*SVTX(I,J)
   & *(TV(I+1,J,k)-TV(I,J,k))+SVTY(I,J-1)*(TV(I,J,k)
   & -TV(I,J-1,k))+0.5D0*SVTX(I-1,J)*(TV(I,J,k)-TV(I-1,J,k))

X1M=X1(I,J,K)
T1M=T1(I,J,K)
X0M=XH(I,J,K)
XM0=CX(I,J,K)
TM0=T(I,J,K)

SAM0=DX(I)*BX(I,K)*DT*SAI(XM0,TM0)*ROSV(TM0)*EPS(I,J)**2*
   & (X0M-XEQ(I,K))

    IF(NFIFLAG(I,K).EQ.1)SAM0=0.0D0

B(I)=-1.0D0*(A(I)+C(I))+DX(I)*DY(J)*ROS
D(I)=D(I)+XH(I,J,k)*DX(I)*DY(J)*ROS-SAM0
END IF


C ————————— FOR GENERAL INTERNAL POINT NO. 9

IF(J.LT.NY.AND.J.GT.1)THEN

C(I)=0.5D0*SVXX(I,J)
A(I)=0.5D0*SVXX(I-1,J)
D(I)=0.5D0*SVXY(I,J-1)*(XH(I,J,k)-XH(I,J-1,k))-0.5D0*SVTX(I,J)
   & *(TV(I+1,J,k)-TV(I,J,k))+0.5D0*SVTY(I,J-1)*(TV(I,J,k)
   & -TV(I,J-1,k))-0.5D0*SVXY(I,J)*(XH(I,J+1,k)-XH(I,J,k))
   & -0.5D0*SVTY(I,J)*(TV(I,J+1,k)-TV(I,J,k))+0.5D0*SVTX(I-1,J)
   & *(TV(I,J,k)-TV(I-1,J,k))

B(I)=-1.0D0*(A(I)+C(I))+DX(I)*DY(J)*ROS
D(I)=D(I)+XH(I,J,k)*DX(I)*DY(J)*ROS
END IF

C ————————— FOR GENERAL SYMMETRY AXIS POINT NO. 8

IF(J.EQ.1)THEN

C(I)=0.5D0*SVXX(I,J)
A(I)=0.5D0*SVXX(I-1,J)

D(I)=0.5D0*SVTX(I-1,J)*(TV(I,J,k)-TV(I-1,J,k))-0.5D0*SVTX(I,J)
   & *(TV(I+1,J,k)-TV(I,J,k))-SVTY(I,J)*(TV(I,J+1,k)
   & -TV(I,J,k))-SVXY(I,J)*(XH(I,J+1,k)-XH(I,J,k))


B(1)=-1.0D0*(A(I)+C(I))+DX(I)*DY(J)*ROS
D(I)=D(I)+XH(I,J,k)*DX(I)*DY(J)*ROS
END IF
C ————————————————————————
E(I)=B(I)-A(I)*H(I-1)
H(I)=C(I)/E(I)
G(I)=(D(I)-A(I)*G(I-1))/E(I)
900 CONTINUE

E(NX)=B(NX)-A(NX)*H(NX-1)
G(NX)=(D(NX)-A(NX)*G(NX-1))/E(NX)
X1(NX,J,K)=G(NX)
IF(X1(NX,J,K).GT.XMAX)X1(NX,J,K)=XMAX
IF(X1(NX,J,K).LT.0.03D0)X1(NX,J,K)=0.03D0
```

```
  DO 920 I=NX-1,1,-1
    X1(I,J,K)=G(I)-H(I)*X1(I+1,J,K)
    IF(X1(I,J,K).GT.XMAX)X1(I,J,K)=XMAX
    IF(X1(I,J,K).LT.0.03D0)X1(I,J,K)=0.03D0
 920  CONTINUE

1000 CONTINUE

CALL CALXGRADXT(GXT,GXX,T1,X1,NX,NY,K)
CALL CALYGRADXT(GYT,GYX,T1,X1,NX,NY,K)

C*****************************************************************
C ***********************************************
5020 CALL CALSUM(T1,X1,T1P,X1P,SUMT,SUMX,AMAXERT,AMAXERX,NX,NY,K)

IF(AMAXERT.LE.AMAXERTV.AND.SUMT.LE.SUMTV.
   & AND.AMAXERX.LE.AMAXERXV.AND.SUMX.LE.SUMXV)GO TO 5100

IF(NITOUT.GT.500)THEN
 WRITE(1,*)'NO CONVERGENCE FOR T1 AND X1',' TIME=',TIME,' K=',K
 WRITE(2,*)'NO CONVERGENCE FOR T1 AND X1',' TIME=',TIME,' K=',K
  GO TO 9000
END IF
C GOING TO NEXT ITERATION SINCE THERE IS NO CONVERGENCE
GO TO 250
 5100 CONTINUE

IFIFLAG=0

PRINT *,'NO. OF OUTER ITERATIONS',NITOUT,'   K=',K

C ************** STARTING A NEW BOARD **********
IF(K.LT.7)THEN
  GO TO 120
END IF

C *******BEFORE GOING TO NEXT TIME STEP,UPDATING NEW X & T(N) WITH OLD
C***  X & T(N+1) EVALUATING THE STACK AVERAGE MOISTURE CONTENT

5500 XAV=0.0D0
  DO 6200 K=1,7
    AVX(K)=0.0D0

    DO 6000 I=1,NX
NFIFLAG(I,K)=0
AX=1.0D0
IF(I.EQ.1.OR.I.EQ.NX)AX=0.5D0
DO 6000 J=1,NY
  AY=1.0D0
  IF(J.EQ.1.OR.J.EQ.NY)AY=0.5D0
  CX(I,J,K)=X1(I,J,K)
  T(I,J,K)=T1(I,J,K)

  XAV=XAV+CX(I,J,K)*DX(I)*DY(J)*AX*AY
  AVX(K)=AVX(K)+CX(I,J,K)*DX(I)*DY(J)*AX*AY

 6000 CONTINUE

  AVX(K)=AVX(K)/(0.0525D0*0.105D0)
6200  CONTINUE
XAV=XAV/(7.D0*0.0525D0*0.105D0)

CALL DEVIATION(CX,AVX,DX,DY,NX,NY,AD,STD,TAD,TSTD,
   & GRADYX,GRADXX,XGRAD,ADMAX,GRADYXMAX,GRADXXMAX,AVGRADYX,AVGRADXX
   & ,XGRADAV,XGRADMAX,CXMIN,CXMAX,IGX,JGX,IGY,JGY,IADMAX,JADMAX,
   & IXMAX,JXMAX,IXMIN,JXMIN,IGRADMAX,JGRADMAX)

C****PREPARATION FOR PRINTING AFTER A CERTAIN NUMBER OFTIME STEPS
NP1TIM=TIME/3600.0D0
NP2TIM=TIME/7200.0D0
NP4TIM=TIME/14400.0D0
NP5TIM=TIME/18000.0D0
N1TIM=TIME-3600.0D0*NP1TIM
N2TIM=TIME-7200.0D0*NP2TIM
N4TIM=TIME-14400.0D0*NP2TIM
N5TIM=TIME-18000.0D0*NP2TIM
NM1TIM=(TIME-DT)/3600.0D0
NM2TIM=(TIME-DT)/7200.0D0
NM4TIM=(TIME-DT)/14400.0D0
NM5TIM=(TIME-DT)/18000.0D0
```

```
        IF (MOD(NTIM,15).EQ.1.AND.TIME.LT.30.0)THEN
     IPRINT=1
     GO TO 660
      ELSE
           IPRINT=2
       END IF

          IF(MOD(NTIM,10).EQ.1.AND.TIME.GE.30.0.AND.TIME.LE.500.0D0)THEN
    IPRINT=1
     GO TO 660
      ELSE
           IPRINT=2
       END IF

        IF (MOD(NTIM,18).EQ.1.AND.TIME.GT.500.0.AND.TIME.LE.7200.0D0)
     & THEN
      IPRINT=1
     GO TO 660
      ELSE
           IPRINT=2
       END IF

C       IF (MOD(NTIM,15).EQ.1.AND.TIME.GT.8000.0.AND.TIME.LT.16200.0D0)
        IF(NP1TIM-NM1TIM.EQ.1.AND.TIME.GE.7200.0.AND.TIME.LT.14400.0D0)
     & THEN
    IPRINT=1
     GO TO 660
      ELSE
           IPRINT=2
       END IF

        IF(NP2TIM-NM2TIM.EQ.1.AND.TIME.GE.14400.0.AND.TIME.LT.57600.0D0)
     & THEN
      IPRINT=1
     GO TO 660
      ELSE
           IPRINT=2
       END IF

        IF(NP4TIM-NM4TIM.EQ.1.AND.TIME.GE.57600.0
     & .AND.TIME.LT.216000.0D0)THEN
     IPRINT=1
     GO TO 660
      ELSE
           IPRINT=2
       END IF


        IF(NP5TIM-NM5TIM.EQ.1.AND.TIME.GE.216000.0
     & .AND.TIME.LT.544140.0D0)THEN
     IPRINT=1
     GO TO 660
      ELSE
           IPRINT=2
       END IF

        IF(NP4TIM-NM4TIM.EQ.1.AND.TIME.GE.544140.0)
     & THEN
      IPRINT=1
     GO TO 660
      ELSE
           IPRINT=2
       END IF

        IF (TIME.EQ.544140.0D0)THEN
     IPRINT=1
     GO TO 660
      ELSE
           IPRINT=2
  END IF

        IF (TIME.EQ.631200.0D0)THEN
     IPRINT=1
     GO TO 660
      ELSE
           IPRINT=2
  END IF

       IF (TIME.GE.631200.0D0.AND.XAV.GE.0.150D0)THEN
      IPRINT=1
```

```
   GO TO 660
    ELSE
        IPRINT=2
 END IF

C**** PRINTING THE TEMPERATURE AND MOISTURE CONTENT FIELDS ***
 660  IF(IPRINT.EQ.1)THEN
    K=1
       WRITE(1,*) 'Zone T="TIME',TIME, '(S)", i=',
    &                NY, ', j=', NX
         DO 1666 I=1,NX
         DO 1666 J=1,NY
         WRITE(1,6600) I,J,XX(I),YY(J),T1(I,J,K),X1(I,J,K),
    &    XGRAD(I,J,K)
1666      CONTINUE

   K=2
      WRITE(2,*) 'Zone T="TIME',TIME, '(S)", i=',
    &                NY, ', j=', NX
         DO 2666 I=1,NX
         DO 2666 J=1,NY
         WRITE(2,6600) I,J,XX(I),YY(J),T1(I,J,K),X1(I,J,K),
    &    XGRAD(I,J,K)
2666      CONTINUE

   K=3
      WRITE(3,*) 'Zone T="TIME',TIME, '(S)", i=',
    &                NY, ', j=', NX
         DO 3666 I=1,NX
         DO 3666 J=1,NY
         WRITE(3,6600) I,J,XX(I),YY(J),T1(I,J,K),X1(I,J,K),
    &    XGRAD(I,J,K)
3666      CONTINUE

   K=4
      WRITE(4,*) 'Zone T="TIME',TIME, '(S)", i=',
    &                NY, ', j=', NX
         DO 4666 I=1,NX
         DO 4666 J=1,NY
         WRITE(4,6600) I,J,XX(I),YY(J),T1(I,J,K),X1(I,J,K),
    &    XGRAD(I,J,K)
4666      CONTINUE

   K=5
      WRITE(5,*) 'Zone T="TIME',TIME, '(S)", i=',
    &                NY, ', j=', NX
         DO 5666 I=1,NX
         DO 5666 J=1,NY
          WRITE(5,6600) I,J,XX(I),YY(J),T1(I,J,K),X1(I,J,K),
    &    XGRAD(I,J,K)
5666      CONTINUE

   K=6
      WRITE(9,*) 'Zone T="TIME',TIME, '(S)", i=',
    &                NY, ', j=', NX
         DO 6666 I=1,NX
         DO 6666 J=1,NY
         WRITE(9,6600) I,J,XX(I),YY(J),T1(I,J,K),X1(I,J,K),
    &    XGRAD(I,J,K)
6666      CONTINUE

   K=7
      WRITE(7,*) 'Zone T="TIME',TIME, '(S)", i=',
    &                NY, ', j=', NX
         DO 7666 I=1,NX
         DO 7666 J=1,NY
         WRITE(7,6600) I,J,XX(I),YY(J),T1(I,J,K),X1(I,J,K),
    &    XGRAD(I,J,K)
7666      CONTINUE

       ENDIF

6600 FORMAT(2(I3),(F7.4,F7.4),F6.1,F8.5,F9.3)

C**** PRINTING FOR DEVIATION PARAMETERS
      IF (MOD(NTIM,15).EQ.1.AND.DT.LE.50.0D0)
    & THEN
   JPRINT=1
   GO TO 9660
    ELSE
        JPRINT=2
```

```
      END IF

        IF (MOD(NTIM,10).EQ.1.AND.DT.LE.100.0D0.AND.DT.GT.50.0D0)
     & THEN
    JPRINT=1
     GO TO 9660
      ELSE
          JPRINT=2
      END IF

        IF (MOD(NTIM,6).EQ.1.AND.DT.LE.150.0D0.AND.DT.GT.100.0D0)
     & THEN
    JPRINT=1
     GO TO 9660
      ELSE
          JPRINT=2
      END IF

        IF (MOD(NTIM,4).EQ.1.AND.DT.LE.300.0D0.AND.DT.GT.150.0D0)
     & THEN
    JPRINT=1
     GO TO 9660
      ELSE
          JPRINT=2
      END IF

       IF (TIME.EQ.544140.0D0)THEN
      JPRINT=1
     GO TO 9660
      ELSE
          JPRINT=2
  END IF

       IF (TIME.EQ.552540.0D0)THEN
      JPRINT=1
     GO TO 9660
      ELSE
          JPRINT=2
  END IF

       IF (TIME.EQ.631200.0D0)THEN
      JPRINT=1
     GO TO 9660
      ELSE
          JPRINT=2
  END IF

      IF (TIME.GE.631200.0D0.AND.XAV.GE.0.15D0)THEN
      JPRINT=1
     GO TO 9660
      ELSE
          JPRINT=2
  END IF


6657 FORMAT(I6,F9.1,3(F8.5),28(F8.5),42(F10.4),35(F8.5),5(7F7.4,7F7.4),84(I3))


 9660   IF(JPRINT.EQ.1)THEN

WRITE(8,6657)NTIM,TIME,XAV,TAD,TSTD,(AVX(K),K=1,7),(STD(K),K=1,7)
     & ,(AD(K),K=1,7),(ADMAX(K),K=1,7),(XGRADAV(K),K=1,7),
     & (XGRADMAX(K),K=1,7),(AVGRADXX(K),K=1,7),(GRADXXMAX(K),K=1,7),
     & (AVGRADYX(K),K=1,7),(GRADYXMAX(K),K=1,7),
     & (CXMAX(K),K=1,7),(CXMIN(K),K=1,7),
     & (CX(IGRADMAX(K),JGRADMAX(K),K),K=1,7),
     & (CX(IGX(K),JGX(K),K),K=1,7),(CX(IGY(K),JGY(K),K),K=1,7),
     & (XX(IGRADMAX(K)),K=1,7),(YY(JGRADMAX(K)),K=1,7),
     & (XX(IGX(K)),K=1,7),(YY(JGX(K)),K=1,7),
     & (XX(IGY(K)),K=1,7),(YY(JGY(K)),K=1,7),
     & (XX(IXMAX(K)),K=1,7),(YY(JXMAX(K)),K=1,7),
     & (XX(IXMIN(K)),K=1,7),(YY(JXMIN(K)),K=1,7)
     & (CMH(1,K),K=1,7),(CMH(2,K),K=1,7),
     & (CMH(3,K),K=1,7),(CMH(4,K),K=1,7),
     & (CMH(5,K),K=1,7),(CMV(1,K),K=1,7),
     & (CMV(2,K),K=1,7),(CMV(3,K),K=1,7),
     & (CMSIDE(K),K=1,7),(CMCENT(K),K=1,7)
C
c     & ,(IADMAX(K),K=1,7),(JADMAX(K),K=1,7),(IGRADMAX(K),K=1,7),
c     & (JGRADMAX(K),K=1,7),(IGX(K),K=1,7),(JGX(K),K=1,7),(IGY(K),K=1,7),
c     & (JGY(K),K=1,7),(IXMAX(K),K=1,7),(JXMAX(K),K=1,7),(IXMIN(K),K=1,7)
```

```
c     & ,(JXMIN(K),K=1,7)

      END IF

      PRINT *,'TIME=',TIME
C  ******* GOING TO THE NEXT TIME STEP  ************************
C
      IF(TIME.LT.548280.0D0)GO TO 100
      PRINT *,'NTIME=',NTIM
 9000 CONTINUE
      CLOSE(1)
      CLOSE(2)
      CLOSE(3)
      CLOSE(4)
      CLOSE(5)
      CLOSE(9)
      CLOSE(7)
      CLOSE(8)
      STOP
      END

C=======================================================================
C=======================================================================
c CALCULATING THE AVERAGE MOISTURE CONTENTS OF DIFFERENT CUTS
      SUBROUTINE CALMCCUT(CMH,CMV,CMSIDE,CMTOP,CMCENT,CX,DX,DY,NX,NY)


      DOUBLE PRECISION CMH(5,7),CMV(3,7),CMSIDE(7),CMTOP(7),CMCENT(7),
     &  CX(0:80,0:80,7),DX(80),DY(80),AX,AY,S1V,S2V,S3V,S1DYDX,S2DYDX,
     &  S3DYDX,SH,SHDYDX,SC,SCDYDX,SS,SSDYDX

      INTEGER NX,NY,I,J,K,NH,NF,NS
      DO 100 K=1,7

        S1V=0.0D0
        S2V=0.0D0
        S3V=0.0D0
        S3DYDX=0.0D0
        S2DYDX=0.0D0
        S1DYDX=0.0D0

        DO 40 I=1,NX
          AX=1.0D0
          IF(I.EQ.1.OR.I.EQ.NX)AX=0.5D0

        S3V=S3V+AX*DX(I)*(0.5D0*DY(1)*CX(I,1,K)+DY(2)*CX(I,2,K)
         &       +DY(3)*CX(I,3,K)+DY(4)/3.0D0*CX(I,4,K))

        S3DYDX=S3DYDX+AX*DX(I)*(0.5D0*DY(1)+DY(2)+DY(3)+DY(4)/3.0D0)

          DO 10 J=5,12
       S2V=S2V+AX*DY(J)*DX(I)*CX(I,J,K)
       S2DYDX=S2DYDX+AX*DY(J)*DX(I)
   10     CONTINUE
          S2V=S2V+AX*2.0D0/3.0D0*DY(4)*DX(I)*CX(I,4,K)
        S2DYDX=S2DYDX+AX*2.0D0/3.0D0*DY(4)*DX(I)

          DO 20 J=13,NY-1
       S1V=S1V+AX*DY(J)*DX(I)*CX(I,J,K)
        S1DYDX=S1DYDX+AX*DY(J)*DX(I)
   20     CONTINUE
          S1V=S1V+0.5D0*AX*DY(NY)*DX(I)*CX(I,NY,K)
        S1DYDX=S1DYDX+0.5D0*AX*DY(NY)*DX(I)

       40 CONTINUE

        CMV(1,K)=S1V/S1DYDX
        CMTOP(K)=CMV(1,K)
        CMV(2,K)=S2V/S2DYDX
        CMV(3,K)=S3V/S3DYDX


        DO 70 NH=1,5
        CMH(NH,K)=0.0D0
          IF(NH.EQ.1)THEN
       NS=1
       NF=16
          END IF

          IF(NH.EQ.2)THEN
       NS=16
```

```
 NF=31
    END IF

    IF(NH.EQ.3)THEN
 NS=31
 NF=46
    END IF

    IF(NH.EQ.4)THEN
 NS=46
 NF=61
    END IF

    IF(NH.EQ.5)THEN
 NS=61
 NF=76
    END IF

    SH=0.0D0
    SHDYDX=0.0D0

    DO 60 I=NS,NF
    AX=1.0D0
     IF(I.EQ.NS.OR.I.EQ.NF)AX=0.5D0

      DO 50 J=1,NY
   AY=1.0D0
   IF(J.EQ.1.OR.J.EQ.NY)AY=0.5D0

   SH=SH+AX*AY*DY(J)*DX(I)*CX(I,J,K)
   SHDYDX=SHDYDX+AX*AY*DY(J)*DX(I)
50 CONTINUE
60     CONTINUE
  CMH(NH,K)=SH/SHDYDX
70  CONTINUE

 SC=0.0D0
 SCDYDX=0.0D0

 SS=0.0D0
 SSDYDX=0.0D0

 DO 95 J=1,12
   AY=1.0D0
   IF(J.EQ.1)AY=0.5D0

   DO 80 I=1,16
AX=1.0D0
IF(I.EQ.1.OR.I.EQ.16)AX=0.5D0
   SS=SS+AX*AY*DY(J)*DX(I)*CX(I,J,K)
   SSDYDX=SSDYDX+AX*AY*DY(J)*DX(I)
80     CONTINUE

   DO 85 I=61,NX
AX=1.0D0
IF(I.EQ.61.OR.I.EQ.NX)AX=0.5D0
   SS=SS+AX*AY*DY(J)*DX(I)*CX(I,J,K)
   SSDYDX=SSDYDX+AX*AY*DY(J)*DX(I)
85  CONTINUE


   DO 90 I=16,61
AX=1.0D0
IF(I.EQ.16.OR.I.EQ.61)AX=0.5D0
   SC=SC+AX*AY*DY(J)*DX(I)*CX(I,J,K)
   SCDYDX=SCDYDX+AX*AY*DY(J)*DX(I)
90     CONTINUE

95  CONTINUE
CMSIDE(K)=SS/SSDYDX
CMCENT(K)=SC/SCDYDX
100     CONTINUE


RETURN
END
C-------------------------------------
C***CALCULATING THE COMPONENTS OF GRADIENTS OF MOISTURE CONTENT
SUBROUTINE CALGRADXX(GRADXX,GRADXXMAX,AVGRADXX,IGX,JGX,CX,DX,DY
   & ,NX,NY)
DOUBLE PRECISION GRADXX(80,80,7),CX(0:80,0:80,7),DX(80),DY(80)
```

```
     & ,GMAX,GRADXXMAX(7),AVGRADXX(7),AX,AY
INTEGER NX,NY,I,J,K,JGX(7),IGX(7)
DO 50 K=1,7
  GRADXXMAX(K)=0.0D0
  AVGRADXX(K)=0.0D0
DO 50 J=NY,1,-1
  AY=1.0D0
  IF(J.EQ.1.OR.J.EQ.NY)AY=0.5D0
DO 40 I=1,NX-1
  AX=1.0D0
  IF(I.EQ.1)AX=0.5D0
 GRADXX(I,J,K)=2.0D0*(CX(I+1,J,K)-CX(I,J,K))/(DX(I)+DX(I+1))
 GMAX=ABS(GRADXX(I,J,K))
  AVGRADXX(K)=AVGRADXX(K)+AX*AY*DX(I)*DY(J)*GRADXX(I,J,K)
 IF(GMAX.GT.GRADXXMAX(K))THEN
    GRADXXMAX(K)=GMAX
    IGX(K)=I
    JGX(K)=J
 END IF
40 CONTINUE
 I=NX
AX=0.5D0
 GRADXX(NX,J,K)=GRADXX(NX-1,J,K)
 GMAX=ABS(GRADXX(I,J,K))
  AVGRADXX(K)=AVGRADXX(K)+AX*AY*DX(I)*DY(J)*GRADXX(I,J,K)
 IF(GMAX.GT.GRADXXMAX(K))THEN
    GRADXXMAX(K)=GMAX
    IGX(K)=I
    JGX(K)=J
 END IF
50 CONTINUE
RETURN
END
C-----------------------------------.
SUBROUTINE CALGRADYX(GRADYX,GRADYXMAX,AVGRADYX,IGY,JGY,CX,DX,DY
     & ,NX,NY)
DOUBLE PRECISION GRADYX(80,80,7),CX(0:80,0:80,7),DX(80),DY(80)
     & ,GMAX,GRADYXMAX(7),AVGRADYX(7),AX,AY
INTEGER NX,NY,I,J,K,JGY(7),IGY(7)
DO 50 K=1,7
  GRADYXMAX(K)=0.0D0
  AVGRADYX(K)=0.0D0
DO 50 I=1,NX
  AX=1.0D0
  IF(I.EQ.1.OR.I.EQ.NX)AX=0.5D0
DO 40 J=NY-1,1,-1
  AY=1.0D0
  IF(J.EQ.1)AY=0.5D0
 GRADYX(I,J,K)=2.0D0*(CX(I,J+1,K)-CX(I,J,K))/(DY(J)+DY(J+1))
  AVGRADYX(K)=AVGRADYX(K)+AX*AY*DX(I)*DY(J)*GRADYX(I,J,K)
 GMAX=ABS(GRADYX(I,J,K))
 IF(GMAX.GT.GRADYXMAX(K))THEN
    GRADYXMAX(K)=GMAX
    IGY(K)=I
    JGY(K)=J
 END IF
40 CONTINUE
 J=NY
 AY=0.5D0
 GRADYX(I,NY,K)=GRADYX(I,NY-1,K)
  AVGRADYX(K)=AVGRADYX(K)+AX*AY*DX(I)*DY(J)*GRADYX(I,J,K)
 GMAX=ABS(GRADYX(I,J,K))
 IF(GMAX.GT.GRADYXMAX(K))THEN
    GRADYXMAX(K)=GMAX
    IGY(K)=I
    JGY(K)=J
 END IF
50 CONTINUE
RETURN
END
C-----------------------------------.
C ******CALCULATING THE DEVIATION PARAMETERS
SUBROUTINE DEVIATION(CX,AVX,DX,DY,NX,NY,AD,STD,TAD,TSTD,
     & GRADYX,GRADXX,XGRAD,ADMAX,GRADYXMAX,GRADXXMAX,AVGRADYX,AVGRADXX
     & ,XGRADAV,XGRADMAX,CXMIN,CXMAX,IGX,JGX,IGY,JGY,IADMAX,JADMAX,
     & IXMAX,JXMAX,IXMIN,JXMIN,IGRADMAX,JGRADMAX)

DOUBLE PRECISION CX(0:80,0:80,7),AVX(7),DX(80),DY(80),TAD,TSTD
     & ,AD(7),STD(7),GRADYX(80,80,7),ADMAX(7),GRADXX(80,80,7)
     & ,XGRAD(80,80,7),GRADYXMAX(7),AVGRADYX(7),AX,AY,CXMAX(7)
     & ,GRADXXMAX(7),AVGRADXX(7),XGRADAV(7),XGRADMAX(7),CXMIN(7)
```

```
     & ,DDD0,DDD1,DDD2

INTEGER NX,NY,I,J,K,JGY(7),IGY(7),JGX(7),IGX(7),IADMAX(7),
     & JADMAX(7),IXMAX(7),JXMAX(7),IXMIN(7),JXMIN(7),IGRADMAX(7),
     & JGRADMAX(7)

TAD=0.0D0
TSTD=0.0D0
CALL CALGRADXX(GRADXX,GRADXXMAX,AVGRADXX,IGX,JGX,CX,DX,DY,NX,NY)
CALL CALGRADYX(GRADYX,GRADYXMAX,AVGRADYX,IGY,JGY,CX,DX,DY,NX,NY)

  DO 200 K=1,7

     AD(K)=0.0D0
     STD(K)=0.0D0
     XGRADAV(K)=0.0D0
     ADMAX(K)=0.0D0
     CXMAX(K)=0.0D0
     CXMIN(K)=1.5D0
     XGRADMAX(K)=0.0D0

     DO 90 I=1,NX
AX=1.0D0
IF(I.EQ.1.OR.I.EQ.NX)AX=0.5D0
DO 90 J=NY,1,-1
   AY=1.0D0
   IF(J.EQ.1.OR.J.EQ.NY)AY=0.5D0
   XGRAD(I,J,K)=DSQRT(GRADYX(I,J,K)""2+GRADXX(I,J,K)""2)
   XGRADAV(K)=XGRADAV(K)+XGRAD(I,J,K)*DX(I)*DY(J)*AX*AY
   DDD0=ABS(CX(I,J,K)-AVX(K))
   DDD1=ABS(CX(I,J,K)-AVX(K))*DX(I)*DY(J)*AX*AY
   DDD2=(CX(I,J,K)-AVX(K))""2*DX(I)*DY(J)*AX*AY
     AD(K)=AD(K)+DDD1
   STD(K)=STD(K)+DDD2

   IF(DDD0.GT.ADMAX(K))THEN
     ADMAX(K)=DDD0
     IADMAX(K)=I
     JADMAX(K)=J
   END IF
     IF(CX(I,J,K).GT.CXMAX(K))THEN
CXMAX(K)=CX(I,J,K)
IXMAX(K)=I
JXMAX(K)=J
     END IF
     IF(CX(I,J,K).LT.CXMIN(K))THEN
CXMIN(K)=CX(I,J,K)
IXMIN(K)=I
JXMIN(K)=J
     END IF

   IF(XGRAD(I,J,K).GT.XGRADMAX(K))THEN
     XGRADMAX(K)=XGRAD(I,J,K)
     IGRADMAX(K)=I
     JGRADMAX(K)=J
   END IF

90 CONTINUE

   AD(K)=AD(K)/(0.0525D0*0.105D0)
   TAD=TAD+AD(K)
   STD(K)=DSQRT(STD(K)/(0.0525D0*0.105D0))
   TSTD=TSTD+STD(K)
   XGRADAV(K)=XGRADAV(K)/(0.0525D0*0.105D0)
200   CONTINUE

  TAD=TAD/7.D0
  TSTD=TSTD/7.D0

RETURN
END
C-------------------------------.


C **THIS SUBROUTINE CALCULATES THE DIFFERENCE BETWEEN THE T AND X VALUES
C ** AT LAST  AND CURRENT OUTER ITERATIONS + SUBSTITUTE THE TK AND XK'X
C **WITH T1 AND X1 VALUES: XK & TK VALUES ARE THE LAST ITERATION VALUES

SUBROUTINE CALSUM(T1,X1,TK,XK,SUMT,SUMX,AMAXERT,AMAXERX,NX,NY,K)

DOUBLE PRECISION X1(0:80,0:80,7),T1(0:80,0:80,7),
```

```
     & XK(0:80,0:80,7),TK(0:80,0:80,7),AMAXERT,AMAXERX,SUMX,SUMT,ERT,ERX

INTEGER NX,NY,I,J,K,LOCXI,LOCXJ,LOCTI,LOCTJ

AMAXERT=0.0D0
AMAXERX=0.0D0
SUMX=0.0D0
SUMT=0.0D0
ERX=0.0D0
ERT=0.0D0

DO 10 I=1,NX
DO 10 J=1,NY
ERT=ABS(T1(I,J,K)-TK(I,J,K))
ERX=ABS(X1(I,J,K)-XK(I,J,K))
IF(ERT.GE.AMAXERT)THEN
LOCTI=I
LOCTJ=J
AMAXERT=ERT
END IF
IF(ERX.GE.AMAXERX)THEN
LOCXI=I
LOCXJ=J
AMAXERX=ERX
END IF
SUMX=SUMX+ERX
SUMT=SUMT+ERT
TK(I,J,K)=T1(I,J,K)
XK(I,J,K)=X1(I,J,K)
C ** BOUNDING THE T1'S
    IF(T1(I,J,K).GT.357.0D0)T1(I,J,K)=357.0D0
    IF(T1(I,J,K).LT.285.0D0)T1(I,J,K)=285.0D0
10 CONTINUE
RETURN
END

C-------------------------------.
C** UPDATING THE CONDITIONS OF THE DRYING AIR

SUBROUTINE XTAIRUPDATENEW2(XH,ROMV,TDIN,TWIN,VTIN,NX,NY,BY,BX
    & ,DX,DY,EPS,AMTIN,AMVIN,TH,HH,BQY,TIN,TM,BQX,FIIN,XEQ,FII
    & ,NFIFLAG,WIN,IFIFLAG)

DOUBLE PRECISION TDIN,TWIN,VTIN,FIIN,PATM,PVIN
    & ,PSV,CVIN,ROVIN,VT,TMS,VMS,DM,DQ,X0M,T0M,SAI,ROSV
    & ,SS,SQ,TQ,DV,SAM,SAM0,AMAIRIN,W,DQM,SQM,WIN,ROTIN,TMIN,TMVIN
    & ,MR

INTEGER NX,NY,I,J,K,nloop,NFIFLAG(80,7),IFIFLAG

DOUBLE PRECISION XH(0:80,0:80,7),ROMV(80,7),AMVIN(7),AMTIN(7)
    & ,BY(80,7,2),BX(80,7),TH(0:80,0:80,7),HH(80,80,3),BQY(80,7,2),
    & BQX(80,7),TIN(7),TM(80,7),DX(80),DY(80),EPS(80,80),XEQ(80,7)
    & ,FII(80,7)


PATM=101325.0D0
     PVIN=FIIN*PSV(TDIN)
     MR=18.01528D0/28.9645D0

C**************
     ROTIN=MR*PATM*(1.0D0+WIN)*28.9654D0/(8314.41D0*TDIN)
    &       /(MR+WIN)

     CVIN=WIN/(1.0D0+WIN)
     ROVIN=ROTIN*CVIN
     TMIN=ROTIN*VTIN
     TMVIN=ROVIN*VTIN
     AMAIRIN=TMIN-TMVIN

   DO 80,NLOOP=1,5
     TMS=0.0D0
     TQ=0.0D0

C** ASSIGNING ZERO VALUES TO NFIFLAG'S AT START OF EACH ITERATION
     DO 7,K=1,7
  DO 7,I=1,NX
    NFIFLAG(I,K)=0
 7  CONTINUE
C***** STARTING CALCULATIONS FOR A NEW BOARD
   DO 70,K=1,7
```

```
C  ASSIGNING THE INLET VALUES FOR K=1
      IF(K.EQ.1)THEN
     TWIN=TWIN
     TIN(K)=TDIN
     AMVIN(K)=TMVIN
     AMTIN(K)=TMIN
     VT=VTIN

   END IF

TMS=AMTIN(K)
VMS=AMVIN(K)
C  STARTING UPDATING FOR A NEW I
    DO 30 I=1,NX
DM=0.0D0
DQ=0.0D0
DQM=0.0D0

C  UPDATING FOR THE LEADING EDGE (I=1)
IF(I.EQ.1)THEN
  DO 10 J=1,NY
     X0M=XH(I,J,K)
     T0M=TH(I,J,K)

     SAM=DY(J)*BY(J,K,1)*SAI(X0M,T0M)*
    &  ROSV(T0M)*EPS(I,J)**2*(X0M-XEQ(I,K))

    IF(J.EQ.1.OR.J.EQ.NY)THEN
 DM=DM+0.5D0*SAM
 DQM=DQM+0.5D0*SAM*HH(I,J,1)

 DQ=DQ+0.5D0*BQY(J,K,1)*(T0M-TM(I,K))*DY(J)
    & +0.5D0*SAM*HH(I,J,1)

    ELSE
 DM=DM+SAM
 DQM=DQM+SAM*HH(I,J,1)

      DQ=DQ+BQY(J,K,1)*(T0M-TM(I,K))*DY(J)+SAM*HH(I,J,1)

        END IF
10   CONTINUE
END IF

C**RESET DM & DQ TO ZERO AFTER USING FOR I=1& REUSE THEM FOR 1;I
 IF(I.NE.1)THEN
DM=0.0D0
DQ=0.0D0
DQM=0.0D0
 END IF

C **** FOR J=NY ON HORIZONTAL WALL
X0M=XH(I,NY,K)
T0M=TH(I,NY,K)

SAM0=DX(I)*BX(I,K)*SAI(X0M,T0M)*ROSV(T0M)*EPS(I,NY)**2*
   & (X0M-XEQ(I,K))

SS=0.5D0*SAM0
SQ=0.5D0*SAM0*HH(I,NY,1)+0.5D0*BQX(I,K)*(T0M-TM(I,K))*DX(I)
SQM=0.5D0*SAM0*HH(I,NY,1)

    IF(I.NE.1)THEN
  DM=SS
  DQ=SQ
  DQM=SQM
END IF

C **** FOR I=N ON VERTICALL WALL AT THE BOARD'S BACK
   IF(I.EQ.NX)THEN
DO 20 J=1,NY
  X0M=XH(I,J,K)
  T0M=TH(I,J,K)

  SAM=DY(J)*BY(J,K,2)*SAI(X0M,T0M)
   & *ROSV(T0M)*EPS(I,J)**2*(X0M-XEQ(I,K))

      IF(J.EQ.1.OR.J.EQ.NY)THEN

   DM=DM+0.5D0*SAM
 DQM=DQM+0.5D0*SAM*HH(I,J,1)
```

```
    DQ=DQ+0.5D0*BQY(J,K,2)*(T0M-TM(I,K))*DY(J)
    & +0.5D0*SAM*HH(I,J,1)

  ELSE

    DM=DM+SAM
 DQM=DQM+SAM*HH(I,J,1)
  DQ=DQ+BQY(J,K,2)*(T0M-TM(I,K))*DY(J)+SAM*HH(I,J,1)

       END IF

 20      CONTINUE

    END IF

    TMS=TMS+DM
    VMS=VMS+DM
TQ=TQ+DQ
    DV=DM/ROSV(TM(I,K))
    VT=VT+DV
    ROMV(I,K)=VMS/VT
TM(I,K)=TIN(1)+TQ/(TMS*1008.0D0)
W=(TMS-AMAIRIN)/AMAIRIN
FII(I,K)=W*PATM/PSV(TM(I,K))/(MR+W)
C **** THIS IS FOR THE CASE FII.1
IF(FII(I,K).GT.1.0D0)THEN
   IFIFLAG=1
   NFIFLAG(I,K)=1
   TMS=TMS-DM
   VMS=VMS-DM
   VT=VT-DV
   ROMV(I,K)=VMS/VT
   W=(TMS-AMAIRIN)/AMAIRIN
   TQ=TQ-DQM
   TM(I,K)=TIN(1)+TQ/(tms*1008.0D0)
   FII(I,K)=W*PATM/PSV(TM(I,K))/(MR+W)
    IF(FII(I,K).GT.1.0D0)THEN
   FII(I,K)=1.0D0
   CALL CALXEQ(XEQ,TM,FII,NX)
END IF
END IF
C **** FOR THE BACK VERTICAL WALL
   IF(I.NE.NX)THEN
     IF(IFIFLAG.NE.1)THEN
 TMS=TMS+SS
 VMS=VMS+DV
 TQ=TQ+SQ
     ELSE
 TQ=TQ+SQ-SQM
     END IF
 END IF

   IF(K.LE.6.AND.I.EQ.NX)THEN
     AMVIN(K+1)=VMS
     AMTIN(K+1)=TMS
     TIN(K+1)=TM(I,K)
     TM(1,K+1)=TM(I,K)
   END IF

c*******going for next I'
30       CONTINUE

c*******going for next K'
70    CONTINUE
   CALL CALXEQ(XEQ,TM,FII,NX)
c*******going for next ITERATION LOOP'
80    CONTINUE

  RETURN
END
C-------------------------------------------------
SUBROUTINE CALXGRADXT(GXT,GXX,T,CX,NX,NY,K)
DOUBLE PRECISION GXT(80,80),GXX(80,80),T(0:80,0:80,7)
    & ,CX(0:80,0:80,7)
INTEGER NX,NY,I,J,K
DO 50 J=1,NY
DO 40 I=1,NX-1
  GXX(I,J)=CX(I+1,J,K)-CX(I,J,K)
  GXT(I,J)=T(I+1,J,K)-T(I,J,K)
40  CONTINUE
```

```
  GXX(NX,J)=GXX(NX-1,J)
  GXT(NX,J)=GXT(NX-1,J)
50  CONTINUE
RETURN
END
C-------------------------------.
SUBROUTINE CALYGRADXT(GYT,GYX,T,CX,NX,NY,K)
C IMPLICIT DOUBLE PRECISION (A-H,O-Z)
DOUBLE PRECISION GYT(80,80),GYX(80,80),T(0:80,0:80,7)
    & ,CX(0:80,0:80,7)
INTEGER NX,NY,I,J,K
DO 50 I=1,NX
DO 40 J=1,NY-1
  GYX(I,J)=CX(I,J+1,K)-CX(I,J,K)
  GYT(I,J)=T(I,J+1,K)-T(I,J,K)
40  CONTINUE
  GYX(I,NY)=GYX(I,NY-1)
  GYT(I,NY)=GYT(I,NY-1)
50  CONTINUE
RETURN
END

C-------------------------------.

C ** CALCULATING THE EQUILIBRIUM MOISTURE CONTENT OF AIR***
SUBROUTINE CALXEQ(XEQ,TM,FII,NX)

DOUBLE PRECISION XEQ(80,7),FII(80,7),TM(80,7)
    & ,AK1,AK2,W,AKK,TT

INTEGER NX,I,K
DO 50 K=1,7
DO 50 I=1,NX
TT=TM(I,K)
AK1=-45.69875133D0+0.321555416D0*TT-5.01228D-4*TT**2
AK2=-0.172194726D0+4.731747D-3*TT-5.55336D-6*TT**2
W=1416.501902D0-9.43022664D0*TT+0.0185328D0*TT**2
AKK=AK2*FII(I,K)
XEQ(I,K)=18.0D0/W*(AK1*AKK/(1.0D0+AK1*AKK)+AKK/(1.0D0-AKK))
50 CONTINUE
RETURN
END

C -------------------------------.
C *** CALCULATING THE INTERNAL ENERGY OF PHASES
C     V=1 VAPOUR    B=2 BOUND     F=3 FREE  S=4  SOLID
SUBROUTINE UHCAL(U,H1,DU,DH,T,K,NX,NY)

DOUBLE PRECISION A1,A2,A3,C1,C2,C3,C4,C5,D1,D2,D3,D4,D5,E1,E2,
    & E3,F1,F2,F3,F4,F5,G1,G2,G3,G4,P1,P2,P3,P4,P5,Q1,Q2,Q3,Q4,TP

DOUBLE PRECISION U(80,80,4),H1(80,80,3),DU(80,80,4),DH(80,80,3)
    & ,T(0:80,0:80,7)
INTEGER NX,NY,I,J,K

A1=-8.991948190716617D-01
A2=1.906495192066809D+03
A3=1.920416956358603D+06

C1=3.911292745066279D-05
C2=-4.803177704172579D-02
C3=2.206972449277908D+01
C4=-3.140814867379426D+02
C5=-7.995171343368989D+05

D1=4.041035127382818D-05
D2=-4.955357718019450D-02
D3=2.274399421234990D+01
D4=-4.476206478354741D+02
D5=-7.895564686971186D+05

E1=-1.236057724917015D+00
E2=2.563524677213299D+03
E3=1.891879255489751D+06

F1=3.966253729589242D-07
F2=-3.801268470618274D-04
F3=1.271772117537275D-01
F4=-1.659458529219993D+01
F5=4.766214787665288D+03
```

```
G1=5.335053488154614D-05
G2=-3.721735569210400D-02
G3=8.968188411027045D+00
G4=1.107373781180579D+03

P1=-2.375401980811967D-06
P2=3.414183570124922D-03
P3=-1.834527555173341D+00
P4=4.316642658134905D+02
P5=-3.320188572621348D+04

Q1=2.317937666947513D-05
Q2=-1.378062015666426D-02
Q3=2.813889900431855D+00
Q4=1.190469447107531D+03

DO 10 I=1,NX
DO 10 J=1,NY
TP=T(I,J,K)
U(I,J,3)=C1*TP**4+C2*TP**3+C3*TP**2+C4*TP+C5
U(I,J,1)=A1*TP**2+A2*TP+A3
U(I,J,4)=123010.0D0-212.05D0*TP+2.425D0*TP**2
H1(I,J,3)=D1*TP**4+D2*TP**3+D3*TP**2+D4*TP+D5
H1(I,J,1)=E1*TP**2+E2*TP+E3
H1(I,J,2)=H1(I,J,3)
DH(I,J,3)=F1*TP**4+F2*TP**3+F3*TP**2+F4*TP+F5
DH(I,J,1)=G1*TP**3+G2*TP**2+G3*TP+G4
DU(I,J,3)=P1*TP**4+P2*TP**3+P3*TP**2+P4*TP+P5
DU(I,J,1)=Q1*TP**3+Q2*TP**2+Q3*TP+Q4
DU(I,J,4)=1112.D0+4.85D0*(TP-273.15D0)
10 CONTINUE
RETURN
END
C-------------------------.
C ** CALCULATING THE DENSITY OF MOISTURE IN EACH PHASE *****
C** AND DRY WOOD HEAT CONDUCTIVITY+ CHARACTERISTICS OF BOUND WATER***
C      V=1 VAPOUR    B=2 BOUND     F=3  FREE

SUBROUTINE ROEPCAL(RO,EPS,EPSD,CX,T,K,NX,NY,ROS,AMBDA,XMAX
     & ,U,H,DU,DH)

DOUBLE PRECISION X0,CT,XF,XFSP,ROS,ROTW,ROBSF,RF,EPSD,UD,HD,
     &  DUD,DHD,XMAX,ROW,ROSV,SAI

DOUBLE PRECISION RO(80,80,4),EPS(80,80),CX(0:80,0:80,7),
     & T(0:80,0:80,7),AMBDA(80,80),U(80,80,4),H(80,80,3),DU(80,80,4)
     & ,DH(80,80,3)

INTEGER NX,NY,I,J,K,NP
EPSD=1-ROS/1500.0D0

  DO 10 I=1,NX
    DO 10 J=1,NY
RO(I,J,4)=ROS
X0=CX(I,J,K)
CT=T(I,J,K)
XF=XFSP(CT)
ROTW=CX(I,J,K)*ROS

IF(X0.GT.XF)THEN
RO(I,J,2)=XF*ROS
RO(I,J,3)=ROTW-RO(I,J,2)
ELSE
RO(I,J,3)=0.0
RO(I,J,2)=CX(I,J,K)*ROS
END IF

  EPS(I,J)=EPSD-RO(I,J,3)/ROW(CT)
RO(I,J,1)=ROSV(CT)*SAI(X0,CT)*EPS(I,J)

IF(X0.GT.XF)RO(I,J,3)=ROTW-RO(I,J,2)-RO(I,J,1)
  EPS(I,J)=EPSD-RO(I,J,3)/ROW(CT)
RO(I,J,1)=ROSV(CT)*SAI(X0,CT)*EPS(I,J)
IF(X0.GT.XF)RO(I,J,3)=ROTW-RO(I,J,2)-RO(I,J,1)

IF(X0.LE.XF)THEN
RO(I,J,3)=0.0D0
RO(I,J,2)=ROTW-RO(I,J,1)
END IF

ROBSF=XF*ROS
```

```
RF=RO(I,J,2)/ROBSF
UD=U(I,J,1)-U(I,J,3)
HD=H(I,J,1)-H(I,J,3)
U(I,J,2)=U(I,J,3)-0.4D0*UD*(1.0D0-RF+RF*RF/3.0D0)
H(I,J,2)=H(I,J,3)-0.4D0*HD*(1.0D0-RF+RF*RF/3.0D0)

DUD=DU(I,J,1)-DU(I,J,3)
DHD=DH(I,J,1)-DH(I,J,3)
DU(I,J,2)=DU(I,J,3)-0.4D0*DUD*(1.0D0-RF+RF*RF/3.0D0)
DH(I,J,2)=DH(I,J,3)-0.4D0*DHD*(1.0D0-RF+RF*RF/3.0D0)

 AMBDA(I,J)=0.0D0
DO 5 NP=1,3
AMBDA(I,J)=AMBDA(I,J)+RO(I,J,NP)
5 CONTINUE


AMBDA(I,J)=ROS/1000.0D0*(0.4D0+0.5D0*AMBDA(I,J)/ROS)+0.024D0


10 CONTINUE
XMAX=EPSD*1000.D0/ROS
 RETURN
END
C————————D————————————————————————
C ——— EVALUATING THE VT'S & VX'S COEFFICIENTS AT THE NODES ———-
C     V=1 VAPOUR    B=2 BOUND     F=3  FREE   S=4  SOLID

SUBROUTINE VTXCAL(VX,VT,RON,T,CX,NX,NY,K,SMIN,XMAX,ALFA,DMU,
   & SKL,EPS,ROS)

DOUBLE PRECISION CM0,CT1,XF1,XFSP,ROS,AS,DEX,SAI,
   &  XMAX,SMIN,ALFA,DMU,SKL,PI,EE,RELT,V,PSV,DD,DPSV,DTSAI
   & ,DXSAI,PL,PV,CLT,DBM,SBT,S,SSS,AKL,FX,RNUL

 DOUBLE PRECISION VX(80,80,3),VT(80,80,3),T(0:80,0:80,7)
   & ,CX(0:80,0:80,7),EPS(80,80),RON(80,80,4)

INTEGER NX,NY,I,J,K

PI=4.0D0*DATAN(1.0D0)
EE=DEXP(1.0D0)

  DO 10 I=1,NX
   DO 10 J=1,NY
CM0=CX(I,J,K)
CT1=T(I,J,K)
RELT=T(I,J,K)/273.15D0
XF1=XFSP(CT1)

V=-1.2146D-4*18.D0*ALFA/8314.41D0*EPS(I,J)*(CT1**0.75D0)
   & /101325.D0

AS=16.3737D0-2818.6D0/CT1-1.6908D0*DLOG10(CT1)
   & -5.7546D-3*CT1+4.007D-6*CT1**2

PSV=102142.621D0/760.0D0*10.0D0**AS

DD=2818.6D0/CT1**2-1.6908D0*DLOG10(EE)/CT1
   & -5.7546D-3+4.007D-6*CT1*2.0D0

DPSV=PSV*DLOG(10.0D0)*DD
VT(I,J,1)=V*(DTSAI(CM0,CT1)*PSV+DPSV*SAI(CM0,CT1))
VX(I,J,1)=V*DXSAI(CM0,CT1)*PSV
DEX=40.0D0*(RON(I,J,2)/ROS-XF1)-6500.0D0/CT1
PL=PV(CM0,CT1)/101325.0D0
CLT=CT1/298.15D0
DBM=DEXP(DEX)
SBT=-1.0D0*(187.D0+35.1D0*DLOG(CLT)-8.314D0*DLOG(PL))

VT(I,J,2)=-1000.D0/18.0D0*DMU*DBM*(SBT+8.314D0*CT1/PV(CM0,CT1)
   & *(DTSAI(CM0,CT1)*PSV+DPSV*SAI(CM0,CT1)))

VX(I,J,2)=-1000.D0/18.0D0*DMU*DBM*8.314D0*CT1/PV(CM0,CT1)
   & *DXSAI(CM0,CT1)*PSV

VT(I,J,3)=0.0D0

IF(CM0.LE.XF1)THEN
VX(I,J,3)=0.0D0
GO TO 8
```

```
END IF

S=(CM0-XF1)/(XMAX-XF1)
SSS=(S-SMIN)/(1.0D0-SMIN)*PI/2.0D0
AKL=1.0D0-DCOS(SSS)
FX=AKL/(RNUL(CT1)*S**0.61D0*(CM0-XF1))
 VX(I,J,3)=-6100.D0*SKL*FX

IF(S.LE.SMIN.AND.CM0.GE.XF1)THEN
 VX(I,J,3)=0.0D0
 END IF

8 CONTINUE

10 CONTINUE
RETURN
END
C ------------------------------------
C ** EVALUATING THE SATURATION PRESSURE OF WATER
DOUBLE PRECISION FUNCTION PSV(T)
DOUBLE PRECISION T

PSV=102142.621D0/760.0D0*10.0D0**(16.3737D0-2818.6D0/T
    & -1.6908D0*DLOG10(T)-5.7546D-3*T+4.007D-6*T**2)

RETURN
END
C ----------------------
SUBROUTINE GRIDY(YY,DY,RY,NY)

DOUBLE PRECISION YY(80),RY(80),DY(80)
DOUBLE PRECISION SR1,YS1,S,ST
INTEGER NY,I,J,NS1
YY(1)=0.0D0
NS1=40
SR1=0.92909D0
YS1=0.0525D0

S=1.0D0
ST=0.5D0
  DO 10 I=1,NS1-2
    S=S*SR1
    ST=ST+S
10   CONTINUE
S=S*SR1
ST=ST+0.5D0*S
DY(1)=YS1/ST

 DO 30 I=2,NS1
   DY(I)=DY(I-1)*SR1
30  CONTINUE
NY=NS1
  DO 120 I=1,NY
    IF(I.EQ.1)GO TO 114
    YY(I)=YY(I-1)+0.5D0*(DY(I)+DY(I-1))
114      IF(I.EQ.NY)GO TO 120
    RY(I)=DY(I)/(DY(I)+DY(I+1))
120   CONTINUE
RETURN
END

C--- GRID GENERATION FOR BOARDS NO. 1 ----------

SUBROUTINE GRIDX1(XX,DX,RX,NX)

DOUBLE PRECISION XX(80),RX(80),DX(80)
DOUBLE PRECISION XS1,XS2,XS3,XS4,XS5,SR1,SR2,SR3,SR4,SR5,S,ST
INTEGER NX,I,NS1,NS2,NS3,NS4,NS5,NT
XX(1)=0.0D0
NS1=17
SR1=1.05D0
XS1=0.010D0
S=1.0D0
ST=0.5D0
DO 10 I=1,NS1-1
S=S*SR1
ST=ST+S
10 CONTINUE
DX(1)=XS1/ST
DO 30 I=2,NS1
DX(I)=DX(I-1)*SR1
```

```
30 CONTINUE
NS2=17
XS2=0.020D0
SR2=1.0D0/1.05D0
S=1.0D0
ST=1.0D0
DO 50 I=1,NS2-1
S=S*SR2
ST=ST+S
50 CONTINUE
DX(NS1+1)=(XS2-XS1)/ST
DO 60 I=2,NS2
DX(I+NS1)=DX(I+NS1-1)*SR2
60 CONTINUE
NS3=26
XS3=0.065D0
SR3=1.1D0
S=1.0D0
ST=1.0D0
DO 70 I=1,NS3-1
S=S*SR3
ST=ST+S
70 CONTINUE
DX(NS2+NS1+1)=(XS3-XS2)/ST
DO 80 I=2,NS3
DX(I+NS1+NS2)=DX(I+NS1+NS2-1)*SR3
80 CONTINUE
NS4=6
XS4=0.090D0
SR4=1.0D0/1.1D0
S=1.0D0
ST=1.0D0
DO 85 I=1,NS4-1
S=S*SR4
ST=ST+S
85 CONTINUE
NT=NS1+NS2+NS3
DX(NT+1)=(XS4-XS3)/ST
DO 90 I=2,NS4
DX(I+NT)=DX(I+NT-1)*SR4
90 CONTINUE
NS5=10
XS5=0.1035D0
SR5=1.0D0/1.2D0
S=1.0D0
ST=1.0D0
NT=NS1+NS2+NS3+NS4
DO 100 I=1,NS5-2
S=S*SR5
ST=ST+S
100 CONTINUE
S=S*SR5
ST=ST+0.5D0*S

DX(NT+1)=(XS5-XS4)/ST
DO 110 I=2,NS5
DX(I+NT)=DX(I+NT-1)*SR5
110 CONTINUE
NX=NT+NS5

C THIS IS A SECTION TO MAKE EQUAL DX'S
c NX=76
DO 111 I=1,NX
DX(I)=0.1035D0/(NX-1)
111 CONTINUE

DO 120 I=1,NX
IF(I.EQ.1)GO TO 114
XX(I)=XX(I-1)+0.5D0*(DX(I)+DX(I-1))
114 IF(I.EQ.NX)GO TO 120
RX(I)=DX(I)/(DX(I)+DX(I+1))
120 CONTINUE

RETURN
END
C--- GRID GENERATION FOR BOARDS NO. 2-7 ----------
SUBROUTINE GRIDX2(XX,DX,RX,NX)

DOUBLE PRECISION XX(80),RX(80),DX(80)
DOUBLE PRECISION XS1,XS2,XS3,XS4,SR1,SR2,SR3,SR4,S,ST
INTEGER NX,I,NS1,NS2,NS3,NS4,NT
```

```
XX(1)=0.0D0
NS1=19
SR1=1.1D0
XS1=0.025D0
S=1.0D0
ST=0.5D0
DO 10 I=1,NS1-1
S=S*SR1
ST=ST+S
10 CONTINUE
DX(1)=XS1/ST
DO 30 I=2,NS1
DX(I)=DX(I-1)*SR1
30 CONTINUE
NS2=7
XS2=0.060D0
SR2=1.2D0
S=1.0D0
ST=1.0D0
DO 50 I=1,NS2-1
S=S*SR2
ST=ST+S
50 CONTINUE
DX(NS1+1)=(XS2-XS1)/ST
DO 60 I=2,NS2
DX(I+NS1)=DX(I+NS1-1)*SR2
60 CONTINUE
NS3=7
XS3=0.095D0
SR3=1.0D0/1.2D0
S=1.0D0
ST=1.0D0
DO 70 I=1,NS3-1
S=S*SR3
ST=ST+S
70 CONTINUE
DX(NS2+NS1+1)=(XS3-XS2)/ST
DO 80 I=2,NS3
DX(I+NS1+NS2)=DX(I+NS1+NS2-1)*SR3
80 CONTINUE
NS4=7
XS4=0.1035D0
SR4=0.84D0
S=1.0D0
ST=1.0D0
NT=NS1+NS2+NS3
DO 90 I=1,NS4-2
S=S*SR4
ST=ST+S
90 CONTINUE
S=S*SR4
ST=ST+0.5D0*S

DX(NT+1)=(XS4-XS3)/ST
DO 100 I=2,NS4
DX(I+NT)=DX(I+NT-1)*SR4
100 CONTINUE
NX=NT+NS4

C THIS IS A SECTION TO MAKE EQUAL DX'S
NX=76
DO 111 I=1,NX
DX(I)=0.1035D0/(NX-1)
111 CONTINUE

DO 110 I=1,NX
IF(I.EQ.1)GO TO 104
XX(I)=XX(I-1)+0.5D0*(DX(I)+DX(I-1))
104 IF(I.EQ.NX)GO TO 110
RX(I)=DX(I)/(DX(I)+DX(I+1))
110 CONTINUE

RETURN
END
C------------------------EVALUATING PSAI FUNCTION
DOUBLE PRECISION FUNCTION SAI(CX,T)
DOUBLE PRECISION CX,T,AS1,AS2
AS1=17.884D0-0.1423D0*T+23.63D-5*T**2
AS2=1.0327D0-67.4D-5*T
SAI=DEXP(AS1*AS2**(92.0D0*CX))
RETURN
```

```
END
C----------EVALUATING DERIVATIVE (DSAI/DX) FUNCTION
C ** EVALUATING DIFFERENTIAL OF PSI TO MOISTURE CONTENT
DOUBLE PRECISION FUNCTION DXSAI(CX,T)
DOUBLE PRECISION CX,T,AS1,AS2,SAI,FS,F1

AS1=17.884D0-0.1423D0*T+23.63D-5*T**2
AS2=1.0327D0-67.4D-5*T
SAI=DEXP(AS1*AS2**(92.0D0*CX))
FS=AS1*AS2**(92.0D0*CX)
F1=DLOG(AS2)
DXSAI=SAI*FS*92.0D0*F1
10 RETURN
END
C----------EVALUATING DERIVATIVE (DSAI/DT) FUNCTION
C ** EVALUATING DIFFERENTIAL OF PSI TO TEMPERATURE
DOUBLE PRECISION FUNCTION DTSAI(CX,CT)
DOUBLE PRECISION CX,CT,AS1,AS2,SAI,DA1,DA2,F3,F4

AS1=17.884D0-0.1423D0*CT+23.63D-5*CT**2
AS2=1.0327D0-67.4D-5*CT
 SAI=DEXP(AS1*AS2**(92.0D0*CX))
DA1=-0.1423D0+23.63D-5*CT*2.D0
DA2=-67.4D-5
F3=AS2**(92.0D0*CX)
F4=AS2**(92.0D0*CX-1.0D0)
DTSAI=SAI*(DA1*F3+AS1*92.0D0*CX*DA2*F4)
10 RETURN
END
C ----------
C ** EVALUATING THE FIBER SATURATION POINT
DOUBLE PRECISION FUNCTION XFSP(CT)
DOUBLE PRECISION CT

XFSP=0.57315D0-0.001D0*CT
RETURN
END
C ----------
DOUBLE PRECISION FUNCTION PV(CX,T)
DOUBLE PRECISION CX,T,PSV,SAI
PV=PSV(T)*SAI(CX,T)
RETURN
END
C ----------
C ** EVALUATING THE DENSITY OF SATURATED WATER VAPOR
DOUBLE PRECISION FUNCTION ROSV(T)
DOUBLE PRECISION A1,A2,A3,A4,A5,T

A1=4.432837625451488D-09
A2=-4.915580026625070D-06
A3=2.064266950940671D-03
A4=-3.886732036460719D-01
A5=2.765818768321988D+01
ROSV=A1*T**4+A2*T**3+A3*T**2+A4*T+A5
RETURN
END
C -- FUNCTION FOR EVAL. DYNAMIC LIQUID WATER VISCOSITY  ROL/MUL(T)
C ** EVALUATING THE VISCOSITY OF LIQUID WATER
DOUBLE PRECISION FUNCTION RNUL(T)
DOUBLE PRECISION A1,A2,A3,A4,A5,T

A1=2.345596395094833D-14
A2=-3.234702454809699D-11
A3=1.678630597315793D-08
A4=-3.890361741373284D-06
A5=3.405747213883450D-04
RNUL=A1*T**4+A2*T**3+A3*T**2+A4*T+A5
RETURN
END
C ------FUNCTION FOR EVAL. DENSITY OF WATER
C ** EVALUATING THE DENSITY OF LIQUID WATER
DOUBLE PRECISION FUNCTION ROW(TT)
DOUBLE PRECISION A1,A2,A3,TT

A1=-3.355930317044745D-03
A2=1.729139535861038D0
A3=7.796945077283663D+02
ROW=A1*TT**2+A2*TT+A3
RETURN
END
C ------SUBROUTINE FOR CALCULATING THE SURFACE COEFFICIENTS
```

```
C For Run 10 of Li, Re=8800, g=1.5 mm
C ** BQ'S=HEAT TRANSFER, B'S=MASS TRANSFER,
C **  X(AT END)=HORIZONTAL SURFACE,  Y(AT END)=VERTICAL SURFACE
C**FOR VERTICAL WALLS:1=LEADING , 2=TRAILING EDGE SURFACE
C*BQY(I,3,1)=HEAT TRANSFER COEFFICIENT ON LEADING SURFACE OF 3ND BOARD

 SUBROUTINE BQXYCAL(BX,BY,BQX,BQY,K,NX,NY,XX,YY)

DOUBLE PRECISION BX(80,7),BQX(80,7),BY(80,7,2),BQY(80,7,2),
   & XX(80),yy(80)

DOUBLE PRECISION X,N
INTEGER NX,NY,I,J,K

C ************************ FOR 1ST BOARD **
IF(K.EQ.1)THEN
 DO 10 I=1,NX
  X=XX(I)

C PART A
    IF(X.LE.0.001131)THEN

  BQX(I,K)=407.1659549788167D0*DEXP(-21024.46684476504D0*x)+
   &         31.93038218791909D0*DEXP(-
   &        190.8939384430411D0*x)

  ELSE

C PART B
    x=DSQRT(x)

    BQX(I,K)=(-40.60055557348986D0+x*(2509.893603562523D0+
   &      x*(-45233.75832392177D0+x*(273474.4522222359D0+
   &    x*(-224405.9111035019D0+x*(-93968.84830620003D0)))))/
   &   (1.0+x*(-46.42031997130932D0+x*(888.2634409851075D0+
   &    x*(-8498.740055879648D0+x*(37096.73029862930D0+
   &   x*(-39029.17241457500D0))))))


  END IF
 END IF

C ** FOR 2ND BOARD
IF(K.EQ.2)THEN

      x=DSQRT(x)

     BQX(I,K)=174.2807102712536D0+x*(-11471.56791646031D0+
   &   x*(427917.5120607024D0+x*(-8941796.863056447D0+
   &   x*(115424760.2449346D0+x*(-964994935.9659027D0+
   &   x*(5316271194.309318D0+x*(-19150314217.03432D0+
   &   x*(43370204089.22347D0+x*(-56001533328.48792D0+
   &   x*31428233192.12275D0)))))))))

  END IF

C ** 3RD BOARD
IF(K.EQ.3)THEN

     x=DSQRT(x)

     BQX(I,K)=118.4032087166884D0+x*(-8073.845057563445D0+
   &   x*(311020.4559430483D0+x*(-6671293.653168771D0+
   &   x*(88027539.62410394D0+x*(-749434781.2624494D0+
   &   x*(4191211371.746140D0+x*(-15287141605.55975D0+
   &   x*(34984067586.48907D0+x*(-45571336480.68352D0+
   &   x*25766029369.19578D0)))))))))

  END IF

C ** 4TH BOARD
IF(K.EQ.4)THEN

C PART A
    IF(X.LT.0.098365215D0)THEN
      x=1.0D0/DLOG(x)

     BQX(I,K)=5054.773499014141D0+x*(177752.2993900421D0+
   1  x*(2787860.724542999D0+x*(25532275.57650707D0+
   1  x*(151139808.8375395D0+x*(604131239.6530711D0+
   1  x*(1651320343.954866D0+x*(3048046160.480916D0+
```

```
     1  x*(3636571573.933142D0+x*(2532827359.046554D0+
     1  x*782153615.7196340D0)))))))))

   ELSE

C PART B
       BQX(I,K)=23.10952507452315D0+5.941267193983624D0*(DATAN((x-
     1  0.1034198926040754D0)/6.566736935923352D-
     1  05)+1.570796326794896619 2D0)/
     1  3.141592653589793238 4D0

   END IF
  IF(X.EQ.0.0D0)BQX(I,K)=102.46D0
END IF
C
C ** 5TH BOARD
IF(K.EQ.5)THEN

C PART A
    IF(X.LT.0.095693486D0)THEN
       x=1.0D0/DLOG(x)
       BQX(I,K)=4985.466572261113D0+x*(176869.6390117575D0+
     1  x*(2799463.437750935D0+x*(25886303.44409218D0+
     1  x*(154786201.5617931D0+x*(625226992.1012339D0+
     1  x*(1727654079.107009D0+x*(3224907363.803606D0+
     1  x*(3892183926.879361D0+x*(2743028550.564295D0+
     1  x*857313257.9576165D0)))))))))

   ELSE
C PART B
       BQX(I,K)=22.53231800096773D0+12.38607048447966D0*(DATAN((x-
     1  0.1034442648309563D0)/3.578110566795277D-
     1  05)+1.570796326794896619 2D0)/
     1  3.141592653589793238 4D0

   END IF
  IF(X.EQ.0.0D0)BQX(I,K)=102.46D0
END IF

C **6TH BOARD
IF(K.EQ.6)THEN

C PART A
    IF(X.LT.0.089588916D0)THEN
       x=1.0D0/DLOG(x)
       BQX(I,K)=4672.918331456752D0+x*(163550.2220439411D0+
     1  x*(2544478.214232123D0+x*(23014960.25183302D0+
     1  x*(133787642.2855464D0+x*(521250449.3777585D0+
     1  x*(1375159115.619343D0+x*(2417782935.635727D0+
     1  x*(2698144702.783632D0+x*(1712594195.263961D0+
     1  x*463347013.2078118D0)))))))))

   ELSE

C PART B
       BQX(I,K)=22.36959481057400D0+15.43823221618957D0*(DATAN((x-
     1  0.1034540460523745D0)/3.147319372719047D-
     1  05)+1.570796326794896619 2D0)/
     1  3.141592653589793238 4D0

   END IF
  IF(X.EQ.0.0D0)BQX(I,K)=104.46D0
END IF

C ** 7TH BOARD
IF(K.EQ.7)THEN
C PART A
    IF(X.LT.0.046845312D0)THEN
       BQX(I,K)=22.34266750091485D0+36.32222888065240D0*(DATAN((x-
     1  0.0002041963816922589D0)/(-
     1  0.0001833134646019605D0))+1.570796326794896619 2D0)/
     1  3.141592653589793238 4D0

   ELSE
C PART B
       SS=(x-0.1457452261719253D0)/0.01572179786938619D0
       BQX(I,K)=22.40770348742958D0+82433.52411079670D0*DEXP(-
     1  DEXP(-SS)-SS+1.0D0)

   END IF
  IF(X.EQ.0.0D0)BQX(I,K)=102.46D0
```

```
END IF

BX(I,K)=8.647342479D-4*BQX(I,K)

10 CONTINUE

DO 20 J=1,NY
  X=YY(J)
IF(K.EQ.1)THEN

      BQY(J,K,1)=(6.261404555418986D0+x*(103.6888025337674D0+
     & x*(-3824.274150279517D0)))/
     & (1.0+x*(63.81817415882764D0+x*(-2258.594958432667D0+
     & x*13463.19268992207D0)))

  BQY(J,K,1)=BQY(J,K,1)*BQY(J,K,1)

ELSE

  BQY(J,K,1)=0.0D0
  BQY(J,K,2)=0.0D0
END IF


IF(K.EQ.7)THEN

      x=DSQRT(x)

      BQY(J,K,2)=(10.65602451129187D0+x*(-233.4898717610709D0+
     & x*(2139.692287625347D0+x*(-8858.828851081354D0+
     & x*13451.44881053568D0))))/
     & (1.0+x*(-19.62189371118493D0+x*(154.3742227517323D0+
     & x*(-554.9441910405214D0+x*749.9127281683968D0))))


END IF
  BY(J,K,1)=8.647342479D-4*BQY(J,K,1)
BY(J,K,2)=8.647342479D-4*BQY(J,K,2)
20 CONTINUE
RETURN
END

C-------------------------------------------------------------
C calculating the enthalpies at the edge of control volumes
SUBROUTINE HXYCAL(HX,HY,H1,DHK,T1R,T,RX,RY,NX,NY,K)

DOUBLE PRECISION HX(80,80,3),HY(80,80,3),H1(80,80,3),DHK(80,80,3)
     & ,T1R(0:80,0:80,7),T(0:80,0:80,7),RX(80),RY(80)

INTEGER NX,NY,I,J,K,np
    DO 50 I=1,NX-1
      DO 50 J=1,NY-1
        DO 40 NP=1,3

HX(I,J,NP)=1.0D0/(RX(I)/(H1(I,J,NP)+DHK(I,J,NP)*
     & (T1R(I,J,K)-T(I,J,K)))+(1.0D0-RX(I))/(H1(I+1,J,NP)+
     & DHK(I+1,J,NP)*(T1R(I+1,J,K)-T(I+1,J,K))))

HY(I,J,NP)=1.0D0/(RY(J)/(H1(I,J,NP)+DHK(I,J,NP)*
     & (T1R(I,J,K)-T(I,J,K)))+(1.0D0-RY(J))/(H1(I,J+1,NP)+
     & DHK(I,J+1,NP)*(T1R(I,J+1,K)-T(I,J+1,K))))

40      CONTINUE
50      CONTINUE

I=NX

     DO 60 J=1,NY-1
     DO 55 NP=1,3

HY(I,J,NP)=1.0D0/(RY(J)/(H1(I,J,NP)+DHK(I,J,NP)*
     & (T1R(I,J,K)-T(I,J,K)))+(1.0D0-RY(J))/(H1(I,J+1,NP)+
     & DHK(I,J+1,NP)*(T1R(I,J+1,K)-T(I,J+1,K))))

55    CONTINUE
60      CONTINUE

J=NY

     DO 80 I=1,NX-1
     DO 70 NP=1,3
```

```
HX(I,J,NP)=1.0D0/(RX(I)/(H1(I,J,NP)+DHK(I,J,NP)*
     & (T1R(I,J,K)-T(I,J,K)))+(1.0D0-RX(I))/(H1(I+1,J,NP)+
     & DHK(I+1,J,NP)*(T1R(I+1,J,K)-T(I+1,J,K))))

70      CONTINUE
80      CONTINUE

RETURN
END
C-------------------------------------.
SUBROUTINE CXVCAL(CXV,CX,X1R,NX,NY,K)

DOUBLE PRECISION CXV(0:80,0:80,7),CX(0:80,0:80,7)
     & ,X1R(0:80,0:80,7)
INTEGER NX,NY,I,J,K

DO 50 I=1,NX
DO 50 J=1,NY
CXV(I,J,K)=(X1R(I,J,K)+CX(I,J,K))/2.0D0
50 CONTINUE
RETURN
END
C-------------------------------------.
SUBROUTINE TVCAL(TV,T,T1R,NX,NY,K)

DOUBLE PRECISION TV(0:80,0:80,7),T(0:80,0:80,7)
     & ,T1R(0:80,0:80,7)
INTEGER NX,NY,I,J,K

DO 50 I=1,NX
DO 50 J=1,NY
TV(I,J,K)=(T1R(I,J,K)+T(I,J,K))/2.0D0
50 CONTINUE
RETURN
END
C-------------------------------------.
SUBROUTINE CALHVXGX(HXVXGX,HYVXGX,HXVXX,HYVXY,X1,DX,DY,NX,NY
     & ,DT,K)

DOUBLE PRECISION HYVXGX(80,80),HXVXGX(80,80),HYVXY(80,80)
     & ,HXVXX(80,80),DX(80),DY(80),X1(0:80,0:80,7),DT

INTEGER NX,NY,K,I,J
     DO 50 I=1,NX-1
       DO 50 J=1,NY-1
HXVXGX(I,J)=HXVXX(I,J)*(X1(I+1,J,K)-X1(I,J,K))*DY(J)*DT
HYVXGX(I,J)=HYVXY(I,J)*(X1(I,J+1,K)-X1(I,J,K))*DX(I)*DT
50      CONTINUE

      I=NX
       DO 60 J=1,NY-1
HYVXGX(I,J)=HYVXY(I,J)*(X1(I,J+1,K)-X1(I,J,K))*DX(I)*DT
60      CONTINUE

      J=NY
     DO 70 I=1,NX-1
HXVXGX(I,J)=HXVXX(I,J)*(X1(I+1,J,K)-X1(I,J,K))*DY(J)*DT
70      CONTINUE

RETURN
END
C-------------------------------------.
C CALCULATING THE A,B,C AND D FOR SOR METHOD
SUBROUTINE CALABCD(VIRCONDX,VIRCONDY,AA,BB,CC,DD,NX,NY)

DOUBLE PRECISION VIRCONDX(80,80),VIRCONDY(80,80),AA(80,80)
     & ,BB(80,80),CC(80,80),DD(80,80)
INTEGER NX,NY,I,J

C POINT NO.9
     DO 10 I=2,NX-1
       DO 10 J=2,NY-1
  AA(I,J)=VIRCONDX(I,J)
  BB(I,J)=VIRCONDX(I-1,J)
  CC(I,J)=VIRCONDY(I,J)
  DD(I,J)=VIRCONDY(I,J-1)
10      CONTINUE

C POINT NO.3
     I=1
```

```
      DO 20 J=2,NY-1
  AA(I,J)=2.D0*VIRCONDX(I,J)
  BB(I,J)=0.D0
  CC(I,J)=VIRCONDY(I,J)
  DD(I,J)=VIRCONDY(I,J-1)
20      CONTINUE

C POINT NO.4
      I=NX
      DO 30 J=2,NY-1
  AA(I,J)=0.D0
  BB(I,J)=2.D0*VIRCONDX(I-1,J)
  CC(I,J)=VIRCONDY(I,J)
  DD(I,J)=VIRCONDY(I,J-1)
30      CONTINUE

C POINT NO.8
      J=1
     DO 40 I=2,NX-1
  AA(I,J)=VIRCONDX(I,J)
  BB(I,J)=VIRCONDX(I-1,J)
  CC(I,J)=2.D0*VIRCONDY(I,J)
  DD(I,J)=0.D0
40      CONTINUE

C POINT NO.7
      J=NY
     DO 70 I=2,NX-1
  AA(I,J)=VIRCONDX(I,J)
  BB(I,J)=VIRCONDX(I-1,J)
  CC(I,J)=0.D0
  DD(I,J)=2.D0*VIRCONDY(I,J-1)
70      CONTINUE

C POINT NO.1
      J=1
      I=1
  AA(I,J)=2.D0*VIRCONDX(I,J)
  BB(I,J)=0.D0
  CC(I,J)=2.D0*VIRCONDY(I,J)
  DD(I,J)=0.D0

C POINT NO.2
      J=1
      I=NX
  AA(I,J)=0.D0
  BB(I,J)=2.D0*VIRCONDX(I-1,J)
  CC(I,J)=2.D0*VIRCONDY(I,J)
  DD(I,J)=0.D0

C POINT NO.5
      J=NY
      I=1
  AA(I,J)=2.D0*VIRCONDX(I,J)
  BB(I,J)=0.D0
  CC(I,J)=0.D0
  DD(I,J)=2.D0*VIRCONDY(I,J-1)

C POINT NO.6
      J=NY
      I=NX
  AA(I,J)=0.D0
  BB(I,J)=2.D0*VIRCONDX(I-1,J)
  CC(I,J)=0.D0
  DD(I,J)=2.D0*VIRCONDY(I,J-1)
RETURN
END
C-------------------------------------
C ** EVALUATING THE E AND F COEFFICIENTS OF THE SOR METHOD
SUBROUTINE CALEFNEW(VIRCONDX,VIRCONDY,EE,FF,CT,T1,X1,CXV,RODU,
     & EPS,BY,BX,XEQ,TM,BQY,BQX,DHK,DX,DY,NX,NY,K,DT,H1,HXVXGX,HYVXGX
     & ,NFIFLAG)

DOUBLE PRECISION VIRCONDX(80,80),VIRCONDY(80,80),EE(80,80),
     & FF(80,80),SAI,ROSV,T1(0:80,0:80,7),X1(0:80,0:80,7),
     & RODU(80,80),EPS(80,80),BY(80,7,2),BX(80,7),XEQ(80,7),TM(80,7)
     & ,BQY(80,7,2),BQX(80,7),DHK(80,80,3),DX(80),DY(80),DT,SAM
     & ,CT(0:80,0:80,7),H1(80,80,3),HXVXGX(80,80),HYVXGX(80,80)
     & ,CXV(0:80,0:80,7)

INTEGER NX,NY,I,J,K,NFIFLAG(80,7)
```

```
      DO 10 I=2,NX-1
       DO 10 J=2,NY-1
EE(I,J)=RODU(I,J)-VIRCONDX(I,J)-VIRCONDX(I-1,J)
     & -VIRCONDY(I,J-1)-VIRCONDY(I,J)

       FF(I,J)=RODU(I,J)*CT(I,J,K)-HXVXGX(I,J)+HXVXGX(I-1,J)
     &   -HYVXGX(I,J)+HYVXGX(I,J-1)
10     CONTINUE

C POINT NO.3
       I=1
       DO 20 J=2,NY-1
       SAM=DY(J)*DT*BY(J,K,1)*EPS(I,J)**2*SAI(X1(I,J,K),T1(I,J,K))
     &   *ROSV(T1(I,J,K))*(CXV(I,J,K)-XEQ(I,K))

       IF(NFIFLAG(I,K).EQ.1)SAM=0.0D0

      EE(I,J)=RODU(I,J)-2.D0*VIRCONDX(I,J)+2.D0*SAM*DHK(I,J,1)
     & -VIRCONDY(I,J-1)-VIRCONDY(I,J)+2.D0*DY(J)*DT*BQY(J,K,1)

       FF(I,J)=RODU(I,J)*CT(I,J,K)-2.D0*HXVXGX(I,J)
     &   -HYVXGX(I,J)+HYVXGX(I,J-1)-2.D0*SAM*(H1(I,J,1)-DHK(I,J,1)*
     &   CT(I,J,K))+2.D0*DY(J)*DT*BQY(J,K,1)*TM(I,K)
20     CONTINUE

C POINT NO.4
       I=NX
       DO 30 J=2,NY-1
       SAM=DY(J)*DT*BY(J,K,2)*EPS(I,J)**2*SAI(X1(I,J,K),T1(I,J,K))
     &   *ROSV(T1(I,J,K))*(CXV(I,J,K)-XEQ(I,K))

       IF(NFIFLAG(I,K).EQ.1)SAM=0.0D0

      EE(I,J)=RODU(I,J)-2.D0*VIRCONDX(I-1,J)+2.D0*SAM*DHK(I,J,1)
     & -VIRCONDY(I,J-1)-VIRCONDY(I,J)+2.D0*DY(J)*DT*BQY(J,K,2)

       FF(I,J)=RODU(I,J)*CT(I,J,K)+2.D0*HXVXGX(I-1,J)
     &   -HYVXGX(I,J)+HYVXGX(I,J-1)-2.D0*SAM*(H1(I,J,1)-DHK(I,J,1)*
     &   CT(I,J,K))+2.D0*DY(J)*DT*BQY(J,K,2)*TM(I,K)
30     CONTINUE

C POINT NO.8
       J=1
      DO 40 I=2,NX-1
EE(I,J)=RODU(I,J)-VIRCONDX(I,J)-VIRCONDX(I-1,J)
     & -2.D0*VIRCONDY(I,J)

       FF(I,J)=RODU(I,J)*CT(I,J,K)-HXVXGX(I,J)+HXVXGX(I-1,J)
     &   -2.D0*HYVXGX(I,J)
40     CONTINUE

C POINT NO.7
       J=NY
      DO 70 I=2,NX-1
SAM=DX(I)*DT*BX(I,K)*EPS(I,J)**2*SAI(X1(I,J,K),T1(I,J,K))
     &   *ROSV(T1(I,J,K))*(CXV(I,J,K)-XEQ(I,K))

       IF(NFIFLAG(I,K).EQ.1)SAM=0.0D0

EE(I,J)=RODU(I,J)-VIRCONDX(I,J)-VIRCONDX(I-1,J)-2.D0
     & *VIRCONDY(I,J-1)+2.D0*SAM*DHK(I,J,1)+2.D0*DX(I)*DT*BQX(I,K)

       FF(I,J)=RODU(I,J)*CT(I,J,K)-HXVXGX(I,J)+HXVXGX(I-1,J)
     &   +2.D0*HYVXGX(I,J-1)-2.D0*SAM*(H1(I,J,1)-DHK(I,J,1)*CT(I,J,K))
     &       +2.D0*DX(I)*DT*BQX(I,K)*TM(I,K)
70     CONTINUE

C POINT NO.1
       J=1
       I=1
       SAM=DY(J)*DT*BY(J,K,1)*EPS(I,J)**2*SAI(X1(I,J,K),T1(I,J,K))
     &   *ROSV(T1(I,J,K))*(CXV(I,J,K)-XEQ(I,K))

       IF(NFIFLAG(I,K).EQ.1)SAM=0.0D0

      EE(I,J)=RODU(I,J)-2.D0*VIRCONDX(I,J)+2.D0*SAM*DHK(I,J,1)
     & -2.D0*VIRCONDY(I,J)+2.D0*DY(J)*DT*BQY(J,K,1)

       FF(I,J)=RODU(I,J)*CT(I,J,K)-2.D0*HXVXGX(I,J)
     &   -2.D0*HYVXGX(I,J)-2.D0*SAM*(H1(I,J,1)-DHK(I,J,1)*
     &   CT(I,J,K))+2.D0*DY(J)*DT*BQY(J,K,1)*TM(I,K)
```

```
C POINT NO.2
     J=1
     I=NX
SAM=DY(J)*DT*BY(J,K,2)*EPS(I,J)**2*SAI(X1(I,J,K),T1(I,J,K))
    &    *ROSV(T1(I,J,K))*(CXV(I,J,K)-XEQ(I,K))

      IF(NFIFLAG(I,K).EQ.1)SAM=0.0D0

    EE(I,J)=RODU(I,J)-2.D0*VIRCONDX(I-1,J)+2.D0*SAM*DHK(I,J,1)
    & -2.D0*VIRCONDY(I,J)+2.D0*DY(J)*DT*BQY(J,K,2)

      FF(I,J)=RODU(I,J)*CT(I,J,K)+2.D0*HXVXGX(I-1,J)
    &    -2.D0*HYVXGX(I,J)-2.D0*SAM*(H1(I,J,1)-DHK(I,J,1)*
    &    CT(I,J,K))+2.D0*DY(J)*DT*BQY(J,K,2)*TM(I,K)


C POINT NO.5
     J=NY
     I=1
SAM=DT*(DY(J)*BY(J,K,1)+DX(I)*BX(I,K))*EPS(I,J)**2*
    &    SAI(X1(I,J,K),T1(I,J,K))*ROSV(T1(I,J,K))*(CXV(I,J,K)-XEQ(I,K))

      IF(NFIFLAG(I,K).EQ.1)SAM=0.0D0

    EE(I,J)=RODU(I,J)-2.D0*VIRCONDX(I,J)+2.D0*SAM*DHK(I,J,1)
    & -2.D0*VIRCONDY(I,J-1)+2.D0*DT*(DY(J)*BQY(J,K,1)+DX(I)*BQX(I,K))

      FF(I,J)=RODU(I,J)*CT(I,J,K)-2.D0*HXVXGX(I,J)
    &   +2.D0*HYVXGX(I,J-1)-2.D0*SAM*(H1(I,J,1)-DHK(I,J,1)*CT(I,J,K))
    &    +2.D0*DT*(DY(J)*BQY(J,K,1)+DX(I)*BQX(I,K))*TM(I,K)

C POINT NO.6
     J=NY
     I=NX
SAM=DT*(DY(J)*BY(J,K,2)+DX(I)*BX(I,K))*EPS(I,J)**2*
    &    SAI(X1(I,J,K),T1(I,J,K))*ROSV(T1(I,J,K))*(CXV(I,J,K)-XEQ(I,K))

      IF(NFIFLAG(I,K).EQ.1)SAM=0.0D0

    EE(I,J)=RODU(I,J)-2.D0*VIRCONDX(I-1,J)+2.D0*SAM*DHK(I,J,1)
    & -2.D0*VIRCONDY(I,J-1)+2.D0*DT*(DY(J)*BQY(J,K,2)+DX(I)*BQX(I,K))

      FF(I,J)=RODU(I,J)*CT(I,J,K)+2.D0*HXVXGX(I-1,J)
    &   +2.D0*HYVXGX(I,J-1)-2.D0*SAM*(H1(I,J,1)-DHK(I,J,1)*CT(I,J,K))
    &    +2.D0*DT*(DY(J)*BQY(J,K,2)+DX(I)*BQX(I,K))*TM(I,K)

RETURN
END

C=============================================================
      SUBROUTINE sor(a,b,c,d,e,f,u,IMAX,jmax,rjac,K,NMAX)
C IMAX=NX+1, JMAX=NY+1
INTEGER jmax,MAXITS,imax
DOUBLE PRECISION rjac,a(80,80),b(80,80),c(80,80),
    * d(80,80),e(80,80),f(80,80),u(0:80,0:80,7),EPS,DX,DY


      PARAMETER (MAXITS=10000,EPS=1.0d-13)
      INTEGER ipass,j,jsw,isw,n,I,K,NMAX
      DOUBLE PRECISION anorm,anormf,omega,resid,PI

PI=4.D0*DATAN(1.D0)
DX=0.105D0/(IMAX-2)
DY=0.525D0/(JMAX-2)

RJAC=(DCOS(PI/(IMAX-1))+(DX/DY)**2*DCOS(PI/(JMAX-1)))
    & /(1.D0+(DX/DY)**2)

      anormf=0.d0

DO 5 I=0,IMAX
U(I,0,K)=0.D0
U(I,JMAX,K)=0.D0
5 CONTINUE

DO 6 J=0,JMAX
U(0,J,K)=0.D0
U(IMAX,J,K)=0.D0
6 CONTINUE
```

```
      do 12 I=1,Imax-1
        do 11 J=1,jmax-1
         anormf=anormf+abs(f(I,J))
11      continue
12     continue
      omega=1.d0
c GO TO 20

      do 16 n=1,MAXITS
       anorm=0.d0

       Isw=1

       do 15 ipass=1,2
         Jsw=Isw

         do 14 I=1,Imax-1

           do 13 J=jmax-JSW,1,-2
             resid=a(I,J)*u(I+1,J,K)+b(I,J)*u(I-1,J,K)+c(I,J)*
     * u(I,J+1,K)+d(I,J)*u(I,J-1,K)+e(I,J)*u(I,J,K)-f(I,J)

             anorm=anorm+abs(resid)
             u(I,J,K)=u(I,J,K)-omega*resid/e(I,J)
13         continue
           Jsw=3-Jsw
14       continue
         Isw=3-Isw
         if(n.eq.1.and.ipass.eq.1) then
           omega=1.d0/(1.d0-.5d0*rjac**2)
         else
           omega=1.d0/(1.d0-.25d0*rjac**2*omega)

         endif
15      continue
NMAX=N
       if(anorm.lt.EPS*10000.D0*anormf)GO TO 20
16     continue

20    omega=2.d0/(1.D0+SQRT(1.d0-rjac**2))

          do 30 N=NMAX,MAXITS
       anorm=0.d0
         do 24 I=Imax-1,1,-1
           do 23 J=1,jmax-1,1
             resid=a(I,J)*u(I+1,J,K)+b(I,J)*u(I-1,J,K)+c(I,J)*
     * u(I,J+1,K)+d(I,J)*u(I,J-1,K)+e(I,J)*u(I,J,K)-f(I,J)

             anorm=anorm+abs(resid)
             u(I,J,K)=u(I,J,K)-omega*resid/e(I,J)

23         continue
24       continue
IF(N.LE.4)GO TO 30
NMAX=N
       if(anorm.lt.EPS*anormf)return
30 continue
     WRITE(1,*)'MAXITS exceeded in sor'
     WRITE(*,*)'MAXITS exceeded in sor'
     pause 'MAXITS exceeded in sor'
return
c      pause 'MAXITS exceeded in sor'
       END

C-----------------------------------------------------------
SUBROUTINE CALHH(H1,HH,DHK,T1R,T,NX,NY,K)

DOUBLE PRECISION HH(80,80,3),H1(80,80,3),DHK(80,80,3)
    & ,T1R(0:80,0:80,7),T(0:80,0:80,7)

INTEGER NX,NY,I,J,K,np
     DO 50 I=1,NX-1
       DO 50 J=1,NY-1
         DO 40 NP=1,3
HH(I,J,NP)=H1(I,J,NP)+DHK(I,J,NP)*(T1R(I,J,K)-T(I,J,K))
 40 CONTINUE
 50 CONTINUE
RETURN
      END
```

```
C-------------------------------------.
SUBROUTINE CALSVTXXY(VT,VX,DX,DY,DT,NX,NY,SVT,SVX,
     & SVTX,SVTY,SVXX,SVXY)

INTEGER NX,NY,I,J

DOUBLE PRECISION VT(80,80,3),VX(80,80,3),SVX(80,80)
     & ,SVT(80,80),SVTY(80,80),SVXY(80,80),DX(80),DY(80),
     & SVXX(80,80),SVTX(80,80),DT

     DO 10 I=1,NX
       DO 10 J=1,NY
  SVT(I,J)=VT(I,J,1)+VT(I,J,2)+VT(I,J,3)
  SVX(I,J)=VX(I,J,1)+VX(I,J,2)+VX(I,J,3)
 10   CONTINUE

 DO 40 I=1,NX-1
   DO 40 J=1,NY
SVXX(I,J)=2.0D0*DY(J)*DT*(DX(I)/SVX(I,J)+DX(I+1)/SVX(I+1,J))**-1
SVTX(I,J)=2.0D0*DY(J)*DT*(DX(I)/SVT(I,J)+DX(I+1)/SVT(I+1,J))**-1
 40 CONTINUE

 DO 50 I=1,NX
   DO 50 J=1,NY-1
SVXY(I,J)=2.0D0*DX(I)*DT*(DY(J)/SVX(I,J)+DY(J+1)/SVX(I,J+1))**-1
SVTY(I,J)=2.0D0*DX(I)*DT*(DY(J)/SVT(I,J)+DY(J+1)/SVT(I,J+1))**-1
 50 CONTINUE

RETURN
     END
C-------------------------------------.
SUBROUTINE CALVIRCOND2(HH,VT,VX,AMBDA,VIRCOND,VIRCONDX,
     & VIRCONDY,HHVX,HHVT,HHVXX,HHVXY,DX,DY,NX,NY,DT)

DOUBLE PRECISION HH(80,80,3),VT(80,80,3),VX(80,80,3),
     & AMBDA(80,80),VIRCOND(80,80),VIRCONDX(80,80),VIRCONDY(80,80)
     & ,HHVX(80,80),HHVT(80,80),HHVXX(80,80),HHVXY(80,80),DX(80)
     & ,DY(80),DT

INTEGER NX,NY,I,J
     DO 10 I=1,NX
       DO 10 J=1,NY
HHVX(I,J)=HH(I,J,1)*VX(I,J,1)+HH(I,J,2)*VX(I,J,2)
     & +HH(I,J,3)*VX(I,J,3)

HHVT(I,J)=HH(I,J,1)*VT(I,J,1)+HH(I,J,2)*VT(I,J,2)
     & +HH(I,J,3)*VT(I,J,3)

VIRCOND(I,J)=HHVT(I,J)-AMBDA(I,J)
 10   CONTINUE

     DO 50 I=1,NX-1
       DO 50 J=1,NY

  VIRCONDX(I,J)=2.0D0*DY(J)*DT*
     &  (DX(I)/VIRCOND(I,J)+DX(I+1)/VIRCOND(I+1,J))**-1

  HHVXX(I,J)=2.0D0*DY(J)*DT*
     &  (DX(I)/HHVX(I,J)+DX(I+1)/HHVX(I+1,J))**-1

50     CONTINUE

     DO 60 I=1,NX
       DO 60 J=1,NY-1

  VIRCONDY(I,J)=2.0D0*DX(I)*DT*
     &  (DY(J)/VIRCOND(I,J)+DY(J+1)/VIRCOND(I,J+1))**-1

  HHVXY(I,J)=2.0D0*DX(I)*DT*
     &  (DY(J)/HHVX(I,J)+DY(J+1)/HHVX(I,J+1))**-1

60     CONTINUE

RETURN
END
C-------------------------------------.
SUBROUTINE CALRODU(RODUP,RODU,RO,DUK,NX,NY,DX,DY)

INTEGER NX,NY,I,J,NP
DOUBLE PRECISION RODUP(80,80,4),RODU(80,80),RO(80,80,4),
     & DUK(80,80,4),DX(80),DY(80)
```

```
      DO 60 I=1,NX
        DO 50 J=1,NY
        RODU(I,J)=0.0D0
10      DO 40 NP=1,4
          RODUP(I,J,NP)=RO(I,J,NP)*DUK(I,J,NP)*DX(I)*DY(J)
          RODU(I,J)=RODU(I,J)+RODUP(I,J,NP)
40      CONTINUE
50      CONTINUE
60      CONTINUE
      RETURN
      END
```

Appendix C

Computer program for one-dimensional diffusion

The following program uses the implicit Crank-Nicholson method for discretization and the TDMA method for solving the one-dimensional diffusion equation.

```
C "" COPYRIGHT"" AHMAD HASHEMI ESFAHANIAN, 1999

real mc(100),mch(100),a(100),b(100),c(100),d(100),dp(100),dd(100),e(100)
     & ,g(100),h(100),avgm(6000),mcin,mcc
al=10.5/2.0
C T=TIME IN SECONDS
t=0.0
mcin=.3
mcc=.033
C  K=NO. OF POINTS
tim=600000.0
k=21
C DX=DISTANCE BETWEEN TWO ADJACENT POINTS
dx=al/(k-1)
dt=30.0
r=dt/(dx**2)
OPEN(UNIT=1,FILE='mc1b1.out')

OPEN(UNIT=2,FILE='mav1b1.out')
r2=r/2.0
aa=.264E-6
bb=16.8
aa1=1.0376652e-6
bb1=8.3520836e-6
aa2=5.17086667e-5
bb2=-8.2266666667e-5
C   S=AVERAGE SURFACE COEFFICIENT
s=2.611634286e-5
C   CCC=AVERAGE DIFFUSION COEFFICIENT
ccc=6.74560392e-5
n=1
ncont=0
C CON=EXPANSION FACTOR FOR TIME STEP
con=1.0
```

```
WRITE(1,*)'Results of Implicit Crank-Nicolson Method for RUN 7
     & of Min Li's case',' dt=',dt,' dx=',dx,'  K=',k,' Mc(initial)= ',mcin
     & ,' Mc(air)= ',mcc,' Dif coef=',ccc,' S=',s

WRITE(2,*)'Dt=',dt,'K=',k,'dx=',dx,'Mc(initial)=',mcin,'Mc(air)='
     & ,mcc,' Dif coef=',ccc,' S=',s

C   MC(J)=MOISTURE CONTENT AT EACH POINT
do 9 j=1,k,1
mc(j)=mcin
c20 mco(j)=mcin
9 continue
10 dt=dt
t=t+dt
n=n+1
con=con*1.0001
do 20 j=1,k,1
C IN CASE THAT THE DIFFUSION COEFFICIENT AT EACH POINT IS DIFFERENT
C DP(J)=THE DIFFUSION COEFFICIENT AT EACH POINT
c dp(j)=aa*exp(bb*mc(j))
c dp(j)=(aa1+bb1*mc(j))/(mc(j)-mcin)
c dp(j)=aa2+bb2*mc(j)
c dp(j)=2.5774e-5
c dp(j)=1.518e-5
dp(j)=ccc
20  continue
do 25 j=1,k,1
if(j.EQ.k)go to 25
C EVALUATING THE HARMONIC AVERAGE OF THE DIFFUSION COEFFICIENT
dd(j)=2./(1./dp(j)+1./dp(j+1))
c dd(j)=0.5*(dp(j)+dp(j+1))
25 continue

do 30 j=2,k-1,1
mch(j)=mc(j)*(1-dd(j-1)*r2-dd(j)*r2)+dd(j-1)*r2*mc(j-1)+dd(j)*r2*mc(j+1)
30 continue
mch(1)=mc(1)*(1-dd(1)*r)+mc(2)*dd(1)*r
c s=9.2e-3
c s=7.27e-4
mch(k)=mc(k)*(1-s*dt/dx-dd(k-1)*r)+dd(k-1)*r*mc(j-1)+mcc*s*dt/dx
c mch(k)=mcc
C IN CASE DIFFUSION COEFFICIENT IS CHANGING DUE TO CHANGES IN MOISTURE CONTENT
do 40 j=1,k,1
c dp(j)=aa*exp(bb*mch(j))
c dp(j)=aa1/(mch(j)-mcin)+bb1*mch(j)/(mch(j)-mcin)
c dp(j)=aa2+bb2*mch(j)
40 continue
do 45 j=1,k,1
if(j.ne.k)dd(j)=2./(1./dp(j)+1./dp(j+1))
45 continue

C EVALUATING THE TDMA ALGORITHM COEFFICIENTS, A,B,C,DE,F,G,H AT EACH POINT
d(1)=mch(1)
c(1)=-dd(1)*r
b(1)=1.0+dd(1)*r
g(1)=d(1)/b(1)
h(1)=c(1)/b(1)
c43
do 60 j=2,k-1,1
a(j)=-dd(j-1)*r2
b(j)=1.0+dd(j-1)*r2+dd(j)*r2
c(j)=-dd(j)*r2
d(j)=mch(j)
e(j)=b(j)-a(j)*h(j-1)
h(j)=c(j)/e(j)
g(j)=(d(j)-a(j)*g(j-1))/e(j)
60 continue

a(k)=-dd(k-1)*r
b(k)=1.0+s*dt/dx+dd(k-1)*r
d(k)=s*dt/dx*mcc+mch(k)
e(k)=b(k)-a(k)*h(k-1)
g(k)=(d(k)-a(k)*g(k-1))/e(k)
mc(k)=g(k)

C EVALUATING THE NEW VALUES FOR MOISTURE CONTENTS
do 90 j=k-1,1,-1
mc(j)=-h(j)*mc(j+1)+g(j)
90 continue
avm=(mc(1)+mc(k))/2.
kk=k-1
```

```
do 160 i=2,kk
avm=avm+mc(i)
160 continue
avm=avm/(k-1)
C AVM=AVERAGE MOISTURE CONTENT OF THE BOARD
ncs=con*20.0
ns=n/ncs
ls=ns*ncs
ps=n-ls
C WRITING THE DATA EVERY 20 TIME STEP
if(ps.NE.0)go to 360
ncont=ncont+1
C   AVGM(NCONT)=AVERAGE MOISTURE CONTENT OF THE BOARD AT THE TIME STEP
avgm(ncont)=avm
tmin=t/60.0
WRITE(1,*)'time=',t

WRITE(1,*)'MC(j) after second half time step'

350 WRITE(1,355)(mc(J),j=1,k)
c WRITE(2,356)582060-t,avgm(ncont)
WRITE(2,356)t,avgm(ncont)
355  FORMAT(21(F13.9))
356 FORMAT(f8.1,f8.4)
360 continue
C CHECKING THE END OF THE PROGRAM
if(abs(avm-mcc).LE.0.00001.and.avm.lt.mcc)go to 370
if(t.lt.tim)go to 10
370 continue
CLOSE(1)
CLOSE(2)
stop
end
```